

ADVANCED TECHNOLOGIES IN EDUCATION, INDUSTRY AND THE ENVIRONMENT

Edited by

Olga Paraska

Khmelnytskyi National University, Ukraine

Norbert Radek

Kielce University of Technology, Kielce, Poland

Oleg Synyuk

Khmelnytskyi National University, Ukraine

Poland

2020

Advanced technologies in education, industry and the environment.
Monograph: edited by Olga Paraska, Norbert Radek, Oleg Synyuk –
2020. – 297 p.

Monograph is prepared at the Department of Chemistry and Chemical
Engineering of Khmelnytskyi National University in cooperation with
Centre for Laser Technologies of Metals, Kielce, Poland.

Monograph recommended by the Senate of Khmelnytskyi National
University (UA), Khmelnytskyi city council (UA), Khmelnytskyi Regional
Council (UA), F. H. Barwa (PL), Centre for Laser Technologies of Metals
(PL), September – October 2020.

Article in monograph are presented in the author's original version. Authors are
responsible for materials and interpretation.

EDITORIAL BOARD:

Radek N. (Poland, Kielce), **Pietraszek Ja.** (Poland, Krakow), **Skyba M.**
(Ukraine, Khmelnytskyi), **Mandzyuk I.** (Ukraine, Khmelnytskyi), **Pelik L.**
(Ukraine, Lviv), **Korycki R.** (Poland, Lodz), **Govorushchenko T.**
(Ukraine, Khmelnytskyi), **Dudek A.** (Poland, Czestochowa), **Gadek-
Moszczak A.** (Poland, Krakow), **Szczotok A.** (Poland, Gliwice),
Korzekwa J. (Poland, Gliwice), **Mironova N.** (Ukraine, Khmelnytskyi),
Beresnenko S. (Ukraine, Kiev), **Hes L.** (Czech Republic), **Slizkov A.**
(Ukraine, Kiev), **Broncek J.** (Slovakia, Zilina), **Bonek M.** (Poland,
Gliwice), **Kozar O.** (Ukraine, Mukachevo), **Saribekova Yu.** (Ukraine,
Kherson), **Zacharkevic O.** (Ukraine, Khmelnytskyi).

REVIEWERS:

Boguslavska-Bochek M. (Poland, Katowice), **Dombrovskiy A.** (Ukraine,
Khmelnytskyi), **Kuleshova S.** (Ukraine, Khmelnytskyi), **Ivanishena T.**
(Ukraine, Khmelnytskyi), **Musial J.** (Poland, Bydgoszcz), **Lochov V.**
(Russia, Perm), **Fabian P.** (Slovakia, Zilina), **Lysenko S.** (Ukraine,
Khmelnytskyi), **Goryashchenko S.** (Ukraine, Khmelnytskyi), **Horbovyi A.**
(Ukraine, Kiev), **Rotar D.** (Ukraine, Chernivtsi), **Polishchuk O.** (Ukraine,
Khmelnytskyi), **Padgurskas Ju.** (Lithuania, Kaunas), **Sniadkowski M.**
(Poland, Lublin), **Mazurkewic A.** (Poland, Bydgoszcz).

Responsible Secretary: Prof. univ. dr hab. Ing. J. Pietraszek

Technical Secretariat: Associate Prof. PhD N. Mashovets

ISBN – 978-617-7600-96-0

©Copyright by the Centre for Laser Technologies of Metals, Kielce University of
Technology, Al. 1000-lecia Państwa Polskiego 7, PL-25314, Kielce, Poland, 2020

CONTENT

Preface	6
Quality-control research of elements of the learning process by an example of studying chemical disciplines Tkachuk H.....	10
Exploration of mobile applications to use in training of clothing patternmakers Zakharkevich O., Koshevko Ju.....	23
New combined technologies of synthesis materials Zhiguts Yu., Kozar O.....	33
Peculiarities of a new method for evaluating fibrous products structure Slizkov A., Avetisyan A.....	47
The effect of moisture on moisture absorptivity and overall comfort index of men's shirts Hes L., Paraska O., Gebrian P.....	59
Selected aspects of aesthetic properties of laminated seams Szafranska H., Korycki R.....	71
Wearing out process of textile materials made of hermoresistant fibers and its impact on the filtering capacity of the hose filters Pelyk L., Pelekh Yu.....	83
Study of influence of the cotton knitted fabric weave on the surface geometry and lightfastness of colours Semeshko O., Asulyuk T., Saribyekova Yu.....	94
Development of a device and methods for assessing the flammability of materials Zasornov A., Zasornova I.....	109
Moisture transport inside textile structures and leather Korycki R., Szafranska H.....	122

Increase of temperature and fire resistance for reinforced-concrete structures by surface treatment with protective coating Demydchuk L., Sapozhnyk D.....	132
Implementation of expert system for clothes style selection Kuleshova S.....	146
Optimization of the technological parameters of wet cleaning process of the textile products Paraska O., Radek N.....	159
Mathematical modeling of heat protective properties of polymeric materials for footwear Horiashchenko S., Horiashchenko K., Polishchuk O.....	172
Determination of the parameters of rheological leather models by the indirect method Ihnatyshyn M., Rosul R.....	183
Applying nonlinear approximation methods in experimental data processing Chesanovskyi I., Katerynchuk I.....	193
Formation of the model of the polymer material structure during orientational drawig Synyuk O.....	205
Physical and mechanical characteristic of leather for the upper of shoes, filled with natural minerals Kozar O, Wozniak B., Zhiguts Yu.....	223
The assessment of the impact of shoe materials on human health on the basis of LCA-analysis Ivanishena T., Ivanishena O.....	235
Acoustic emission diagnostics of composite materials in capacitor assembly under thermal impacts Kovtun I., Petrashchuk S., Boiko J.....	248

Investigations on utilisation chromium tanned leather residues by chrome recovery and biogas production Flisek M., Woźniak B., Schadewell Ch.....	261
Characterization and properties of lubricants obtained by technologies of recycling waste products of thermoplastics Prysiashna K., Mandzyuk I., Padgurskas Ju.....	269
Diagnosing the condition of the temporomandibular joint on the basis of medical image extraction Głowacki M., Mazurkiewicz A., Nowicki K., Słomion M.....	280

PREFACE

Technology in the modern world occupies an important place. It affects all spheres of life, make life easier and better. The modern world is a technical space. The development of innovative technologies and automation of production open new opportunities for industrial enterprises. This allows to optimize and accelerate production processes, to use more rationally funds, energy, natural resources.

Translated from the ancient Greek word "technology" means – art, skill. In a broader sense – the application of scientific knowledge in solving practical problems. The technological process includes methods of work, the sequence of actions in creating finished products or providing services to consumers.

Currently, innovation in industry and business can be divided into two major groups. The first are hardware and software complexes that directly affect the production process. The second are systems that allow to expand the knowledge of manufacturers about the consumers' needs and the operating conditions of certain products. In today's world, the term "technology" refers to the means and actions by which a person improves and changes the world around.

Due to the fact that the needs of society are constantly changing, production technologies do not stop evolving. The introduction of the latest achievements of science in production is a source of industrial technology. It is impossible to imagine modern production without the use of the latest technologies. This applies to materials and equipment that must meet international standards.

Powerful equipment, information tools, automation of production, methods of energy saving and energy supply, methods of waste disposal –

Advanced technologies in education, industry and the environment

these technologies directly affect the competitiveness of the enterprise. Due to the production and technology automation here is an increase in productivity and product quality, which has a positive impact on business development and customer satisfaction.

The textile industry is an important component of the economy, as it provides not only consumers but also various industries where textile materials are used (automotive industry, furniture, defense, medical, food, etc.).

Currently, manufacturers automatize technological processes, optimize the business management system. Automatic fabric cutting with the help of an automated design system, successfully used in the garment and leather goods industry. Automated processes help to accelerate the creation of new models, reduce the complexity of work, improve the quality of clothing and footwear. Unified databases allow to automatize production processes with an enterprise management system and help reduce production costs.

Thanks to modern software and technology, it has become possible to take contactless measurements and produce clothing, taking into account the individual characteristics of the person. Such systems allow to measure remotely a large number of people, which increases the number of consumers. The innovative materials use, such fabrics as microfiber, have unique characteristics and are superior in their properties to natural fabrics (silk, cotton).

The application of innovations in the food industry helps to improve product quality and allows the rational use of raw materials. The latest developments in the field of chemistry, physics, biology and electrical engineering are widely used in the production and storage of products (treatment with radioactive radiation, ultraviolet; heating by infrared

Advanced technologies in education, industry and the environment

radiation, alternating electric field, cryo-freezing). These technologies destroy all known microbes without harming the environment, do not cause the formation of toxins and do not change the chemical composition of products.

With the help of modern food packaging significantly increases the shelf life of products without changing their taste and appearance (vacuum, aseptic packaging, packaging in a gaseous medium). Such technologies ensure the tightness of packaging, reduce the development of microflora and increase the shelf life of products without the use of preservatives.

Currently, waste is generated in various industries in the production process. Recycling technologies are carried out in accordance with legal norms and standards. The future of the world's ecology, life and health of citizens depends on the choice of waste processing technology. Modern recycling technologies allow not only to completely neutralize potential damage, but also to obtain secondary raw materials after disposal.

Innovative technologies are an important part of production in all industries. They increase the efficiency of enterprises, quantity and quality of products. The logistics technologies development that are focused on consumer demand contribute to the successful operation of corporations in the international market. Modernization of technologies and equipment, the latest technologies, modern materials are the main components of industrial development in the world.

The innovative technologies introduction is based on the latest advances in science and technology. A large number of specialists take part in this process – scientists, industrialists, businessmen, experts. Training and education of professional specialists make an invaluable contribution to the development of modern industrial technologies.

Advanced technologies in education, industry and the environment

The monograph presents the results of research by scientists from Ukraine, Poland, Lithuania, Germany and the Czech Republic. Long-term international cooperation between researchers, scientists, entrepreneurs, business owners contributes to the introduction of new technologies in production. Implementation of joint projects strengthens the world's research and production infrastructure, R&D centers and technology parks. The monograph will be useful for professionals in various industries, scientists and researchers.

We are sincerely grateful to all the authors and individuals for your valuable contribution to the publication of the monograph. We express our general gratitude for the help in preparing the monograph to the Rector of Khmelnytskyi National University Mykola Skyba, the Mayor of Khmelnytskyi Oleksandr Symchyshyn, the Deputy Chief of Staff of the Regional Council Tetyana Zelenko, the head of the Centre for Laser Technologies of Metals Bogdan Antoszewski, and head of the company F.H. BARWA Jaroslaw Czajkowski for their support and cooperation in preparing for publication of monographs, as well as the entire editorial board and respected reviewers. It is a pleasure to cooperate with you.

With best wishes and respect

Monograph editor

Olga Paraska

Norber Radek

Oleg Synyuk

**QUALITY-CONTROL RESEARCH OF ELEMENTS OF THE
LEARNING PROCESS BY AN EXAMPLE OF
STUDYING CHEMICAL DISCIPLINES**

Tkachuk H.

Khmelnytskyi National University, Ukraine

Introduction

Ukraine's European integration in the field of education and science determines the needs of developing and optimizing the methodological and organizational system of the educational process in universities. As an integral part of the educational process is learning, which with the introduction of quarantine restrictions and virtually continuous distance technologies, has become even more dominant over the teaching process, qualimetric monitoring assessment of learning outcomes is important and relevant [1].

In [2] we revealed the formation of learning technology in the study of chemical disciplines in classical universities as the main component of the educational process and considered the possibilities of solving the practical implementation of all eight proposed elements of learning technology. These elements are: preparation for learning, perception, understanding, memorization, ensuring the strength of knowledge, generalization, systematization, achievement of developed skills and abilities. However, this paper is devoted to an analysis of the influence of input and output parameters of the elements of learning technology.

Methods

Theoretical research methods, pedagogical experiment, experimental methods of measuring physical quantities, methods of mathematical statistics, mathematical modeling and computer processing of experimental data are used in the work.

Experimental

Elements of the technology of the learning process, such as perception, understanding, memorization, have a certain significance in the mechanism of learning technology. We will assume that all individual elements of learning technology are not functional or correlated and have the same weights, as noted in the paper [3], monitoring the quality assessment of each of the individual elements of learning technology, followed by evaluation the quality of all learning technology is associated with significant methodological and mathematical difficulties, due to the different physical nature of these elements. This is the main reason for the use of qualimetry methods [4] to measure qualitative quantities and processes by quantitative methods. For most elements of learning technology, direct assessment of academic achievement is not possible.

To solve such a difficult problem is proposed in the paper [3], namely: all structural elements of learning technology set three levels of assessment: unsatisfactory, when this element of technology does not show its inherent functions in the mechanism of learning technology, or when it is numerically unsatisfactory assessment; satisfactory, when it mainly manifests itself sufficiently in the mechanism of formation of a certain component of learning technology; and, a sufficient level. Numerically named levels of assessment of student achievement (students) are expressed by the numbers 0; 1; 2.

If in this way to make a monitoring assessment of the level of academic achievement in learning by elements of its technologies, it will allow to make a general qualimetric assessment of the level of the learning process. It should be borne in mind that the implementation of a qualimetric approach to the learning process requires the introduction of a whole system of detection, collection and processing of information about the learning process and its results. This system should include control measures, starting with the current survey, work with test materials and ending with the types of control measures performed. Qualimetry should not be considered as an isolated canned system, but as an integral part of

learning technology, given the feedback of the technology of these processes with the search for effective forms and methods of influencing the quality of the learning process. Qualimetry can be considered as an active and integral part of the technology of the learning process.

Let's find dependences between input and output parameters of technology. The input parameter should be considered elements of the technology of the learning process [2]. For example, the technology of understanding involves the use of certain subordinate actions: visual aids, visualization tools, samples of chemicals and equipment, demonstration of a chemical experiment, molecular modeling, and so on. The initial parameters are the result of the application of a technology measured by the academic achievements of students in the learning process. The qualimetric measure of these achievements is the place of this position in the grading system 0; 1; 2 levels of learning process technologies. These results allow us to identify a characteristic measure of the impact of input parameters on academic achievement.

We will consider a certain value of x , which is taken as the starting point in the technology of the learning process as a one-dimensional continuous random variable. The set of possible values of a random variable and the probability that it will take these possible values form the law of its distribution. Exhaustive probabilistic characteristics of a random variable are its distribution laws [5]. There are two types of distribution of random variables: integral and differential. The differential distribution law $f(x)$, the random variable x , is called the derivative of its integral distribution law. It is necessary to take into account the possibilities of distribution laws that are revealed in the process of their use: the range of possible values of x ; the probability density $\varphi(x)$ in the middle of this interval, and outside the range of possible values, the probability density is zero, and the probability density $\varphi(x)$ is the probability limit that the value of x has a value in the range $(x, x + \Delta x)$ to the value of the interval Δx ,

when $\Delta x \rightarrow 0$ [5]. It should be borne in mind that $\int_{-\infty}^{+\infty} \varphi(x) dx = 1$, and the unit of probability density $\varphi(x)$ is the inverse of the unit of measurement of x .

Such properties of the law of distribution of a random variable (in this case, a qualimetric assessment of the technology of the learning process) allow the use of the laws of its distribution for modeling. It can occur first at the level of creating graphical models of technological processes, first in the form of histograms or polygons of distribution of experimental data, and then already proven worked out and smoothed curves of distribution of initial values, which are presented as graphical models of technological processes. The next stage is the creation of mathematical models of technological processes of learning by approximating the obtained graphical dependences of the laws of distribution by analytical dependences or their elements.

Results

Consider the components of the technological process of learning in the sequence presented in the paper [2]. Each of the components of learning technology is assigned a number that corresponds to its place in the structure of technology as a whole using the text of references to these numbers. Moreover, we note that each of the eight elements of learning technology is represented by the number of students, which varied from $N = 250$ people to $N = 320$ people.

In Fig. 1 according to experimental data, a histogram of the distribution of learning technology element 1 – preparation for learning at $N = 250$. Preparation of chemistry students for the learning process is to actualize their interest in learning, providing positive motivation by demonstrating the prospects of higher education in the chosen specialty scholarship support, interesting teaching of educational material, which is not difficult to implement due to the large volume of laboratory workshops and internships in the curriculum for the training of chemists [2].

In Fig. 1 indicates that n_i is the number of observations of learning monitoring results; n_i^* – the number of observations in the i -th digit of the array of N observations. We have accepted the number of digits k of observations. It should be noted that.

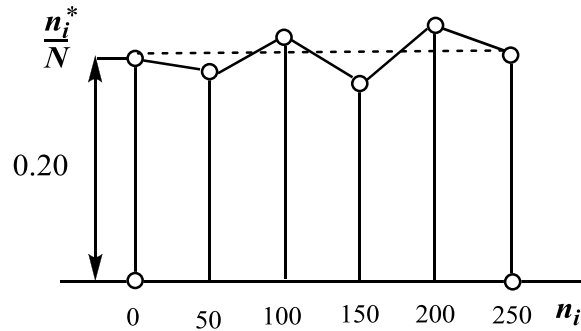


Fig. 1. Histogram of the distribution of the output parameter element 1 of learning technology

The appearance of the histogram of the distribution of preparation for learning allows you to make sure that it is a distribution of levels of probability or the law of uniform distribution (Fig. 2).

The range of possible values of the random variable x , subject to the law of equal probability from b to c in fig. 2, or from $a - 1$ to $a + 1$. In this law there are two parameters: b and c , or from a and l .

Received the probability density (1) [5], and the distribution function, or the integral law of uniform distribution (2) [6].

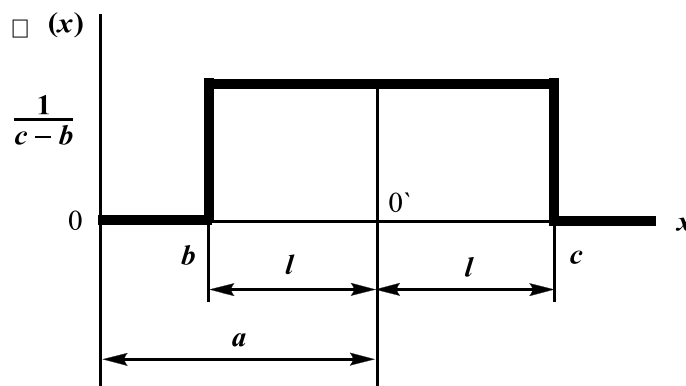


Fig. 2. Differential law of uniform distribution the output parameter of element 1 of the learning technology

$$\varphi(x) = \begin{cases} 0 & \text{при } x < b, \\ \frac{1}{c-b} & \text{при } b \leq x \leq c, \\ 0 & \text{при } x > c. \end{cases} \quad (1)$$

$$F(x) = \begin{cases} 0 & \text{при } x < b, \\ \frac{x-b}{c-b} & \text{при } b \leq x \leq c, \\ 1 & \text{при } x > c. \end{cases} \quad (2)$$

The law of uniform probability density is symmetric. In our case, the function x has an upper bound $x = 2$, so $c = 2$, and $m_1(x) = 1$. The initial factor of technology can be the sum of two or more mutually independent random variables x, y, z, \dots [6]. In this case, the law of distribution will refer to their sum, ie finding the composition of the law of distribution. This operation is called the layout of the distribution law and is denoted by the symbol $*$ [5]. The probability density of the sum of two independent random variables is determined by equation (3), where $u = x + y$.

$$\varphi(x+y) = \varphi_1(x) * \varphi_2(y) = \int_{-\infty}^{+\infty} \varphi_1(x) \cdot \varphi_2(u-y) dx = \int_{-\infty}^{+\infty} \varphi_2(y) \cdot \varphi_1(u-y) dy, \quad (3)$$

There may be cases when the law of distribution of a random variable that characterizes the output of the parameter element 2 of the technology of the learning process is described by a trapezoidal distribution, the geometry of which is given in Fig. 3.

Perception as the second element of learning technology is the process of student reflection of objects and phenomena in general, in the aggregate of all other qualities and properties with their direct impact on the senses. Attentively, students perceive mostly only interesting or very necessary information that arouses their spontaneous interest or when they are in a state of surprise and creative activity [2].

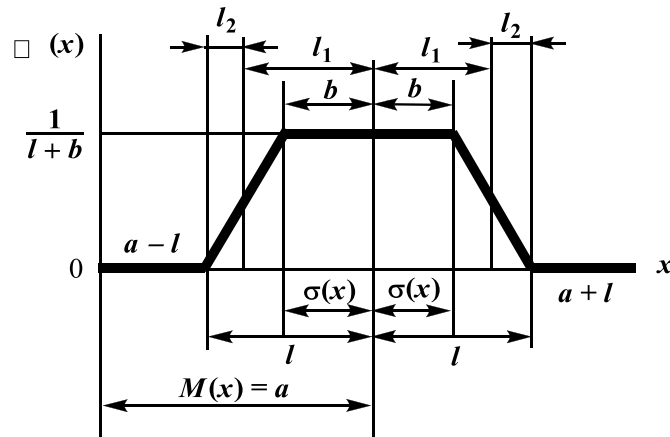


Fig. 3. Trapezoidal distribution of the output parameter element 2 of learning technology [5]

The parameters of the law shown in Fig. 3 are three one [5]: $a = M(x)$; $l = l_1 + l_2$ – half of the range of possible values; $b = |l_1 - l_2|$ – half of the horizontal section of the distribution curve.

Trapezoidal probability density [5] (4).

Mathematical expectation is simply determined by fig. 3:

$$m_2(x) = l = 1.$$

$$\varphi(x) = \begin{cases} 0 & \text{при } x < a - l, \\ \frac{x - a - 1}{l^2 - b^2} & \text{при } a - l \leq x \leq a - b, \\ \frac{1}{l + b} & \text{при } a - b \leq x \leq a + b, \\ \frac{a + l - x}{l^2 - b^2} & \text{при } a + b \leq x \leq a + l, \\ 0 & \text{при } x > a + l. \end{cases} \quad (4)$$

The third element of learning technology is understanding. The language of chemical symbols, equations of chemical reactions, schemes, graphical formulas, results and analytical effects of laboratory workshops and chemical experiments are very important for the transmission and understanding of information to chemistry students [2].

Implementation of element 3 – understanding of the technology of learning. It is represented by the histogram of distribution of element 3 constructed according to experimental data – understanding among participants of training in number of 250 persons that is shown in Fig. 4.

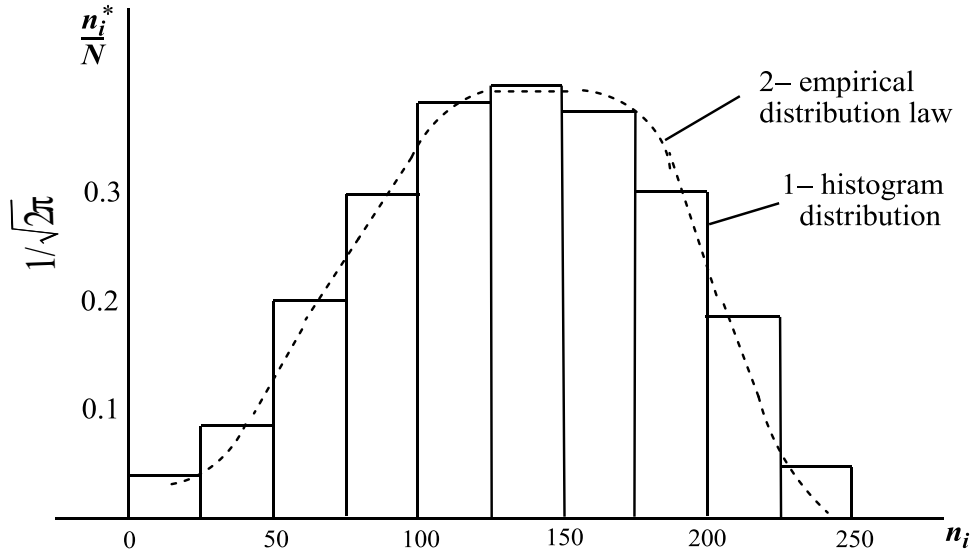


Fig. 4. Empirical law of distribution of initial parameter element 3 of learning technology

The theoretical distribution law in this case is the normal Gaussian distribution law [5]. The density distribution of the probability of a random variable having a Gaussian distribution depends on two parameters: the mathematical expectation $a = m(x)$ and the standard deviation $\sigma = \frac{(x-a)^2}{2\sigma^2}$ and is determined by equation (5) [5]:

$$\varphi(x) = \frac{1}{\sigma\sqrt{2\pi}} \cdot \exp, \quad x \in [-\infty; +\infty]. \quad (5)$$

The mathematical expectation of element 3 of the understanding of learning technology is equal to [6]: $m_3(x) = 0.9973 / 2 \approx 0.5$.

Curve 2 (Fig. 4) depicts the law of distribution of the initial parameter of element 3 – understanding the technology of learning.

Memorization is the fourth element of technology, which is also a property of man, without which learning as a process is not possible, it is to consolidate, store and subsequently reproduce the student's previous experience. Memorization plays a significant role not only in conducting control measures to demonstrate the degree of mastery of theoretical material, but also required in the reproduction and use of this experience in solving situational problems in chemistry, as well as production problems [2]. Consider element 4 – memorizing of the learning technology in Fig. 5.

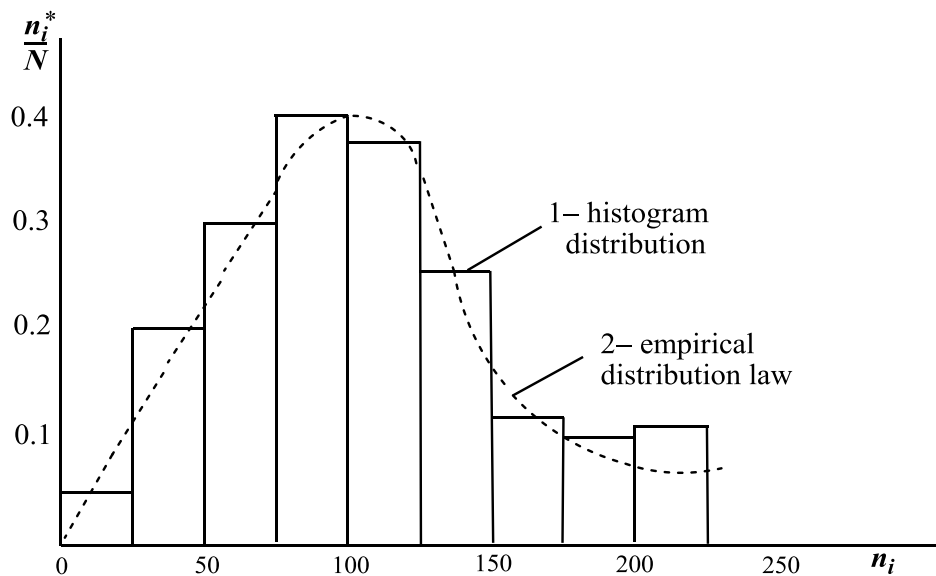


Fig. 5. Histogram and empirical law of distribution of the initial parameter of element 4 of learning technology

In figure $N = 250$, and this histogram on its external features is a composition of the distribution law and the law of equal probability, ie the sum of random variables $u = x + y$. Let's find the analytical dependence for the distribution law of the composition, which is characterized by equation (6). The probability density of a random variable is determined by Gauss's law and is given by the value. The probability density of the value of y is given by the dependence (7) [6].

$$\varphi_1(x) = \frac{1}{\sigma_0 \sqrt{2\pi}} \cdot \exp\left(-\frac{x^2}{2\sigma^2}\right), \quad \text{при } -\infty \leq x \leq +\infty. \quad (6)$$

$$\begin{aligned}\varphi_2(y) &= \frac{1}{2\delta} & \text{при } |y| \leq \delta, \\ \varphi_2(y) &= 0 & \text{при } |y| > \delta.\end{aligned}\quad (7)$$

From the boundaries of integration over x in equation (6) is excluded only the range of values in which $\varphi_2(y) = 0$, since within $\varphi(x) \neq 0$. These are the following areas: $-\infty < y - x < +\infty$, ie $-\infty < x < u - \delta$. From this we obtain the boundaries of integration on x from $u - \delta$ to $u + \delta$. And take into account that δ is half the value of a given field. The differential law of distribution of compositions of the Gaussian law of distribution and the law of true probability on the basis of the above is described by dependence (8) [5]. Using the Laplace function [6] expression (8) is written in the form (9) [5]:

$$\varphi_1(u) = \frac{1}{\delta} \cdot \frac{1}{\sigma_c \sqrt{2\pi}} \cdot \int_{a-\delta}^{a+\delta} \exp\left(-\frac{x^2}{2\sigma_c^2}\right) dx, \quad [-\infty < u < +\infty]. \quad (8)$$

$$\varphi(u) = \frac{1}{2\delta} \left[\Phi\left(\frac{u+\delta}{\sigma_0}\right) - \Phi\left(\frac{u-\delta}{\sigma_0}\right) \right], \quad (9)$$

This is an analytical dependence for the law of distribution of the output parameter of the element of technology 4 – memorization. Calculate it for $\delta = 0.5$ and $\sigma_0 = 1$, given that the Laplace function is odd and $\Phi(-u) = -\Phi(u)$. The theoretical laws of probability distribution $F(u)$ and the law of probability density distribution $\varphi(u)$ for the initial parameter of element 4 – memorization of learning technology are obtained as a result of the composition of the Gaussian distribution law and the law of equal probability shown in Fig. 6.

Ensuring the strength of knowledge is the fifth element of learning technology. The most strongly stored in the student's memory is information that is associated with a bright emotional and figurative background. Effective means of strengthening knowledge are not only a vivid emotional presentation of educational material, but also the skillful use of laboratory workshops in chemical disciplines [2].

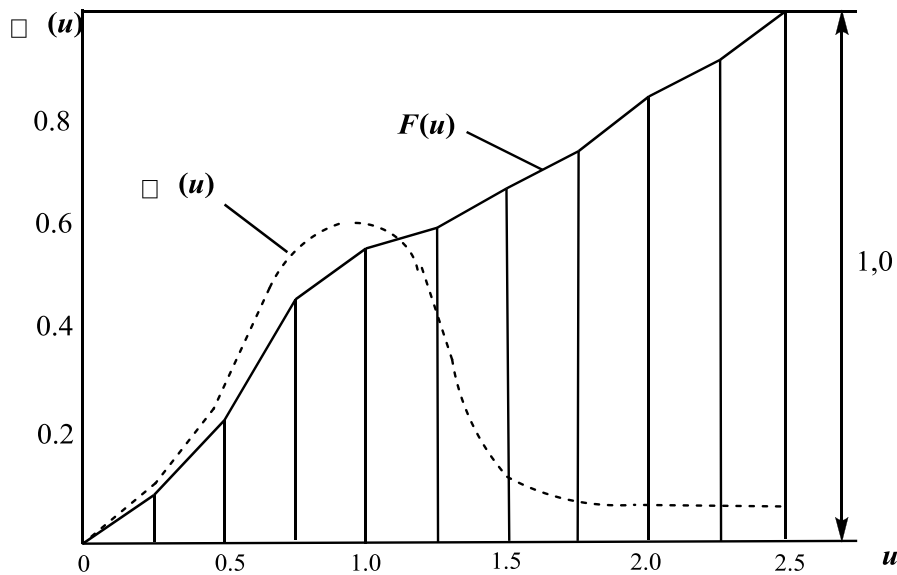


Fig. 6. Theoretical laws of probability distribution and the law of distribution of probability density for the initial parameter of element 4 of the learning process

In the implementation of the element of technology 5 – ensuring the strength of knowledge, it is characterized by a histogram of the distribution of the initial parameter of the element 5 of the technology, obtained empirically (Fig. 7).

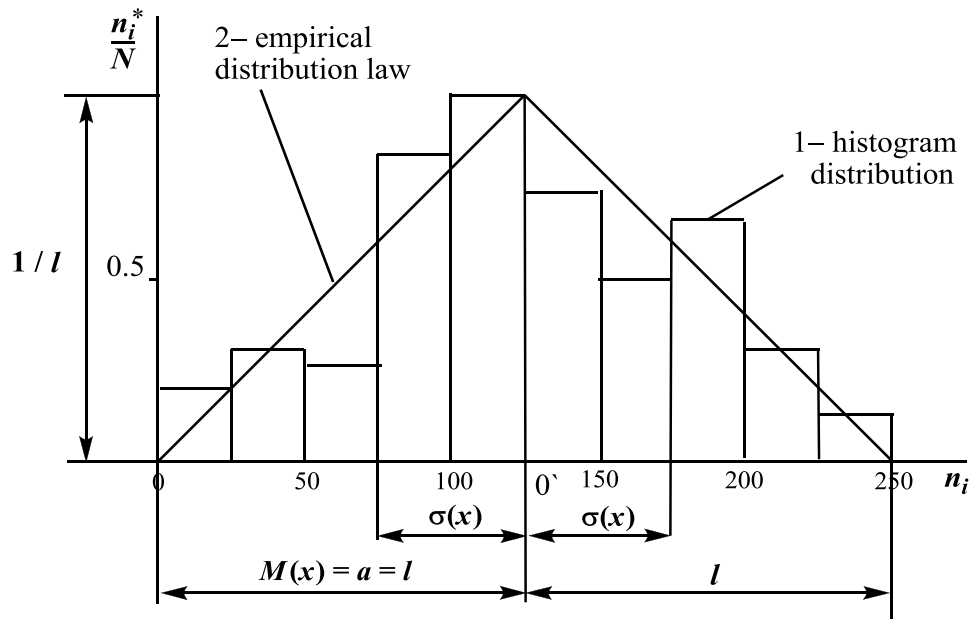


Fig. 7. Illustration of the law of distribution of qualimetric evaluation the level of ensuring the strength of knowledge in the process of actions

The law of distribution of qualimetric assessment of the level of ensuring the strength of knowledge in the learning process corresponds to the analytical equation (10). The probability density of the distribution of qualimetric estimation of the level of ensuring the strength of knowledge on the basis of the above provisions is determined by Simpson's law [6] – the distribution of an isosceles triangle.

Mathematical expectation was calculated by the expression: $m_5(x) = a = 1.0$.

$$\varphi(x) = \begin{cases} 0 & \text{при } x < a - l, \\ \frac{l + x - a}{l^2} & \text{при } a - l \leq x < a, \\ \frac{l + x + a}{l^2} & \text{при } a \leq x \leq a + l, \\ 0 & \text{при } x > a + l. \end{cases} \quad (10)$$

We had explored five elements of learning technology. Further research will determine the initial parameters of the next three elements of learning technology and test the plausibility of the assumption, how the empirical results are consistent with the hypothesis of whether the random variable under consideration is subject to the theoretical distribution law. The important question is whether the tendency found in empirical data for a relationship between two random ones is really an objective relationship, or whether it is due to random causes, which is due to insufficient research.

Conclusions

1. The initial parameters of the studied five elements of learning technology are not random and are subjects to mathematical laws.
2. The histogram of the distribution of preparation for learning is described by the law of uniform distribution.
3. The histogram of distribution of the initial parameter of perception has trapezoidal character.

4. The empirical distribution law of the initial parameter of understanding is described by the normal Gaussian distribution law.

5. The theoretical laws of probability distribution and the law of probability density distribution for memorization are obtained as a result of the composition of the Gaussian distribution law and the law of equal probability.

6. The probability density of the distribution of qualimetric estimation of the level of ensuring the strength of knowledge is determined by Simpson's law – the distribution of an isosceles triangle.

References

1. Tkachuk H. S. (2019). Uchinnya yak bazovyi element tekhnolohii navchalnoho protsesu [Learning as a basic element of the technology of the educational process] *Teoriya ta metodyka navchannya ta vychovannya*, 47, 133–147.

2. Tkachuk A. & Karvan S. (2013). The Discipline Problem of Students under Condition of Academic Mobility. International Conference “New Perspectives in Science Education”, Florence, Italy. <http://www.pixel-online.net/npse2013/acceptedabstracts.php>.

3. Skyba M. Ye., Kostohryz S. H. & Krasylnykova H. V. (2009). Monitorynh yakosti navchalnoho protsesu u vyshchomu zakladi osvity [Monitoring the quality of the educational process in a higher education institution] *Khmelnytskyi, KhNU*.

4. Tsyba V. T. (2002). *Matematychni osnovy sotsiologichnykh doslidzhen: kvalimetrychnyi pidkhid* [Mathematical foundations of sociological research: a qualimetric approach.] Kyiv, MAUP.

5. Livshits N. A. & Pugachev N. A. (1963). *Vieroyatnostnyi analiz sistem avtomaticheskogo upravlieniya* [Probabilistic analysis of automatic control systems] Moskva, Sovetskoye radio.

6. Vientsel Ye. S. (2006). *Teoriya vieroyatnosti* [Probability theory] / Ye. S. Ventsel. Moskva, Vysshaya shkola.

EXPLORATION OF MOBILE APPLICATIONS TO USE IN TRAINING OF CLOTHING PATTERNMAKERS

Zakharkevich O., Koshevko J.

Khmelnyskyi National University, Ukraine

Introduction

In the past decade it is not so difficult to imagine that all the tasks of apparel designer might be handled by using smartphone tools such as mobile applications. As it was discovered in the work [1], the opportunities for mobile apps in the fashion domain are very versatile. Among them most frequently mentioned are wardrobe organizers apps. It does not mean though that the purpose of mobile apps in apparel design is restricted to the domain of ready-made clothing. There are a lot of different tools on the market of mobile apps those are or might be used for designing clothing.

The necessity to have such an instrument as mobile app is proven during the COVID-19 pandemic that forced all the industries and educational institutions to work mostly online.

Every student of every university of the world has a smartphone. However, most of them do not have a computer. Especially, when we are talking not about the laptop but the computer. The computer is the hardware that is almost obligatorily when computer aided design of clothing patterns is concerned. Pattern drafting systems (PDS) are very costly and they are very demanding systems in regard to the computer hardware. That is why, when the student is forced to work on their class work not in the laboratory but at home the necessity of alternative tools is evident.

The question of using the mobile apps while learning and teaching was addressed by many researchers of the world. The evidence of great variety we can see in the works [2-11]. The most prominent of them are Kim Y. and Smith D. [1], Zaranis N., Kalogiannakis M., Papadakis [3], Mackaya B.J., Andersona J., Hardingb T. [4].

Advanced technologies in education, industry and the environment

Some of them are working on specific issues of using the mobile apps as a part of the smart technology [12-13]. Others are studying possibilities of using the mobile applications as 3Dscanners of some sort [14-16].

It is evident that some of their results might be used in the process of clothing designers training. However, specific issues of using mobile apps in the training of future experts in apparel design are scarcely observed until now.

The paper [17] presents different examples of using mobile applications during educational simulation of a design product, in managing students' remote independent work. With the example of such mobile applications as Pinterest, Fashion Design, Sketch, Bamboo Paper, SCANN3D, True Sculptor, d3D Sculptor and RealtimeBoard in the work [17] practical details of how to attract mobile technologies at different stages of the project development of product design were shown.

Methods

Statistical analysis was performed in order to determine the state of the mobile market in the fashion and apparel domain. The explorations were performed on both Google Play and App Store platforms.

The population of mobile apps was formed by using search words such as “pattern”, “clothing”, “sewing”, “wardrobe”, “clothes” etc.

Discovered mobile applications were analyzed in regard to their applicability for the education process. To assess the applicability a survey was conducted. There were 10 respondents of the survey. All of them are experts in the field of education as well as in the field of apparel design.

Aiming to obtain an algorithm that will allow choosing a specific app for the certain design activity or the certain apparel design process we categorized all apps by 14 categories. The categories were compared for the different operating systems.

Experimental

The size of population of mobile applications, which have something to do with clothing and its design or manufacturing, is about 500 mobile application both for Android and iOS operating systems. All of the mobile apps were divided into 14 groups, each of them addresses one of the important questions in apparel design and clothing distribution. The results of categorization are shown in the table 1.

The applicability for the education was estimated in points from 0 to 5, where 0 – absolutely inapplicable, and 5 – absolutely applicable and advisable. In the table 1 the average values of estimated marks given by 10 different experts are shown.

Table 1. Categorization of mobile applications in fashion domain

No	Category	Number of discovered applications in operating system		Applicability for the education	Coefficient of variation, %
		Android	iOS		
1	Galleries of ready-made clothing patterns	141	8	4.4	18.18
2	Apps to create a capsule wardrobe	10	9	4.6	14.42
3	Online shops apps	97	38	4.2	20.76
4	Sewing tutorials	10	6	4.9	6.12
5	Galleries of clothing styles	70	11	4.2	17.82
6	Wardrobe organizers	6	14	3.9	24.2
7	Body measurements	4	9	4.5	14.91
8	Fashion and clothing glossary apps	3	1	4.8	8.33
9	Apps to create a sketch of fashion design	2	11	4.5	17.92
10	Apps to organize tailor's work	2	3	3.7	27.16
11	Pattern calculators	4	0	4.9	6.12
12	Virtual fitting apps	1	4	4.1	25.46
13	Clothing color matching apps	1	4	4.3	23.37
14	Fabrics calculators	1	9	4.7	9.75

As one can see in the table 1, basically all of discovered applications might be used in the educational process while teaching students who study apparel design (Fig. 1).

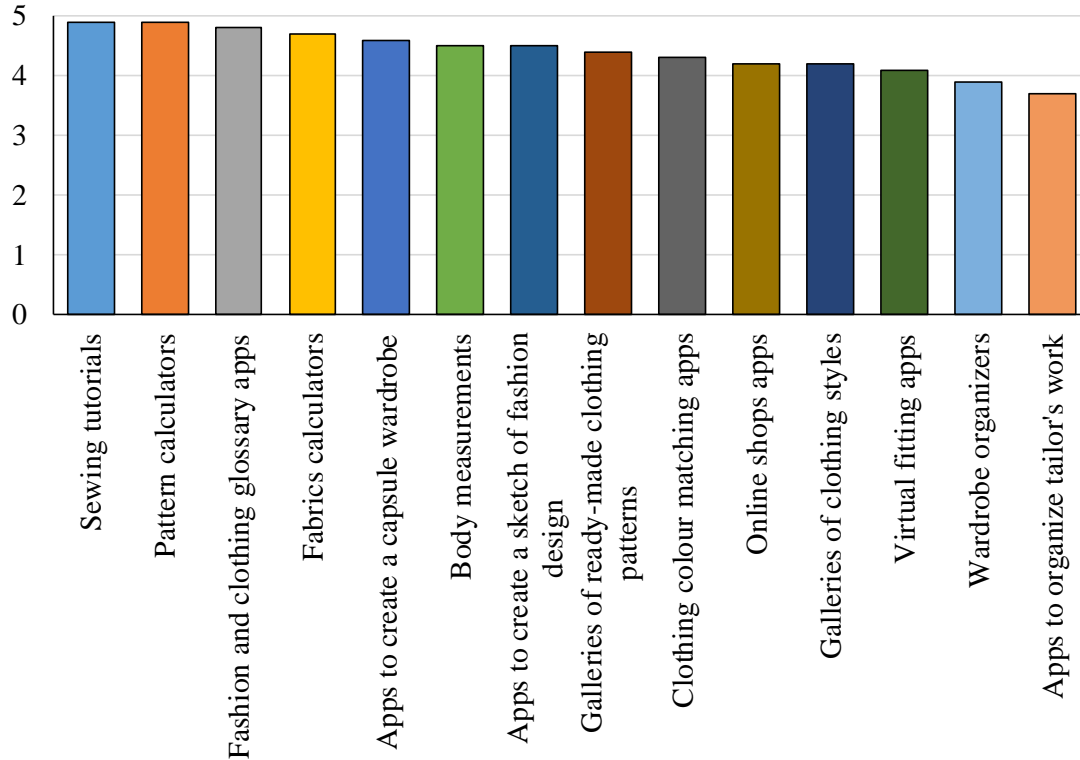


Fig. 1. Comparison of apps applicability for the education

The coefficients of variation show that the experts' opinions are coordinated (the coefficients values are less than 30%). The most versatile answers regard the following categories: “Online shops apps”, “Wardrobe organizers”, “Apps to organize tailor's work”, “Virtual fitting apps”, “Clothing color matching apps” (Fig. 2).

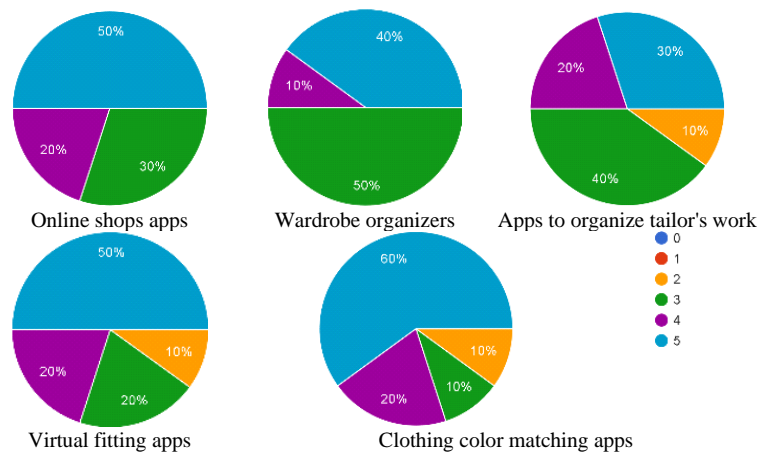


Fig. 2. Results of the survey

Results

All of considered mobile apps were categorized according to the stage of the clothing life cycle they refer to (Table 2 – Table 6).

Table 2. Mobile applications to support apparel design

Category	Operating system		
	iOS	Android	iOS + Android
Galleries of ready-made clothing patterns	Sewing and Patterns, My Sewing Patterns, Maven Patterns, Pattern Yardage, Megan Nielsen Patterns, Patternbox Premium, George + Ginger	Free clothes patterns; Clothing pattern design; How to make a sewing pattern from a picture; Clothing patterns; Pattern Kids Clothes; Patterns of Clothes; Women's Clothing Pattern Plan	Sewing patterns
Apps to create a sketch of fashion design	Fashion Design Sketches, Fashion Design FlatSketch, Prêt-à-Template, Cloth Design 2, Clothing Designer AR, Super T-shirt Designer, Yoshirt, Fonxy, YoTee –T-shirt Design and Print, Snaptee – Print Design Clothing, T-Shirt Editor	Fashion Design App	-
Clothing color matching apps	My colorist, Colors Chat, Ask Hue – Color in Fashion, Recolor Dress	Discover Color	-
Pattern calculators	-	Circle Skirt Calculator; Chalk; JSK Patrones; Solo Patrones App; CloStyler	-
Body measurements	-	Measurements notebook; Measurement Book; TailorGuide; Генетика кроя new	-

Table 3. Mobile applications to support apparel manufacturing process

Category	Operating system		
	iOS	Android	iOS+Android
Sewing tutorials	How to Sew – Sewing Patterns and Tips for Beginners, Couture Sewing for Beginners – Guide and Tutorials, How to Sew – Sewing Guide, Couture Sewing Handbook – Techniques and Tutorials, How to Design Clothes: Tutorial and Beginners Tips	How to Cut and Sew; Expert Tailoring Design; Home Sewing Complete Guide; Knowledge of Sewing Lessons; Puff Sleeve Cutting and Stitching Videos; Tulip Salvar Cutting and Stitching Videos; Tailor Course; Tank Top Cutting Stitching Videos; Learning how to sew; Cutting stitching videos: DIY Fashion Designer	–
Virtual fitting apps	Lectra 3D Review, Avattire, Dressed	Beautiful Dress	–
Apps to create a capsule wardrobe	Chloe; ClothesOn; Clothe to me; Covet Fashion; Combyne – your perfect Outfit; What to Wear; Dress Combinations for Women; Tweed	Women’s clothing styles (New); Daily clothing styles (New); Your closet – smart; Smart closet; Outfit ideas 2018; Everyday clothing; Fashion clothing; Business Women Work Outfits Suit Dress Idea Design	–
Fabrics calculators	All about Fabrics; Curtain Fabric Calculator; Cross Stitch Calculator; ACE Fabric Calculator; Cora Fabric; Fabric Stash; Stash Star Fabric; Fabric Selector; Sense Fabric	Fabrics; MatVed – Fabric Properties Calculator	–
Apps to organize tailor's work	iSewMe	–	Sew Organized; Tailor Manager

Table 4. Mobile applications to support clothing distribution

Category	Operating system		
	iOS	Android	iOS+Android
Online shops apps	Zara Home Shop Online, H&M; Bonprix; ...	Zara Home Shop Online, H&M; Bonprix; ...	Zara Home Shop Online, H&M; Bonprix; ...
Galleries of clothing styles	Free women clothing style idea; Trending Fashions; Nu outfit – style ideas; Grazia – Beauty & Fashion News...	Salwar sleeve idea gallery; Women African styles 2018; ...	Pinterest

Table 5. Mobile applications to support clothing exploitation

Category	Operating system		
	iOS	Android	iOS+Android
Wardrobe organizers	Dress Assistant; Manage Attire Dress Wardrobe; GetWardrobe – virtual wardrobe; My Wardrobe - Clothes Tracker; Wardrobe Assistant; My Simple Closet; Personal Lookbook; Cloth; Wardrobe Planning and Design; Mix & Style – Dressing Room and Virtual Closet...	Stylicious; Medini; Mix Me; Clamotty; LookBook; GoodLook; Women’s clothing styles 2018; Women’s wear; Getwardrobe; My Wardrobe – Organize your clothes; Your Closet – Smart Fashion; My Dressing – Penderie&Mode; My Wardrobe; XZ(Closet); What’s in my Closet/Wardrobe App	Smart Closet - Fashion Style,

Table 6. Mobile applications to support all processes of garment design

Category	Operating system		
	iOS	Android	iOS+Android
Fashion and clothing glossary apps	Sewing Translator	Sew Awesome: Sewing Tracker; Sewing; Basic Fashion Design	–

As one can see from the given tables, a lot of mobile applications were developed only for one specific operating system (OS) and have no analogs in another OS. Thus, when education process is concerned it is

Advanced technologies in education, industry and the environment

very difficult to choose only one basic application for the given task at hand.

It is evident from the given tables that a lot of stages in apparel design is in dire need of specific mobile applications. Besides that, some applications must be replicated in another operating system. It would allow preparing unified instructions for all the students with no regard to what exactly smartphones they have.

On the other hand, some stages of garment design are perfectly equipped with mobile tools in both operating systems. There is a variety of applications to choose from in categories of “Wardrobe organizers”, “Online shops apps”, “Galleries of clothing styles”, and “Galleries of ready-made clothing patterns”. Every one of them consists of several apps those have both Android and iOS versions beside all applications those have not.

In order to demonstrate a possible solution in choosing the mobile apps for the teaching courses in educational program for master degree, we constructed the Table 7. In the table there is at least one app selected out from the population of apps given above.

Table 7. Selected mobile apps for the educational program of master in apparel

Course	Mobile application	
	iOS	Android
Methods of development competitive garments	Sewing Translator; Zara Home Shop Online, H&M; Bonprix; ...	Sew Awesome: Sewing Tracker; Zara Home Shop Online, H&M; Bonprix; ...
Computer technologies in garment industry	Fashion Design Sketches	CloStyler Fashion Design App
Innovative technologies in garment industry	Sew Organized; Tailor Manager	Sew Organized; Tailor Manager
Drafting design documentation	–	CloStyler
Master thesis	ACE Fabric Calculator	CloStyler; MatVed – Fabric Properties Calculator
Foreign language (in professional direction)	Sewing Translator	Sew Awesome: Sewing Tracker

Conclusion

Exploration of mobile applications to use in training of clothing patternmakers shows the great diversity of them. On the mobile market there is an accessible tool for almost any task in apparel design. However, the exploration displayed the necessity to develop applications that would be purposely adjusted for the educational processes. Besides that, there are categories of applications those are to be additionally studied due to their significant amount and immense diversity.

References

1. Zhylenko T. I., Kudryavtsev A. M., & Zakharkevich O. V. (2019). Mobile application to calculate the parameters of top wear basic design. *Nauka innov.*, 15(3), 24–34 pp. https://www.researchgate.net/publication/333985538_Mobile_Application_to_Calculate_the_Parameters_of_Top_Wear_Basic_Design
2. Kim, Y., & Smith, D. (2017). Pedagogical and technological augmentation of mobile learning for young children interactive learning environments. *Interactive Learning Environments*, 25(1), 4–16 pp. <https://doi.org/10.1080/10494820.2015.1087411>
3. Zaranis, N., Kalogiannakis, M., & Papadakis, S. (2013). Using Mobile Devices for Teaching Realistic Mathematics in Kindergarten Education. *Creative Education*, 4(7), 1–10 pp. <http://dx.doi.org/10.4236/ce.2013.47A1001>
4. Mackaya, B.J., Andersona, J., Hardingb, T. (2017). Mobile technology in clinical teaching. *Nurse Education in Practice*, 22, 1–6 pp. <https://doi.org/10.1016/j.nepr.2016.11.001>
5. Lumsden, C. J., Byrne-Davis, L. M. Th., Mooney, J. S., & Sandars, J. (2015). Using mobile devices for teaching and learning in clinical medicine. *Archives of Disease in Childhood - Education and Practice*, 100 (5), 244–251 pp. <http://dx.doi.org/10.1136/archdischild-2014-306620>
6. Rosell-Aguilar, F. (2017). A Taxonomy and Framework for Evaluating Language Learning Mobile Applications. *Calico journal*, 34.2, 243–258 pp. <https://doi.org/10.1558/cj.27623>
7. Pereira, C.H., & Terra, R. (2018). A mobile app for teaching formal languages and automata. *Computer Applications in Engineering Education*. <https://doi.org/10.1002/cae.21944>
8. Khaddage, F., & Lattemann, C. (2013). iTeach We Learn Via Mobile Apps "a Case Study in a Business Course". In R. McBride & M. Searson (Eds.),

Advanced technologies in education, industry and the environment

Proceedings of SITE 2013-Society for Information Technology & Teacher Education International Conference, 3225–3233. New Orleans, Louisiana, United States: Association for the Advancement of Computing in Education (AACE). Retrieved June 19, 2020 from <https://www.learntechlib.org/primary/p/48591/>.

9. Mouzaa, Ch., & Barrett-Greenlyb, T. (2015) Bridging the app gap: An examination of a professional development initiative on mobile learning in urban schools. *Computer & Education*, 88, 1–14 pp. <https://doi.org/10.1016/j.compedu.2015.04.009>

10. Shraim, Kh., & Crompton, H. (2015). Perceptions of Using Smart Mobile Devices in Higher Education Teaching: A Case Study from Palestine. *Contemporary Educational Technology*, 6(4), 301–318 pp.

11. Thomas, R. L., & Fellowes, M. D. E. (2017). Effectiveness of mobile apps in teaching field-based identification skills. *Journal of Biological Education*, 51 (2), 136–143 pp. <https://doi.org/10.1080/00219266.2016.1177573>

12. Chandekar, T., Chouhan, R., Gaikwad, R., Gosavi, H., & Darade, S.A. (2017). Implementation of Obstacle Detection and Navigation system for Visually Impaired using Smart Shoes. *International Research Journal of Engineering and Technology (IRJET)*, 4(4), 2125–2129 pp.

13. Deshmukh, G., Gawade, V., & Gawari, D. (2018). Smart Navigational Shoes for Bikers/Cyclists. *International Journal of Computer Applications*. <https://doi.org/10.5120/ijca2018917062>

14. Parrilla, E., Ballester, A., Solves-Camallonga, C., Nacher, B., Puigcerver, S., Uriel, J., Pierola, A., Gonzalez, J. C., & Alemany, S. (2015). Low-cost 3D foot scanner using a mobile app. *Footwear Science*, 7(1), 26–28. pp. <https://doi.org/10.1080/19424280.2015.1038308>

15. Cheung, K. Y., Reth, D., Song, C., Li, Z., Li, Q., & Xu, W. (2019). BigFoot: A Mobile Solution toward Foot Parameters Extraction, *IEEE 16th International Conference on Wearable and Implantable Body Sensor Networks (BSN)*, Chicago, IL, USA, 1–4 pp. <https://doi.org/10.1109/BSN.2019.8771077>

16. Alfaro-Santafé, J., Gómez-Bernal, A., Lanuza-Cerzócimo, C., Alfaro-Santafé, J. V., Pérez-Morcillo, A., & Almenar-Arasanz, A. J. (2020). Three-axis measurements with a novel system for 3D plantar foot scanning: iPhone X. *Footwear Science*, 12(2), 123–131 pp. <https://doi.org/10.1080/19424280.2020.1734867>

17. Borisenko D. (2018) The use of mobile applications in the development of a design product in the training of future design professionals. *Information Technologies and Learning Tools* 68(6):47, 47–63 pp. <https://doi.org/10.33407/itlt.v68i6.2224>

NEW COMBINED TECHNOLOGIES OF SYNTHESIS MATERIALS

Zhiguts Yu.¹ Kozar O.²

¹Uzhhorod National University, Ukraine

²Mukachevo State University, Ukraine

Introduction

The lack of materials with required complex of physical, chemical, mechanical, technological and auxiliary properties for the relevant functional purposes has raised an urgent problem of synthesizing corresponding alloys and developing technologies of their production. Synthesis of materials with specific properties will allow not only the new areas of their application to be opened, but also the new trends in further scientific research to be formulated. Combined methods of material synthesis are based on the use of the two types of reactions, namely, the metallothermic ones and the self-propagating high-temperature synthesis (SHS). Combined processes versatility is related to the possibility of synthesizing almost any cast material, i.e. ferrous alloys, instrumental, high-speed and special steels, as well as materials being produced earlier by the metal powder industry techniques only, i.e. hard alloys, carbide steel etc.

Subject relevance

The urgent industrial problem of nowadays is not only creation of new materials but also improvement of traditional material properties and advance development of technologies of their production. Detailed studies of the problem allow us to state that this task could be successfully solved by using specially synthesized alloys produced by combined processes based on the combustion of exothermic powder mixtures.

The above technologies are based on the combined processes and allow the predetermined structure to be synthesized with specified alloy properties at cast formation with the use of synthesized materials for the

emergency repairs of products, part surface layer recovery and for the use of the synthesized alloy for the cast saving in the exothermic cast additive technologies.

The synthesis technologies developed in this work differ from traditional ones by a series of obvious advantages: the lack of need in the powerful electric energy power supplies, the possibility to use simple and cheap casting equipment, the high process productivity (alloy synthesis time may vary from 30 seconds to a couple of minutes), the possibility of using secondary production waste – graphite electrode grinding, aluminium or magnesium chips, iron cinder, blue powder, i.e. the dust from the filters of the casting shops producing manganese alloys. All the aforementioned have caused an urgent need in carrying out research described in this paper. The above technologies could be successfully applied to save metal at the high-volume and mass production factories producing casts and instruments. Creating materials on the basis of the self-propagating high-temperature synthesis (SHS) and combined (metallothermy + SHS) processes as well as studying the influence of new technological methods of metal production on the cast microstructure, chemical composition and mechanical properties have gained large practical importance. Their use in the existing casting technologies, e.g. in producing steel casts with thermite cast additives increases considerable process efficiency.

Research goal

The main goal of the present research was to predict the structure and the phase composition of the synthesized alloys, to elucidate the influence of combined technologies on the material properties and to determine the most optimal areas of the above alloys application. In addition, this work is intended to study the synthesized materials, namely the thermite cast iron, alloy steel, construction steel, stainless steel, rapid tool steel, hard alloys, carbide steel, non-ferrous alloys etc.

Materials and research technique

The following materials were used in this work: the smoke black, the aluminium powder “ПA-3” – “ПA-4”, the iron cinder (rolling made) with

the following average chemical composition (in mass %): 0.05 C; 0.10–0.35 Si; 0.10–0.35 Mn; 0.01–0.03 S; 0.01–0.03 P; 40–50 Fe₂O₃; 50–60 FeO and others. The powder burden was dried, mixed, consolidated and placed into the metallothermic reactor, in the simplest variant – into the metallothermic pot.

The essence of the metallothermic and combined syntheses is quite simple, i.e. the powder-like burden ingredients are loaded into the metallothermic reactor and then are burnt up using a special igniter. After combustion completion, in the bottom part of reactor the cast is formed, whereas the slag is collected in the upper part due to a considerable difference in the specific masses of the reaction products.

To determine the cast mass and alloy yield, at the first stage of our studies the microsmelting's were carried out in the metallothermic pot at the burden mass of 100–150 g. Combustion process was initiated by a special titanium powder (PX-2)-made igniter.

After determining the burden composition by the chemical reaction stoichiometric coefficients and its correcting by the component fixation coefficients, the adiabatic combustion temperature of the metallothermic reaction was calculated to find the possibility to separate the alloy from the slag.

The technique developed allows the metallothermic burden composition to be found and its adiabatic combustion temperature to be calculated. The principal condition of the synthesis process is the necessity to keep the actual burden combustion temperature above the slag melting temperature (for Al₂O₃ – 2400 K).

To minimize the high temperature influence on the thermite metal, as well as to eliminate the related high porosity and cast shrinkage, the inert additions were introduced into the burden in a form of the relevant alloy chips and ferrous alloys. To increase the combustion stability and to improve the kinetic characteristics of reaction, 1–2% (of the burden mass) of fluorspar CaF₂ were added to the burden. This addition not only reduces

the ignition temperature of the exothermic powder mixture but also increases the metal yield from it.

Theoretical part

Taking into account the necessity to predict the alloy structure, phase composition and properties, the authors have developed the principles of the synthesized alloy formation. The techniques based on the above principles allowed the exothermic burden adiabatic combustion temperatures to be determined. The methods of geometric thermodynamics for the structure optimization and prediction were modified as well.

Theoretical grounds of synthesis reaction

When organizing the ferrous alloy synthesis process, we used the thermite reactions based on the aluminium acidification and iron reduction: $\text{Fe}_3\text{O}_4 + \text{Al} \rightarrow \text{Fe} + \text{Al}_2\text{O}_3$, or the metallothermic metal oxide reactions with oxidizer and the classical "oxygen-free" combustion SHS reactions.

Microsmeltings carried out by us have shown the regularities of the carbon (in a form of silver graphite) and other doping elements fixation by the thermite metal that is necessary to synthesize the desired thermite steel chemical composition when calculating the exothermic burdens.

Method of recovering the exothermic mixture adiabatic combustion temperature and selecting reactions suitable for the alloy synthesis

To find the boundary conditions of the alloy synthesis the authors have developed a method on the basis of adiabatic temperature dependence on the molar composition of synthesized compounds. This allowed the synthesis reactions to be divided into two principal groups. The first of them includes those reactions, the adiabatic temperature of which is higher than the temperature of separation of the synthesized alloy and slag. These reactions are applicable for the alloy formation. The second group of reactions occurring at the ingredient interaction results in the formation of an alloy in a form of separate "grains" in the slag or leads to the slag part

non-separation from the alloy itself. These reactions are not acceptable for further experimental use.

After determining the burden composition according to the stoichiometric coefficients and after correcting them by the burden component fixation coefficients, it is recommended to calculate the metallothermic reaction adiabatic combustion temperature T_a [1–3]. In these calculations of the burden adiabatic combustion temperature according to the methods developed, the aluminum sublimation was not taken into account giving the error of finding T_a and the reaction heat Q_r . However, in spite notwithstanding, the mixture reaction temperatures must (heat sink being taken into account) be sufficient to smelt the reaction components and products ($T_{mel(FeO)} = 1640K$; $T_{mel(Fe_3O_4)} = 1810K$; $T_{mel(Fe)} = 1800K$; $T_{mel(Al)} = 830K$; $T_{mel(Al_2O_3)} = 2320K$). That is, the principal criterion of the cast production is that T_a for all reactions must exceed the reaction product temperature T_{mel} . The T_a value calculation, obviously, does not take into account the heat losses during combustion and the completeness of reactants transformation into reaction products.

Taking into account the condition that all the heat is spent to heat the burden up, i.e. the enthalpies of the initial and final products are equal, we find:

$$\sum_{i=1}^k (H(T_a) - H(T_o)) = Q, \quad (1)$$

where T_a is the adiabatic combustion temperature; T_o is the initial temperature; Q is the reaction heat and k is the number of reaction products.

In more complex equations, when more than three reaction products were produced, T_a was found in accordance with the following formula:

$$T_a = \frac{Q - \sum H_i(T_{meli}) - \sum L_i + \sum C_{ip} \cdot T_{meli}}{\sum C_{ilic}}, \quad (2)$$

where C_i and L_i are the reaction product heat capacity and smelting heat, respectively; γ is the liquid phase part in the combustion product;

$$\begin{cases} \gamma = 0 \text{ at } T_a < T_{mel}; \\ \gamma = 0 \text{ at } T_a > T_{mel}. \end{cases} \quad (3)$$

Obviously, due to the lack of the full data table on the C dependence on T at high temperatures [1–3], we extrapolated the values in accordance with the suggested conclusions:

$$C_{sol}(T_{mel}) = 7n \cdot b \text{ (J/mole} \cdot \text{deg)}, \quad (4)$$

where $C_{sol}(T_{mel})$ is the product heat capacity at the smelting temperature; n is a number of atoms in the product molecule and b is the coefficient of transition from kkal to J.

Using the simplified calculation scheme, T_a was determined with no accurate specific heat values being taken into account, while the reaction heat was determined at the average temperature (e.g. 2500 K). As regards the reaction heat variation, when the reaction products are in the liquid state, it should be neglected.

This method was taken as a basis of the T_a and Q_r calculation for the special alloy steels, cast irons, hard alloys, carbide steels, copper, aluminium and other alloys [3–10].

Afterwards, based on the stoichiometric ratio between the reaction components, the burden composition was found being checked according to the thermodynamic parameters. Then the coefficients of fixation of certain burden components were taken into account. After the burden chemical composition correction, the burden was composed, dried and loaded into the graphite and/or metal pot. The burden was then consolidated and ignited.

The synthesis process lasted dozens of seconds, the metal was then separated from slag and the material structure was evaluated. After the control weighing, the metal yield from the burden was estimated and the synthesized cast was studied. The third stage [1, 3] dealt with the burden composition correction due to the introduction of the relevant ferrous additives (i.e. ferrous manganese, ferrous chromium etc.) that allowed the desired alloy chemical composition to be obtained.

When performing calculations, we had to extrapolate $C(T)$ into the higher temperature region [1–3]:

$$C_{sol}(T_{mel}) = 29,3n \left(\frac{J}{mole \cdot deg} \right), \quad (5)$$

$$C_{lik} = 33,5n \left(\frac{J}{mole \cdot deg} \right), \quad (6)$$

where $C_{m6}(T_{nl})$ is the solid product specific heat at the melting point; C_{lik} is the liquid product specific heat independent of the temperature; n is the number of atoms in the product molecule.

For the linear dependence of the specific heat on the temperature at $T_{lik} < T < T_{mel}$:

$$C(T) = C^* + \frac{C_{mel} - C^*}{T_{mel} - T^*} (T - T^*), \quad (7)$$

where C^* is the experimental specific heat value at $T = T^*$; T^* is the maximal experimental temperature at the $C(T)$ determination.

At $T < T^*$:

$$C(T) = \alpha + \beta T + \gamma T^2. \quad (8)$$

Using (6) and (7), we find:

$$\Delta H(T_{mel}) = \Delta H(T^*) + \frac{C^* + C_{mel}}{2} (T_{mel} - T^*), \quad (9)$$

where $C^* = \alpha + \beta T^* + \gamma (T^*)^2$.

For $T_a > T_{nl}$:

$$\Delta H(T^*) = \left[\alpha + \frac{\beta}{2} (T_o + T^*) \right] (T^* - T_o) + \gamma \left(\frac{1}{T_o} - \frac{1}{T^*} \right). \quad (10)$$

At the determined combustion product enthalpy values, T_a is easily calculated by the following formula:

$$T_a = T_{mel} + \frac{Q - L - \Delta H(T_{mel})}{C_{lik}}. \quad (11)$$

Experimental and results

The experimental studies carried out by the authors were stimulated by the necessity to confirm the development of a complex of theoretical notions. This work was carried out to synthesize the different-class thermite steels, alloyed steels, tool materials (high-carbon, high-speed and highly alloyed steels), carbide steels.

High percentage content of impurities and ferrous alloys excessively "cools" the exothermic reaction, and then the calculated burden composition for the high alloy steel does not ensure the optimal combustion temperature of the exothermic mixture. In this case it is necessary to use the other, different from the above one, direction of the alloy steel synthesis. It is related to the synthesis of a preset alloy chemical composition not by adding a certain quantity of ferrous alloys but by composing a special exothermic burden comprising the alloying oxides (e.g., Cr_2O_3 , CrO_3 , NiO , CuO , V_2O_5 and others) and the iron cinder reduced by aluminium in the course of the aluminothermic process. The technique of the relevant calculations and the synthesis technology have been developed to obtain the thermite high alloys. For instance, this allowed the 12X18H10T steel on the basis of the Fe, Ni, Cr oxide to be synthesized [11]. Titanium was introduced into the exothermic burden not in the form of TiO_2 but as the 30% ferrous titanium due to the low titanium reducibility from its oxides using aluminium. The burden composition was as follows: Cr_2O_3 – 17,2%; Fe_3O_4 – 50%; NiO – 6,6%; Al – 26,2% [3, 11]. Both carbon and titanium at their introduction into the metallothermic burden move the synthesis reaction from the metallothermic class to the combined one, i.e. to that involving the metallothermic reaction and the SHS reaction. The chemical analysis of the synthesized metal samples has demonstrated poor chromium reducibility from its oxides.

When carrying out the thermite smelting according to the suggested method, one has to take into account the "activity" of the elements that compose the metallothermic burden. Speaking about the inhomogeneity of the element distribution in the casts synthesized by the aluminothermic reduction of oxides, one must indicate the sequence of the above oxides

reaction with aluminum. First the most easily reducible elements (Fe, Ni, etc.) are reduced, whereas hardly reducible oxides move to the slag melt. Afterwards the thermite metal that contains the excessive aluminium, while passing the slag layer, reduces the hardly reducible oxides as well.

At the “12X18H10T” (analogue 321S31) steel synthesis, first the nickel and iron oxides, then the chromium oxides, are reduced. This stipulates not sufficient Cr content in the thermite alloy steel produced. To improve the completeness of all oxides reduction, one has to carry out the exothermic smelting with larger burden masses.

Continuing this work, we have carried out the experiments in the research-production conditions with the use of the above burden compositions for the cast additions of the alloy steels [3].

Continuing this work, we succeeded to combine the metallothermic and the SHS processes to obtain the tungsten-cobalt hard alloys according to the following reaction scheme:



where A, B, C are the synthesis elements; O is the oxidizer (say, oxygen etc.); AC are the reaction products (i.e. carbides, silicide's and so on); BO is a slag.

Technologies developed on the basis of the above schemes allowed us to produce by using the "non-traditional" method the rapid steels (P9, P6M5 – analogue S6-5-2, P12 with the microstructure shown in fig. 1), the cast hard alloys (BK3 – analogue HG012, BK4, BK6, BK8, BK15-like [12]), and others. The microstructure of the carbide steel produced in accordance with the classical SHS-reaction with the tungsten carbide (15 mass % of the thermite mixture) is shown in fig. 1.

The so-called "carbide steels" have been synthesized for the first time being the analogue of the hard tungsten-cobalt alloy having a structure with soft and pliable cobalt being replaced by the rapid steel. The microstructure of one of the carbide steel types is shown in fig. 2 [12, 13].

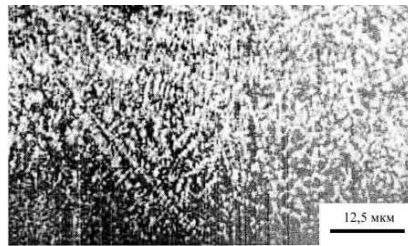


Fig. 1. The dendrite microstructure of the tool steel P12 [3]

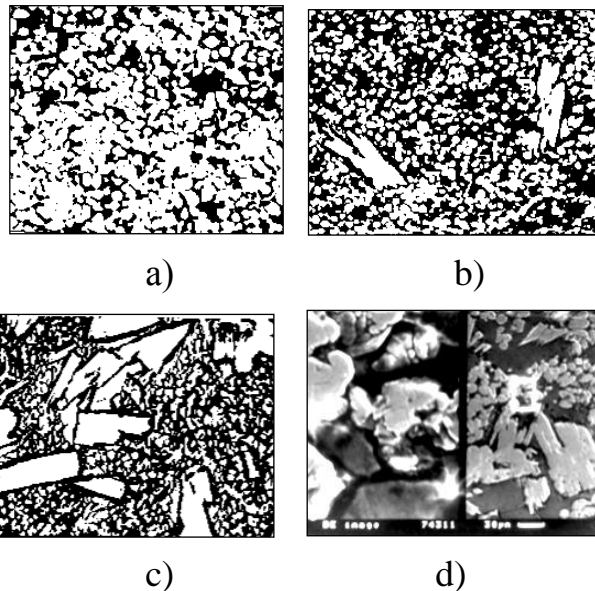


Fig. 2. Microstructure of: a) hard alloy BK41, b) carbide steel B(P18)15I with a matrix in a form of a rapid steel P18 – 15% and tungsten carbides W_2C (small globular light inclusions) and WC (large grains) – 85%, c) – the massive carbides WC in the rapid steel matrix; d) – the rapid steel matrix with a sphere-like complex carbides of the W_2C type (left – x1500, right – x250)

The studies of the microstructure and the properties of the alloys produced allow the following results to be presented, e.g., for the high-speed steel “P18” (analogue 3355): grain size – 10, hardness HRC – 65–67, $\sigma_b=2600$ MPa, heat resistant 913–928 K.

One more direction of the use of the combined (SHS + metallothermy) synthesis processes is the hard alloy material smelting onto the steel or cast iron surfaces. Especially promising from this viewpoint are the technologies that combine the laser surface hardening (LSH) with the

SHS-based smelting. An example of such use of the complex technologies is given below [13].

The mixture of the Ti powder (68 mass %), C powder in a form of a smoke black (18 mass %) and the Fe powder (14 mass %) was used instead of the light-absorbing paint. The above mixture was deposited onto the Steel 10 and Steel 20 surfaces with the subsequent drying in the air producing the 80, 200 or 500 μm layer. Thermochemical calculations have shown that in such mixture almost all Ti reacts at the expense of the oxygen-free combustion with carbon producing the TiC carbide. Carbon excess and very small amount of titanium jointly alloy iron producing a liquid steel of eutectoid composition that at rapid cooling is transformed into troostite in the 80 μm thick layers. These layers were ignited by the ray of the continuous CO_2 laser with longitudinal pumping at the 150 W power and $25\text{--}35 \text{ W}\cdot\text{m}^{-2}$ (at the 0.3–2.0 mm "spot" diameter). Scanning speed was varied within the $10\text{--}20 \text{ mm}\cdot\text{s}^{-1}$ range. In series of studies to provide additional protection of the melted surface we have used a focusing attachment with a possibility of additional surface blowing with inert and less active gases (Ar, CO_2 , N_2 etc.). After the experiment, we measured the macro- and microhardness in the alloyed layer, thermal influence zone and in the main alloy. Fig. 3 shows a typical microstructure of such $\sim 500 \mu\text{m}$ thick layer strengthened by combined processes due to the SHS and LSH combination.

This layer consisted of about 50 volume % of the TiC carbides and about 50 volume % of the metal bond – the U8 carbon tool steel.

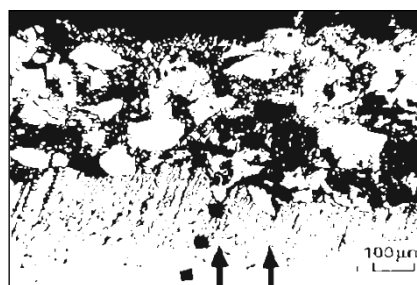


Fig. 3. Microstructure of the strengthened layer with the semi-melted TiC particles after its combined strengthening by LSH and SHS. Etching was carried out by nital

It is also seen that in the area of intense thermal influence the steel microstructure acquired very fine column-like structure with a small slope of thin dendrites (almost not having branches) towards the direction opposite to the laser ray scanning direction. A light inclined arrow (up) shows direction, along which the microhardness was measured using the diamond pyramid. As our studies have shown the microhardness of the TiC carbides is almost several times higher than that of the steel. Thus, in these studies we succeeded to organize the SHS process in the relatively thin layer at the expense of using the LSH to solve two tasks simultaneously: heating, smelting and carbonization of iron, as well as the Ti particles smelting and "burning" in carbon with the TiC carbide production. The adiabatic temperature of the oxygen-free combustion of the equiatomic Ti-C mixture is equal to 3200 K. The actual combustion temperature of the 68%Ti + 18%C + 14%Fe (mass %) mixture exceeds 1850 K that provides formation of the solid-liquid "melt-TiC" slurry with a large interval between the liquidus and the solidus lines.

Formation of the slurry instead of the single-phase melt influences positively the quality of the strengthened layer surface after its complete solidification and cooling and after this layer fixation even on the inclined surfaces. It is important to note that at the above oxygen-free combustion no non-metallic phases and their inclusions are produced. The strengthened layer welding with the principle metal is automatically produced "metallurgically", excluding the necessity of soldering or other methods of alloy connection (for instance, instrumental) with, e.g., the cutter holder.

A brief survey of the technologies of the material synthesis and their use gives one a possibility to judge about the closest future prospects of the SHS and combined processes application.

Despite the overestimated price of the burden components the technologies considered have incontestable advantages: the lack of the complex and expensive equipment (casting furnaces, powerful electric energy power supplies), full autonomy of the technological process (this technology could be used at the movable maintenance platforms,

workshops and even in the field conditions), high productivity and high-speed performance (synthesis time is a few minutes). All this testifies to the possibility of their wide application in various conditions.

Conclusions

The results of the theoretical and experimental studies presented above are related to the synthesis of materials by combined technologies based on the metallothermy and SHS. On the basis of developed methods of calculations the compositions of burdens have been found and a wide spectrum of different-type alloys have been synthesized.

The specific features of smelting using combined methods have been found, the mechanical properties and the structure of alloys produced have been studied, the recovery coefficients for the alloy elements in the metallothermic and combined processes have been found. In addition, the technologies of the thermite welding and smelting onto the super-hard surfaces have been developed, while combining the LSH and SHS processes in one operation allowed one to solve a complex of technical problems of production of the carbide steel-like materials and hard alloys on the metal surface.

References

1. Zhiguts, Yu.Yu. (2004). The method for calculating the metallothermic charge for the supply of cast irons. *Engineering Science*, 9, 43-46.
2. Zhiguts, Yu.Yu., & Pokhmurski, V.I. (2005). The materials, synthesized metallothermy and SHS-processes. Report of the National Academy of Sciences of Ukraine, 8, 93-99.
3. Zhiguts, Yu.Yu., & Lazar, V.F. (2014). The technologies and features of alloys synthesized by combined processes. *Uzhgorod, Invazor*.
4. Zhiguts, Yu.Yu. (2003). Gray and white special thermite cast irons. *Optimization of production processes and technical control in mechanical engineering and instrument making*, 480, 148-153.
5. Zhiguts, Yu.Yu. (2005). High-duty cast iron for thermite welding workpieces. *East-Europe magazine high technologies*, 1 (13), 56-58.

Advanced technologies in education, industry and the environment

6. Zhiguts, Yu., & Kurytnik, I. (2008). Special thermite cast irons. Archives of foundry engineering Polish Academy of sciences, 8(2), 162-166.
7. Zhiguts, Yu.Yu. (2007). Špeciálna termitova liatina. Výrobné inžinierstvo, 6(2), 45-48.
8. Zhiguts, Yu. Yu. (2008). White special thermite cast irons. Metals and casting of Ukraine, 11/12, 9-11.
9. Zhiguts, Yu. Yu. (2007). Thermite high-speed steels. Engineering Science, 1, 41-44.
10. Zhiguts, Yu. Yu. (2007). Aluminium, where smelled metallotermy. Technology of machinery, 10 (64), 11-13.
11. Zhiguts, Yu.Yu. (2007). Use of thermite high-alloy steels for feeding olives. Foundry production, 5, 5-7.
12. Zhiguts, Yu.Yu. (2009). Synthesis and properties of cast carbide alloys. Physical metallurgy and heat treatment of metals, 3, 26-29.
13. Zhiguts, Yu.Yu. (2007). Exothermic welding of high-manganese steels. Welder, 5, 14-16.

**PECULIARITIES OF A NEW METHOD
FOR EVALUATING FIBROUS PRODUCTS STRUCTURE**

Slizkov A., Avetisyan A.

Kyiv National University of Technologies and Design, Ukraine

Introduction

In the course of textile processing, spinning industry products such as slivers, rovings and yarns are sequentially formed from the pulp. All these processes are associated with significant difficulties and their implementation efficiency is entirely evaluated by the complex of properties of fibres, being processed, and their arrangement in semi-processed products structure.

One of the main indexes characterizing the state of a semi-processed product for further processing is an index of fibres straightening and orientation in semi-processed product structure. Correct and timely evaluation of this index in conditions of constant changes in the quality of raw materials will allow maintaining the efficiency of textile processing at the appropriate level. This will lead to the rational use of expensive raw materials and an increase in the quality of finished products.

According to the classification of methods for evaluating indexes of fibrous products structure, all research methods, depending on peculiarities of the effect on textile material, are divided into direct and indirect. Methods classification scheme is based on the principle of dividing methods into classification categories: class, group, subgroup, sort and kind. The class of a method evaluates the peculiarities of product structure study, the group – degree of impact on a sample under study, the subgroup – type of physical or mechanical impact on a sample, the sort – methodical aspect of index study, and the kind – measuring index [1].

Direct research methods consist in direct measurement of fibres size and position relative to the axis of a fibrous product. Direct research methods include the method of measuring fibres after extraction from the sample, projection methods, methods of labelled fibres (dyed fibres, radiography, luminescent) [2-4].

In direct methods for estimating the structure of fibrous products, fibres straightening and orientation is evaluated by direct analysis of fibres or their images in a sample. The advantage of direct methods is that most of them give or can give comprehensive information on fibres arrangement in a sample and fibres shape. At the same time, it can be noted that direct methods are very laborious, since they are all associated with obtaining characteristics for a large number of individual fibres. Some of them require additional pretreatment of samples (labelled fibre methods). For these reasons, direct methods cannot be recommended in those cases when it is necessary to quickly estimate the orientation or straightening of fibres in fibrous samples of textile materials and their semi-processed products.

In indirect methods, fibres orientation and straightening in the structure of fibrous products samples is evaluated according to dependence of fibrous product structure and some physical quantity. Depending on what physical quantity change is recorded, indirect research methods are divided into groups: mechanical and weight, mechanical, optical, capillary and others [2, 4-6].

The most widespread indirect method is the mechanical and weight method for evaluating fibres straightening and orientation in spinning industry – the method of combing sample fibres in a special clamp. The method consists in estimating the longitudinal orientation of fibres by preliminary cutting the sample end of an investigated fibrous product at the point of its clamping. After releasing a certain length of a product, one should card and weigh the loose parts of fibres ends, cut and weigh the straightened fibres ends, went beyond the initial clamping line due to straightening at carding. Finally, it is necessary to cut and weigh fibres ends that remain in the area released from the clamp.

Optical methods are quite simple, have low labour intensity. However, the dependence of values characterizing the orientation of fibres is subject to the condition of sample fibres surface, which complicates the interpretation of results or requires rather laborious calibration for each type of fibres. Considering the dependence of sample thickness indexes, optical methods are recommended for sufficiently thick or, conversely, sufficiently thin samples, limiting the possibilities of their use. In addition, these methods make it possible to evaluate the parallelization, straightening, and orientation of the fibres only from sample surface layers and cannot evaluate its internal structure [2, 5, 6].

The indirect methods of estimating straightness and orientation indexes are also quite time-consuming, but their labour intensity is significantly lower than the labour intensity of direct methods. Known indirect methods cannot be applied to various fibrous structures. Indirect methods are used in most cases to obtain comparative, relative characteristics of fibrous products structure. The values of fibrous material structure in the considered indirect methods depend on a number of side factors (fibres properties, sample geometric parameters, etc.), which require testing the method in new conditions or limit its scope. Most indirect methods are used only in static conditions, and just some are used in dynamic conditions, but with sufficiently significant thickness of the investigated fibrous product.

Based on the above, it can be stated that to evaluate the structural peculiarities of sliver-like fibrous products (straightening and parallelization of fibres) one should use methods that have different approach. The above methods are quite complex and require considerable time to evaluate structural indicators. In addition, all of them cannot be used in production conditions, so the development of new rapid methods for estimating the structure of sliver-like fibrous products is relevant.

Methods

To quickly evaluate the characteristics of fibres location in fibrous products, the most promising are indirect methods that can be used in dynamic production conditions. Among the indirect methods of evaluating fibrous products structure, which can be used in production conditions, it is most appropriate to use methods to evaluate a complex index that takes into account both fibres straightening and orientation [7, 8].

Given the above, the resonance method is considered to be the most promising for estimating the structure, because it can be used in dynamic production conditions and it allows you to evaluate the complex index of fibres straightening and orientation. The resonance method belongs to the group of electrowave methods and is based on the anisotropy of textile fibres dielectric constant in different directions [9, 10].

It is known that the study of textile materials' electrical and dielectric parameters was carried out mainly for technical-purpose textiles. However, due to the development and introduction of new electrophysical methods in the textile industry, an interest to the processes occurring in fibrous products under the action of constant and alternating electric fields has significantly increased.

Studies of electrophysical textile fibres properties were caused by the introduction of a capacitance method for measuring the unevenness of yarn products, a resistive method for evaluating the moisture content of fibres, as well as problems of occurrence and elimination of textile fibres static charges during processing on manufacturing equipment.

Nowadays, the influence of electric and magnetic fields on textile materials is widely used in textile industry for fibres orientation and straightening during carding, in the production of carcass yarn, for obtaining compound yarn and nonwovens.

However, for the design and rational use of devices for evaluating the structural characteristics of fibrous products by electrophysical methods, it is necessary to have basic information about the processes

occurring in fibres under the action of constant and alternating electric fields [11, 12].

Since almost all textile fibres have more or less anisotropy, the dielectric constant is also different in different directions. Thus, cotton fibres were pre-dried to constant weight and had a dielectric constant $\varepsilon = 6$, when arranged along the field lines, and $\varepsilon = 3$ in the case of their transverse arrangement. Measurements were performed at a frequency of 1.755 MHz.

The main disadvantage of evaluating structural indexes by indirect methods, including resonance, is the presence of various side factors that create measurement errors. After analyzing the existing resonant devices for evaluating the structure of fibrous products, it was found that the device circuits contain multiple conversion of the information signal, which leads to uncontrolled parameters. To eliminate this drawback, we set the task of creating the device for evaluating the dielectric parameters of materials. The introduction of new circuit elements and change in functional connections between them in the electrical circuit would ensure the evaluation of textile materials properties with increased accuracy by directly measuring the resonant frequency of the reference and measuring resonators, and exclusion of information signal multiple transformation. This significantly reduces the number of uncontrolled parameters that affect the errors in evaluating the properties of textile materials, namely straightening and orientation factor.

Experimental and results

The offered resonant device for evaluating the structure of fibrous materials contains a super-high-frequency (SHF) generator G, connected by the first output from a two-position SHF switch SW, to the outputs of which the reference Q1 and measuring Q2 resonators are connected. To the second output of SHF generator a prescaler ST is connected, from the output of which the pulse sequence is fed to the input of the microprocessor MR. An indicator device (digital) HL is connected to the

first output of the microprocessor MR, and the second output is connected to the second SHF switch SW.

The device works as follows: in the first operating cycle, on command from the microprocessor MR, two-position SHF switch SW commutates to a certain position 1 and connects the reference Q1 resonator to the SHF generator G, the settings of which will evaluate the operating frequency of the SHF generator G. From the second output of SHF generator G, electromagnetic oscillations are fed to the previous ST frequency divider, which is required to match the high operating frequency of SHF generator G (hundreds of MHz) with the operating frequency of the microprocessor MR (units or tens of MHz) [11, 12].

Generated frequency value in the digital code is entered in the first memory register of the microprocessor MR. In the second operating cycle on command from the microprocessor MR, two-position SHF switch SW commutates to another position 2 and connects to the SHF generator G measuring Q2 resonator tuned to the value of SHF G. From the second output of the SHF generator G, electromagnetic oscillations are fed to the previous frequency divider ST and generated frequency value in the digital code is entered into the second memory register of the microprocessor MR. In the following operating cycles of the microprocessor MR, the program calculates the change in generation frequency, its relative change and, in fact, fibres straightening and parallelization factor according to the formula:

$$\eta_f = 1 - \frac{\Delta f_1 / f_{01}}{\Delta f_2 / f_{02}}; \quad (1)$$

where f_1 is the quality factor of resonator during contact with the fibrous sample along its axis; f_2 is the quality factor of resonator in contact with the fibrous sample perpendicular to its axis;

The measurement result is fed from the first output of the microprocessor MR to the indicator device HL.

The objects of research to evaluate the optimal position of the fibrous products on the resonant device were slivers for obtaining wool yarn by worsted spinning system. Evaluation of the optimal sliver position was carried out on the device shown in Fig. 1, according to our methodology.

The device consists of clamps 1 that rotate around the axis and the resonant device 2. Before filling the tape in the clamp is determined by the position of the tape at the exit of the equipment on which it was received. To study the anisotropy of the propagation of an electromagnetic wave through a fibrous product, the tape was tucked into a clamp under preload and the value of the frequency of the electromagnetic wave as it passed through the textile material was determined. For the initial position of the tape - the angle 0° took its position when released from the equipment. Then the clamps were simultaneously rotated counterclockwise at an angle of 30° , 60° , $90^\circ \dots 360^\circ$ and again recorded the value of the change in the indicator.

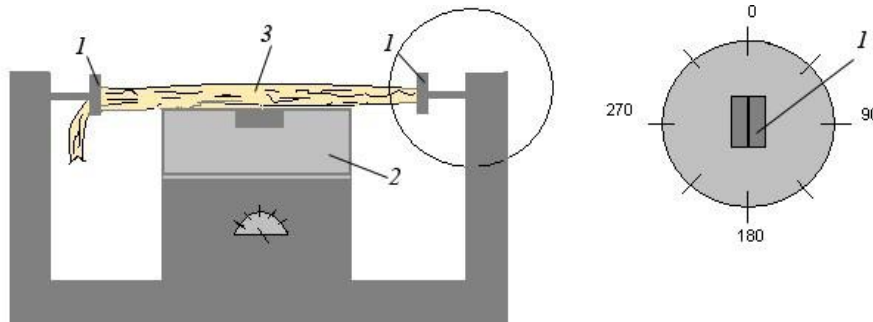


Fig. 1. Attachment for evaluating sliver anisotropy structure
1 - clamps; 2 - resonant device; 3 - fibrous product (sliver)

To estimate the anisotropy of fibrous products structure by electrowave method, a polar coordinate system was used. You can use it to display the relationship between the angles of fibrous product rotation and the magnitude of the change in parameters of electromagnetic wave.

The polar coordinate system is given by a ray called zero or polar axis. The polar axis in a fibrous product is the line passing through the centre of cross section of the product parallel to the position of a sliver when it exits the equipment. The point from which the polar axis emerges

is called the origin or pole. Any other point on the graph is defined by two polar coordinates: radial and angular.

The radial coordinate corresponds to the distance from a certain point to the origin. In the offered method of evaluating the structure of fibrous products, the radial coordinate evaluates the amount of change in the frequency of electromagnetic wave.

The angular coordinate, called the polar angle φ , is equal to the angle at which counterclockwise the polar axis of the fibrous product must be rotated in order to reach the above point. The radial coordinate determined in this way can take values from zero to infinity, and the angular coordinate varies in the range from 0° to 360° .

Graphs of change in the resonant frequency depending on the position of a sliver are presented in Fig. 2.

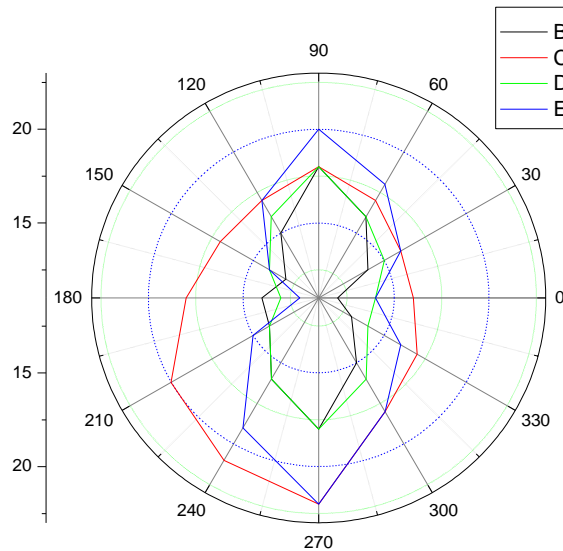


Fig. 2. Change in the resonant frequency when an electromagnetic wave passes through the sliver, depending on its position

$$t_R = \frac{|\bar{Y}_1 - \bar{Y}_2|}{S\{\bar{Y}_1 - \bar{Y}_2\}} = \frac{|\bar{Y}_1 - \bar{Y}_2|\sqrt{m}}{2S\{Y\}} \quad (2)$$

where \bar{Y}_1 and \bar{Y}_2 – the arithmetic mean, $S^2\{Y_1\}$ and $S^2\{Y_2\}$ – the standard deviation, m_1 and m_2 – the sample sizes ($m_1 = m_2 = 30$).

The complex index of fibres straightening and orientation, evaluated by formula (1), is practically not affected by the change in resonant frequency depending on the amount of a fibrous product. In fact with an increase in resonant frequency, the frequency difference also increases when the fibrous samples are placed along and across the resonator. Table 1 shows the change in the complex index of fibres straightening and orientation, according to the position of sliver sample from the carding machine.

Student's t-test (t) was used to estimate whether the differences between the two adjacent mean values of fibres straightening and orientation factor were significant. In this case, the formula (2) is used for two dependent samples, the size of which differs insignificantly.

The calculations results are given in the table 1.

Table 1. Changes in fibres straightening and orientation index according to the position of sliver sample from the carding machine (for $T_c = 17.3$ kTex)

Sample position, degrees	Along resonator f_1	Across resonator f_2	Fibres straightening and orientation factor
0-360	9	12	0,67
30	10,5	14	0,67
60	12	16	0,67
90	13,5	18	0,67
120	11	15	0,64
150	9,5	13	0,63
180	10,5	14	0,67
210	10,5	14	0,67
240	12	16	0,67
270	13,5	18	0,65
300	11	15	0,63
330	9,5	13	0,65

Table 2. Evaluation of an impact in changing two average values of fibres straightening and orientation factor according to the sample position

Sample position, degrees	Fibres straightening and orientation factor \bar{Y}_n	Samples under study, at angles, degrees	Expected value t_R	Tabular value t_T	Null hypothesis $M\{Y_1\}=M\{Y_2\}$
0 (360)	0,67	0-30	0	1,980	is not rejected
30	0,67	30-60	0	1,980	is not rejected
60	0,67	60-90	0	1,980	is not rejected
90	0,67	90-120	1,172	1,980	is not rejected
120	0,64	120-150	0,455	1,980	is not rejected
150	0,63	150-180	1,831	1,980	is not rejected
180	0,66	180-210	0,037	1,980	is not rejected
210	0,67	210-240	0	1,980	is not rejected
240	0,67	240-270	1,921	1,980	is not rejected
270	0,65	270-300	1,833	1,980	is not rejected
300	0,63	300-330	1,724	1,980	is not rejected
330	0,65	330-0	1,910	1,980	is not rejected

If the calculated value of Student's t-test is greater than the tabular one $|t_R| > t_{T2}[\alpha, f]$, the null hypothesis was rejected. If $|t_R| > t_{T2}[\alpha, f]$, there was no reason to reject the hypothesis H_0 of equality of means, that is, both series of measurements were attributed to the same set.

Similar results were obtained for slivers from other processing steps of spinning production. The straightening and orientation factor is relative, so the position of the sliver will not affect its change. The main condition for the study is only the constant position of the sample during the process both along and across the resonator. Therefore, it can be stated that sliver position affects the value of resonant frequency, but does not affect the value of complex factor for fibres straightening and orientation.

In the course of textile processing, the pulp is sequentially formed into slivers, rovings and then yarns. All these processes are associated with significant difficulties and their implementation efficiency is entirely evaluated by the complex of properties of fibres, being processed, and their arrangement in semi-processed products structure.

One of the main indexes characterizing the state of a semi-processed product for further processing is an index of fibres straightening and orientation in its structure.

Correct and timely evaluation of this index in conditions of constant changes in the quality of raw materials will allow maintaining the efficiency of textile processing at the appropriate level. This will lead to the rational use of expensive raw materials and an increase in the quality of finished products.

Conclusions

The device for evaluating the dielectric parameters of materials with increased accuracy due to direct measuring the resonant frequency of reference and measuring resonators, eliminating multiple conversion of the information signal was offered. This significantly reduces the number of uncontrolled parameters that affect the errors in evaluating the properties of textile materials, namely straightening and orientation factor. To estimate fibres straightness and orientation, it is advisable to use the frequency range between 500 and 1500 MHz. In the offered device, the operating frequency of 800 MHz is selected.

References

1. Kostrytskyi V.V., Slizkov A.M. (2010). Klasyfikatsiia metodiv otsinky strukturnykh pokaznykh voloknystykh produktiv; Visnyk KNUTD, 6, 97-102. [in Ukraine].
2. Slizkov A.M. (2007). Analiz metodiv otsinky struktury strichkopodibnykh voloknystykh produktiv; Problemy lehkoi y tekstylnoi promyshlennosti Ukrainy. 1(13). 53-56 [in Ukraine].

3. Kudryavtseva T.N. (1987). Tekhnicheskaya diagnostika sherstopryadil'nogo proizvodstva. – M.: Legprombytizdat [in Russian].
4. Gusev B.N. (1988). Problemy razrabotki metodov diagnostiki tekhnologicheskikh protsessov khlopkopryadil'nogo proizvodstva; Tez. dokl. Vsesoyuzn. konf.: „Perspektivy razvitiya khlopkopryadil'nogo proizvodstva, povyschenie ego tekhnicheskogo urovnya i konkurento–sposobnosti”.- Penza, 67-68. [in Russian].
5. Korniyukhina T.A., Borzunov I.G. (1975). Opredelenie orientatsii i raspryamlenosti volokon metodom rassevaniya izlucheniya; Izv. vuzov. Tekhnologiya tekstil'noy promyshlennosti. 5. 21-25. [in Russian].
6. Korniyukhin I.P., Korniyukhina T.A. (2006). Metody rassevaniya sveta v issledovaniyakh voloknistykh struktur. M.: MGTU im. A.N. Kosygina [in Russian].
7. Shtut I.I., Yarulova N.A., Aronikov A.M. (1986). Kompleksnaya otsenka raspryamlenosti i raz"edinennosti volokon; Izv.vuzov. Tekhnologiya tekstil'noy promyshlennosti. 6. 29-31 [in Russian].
8. Slizkov A.M., Shcherban V.Yu., Potapenko A.O. (2008). Teoretychni osnovy pobudovy fizychnoi modeli elektromahnitnoho rezonatora dlia otsinky struktury strichkopodibnykh voloknistykh produktiv; Visnyk KNUTD. 2. 24-29 [in Ukraine].
9. Slizkov A.M., Shcherban V.Yu., Potapenko A.O. (2008). Rozrobka rezonansnoho metodu otsinky struktury kharakterystyk strichkopodibnykh voloknistykh produktiv; Visnyk KNUTD. 4. 59-65 [in Ukraine].
10. Potapenko A.O., Slizkov A.M., Shcherban V.Yu. ta in. (2008). Patent na korysnu model № 34897, zareiestrovano 26.08.2008. Sposib vyznachennia vlastyvostei tekstylnykh materialiv, zaiavnyk ta patentovlasnyk Kyivskiy natsionalnyi un-t tekhnolohii ta dyzainu. № 200804141, Biul. 16. [in Ukraine].
11. Slizkov A.M., Shcherban V.Yu., Potapenko A.O. (2008). Rozrobka rezonansnoho prystroiu dlia otsinky struktury voloknistykh produktiv; Problemy lehkoï y tekstyl'noï promyshlennosti Ukrainy. 1 (14). 18-21. [in Ukraine].
12. Potapenko A.O., Slizkov A.M., Shcherban V.Yu. ta in. (2008). Patent na korysnu model № 37282, zareiestrovano. Rezonansnyi prystrii dlia vyznachennia vlastyvostei tekstylnykh materialiv ; zaiavnyk ta patentovlasnyk Kyivskiy natsionalnyi un-t tekhnolohii ta dyzainu. № 200806957, Biul. 22. [in Ukraine].

THE EFFECT OF MOISTURE ON MOISTURE ABSORPTIVITY AND OVERALL COMFORT INDEX OF MEN'S SHIRTS

Hes L.¹, Paraska O.², Gebrian P.³

^{1,3} Technical University of Liberec, Czech Republic

² Khmelnytskyi National University, Ukraine

Introduction

The human organism is a self-regulatory system, whose physiological mechanism is focused on maintaining the stability of the internal environment on the principle of balance between the amount of heat generated by the organism and the amount of heat transferred to the environment. The human body can be considered an open system that is always in a state of physical, chemical and biological interaction with the environment [1]

The human body is able to maintain a constant internal ambient temperature of approximately 36,5 °C by various thermoregulatory mechanisms. This temperature can fluctuate within ± 4 °C. Fluctuations are caused by various external and internal influences.

Thermoregulation is a process that combines physiological processes controlled by the central nervous system, maintaining the body temperature at the optimal value at which metabolic transformations take place [1, 2].

The absorption, transmission and desorption method depends greatly on the atmospheric humidity and moisture regain of the textile [3]. Hence, the hydrophilic or hydrophobic property of fibres is important [4, 5]. The mechanism of water vapour transfer through the fabrics is principally diffusion, driven by difference of water vapour concentration or difference of water vapour partial pressure on both parts of fabrics. In porous fabrics, well permeable for air, water vapour transfer is amplified by forced convection of the penetrating air [2, 3, 5 – 7].

The suitable choice of clothing, preferably made of breathable and vapor-permeable materials, is critical to increase overall comfort during

excessive sweating, so that the skin can breathe freely and the body does not overheat. Condensed moisture in the form of sweat is removed from the surface of human skin as quickly as possible through clothing to the environment [7, 8]. Therefore the chosen clothing should have the highest possible values of relative water vapor permeability (or lowest water vapor resistance) and moisture absorption and in-plane transfer.

Methods

The study was carried out on samples of shirting fabrics chosen from fourteen different fabrics compositions. Characteristics of the fabrics are given in Table 1.

Table 1. Composition of shirting fabrics

SAMPLE	COMPOSITION	SQ. MASS [g/m ²]	STRUCTURE
1	100 % bio - cotton	120	plain
2	100 % cotton	105	plain + twill
3	80 % cotton, 20 % polyamide	69	plain
4	70 % cotton, 30 % polyester	108	plain
5	65 % cotton, 35 % polyamide	113	plain
6	60 % cotton, 40 % polyester	104	point twill
7	100 % linen	140	plain
8	55 % linen, 45 % viscose	133	plain
9	50 % linen, 50 % cotton	198	plain
10	100 % viscose	101	twill
11	70 % viscose, 30 % PAN	134	plain
12	100 % polyester	161	plain
13	50 % polyester, 50 % cotton	97	plain
14	100 % Lyocell	182	twill

The shirt fabric where of similar thicknesses with specific mass ranging roughly between 100 and 200 g/m². Images of samples are shown in the Figure 1.



Fig.1. Images of textile samples

The influence of the material composition on thermal and moisture absorptivity b and b_v was investigated on the ALAMBETA device [6, 9]. The measurement takes place in the laboratory, under constant air-conditioned conditions.

The measurement of thermal absorptivity b depends on measurement of amount of heat flowing at a temperature difference of 1 K per unit area per unit time due to heat conduction and accumulation in the unit volume.

The measurement consists in inserting individual samples between the pad and the measuring head of the instrument. All other measuring and mechanical operations are provided by the ALAMBETA. Thermal absorptivity b and b_T [$\text{W} \cdot \text{m}^{-2} \cdot \text{s}^{1/2} \cdot \text{K}^{-1}$] of dry and wetted fabrics is defined by the equation (1):

$$b_T = \sqrt{\lambda \cdot \rho \cdot c} \text{ [W} \cdot \text{m}^{-2} \cdot \text{s}^{\frac{1}{2}} \cdot \text{K}^{-1}] \quad (1)$$

where λ means specific thermal conductivity, [$\text{W} \cdot \text{m}^{-1} \cdot \text{K}^{-1}$]

$\rho \cdot c$ is heat capacity, [J/m^3]

Measurement of moisture absorptivity of textile fabric is also performed on the commercial instrument ALAMBETA and consists in evaluation of level of heat power $q(t)$ which passes through the upper surface of moistened special thin fabric, which simulates wet (sweated) human skin and which is in contact with surface of the measured sample. After mutual contact of both textile fabrics under defined pressure (200 Pa) the moisture is due to surface sorption taken away from the skin simulating fabric and conducted outside of the surface of heat power sensing disc of small diameter. Textile fabrics with higher sorption and higher capillary conduction of moisture (with higher wetting and wicking capacities) then make the skin simulating fabric more dry and indicate drier (warmer) warm-cool feeling and vice versa. As a textile fabric which is in contact with a model of wet human skin (skin simulator) serves thin knitted fabric COOLMAX-FC 205 (square mass $170\text{g}/\text{m}^2$) moistened by 0,5 ml of solution of detergent with water 1:50. As the objective parameter of warm-cool feeling felt by the testing instrument serves the thermal absorptivity.

One layer of fabric was used to measure moisture absorption, due to the use of a moistened COOLMAX-FC 205 knit simulating a damp skin model.

To measure the moisture content, it is necessary to prepare a sample of COOLMAX-FC 205, to which a mixture of 0,3 ml of water and 1 % detergent is applied before each measurement. The mixture is applied from close proximity directly to the structure of the knitted fabric. After application of this solution, it is necessary to wait 1 min in order for sufficient and even distribution of moisture in the structure of the sample. After this time, the test sample is placed in the instrument and a moistened COOLMAX-FC 205 is placed loosely in the center under the measuring head and the instrument is started.

Contact of the dry fabric with the moistened COOLMAX-FC 205 knit leads to an increase in heat from the absorbed moisture of the sample. The heat generated is then dissipated from the lower surface of the sample by conduction to the ceramic plate below it.

Each sample was measured 3 times, each time at a different location on the fabric so as not to distort the measured data. The samples are inserted upside down, towards the measuring head. COOLMAX-FC 205 knit is inserted on the reverse side of the sample.

To determine the overall comfort of wearing a shirt during excessive sweating, under discomfort conditions starting at 50 % fabric moisture, it was necessary to introduce the so-called index of overall comfort OCI. This comfort parameter was introduced by L. Hes only for the purposes of this experiment.

This newly established comfort parameter describes the effect of material composition on the overall comfort of wearing a shirt during excessive sweating, taking firstly into account previous measurements of the effective relative water vapor permeability (ERWVP) of the studied shirt fabric at their 50 % humidity (wetness) [6], and it also newly involves the above explained moisture absorptivity of the studied fabrics.

By combining these comfort properties of the wetted sample, it is possible to obtain information about the fabric, to what extent it is able to let water vapor through even when wet, and how quickly it can carry this moisture further into the environment

Index of overall comfort OCI is measurement based on the equation

(2):

$$OCI = \frac{ERWVP_{U50}}{\frac{b_V}{b_{Vmax}}} \quad (2)$$

where, $ERWVP_{U50}$ – effective water vapor permeability at 50 % humidity, % see in [6];

U – humidity of the wetted (and stepwise manually dried) sample, %;

b_V – moisture absorptivity of shirt fabrics;

b_{Vmax} – maximum level of moisture absorptivity [$800 \text{ W} \cdot \text{m}^{-2} \cdot \text{s}^{1/2} \cdot \text{K}^{-1}$].

Results and discussions

Thermal absorptivity describes the thermal contact perception of a skin in contact with a fabric, the thermal touch. The higher the values of thermal absorptivity b , the colder the feeling of contact with the fabric. With decreasing values of the fabric, it achieves a warmer touch. The measured values of thermal absorptivity are shown in the Table 2.

Table 2. Parameters measured by the ALAMBETA device (CV is Coefficient of Variation [%], a means thermal diffusivity [mm^2/s], r is thermal resistance [$\text{m}^2\text{K}/\text{W}$])

N ^o	Fibre composition	a	CV_a	λ	CV_λ	r	CV_r	b_T	CV_{bT}	b_V	CV_{bV}
1	100% BIO-CO	0,056	5,8	0,042	5,7	0,006	6,5	179	4,1	694	1,3
2	100% CO	0,042	6,9	0,039	2,7	0,005	3,3	190	3,7	772	2,5
3	80% CO	0,063	4,6	0,037	3,3	0,006	1,2	146	1,3	767	4,1
4	70% CO	0,069	6,9	0,042	3,5	0,008	0,8	159	4,3	645	0,4
5	65% CO	0,053	12,9	0,040	8,9	0,007	6,0	176	4,4	674	2,1
6	60% CO	0,173	4,2	0,039	2,6	0,018	5,2	94	1,8	590	4,6
7	100% LI	0,060	8,8	0,042	7,0	0,009	5,0	173	3,3	665	1,7
8	55% LI	0,069	6,8	0,046	3,9	0,009	1,9	174	2,9	639	5,8
9	50% LI CO	0,057	3,4	0,059	4,5	0,007	5,6	248	3,7	647	1,6
10	100% VI	0,053	8,5	0,038	5,9	0,007	2,4	166	3,0	668	2,5
11	70% VI	0,078	5,0	0,042	5,6	0,010	2,4	149	3,1	633	2,7
12	100% PES	0,089	8,0	0,049	5,9	0,010	1,2	157	1,7	611	0,7
13	50% PES CO	0,134	10,6	0,037	4,5	0,013	2,7	109	1,5	612	2,9
14	100% LYOCELL	0,082	4,9	0,049	3,8	0,011	3,6	173	3,1	615	1,3

Values of thermal absorptivity b of climatized fabrics shows the Figure 2.

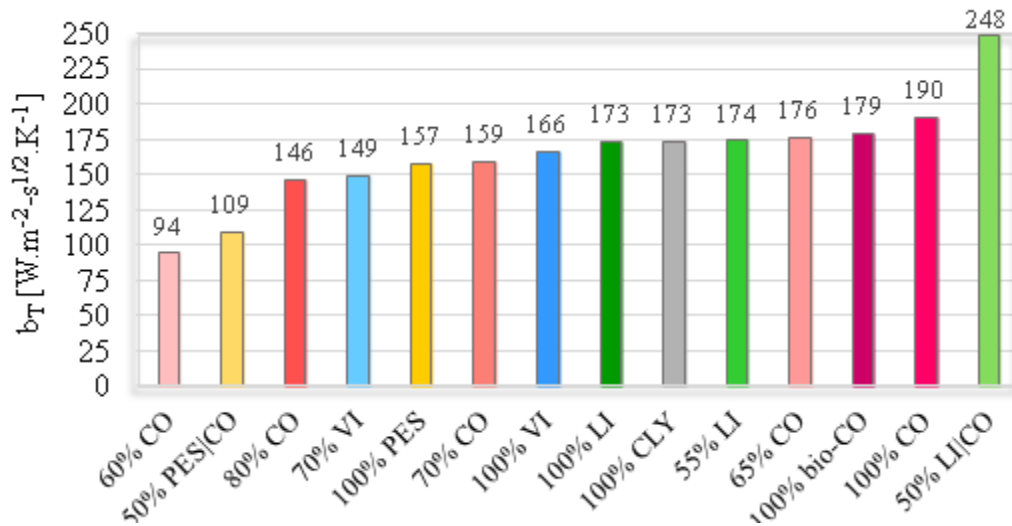


Fig.2. The effect of material composition on thermal absorptivity b of non – wetted shirt fabrics

From the calculated values it can be deduced that the lowest values of thermal absorptivity and thus the most pleasant warm touch in contact with the skin are achieved by those samples which were arrested with a crepe effect. These low values are caused by the corrugated structure of the fabric, which results in an increase in the specific thermal conductivity of the sample, i.e. the ability of the fabric to equalize the temperature more quickly; the heat in the fabric is retained longer, even when the heat source cools.

Furthermore, it can be argued that all samples with man-made filament yarns have a warmer feel, both natural and synthetic polymer. This is due to the good heat conduction properties of the chemical fibers in both the longitudinal and transverse directions.

Depending on the material composition, both fabrics made of pure cotton fibers achieve the coldest feel, because in the transverse direction these fibers conduct heat up to 5 times less than in the longitudinal direction.

Sample No. 9 differs greatly from all samples with its high values of thermal absorptivity. This deviation is caused by the very rough surface of the fabric, using 50 % of flax fibers, which generally have a heat-contact feel. The determined values of moisture absorptivity (b_v) are shown in the Figure 3.

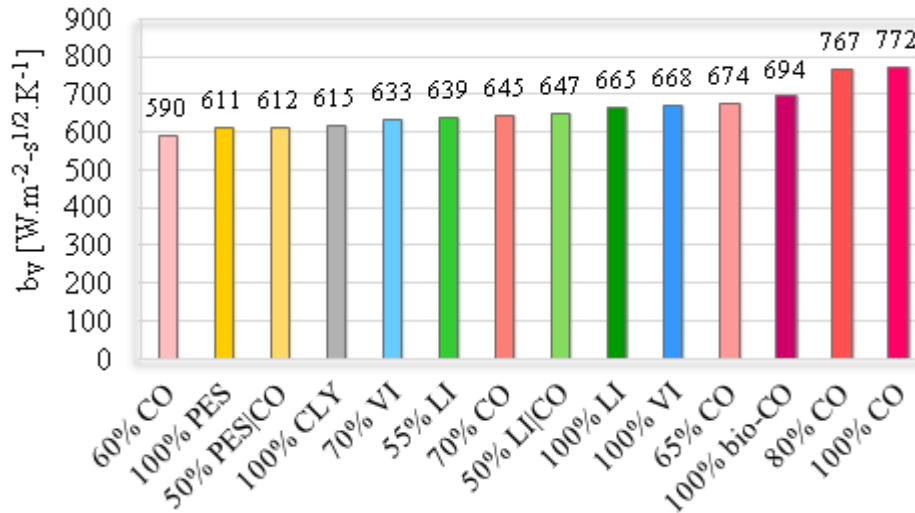


Fig.3. The effect of material composition on moisture absorptivity b_v of the analyzed shirt fabrics

Moisture absorptivity indicates the extent to which the fabric is able to remove moisture from the place of sweat formation to places where there are far fewer sweat glands and where due to the larger area of these places there is several times greater evaporation, which causes much faster moisture removal. High values of moisture absorption indicate that the fabric does not have sufficient moisture resistance during wetting, which increases the heat capacity and the user registers the feeling of cold (moisture). Conversely, if the samples have a good ability to wick away moisture, the heat capacity decreases and a warm (dry) feeling occurs while wearing the garment.

From the measured values it can be deduced that the fastest removal of moisture to the surroundings takes place in samples that were arrested with a crepe effect. These low values are caused by the corrugated structure of the fabric, which reduces the contact area of the fabric and thus its contact resistance, thus facilitating the removal of moisture.

Samples made of chemical fibers show very good values of moisture absorptivity due to the previously mentioned ability of polymer fibers to distribute heat evenly in the longitudinal and transverse directions.

Higher values of moisture absorption are achieved by textiles made mainly of flax fibers, which is due to their generally cold feel and coarse uneven structure.

The samples with the highest ratio of cotton fibers show the worst and thus the slowest removal of moisture to the surrounding environment when the fabric is moistened. This means that after wetting (sweating) the cotton fiber shirt holds moisture and cannot remove it quickly enough, creating unwanted sweat stains.

As mentioned earlier, the overall comfort index expresses the ability of the fabric to let water vapor through the wet state (when sweating) and at the same time the speed at which we can dissipate this moisture into the environment. The highest values of the OCI comfort index correspond to the best comfort when wearing a shirt during excessive sweating and vice versa. The measured and calculated values of the overall comfort index are shown in the Table 3.

Table 3. Parameters of measured and calculated values of the overall comfort index

Sample	Fibre composition	b_{Vmax}	b_V	ERWVP _{U50} effective water vapor permeability at 50 %	Overall comfort index (OCI)
1	100% BIO-CO	800	694	6,42	7,40
2	100% CO	800	772	7,96	8,25
3	80% CO	800	767	10,95	11,42
4	70% CO	800	645	12,10	15,00
5	65% CO	800	674	12,99	15,42
6	60% CO	800	590	19,11	25,91
7	100% LI	800	665	12,57	15,12
8	55% LI	800	639	11,54	14,45
9	50% LI CO	800	647	7,77	9,60
10	100% VI	800	668	14,76	17,68
11	70% VI	800	633	15,37	19,43
12	100% PES	800	611	9,63	12,61
13	50% PES CO	800	612	21,98	28,73
14	100% LYOCCELL	800	615	16,51	21,48

The effect of material composition on the overall comfort index (OCI) of shirt fabrics are shown in the Figure 4.

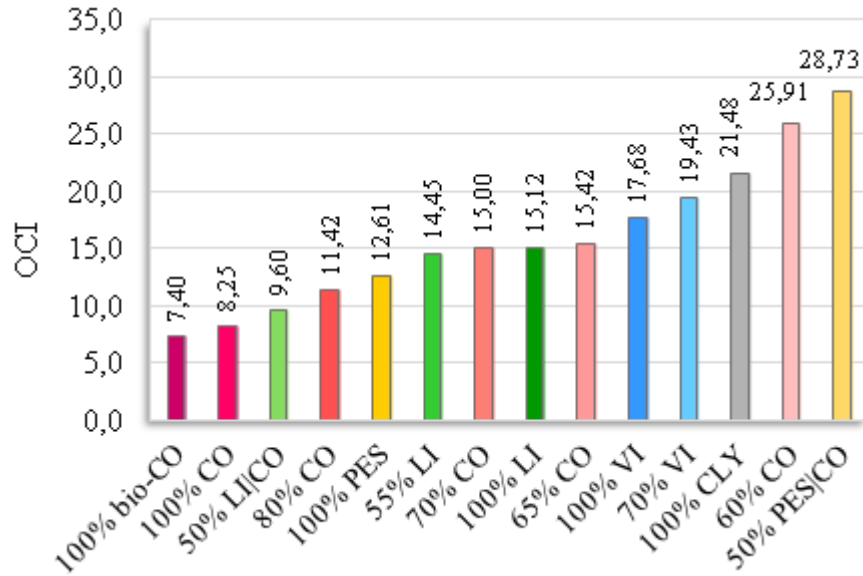


Fig. 4. The effect of material composition on the overall comfort index (OCI) of shirt fabrics

From the calculated values it can be determined that the best choice of a shirt for conditions evoking excessive sweating are the most suitable those that are arrested by the crepe effect, namely those that have a wavy surface, which in both cases is achieved by weaving cotton and polyester yarns, resulting in unique comfort properties. Fabrics with this effect boast both the highest permeability to water vapor when the fabric is wetted, as well as the fastest removal of moisture to the surroundings.

All cellulose viscose and Lyocel fabrics achieve higher values of overall comfort, mainly due to their very good vapor permeability when wet.

Worse results are achieved by fabrics made of primarily linen fibers and generally fabrics with a tighter and coarser fabric structure, causing higher water vapor resistance.

3 of the 4 worst results of overall comfort are achieved by fabrics with the highest ratio of cotton fibers. This fact is caused by the very slow

removal of moisture to the environment as soon as these fibers absorb water (sweat).

Among these very poor values of overall comfort, a sample of a mixture of flax and cotton fibers with a very tight and coarse structure, which prevents sufficient moisture penetration through the fabric, was wedged.

Conclusion

In the dry state, men's shirts made of natural fibres provide very good sensorial and thermal comfort to their wearers. However, in wet state these fibres may exhibit lower moisture transfer in liquid and gaseous state, thus causing higher friction of the fabric against skin resulting in sensorial discomfort.

The study was compared the thermophysical properties of several types of shirt fabrics with different material composition.

Analysis of currently available options for men's shirts was conducted. The influence of the material composition on thermal and moisture absorptivity b and b_v was investigated on the ALAMBETA device. It is a new non-destructive testing instrument, which provides relatively short testing times.

Measurements and comparisons of individual shirt fabric samples with different material composition were made to determine the best possible combination of moisture absorption and other parameters of a particular shirt, which will provide the best possible thermophysiological comfort when worn even during excessive sweating.

References

1. Ozdemir H. (2017). Thermal comfort properties of clothing fabrics woven with polyester/cotton blend yarns. *AUTEX Research Journal*, 17 (2), P.135 – 141.
2. Mansor A., Ghani S. A., Yahya M. F. (2016). Knitted fabric parameters in relation to comfort properties. *American Journal of Materials Science*, 6 (6), P. 147 – 151.

Advanced technologies in education, industry and the environment

3. Lee S., Obendorf S. K. (2012). Statistical modelling of water vapor transport through woven fabrics. *Textile Research Journal*, 82 (3), P.211 – 219.
4. Das S. (2016). Study on comfort properties of different woven fabric. *International Journal of Management and Applied Science*, 2 (8), P. 57 – 61.
5. Paraska O., Rak T., Rotar D., Radek N. (2019). The research on the effect of compositions of ecologically safe substances on the hygienic properties of textile products. *Eastern-European Journal of Enterprise Technologies*. 10 (97), P. 43 – 49.
6. Hes L., Boguslawska – Baczek M. (2018). The effect of the surface roughness on determination of water vapour resistance of fabrics tested by a Skin model. *Internat. Conf. CIRAT 8, Monastir, Tunisia*.
7. Kandi I., Das K. N., Mahish S. S. (2013). Thermo-physiological comfort properties of P/B belnded suiting fabrics. *International Journal of Innovative Research in Science, Engineering and Technology*, 2 (12), P. 7620 – 7629.
8. Jordeva S., Čortoseva S., Mojsov K., Zezova S., Risteski S., Kuzmanoska V. (2017). The influence of the structural characteristics of cotton and polyester knitted fabrics on the thermo-physiological comfort. *Advanced Technologies*, 6 (1), P. 88 – 92.
9. Hes L., Boguslawska-Baczek M. (2014). Analysis and experimental determination of effective water vapor permeability of wet woven fabrics. *Journal of Textile and Apparel, Technology and Management*, 8 (4), P. 1 – 8.

SELECTED ASPECTS OF AESTHETIC PROPERTIES OF LAMINATED SEAMS

Szafrańska H.¹, Korycki R.²

¹ University of Technology and Humanities in Radom, Poland

² Lodz University of Technology, Poland

Introduction

The definition „working clothing” denotes the wide spectrum of clothes. Depending on the work performed, they can be dedicated to the particular professional group (e.g. healthcare, hotel service employees etc.) or can be the single articles, e.g. aprons, shirts etc. The main task of working clothing is to replace the employee's clothes or protect them from damage and dirt, it can also play a representative role. The aesthetic appearance and high usability of the clothing depend not only on the type of materials used (e.g. various tapes, adhesive clothing inserts, threads), but also on manufacturing technology [1-2].

From technological point of view, the durability of product is significantly affected by the structural properties of the seams. In clothing are implemented threaded, glued and welded connections [3-4, 11]. Application of the particular method depends on the type of materials used to create the individual elements, the stage of production process, as well as the strength and aesthetic requirements of individual elements of clothing [5-6, 10].

The main goal of the paper is to analyze the aesthetic properties and technological assumptions for three types of laminated seams created with the participation of transfer foils in the form of a tape of different width. The aesthetic properties of the designed seams were evaluated using the bending stiffness index for the seams formed in the weft direction. The analysis is a continuation of previous works [5-8] concerning the adhesive joints in the seams of working clothing.

Materials

The research objects are the textile material (the clothing fabric) and the transfer tapes, cf. Table 1 and Table 2. The fabric can be applied for working clothing, in particular for healthcare professionals, catering and hospitality (e.g. aprons, shirts, blouses). Cotton fibers make the fabric more airy, which increases the comfort of use.

Table 1. Characteristics of the research material

Name	Raw material composition	Surf. mass M_p , g/m ²	Thickness h, mm	Type of weave	Nr of threads /dm	Max force to rupture P[N]	Relative elongation ϵ [%]
Fabric Z	Cotton 100%	180	0,34	Splot 1/1	warp: 290 weft: 220	warp: 445 weft: 408	warp: 7 weft: 34

Table 2. Characteristics of transfer foil 8735 of 3M™ Scotchlite™ as a tape

Description	Raw material composition of polymer	Surf. mass M_p , g/m ²	Thickness h, mm	Width of tape b[mm]	Max force to rupture P[N]	Relative elongation ϵ [%]
Tape B	Polyester	350	0,21	10 15 20	44	770

3M™ Scotchlite™ reflective material – transfer films are designed for use in protective, working and sport clothing, as well as for everyday use. When properly used, the reflective materials help to increase the visibility of the wearer in night or low light conditions. The reflective thermal transfer film is composed of light-reflecting glass lenses thermally bonded to the heat activated base. The tape is a flame retardant film and can be laminated directly to compatible substrates.

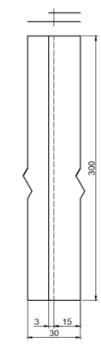
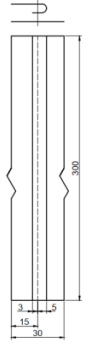
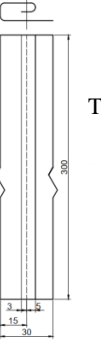
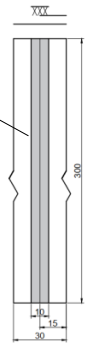
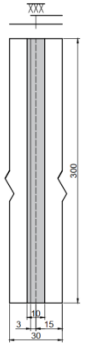
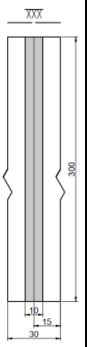
Sewn seams			Laminated seams		
1.02.01/301	5.31.02/301	6.03.01/301	1.02.k	1.02.01/301.k	4.01.k
N1	N2	N3	L1	L2	L3
					

Fig. 1. Technological project of thread and laminated seams according to ISO 4916

Three variants of laminated seams *L1*, *L2* and *L3* were selected for the tests, correspondingly to the modified version of the plain seam (*1.02.k* and *1.02.01 / 301.k*), as well as the flat seam *4.01.k* consisting of the fabric *Z* and the tape *B* on right side of the product. The seams are so designed that both fabric layers are shifted each other and the center line of tape coincide with the connecting line of these layers. Additionally, a thread connection is used in the *L2* seam. Such seam structures provide connection in the seam and decoration of the product (Figure 1) as well as reduce the fabric consumption during manufacturing of clothing.

The samples of seam for the tests were formed along the weft thread of fabric. Each laminated seam *L1*, *L2* and *L3* is provided with the tape *B* of three widths, respectively $10[mm]$, $15[mm]$ and $20[mm]$.

The seams are laminated on a Schulze Airpress 4 plus automatic. It is an automatic transfer press with four bottom plates and one top-heating plate equipped with: (i) the electronic temperature and time programming on the display; and (ii) the smooth pressure adjustment.

The sewing conditions are the following: (i) industrial Juki sewing machine; (ii) stitch type – the quilted seam; (iii) number of stitches – $3/cm$; (iv) type of sewing thread – threads from the company Coats Epic 150, 100% PES; (v) needle type – Schmetz R 90 nickel coating.

Determination of bending stiffness by the constant angle method

The bending stiffness of the laminated and sewn seams was measured by the constant angle method on the test stand, by means of the variable overhang length L of the samples bent at the constant angle of $41^{\circ}30'$. Samples of the dimensions $(300 \times 30)mm$ are cut from the materials and seams intended for tests and placed on the instrument table. After loading with a metal gauge, the samples were displaced and the length of the overhang L was read on the gauge when the overhanging end of the sample coincided with the plane formed between the scratch on the indicator and its reflection in a flat mirror (Fig. 2).

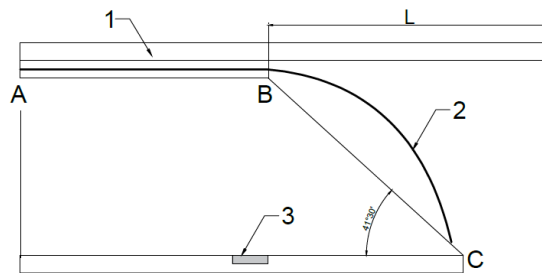


Fig. 2. Scheme of measuring instrument determining the variable length of sample overhang

1 – gauge, 2 – sample of product, 3 – water level, L – sample overhang

Ten measurements were made for the tested seams. Based on the performed tests, the following was determined (Table 3).

Table 3. Parameters determining during the bending stiffness

Parameter	Mean sample overhang L [cm]	Bending length [cm]	Bending stiffness [$\mu\text{N m}$]
Description	$\bar{L} = \frac{\sum_{i=1}^{n=10} L_i}{n}$	$c = \frac{\bar{L}}{2}$	$G = 10^{-3} M_p c^3 g$

Where M_p is a surface mass of the product [g/m^2]; g is gravitational acceleration.

Analytical determination of deflection and angle of rotation

The sample is tested under repeatable conditions and geometry, its shape is planar (i.e. two-dimensional). Let us also determine the cross-

section of the structure by the plane perpendicular to the material. The problem of sample overhang loaded by a gauge is equivalent to the bending of the beam subjected to the continuous load, cf. Figure 3. The load of a gauge can be determined using the simple formula: $q=Q_{gauge}/L$ [N/m]; where Q_{gauge} is weight of a gauge [N]; L is the length before test [m].

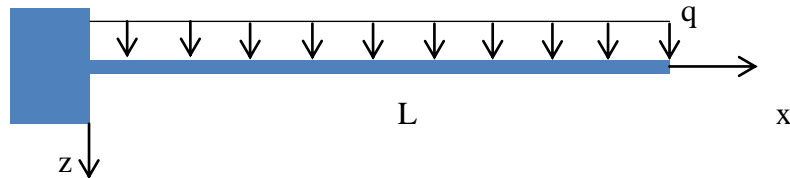
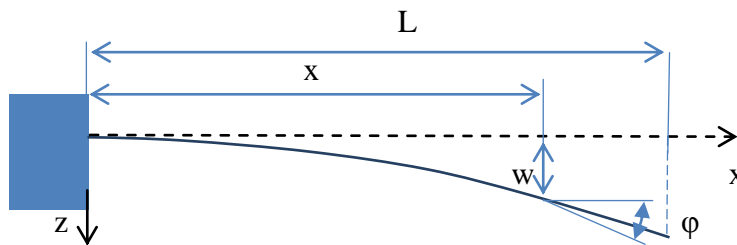


Fig. 3. Scheme of loading system for the tested sample

The sample can be deformed under the load to the form shown in Fig.4.



**Fig. 4 Scheme of deformation line and deformation parameters
w – current deflection of sample; φ – current angle of rotation**

The parameters of deformation line are the deflection and the angle of rotation. The maximal values can be determined at the end of sample i.e. for the coordinate $x=L$. The equation of deflection curve can be formulated by means of a simple theory of strength of materials in the following form.

$$\frac{d^2w}{dx^2} = -\frac{M}{EJ}; \quad \frac{dw}{dx} = \varphi \quad (1)$$

Where M is the bending moment [Nm], E is the Young's modulus of the fabric and seam [GPa], J is the moment of inertia of the cross-section [m^4].

The first step is to determine the distribution of the bending moment along the length of sample. The structure shown in Fig.3 can be described as follows.

$$M = -\frac{q}{2}(L-x)(L-x) \quad (2)$$

Introducing Eq.(2) into Eq.(1), we formulate the relationship.

$$\frac{d^2w}{dx^2} = \frac{q}{2EJ}(L^2 - 2Lx + x^2) \quad (3)$$

Integrating twice in respect of the coordinate x , we can denote.

$$\begin{aligned} \frac{dw}{dx} = \varphi &= \frac{q}{2EJ}\left(L^2x - Lx^2 + \frac{1}{3}x^3\right) + C_1 \\ w &= \frac{q}{2EJ}\left(\frac{1}{2}L^2x^2 - \frac{1}{3}Lx^3 + \frac{1}{12}x^4\right) + C_1x + C_2 \end{aligned} \quad (4)$$

Where C_1 and C_2 are the integration constants. The boundary conditions can be formulated at the beginning of a sample i.e. $w(x=0)=0$; $\varphi(x=0)=0$. Introducing the conditions into the Eqs.(4), we obtain the constants $C_1=0$; $C_2=0$ which allows to define the equations of deflection curve and angle of rotation.

$$\begin{aligned} \varphi &= \frac{q}{2EJ}\left(L^2x - Lx^2 + \frac{1}{3}x^3\right) \\ w &= \frac{q}{2EJ}\left(\frac{1}{2}L^2x^2 - \frac{1}{3}Lx^3 + \frac{1}{12}x^4\right) \end{aligned} \quad (5)$$

It is evident, that the maximal values are at the end of sample for $x=L$. We can also denote.

$$\varphi(x=L) = \frac{qL^3}{6EJ} \quad w(x=L) = \frac{qL^4}{8EJ} \quad (6)$$

The problem can be solved analytically and the obtained relationships can help to predict the value of the sample overhang.

Research results and their analysis

During the tests the following was determined:

- The influence of the lamination process parameters i.e. temperature $T[^\circ C]$, time $t[s]$, pressure $p[N/m^2]$ on the value of bending stiffness index $G[\mu N m]$ for the seam $L1$ with the tape B of the width $10[mm]$;
- The influence of the seams structure on the value of the bending stiffness index G .

The properly prepared material samples (Fig.1, seam L1) are laminated based on a three-factor plan 3^3 with the input factors: $X1$ – temperature $T[^\circ C]$, $X2$ – time $t[s]$, $X3$ – pressure $p[N/m^2]$. On the basis of preliminary studies, the ranges of factor variability were determined (Table 4).

Table 4. Ranges of factor variation for seams with the tape B

Factor	Code description	Central value	Unit of variation	Unit of measure
Temperature T	X_1	170	20	$[^\circ C]$
Time t	X_2	15	5	[s]
Pressure p	X_3	35	20	$10^4 [N/m^2]$

The code values $X1$, $X2$ and $X3$ changes inside the range $\langle -1, 1 \rangle$. The values of $X1$ equal to $-1, 0, 1$ determine the lamination temperature of $150[^\circ C]$, $170[^\circ C]$, $190[^\circ C]$, respectively. Similarly, the values of $X2$ equal to $-1, 0, 1$ mean the time of $10[s]$, $15[s]$, $20[s]$; whereas values of $X3$ equal to $-1, 0, 1$ the pressure $15 \cdot 10^4 [N/m^2]$, $35 \cdot 10^4 [N/m^2]$, $55 \cdot 10^4 [N/m^2]$, respectively. The bending stiffness G was selected as the optimization criterion Y for the seams formed in the weft direction.

The program of experiment include the average results from the calculations. The regression functions defining the relationships between the considered factors and the examined features were estimated using the SAS computer program. The obtained test results were used during the regression analysis, in which the relationship between the examined factors and the considered feature was estimated based on the second-degree polynomials. The value of the regression coefficients is assessed according to the Student's

test, and the adequacy of the developed model according to the value of the multiple correlation coefficient R . Introducing the values of regression coefficients, the second-degree regression equation of the bending stiffness is the following function of the lamination process parameters.

$$G = 147,3155 - 1,9371T - 0,5036t + 0,0058T^2 + 0,0055tT \quad (7)$$

$$+ 0,0329t^2 + 0,0074pT - 0,0355t^2 - 0,0457p^2$$

$$R^2 = 0,93$$

The obtained model adequately describes the lamination process, which is proved by the value of the correlation coefficient R^2 . The established analytical relationships allow to predict the changes in value of the bending stiffness index of the laminated seams formed in the weft direction. Figure 5 shows the dependence of the bending stiffness $G[\mu N m]$ on the parameters of lamination process (T, t, p) for seams with the tape B .

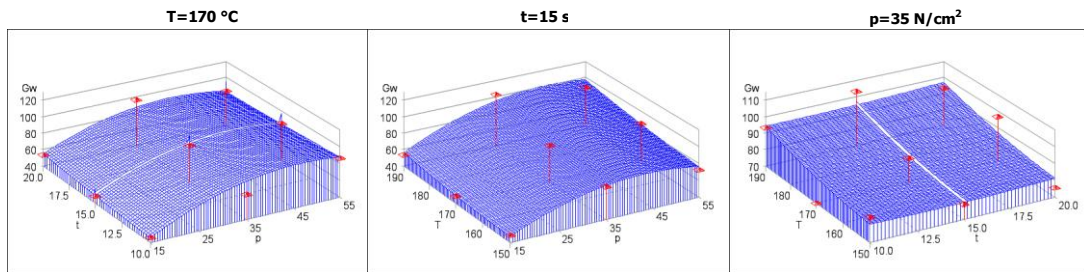


Fig. 5. Response areas / graphs of regression function describing the sensitivity of bending stiffness G of seams formed along the weft direction on the lamination process parameters:

- Time t and pressure p for the constant temperature $T=170[^\circ C]$;
- Temperature T and pressure p for the constant time $t=15[s]$;
- Temperature T and time t for the constant pressure $p=35[N/m^2]$.

For the seams formed on the thermal press, the lowest recommended values of the bending stiffness index are obtained in the area of the lower values of temperature and pressure. Therefore, the recommended values of the analyzed parameters for seam B are: (i) temperature $T=150[^\circ C]$ and $170[^\circ C]$; (ii) pressure $p=15 \cdot 10^4 [N/m^2]$.

It was noticed that in the selected area the analyzed values of time parameter ($10-20$)s are irrelevant. The nature of changes in the presented

response surfaces confirms that the stiffness of seams can be designed by the variable conditions of lamination process. As a result, the quality of seam can be predicted in respect of the requirements of the product and the location of seam in the clothing.

Next, the seams were laminated with the tape B of the different width, under the conditions selected and recommended above, i.e. $T=170[^\circ C]$, $t=15[s]$, $p=15 \cdot 10^4 [N/m^2]$. The obtained test results allow to show a comparative analysis of:

- the influence of the structure of laminated and thread seams on the value of bending stiffness index for seams formed in the weft direction, and
- the effect of variable width of the tape B on the value of the bending stiffness index G .

As presented in literature [10], the thread and adhesive connections used in clothing increase the value of the bending stiffness index compared to the fabric.

During the manufacturing of clothing, the thread seams $N1$ and $N2$ can be used, for example, to sew on the pockets, to finish the bottom of a sleeve. The seam $N3$ can be used to finish the front edge of e.g. a blouse, apron, and also to finish the bottom of trousers, apron or skirt. The presented tests (Fig. 5) show that the value of the bending stiffness index increases with the change in the structure of sewn seams from $N1$ to $N3$. Comparing to the Z fabric ($G=11 \mu N m$), the values of the bending stiffness index for the sewn seam $N1$ were 4 times higher, for the seam $N2$ 8 times higher, and the seam $N3$ as much as 10 times higher, reaching the value of $G=113 [\mu N m]$. Most likely, it results from the number and arrangement of the particular layers of material relative to each other, as well as the application of a quilted stitch, which confirms the significant influence of the seam structure on the value of bending stiffness index.

The arrangement of fabric layers in the seams $L1$ and $L2$ is similar to the seam $N1$, but the method of joining is completely different. The laminated seams $L1$ and $L2$ made with a tape of the width $10[mm]$ are characterized by

the increase in the value of bending stiffness index equal to 100% in relation to the seam $N1$. The sewn seams $N2$ and $N3$ are also very often used in clothing technology. The obtained values of the index G for the seams $L1$ and $L2$ ($80\mu N m$) are close to the values for the seam $N2$ ($83\mu N m$), and much lower (by 30%) than for the seam $N3$ ($113\mu N m$). The lowest values of the bending stiffness index were obtained for the flat seam $L3$ ($59\mu N m$), which can be used to connect the clothing elements, for example on the neck line. The obtained results indicate that it is possible to replace the sewn seams frequently used during the manufacturing of garments by the laminated seams $L1$, $L2$ and $L3$.

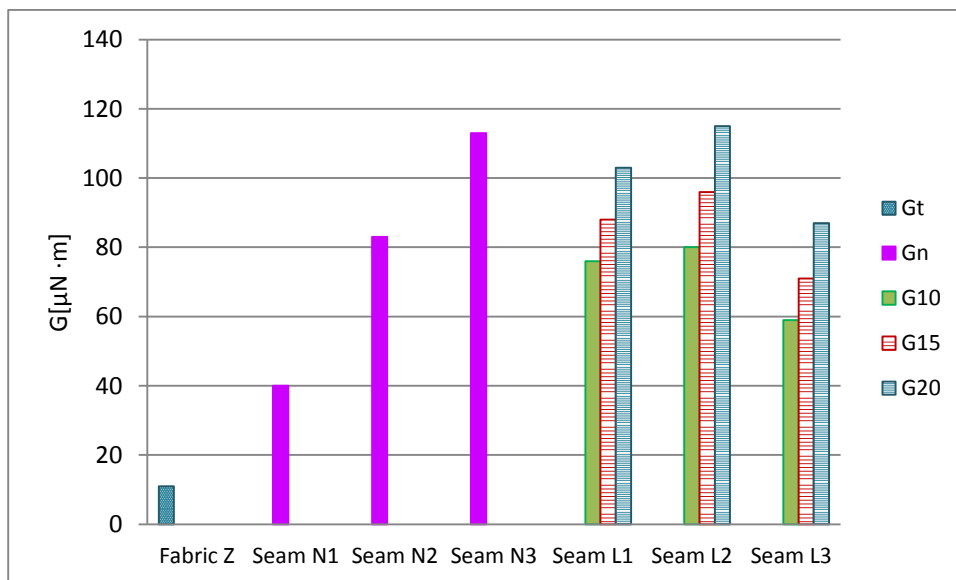


Fig. 6. Influence of the type and structure on the value of bending stiffness index G of the seams formed along the weft thread.

- **Gt** – bending stiffness for the fabric Z ;
- **Gn** – bending stiffness for sewn seams;
- **G10, G15, G20** – bending stiffness for the laminated seams with the different width of the tape B 10[mm],15[mm], 20[mm].

Figure 6 presents the values of the bending stiffness index obtained during the tests for laminated seams with the tape B of variable width. The tests showed that as the width of the tape B increased from 10[mm] to 15[mm] and up to 20[mm], the value of the bending stiffness index of the created seams increased by 20% and 40%, respectively, regardless of the structure of

the laminated seam. This is important information when designing the aesthetic properties of seams.

Compared to the sewn seam $N3$ determined by the highest value of bending stiffness index ($113 \mu N m$), almost all analyzed laminated seams with a tape of the variable width B are characterized by lower values of bending stiffness index. The seam $L2$ with the tape of the largest width shows the similar values.

Compared to the seam $L1$, the application of a thread joint in the laminated seam $L2$ had a slight increase (5-12)% in the value of the bending stiffness index, which proves the dominant effect of the adhesive joint. However, it can have a significant effect on the change of the strength properties of the seam.

Conclusions

The obtained analytical correlations allow to determine and predict the changes in properties of laminated seams in respect of manufacturing parameters such as temperature, time and pressure. Thus, the presented analysis can help to optimize the basic parameters of seams.

Taking into account the recommended softness of seams, the best values of the lamination process parameters were determined, i.e. temperature $T=170[^\circ C]$ and pressure $p=15[N/m^2]$ for the seams formed in the weft direction.

As the width of tape B increases from $10[mm]$ to $15[mm]$ and up to $20[mm]$, the value of the bending stiffness index increases by 20% and 40%, respectively, regardless of the structure of the laminated seam.

In case of the laminated seams, the values of bending stiffness index were close to or lower than the same index for the sewn seams $N2$ and $N3$ commonly used in clothing. The analysis confirms that it is possible to replace the selected sewn seams with the laminated seams.

The problem can also be analyzed using analytical methods. Theoretical considerations concerning some selected questions (cf. the sample overhang) can help to replace the experimental problems by analytical

solutions. Thus, it will not be necessary to conduct time- and labor-consuming tests, but to replace them by the theoretical analysis. The problem is developed theoretically and will be presented in subsequent works.

References

1. Hayes, S.G., McLoughlin, J. (2007), Welded and sewn seams: A comparative analysis of their mechanical behaviour. In: Ariadurai, S.A., Wimalaweera, W.A. (eds) The Textile Institute 85th World Conference, Colombo, Sri Lanka, 131–142.
2. Jakubčionienė, Ž., Masteikaite, V., (2010), Investigation of textile bonded seams. *Mater Sci (Medžiagotyra)*, 16, 76–79.
3. Jevšnik, S., Vasiliadis, S., Kurson Bahadir, S., Grujić, D., Stjepanović, Z., (2016), Applying heat for joining textile materials. In *Open Access Book: Joining Technologies*, <http://www.intechopen.com/books/joining-technologies>
4. Jevšnik, S., Eryürük, S.H., Kalaoğlu, F., Karaguzel Kayaoğlu, B., Komarkova, P., Golombikova, V., Stjepanović, Z., (2017), Seam properties of ultrasonic welded multilayered textile materials. *Journal of Industrial Textiles*, 46, 5, 1193-1211.
5. Szafrńska H., Pawłowa M., Mitak K., Korycki R., (2016), Kształtowanie wytrzymałości połączeń szytych w wyrobach odzieżowych, [w:] *Ocena jakości wybranych wyrobów przemysłowych*, pod red. R. Zielińskiego, J. Żuchowskiego, Wyd. UTH Radom, Instytut Technologii Eksploatacji – PIB, Radom, 62 -70.
6. Szafrńska H., Pawłowa M., Korycki R., (2018), Wybrane aspekty zapewnienia jakości w odzieży wodochronnej, [w:] *Wybrane problemy jakości wyrobów przemysłowych*, pod red. M. Paździor, J. Żuchowski i in., Wyd. UTH Radom, 23-32.
7. Szafrńska H., Pawłowa M., Korycki R., (2017), Analysis of The Mechanical Properties of Seams in Waterproof Clothing, W.: *Innovations in Clothing 3D Design, Products, Fashion, Technologies and Testing of Clothing Materials*, pod red. Frydrych I., Bartkowiak G., Pawłowa M., Wyd. Politechnika Łódzka, Łódź, 156 - 163.
8. Szafrńska H., Korycki R., (2019), Tests of applications of transfer films in seams lamination technology, *Journal of Natural Fibers*, 16, 6, 898-912.
9. <http://www.romanik.pl/sklep/transfer/prasy-wg-typu/prasy-pneumatyczne/prasa-schulze-airpress4x-automatic-detail>
10. Szafrńska H., Pawłowa M., (2007), Aesthetical aspects of clothing products in the context of maintenance procedures. *Fibres & Textiles in Eastern Europe*, Vol. 15, No. 5-6(64-65), 109-112.
11. Vujasinovic, E., Rogale, D., (2013), Properties and performance of welded or bonded seams. In: Jones, I., Stylios. G.K., (eds) *Joining textiles. Principle and application*, 1st edn. Philadelphia: Woodhead Publishing Series in Textiles, 435–461.

WEARING OUT PROCESS OF TEXTILE MATERIALS MADE OF THERMORESISTANT FIBERS AND ITS IMPACT ON THE FILTERING CAPACITY OF THE HOSE FILTERS

Pelyk L., Pelekh Yu.

Lviv Trade and Economics University, Ukraine

Introduction

After industrial use, the surface of the material acquires a strongly distinct roughness due to the adhesion of dust particles during filtration. The unevenness of the material surface significantly affects the filtering capacity of a bag hose filter during its operation. Taking into account rather dense structure of the studied fabrics, small pore size of nonwoven materials, as well as the presence of polytetrafluoroethylene treatment, filter materials are quickly contaminated with dust particles, resulting in reduced permeability. Fine dust fractions, filling the porous layers, are able to form dust formations on the surface and inside the material, which is directed to the flow of the dusty air. Filling the pores, these formations cause a rapid increase in hydraulic resistance.

Application of textile materials made of thermoresistant fibers in bag hose filters is complicated by the fact that increasing filtration temperature leads to the significant increase of the activity of the filter medium components and the speed of reactions of their interaction with materials.

This reduces their service life depending on the nature of the filter material and its operating conditions. The destruction of polymers occurs as a result of: the interaction of polymers with water vapor at raised temperatures (hydrolysis of the material), because they are based on heterochain polymers; interactions with oxidants (mainly materials resistant to hydrolysis - polypropylene, wool are exposed to); thermal destruction (materials with high chemical resistance are exposed to (polytetrafluoroethylene), material destruction occurs due to the cleavage of the polymer chain links); material destruction as a result of its

interaction with dust (thermoresistance reduces in the dusty state, sometimes very significantly) [1].

During operation, filtering materials appear under significant physical and chemical affect, therefore, the threads (yarns) must meet the specific conditions of the filtration process. For example, yarn for filtering materials must be made of fibers of low linear density, as the thinner the fiber is, the higher the filter properties of this material are. Domestic regulations characterize filtering materials by the linear density of the yarn, its strength, thickness of the material, its surface density, tensile strength, and relative elongation. Although these indicators give an idea of the physical and mechanical properties of filtering materials, they are useless in assessing their filtering ability.

Analysis of the regulatory documentation of filtering materials shows that the input breaking characteristics are set by the value of the breaking load on the weft and the warp for the material strips of a certain width [2]. For most filtering materials, this characteristic is not a sufficiently defined value, which makes it difficult to evaluate the newly developed materials, including the evaluation of the service life of bag filters, which during operation are often exposed to long-term action of high temperatures. This leads to the aging process and changes in the properties of filtering materials and their fibers because of structural reconstruction and destructive processes. Three main cases of thermal exposure on fibers and fibrous materials can be pointed out, which require different methodological approaches:

- heat treatment of chemical fiber in technological production processes in order to give them the required level of properties and structural balance.

- operational exposure to low temperatures, which cause irreversible structural and thermochemical changes in fibers and materials.

- thermal aging under long-term exposure to high temperatures with thermochemical processes that lead to both irreversible chemical changes and changes in the supramolecular fibers structure.

Changes in filter materials that occur during their thermal aging can be divided into two stages: structural aging, determined by structural changes and relaxation processes, and thermochemical aging, determined primarily by thermochemical changes.

Changes in the properties that occur allow to assess the behavior of fibers and fibrous materials during operation (their operational reliability). Changing of filtering material properties, depending on the conditions of thermal treatment, takes place differently. During the first period of thermal aging, a change in the linear dimensions of the materials occurs, which leads to increased elongation and reduced strength. With the increase of duration of thermal treatment, the relaxation processes are completed and the process of thermal destruction becomes crucial, thus, the breaking load and elongation are reduced - this is the second stage of thermal aging.

Analysis of the literature has shown that recent studies are based on determining the filtering capacity of materials made of polyester fibers with a temperature of process gases up to 130 ° C. Application of filtering materials made of synthetic fibers with the enhanced thermal resistance (oxalone, sulfone, arcelon, phenylene, nomex, teflon, tefer-felt, etc.) allows to increase gas temperature from 100-140 to 250-300 °C and improve the filtering capacity of bag filters [3].

Objects and research methods

Testing of bag filters made of woven materials was carried out on an open-type bag filter (with a regeneration system – back-purge and the total filtration area of 17280 m²), and for nonwoven ones – on bag filters with pulse regeneration system (the total filtration area of 5600 m²).

Back-purged bag filters, sewed of the tested fabrics (sample 1, sample 9, sample 10) and with a pulse regeneration system, sewed of the tested nonwoven materials (sample 11, sample 13, sample 14), provided dust and gas flow purification with a maximum allowable residual dust content of not more than 0.01 g/m³. The technological equipment of gas purification worked continuously for 8 hours per shift, 3 shifts per day, 7

days a week. In this operation mode, the hose filters worked for the specified service life.

Research results

The conducted researches proved that there was a decrease in the indicator of air permeability in the tested samples after operation in the filtering unit during the determined service life. The data shown in table 1 indicate that the permeability of the "filter material-dust layer" system depends on many factors.

Analyzing the data shown in table 1, it was found out that there was a decrease in air permeability in the test samples after operation in the filter unit during the determined service life. The data obtained prove that the permeability of the "filter material-dust layer" system depends on many factors.

Table 1. Changes in the physical properties of the studied filter during operation

Tested sample		Surface density, g/ m ²	Bulk weight mg/mm ³	Total porosity, %	Air permeability, dm ³ /m ² ·s
Polyester fabric (sample 1)	before operation	318	0,318	77,1	136
	after 12 months	397	0,361	74,0	93
Arcelon fabric (sample 9)	before operation	286	0,286	80,0	142
	after 18 months	326	0,326	77,2	101
Glass fiber (sample 10)	before operation	430	0,878	66,2	165
	after 18 months	458	0,916	64,8	135
Nonwoven polyester material (sample 11)	before operation	500	0,278	80,0	90
	after 12 months	640	0,337	75,8	71
Nonwoven arcelon material (sample 13)	before operation	500	0,263	81,6	104
	after 18 months	583	0,292	79,6	90
Nonwoven material of nomex fibers (sample 14)	before operation	516	0,246	82,8	106
	after 18 months	590	0,281	80,3	92

This is due not so much to the amount of dust left in the material as to the state of dust aggregation in the fabric and cracks in the dust layer. It is found out that the cracks area and, accordingly, the permeability of the system will be greater, the bigger size of the through pores and their area in the clean material is, and the better it is deformed. Thus, the largest area of one pore is in a glass fiber sample 10, which is $2428 \cdot 10^{-4} \text{ mm}^2$ at their smallest number – 162 per 1 cm^2 and at the highest air permeability after its operation – $135 \text{ dm}^3 / \text{m}^2 \cdot \text{s}$. The smallest area of one pore is of the polyester reference sample (sample 1), which is $269 \cdot 10^{-4} \text{ mm}^2$ at their largest number – 536 per 1 cm^2 and at the lowest air permeability after operation – $93 \text{ dm}^3 / \text{m}^2 \cdot \text{s}$.

It was found out that in a clean filter cloth the increasing size of through pores leads to the increase of air permeability. Thus, filter cloth made of glass fiber (sample 10) has got the largest through pores size, it is 0.322 mm at the warp and 0.755 mm at the weft at the highest air permeability after operation – $135 \text{ dm}^3/\text{m}^2 \cdot \text{s}$. Polyester reference sample (sample 1) has got the smallest through pores size, it is 0.068 mm at the warp and 0.395 mm at the weft at the lowest air permeability after operation – $93 \text{ dm}^3/\text{m}^2 \cdot \text{s}$. Air permeability in the filter arcelon fabric (sample 9) after operation is $101 \text{ dm}^3/\text{m}^2 \cdot \text{s}$ with a larger through pores size of 0.140 mm at the warp and 0.319 mm at the weft than in sample 1.

In nonwoven materials, under the condition of through pores absence, air permeability depends on the total porosity. This dependence is of linear nature: the larger the porosity is, the greater air permeability will be. Analyzing table 1, it can be noted that the highest index of air permeability after operation belongs to the sample of nomex fibers (sample 14) and is $92 \text{ dm}^3/\text{m}^2 \cdot \text{s}$ at the highest value of the total porosity – 80.3%. The total porosity of the polyester nonwoven fabric (sample 11) during 12 months of operation reduced by 4.2%, which led to a decrease of air permeability, which is $71 \text{ dm}^3/\text{m}^2 \cdot \text{s}$. Air permeability in the arcelon nonwoven filtering material (sample 13) after operation is $90 \text{ dm}^3/\text{m}^2 \cdot \text{s}$ at a

decrease of total porosity by 1.4% during 18 months of operation, compared to the reference sample (sample 11).

Analysis of the obtained data shows that deposition of dust particles results in reduction of air permeability of the "filtering material – dust layer" system. At the beginning of the filtration of dusty gases, the bulk of the aerosol gets into the pores between the threads of the material. Dust particles settle on the fibers that are on the surface of the threads, between the weaves of the threads, and on the walls of the fibers. The fibers inside the twisted threads are practically not involved in particles settling, because the gas flow passes mainly through the holes between the threads. Dust growths are formed on the fibers that enlarge, and the process of particle settling and the formation of "bridges" over the pores and in the pores themselves is observed, resulting in formation of a continuous layer that turns into a "secondary" filter medium itself, thus, sharply increasing purifying efficiency. This layer has a significant porosity, it is permeable to aerosol, but almost impermeable to dust. During this period, the resistance of the material grows as a result of increasing the velocity of the gas in the pores between the weaves of the threads, caused by size reduction of these pores due to dust fouling [3]. Since the size of the through pores in the material is much larger than the size of dust particles, it is possible to assume that the basis of this solid layer of dust is a cross section of the pore of the smallest area. By the end of the formation of a solid layer of dust, some particles, especially large and heavy, are likely to settle (mainly due to the forces of inertia) on the fibers, which are located on the surface of the material from the dusty gas side.

Thus, in the "filter material - dust layer" system, the latter is the main filter medium, in which, as a result of the open pores area reduction (open is a pore permeable to aerosol) and because of their dust fouling, permeability decreases. However, the filtering material does not only act as a substrate, but efficiency of dust gathering and hydraulic resistance depend on its properties, the latter significantly affects the service life of the material in bag filters. With the reduction of hydraulic resistance in

materials with high air permeability, the efficiency of dust capture increases at the same time. The limiting hydraulic resistance depends on the properties of the filtering material, dust, regeneration parameters and is always set not higher than 2.5 kPa. Its further increase leads to reduction of the purification degree.

Studying the influence of operating conditions, as well as the regeneration process on the change of physical properties of new filtering materials, it was found out that long-term operation leads to reduction of their air permeability at a slight change in filtration capacity. This happens because of the accumulation of dust inside the material, growth of its mass and thickness, displayed by the increased indicators of surface density and bulk weight.

Filtration of dusty industrial gases in bag filters is a radical technical solution to achieve high dust capture efficiency. Capture efficiency is the main indicator of the bag filter work, which determines its filtering capacity. It can decrease in the set operation mode because of two reasons: as a result of micro deformation of the material caused by the gas flow impact and as a result of the formation of cracks in the dust layer during the period that comes right after regeneration. This can be explained by the fact that the high coefficient of purification efficiency is achieved due to the filtering impact of the dust layer on the material. The technological parameters that have the greatest impact on the capture efficiency are the filtering velocity and the parameters of the filter operating mode. These parameters were determined by technical devices on filter units with the tested bag filters.

For all types of bag filters, the upper limit of the input dust content is limited by the need of the abrupt reduction of the filtration rate, the lower limit is a reduction in capture efficiency. The maximum filtration rates for different types of bag filters are mainly determined by the material properties. Thus, the conducted research revealed that, based on the structural characteristics and indicators of mechanical properties, in the tested glass fiber (sample 10) the rate of filtration was the lowest and did

not exceed 9.2 m/sec. The highest filtration rate was observed in bag filters made of nonwoven materials and was in the range of 20.14 – 24.18 m/sec. Nonwoven materials allow to work at higher rates due to the fact that the capturing process takes place not only on the outside, but also, to a great extent, inside the filtering material. In the metallurgical industry, permitted rates for glass fiber should not exceed 30 m/sec, and for synthetic materials – not more than 90 m/sec. [5].

At higher rates, the difference in pressure increases, resulting in the leakage of dust in the direction of clean gas. At a high filtration rate under the action of air flow, the fibers begin to vibrate, dust particles shift from the settled places, penetrate into the depth of the dust layer and material, resulting in secondary dust removal immediately after conducted regeneration. In addition, when operating at high filtration rates, the service life of the bag filters reduces due to the deformation of the fabric partition.

Studies of hose filters with different input dust content indicate that the higher the dust content is, the more the dust removal is needed. When input dust content reduces, this dependence acquires significant meaning, because the formation of a dust layer on the material requires more time, the lower the concentration of dust in gases is. The data show that the higher dust emissions are, the higher its concentration will be. So, in the investigated hose filter made of arcelon fabric, code 37/T/300 (sample 9), at an input dust content of 96.2 g/sec, dust concentration in gases was 1.102 g/nm^3 , and at 64.67 g/sec – 0.52 g/nm^3 , accordingly. When input dust content of gases changes at short intervals, it is difficult to detect the difference in remaining concentrations.

Increasing of intensity and duration of regeneration immediately after it was carried out reduces the capture efficiency. Thus, the more often the regeneration is carried out, the more often the periods of reduced efficiency are observed. On the other hand, with long intervals of regeneration, the cases of dust leakage are higher, which increases at high pressure difference as a result of micro deformation of the material.

To achieve the efficiency and reliability of woven and nonwoven filters work is possible by observing the parameters of the dust-gas flow (temperature, humidity, the amount of gas-dust flow used, etc.) [6]. Exceeding the temperature of the gases above the allowable leads to the filtering material service life reduction, which becomes tough and brittle. When temperature of gases drops to the dew point, water vapor condenses, moistening the dust settled on the material, so dust particles stick together, obscure the pores, resulting in an abrupt increase of the gas-dynamic resistance of a filter.

Thus, keeping to the technological parameters of the hose filter work in the optimal range leads to high efficiency of gas cleaning. The results of the study are presented in table 2.

Table 2. Efficiency of hose filters gas cleaning made of thermoresistant fibers

Sample variant	Capture efficiency (throughout the melting process), %				
	1 measuring	2 measuring	3 measuring	4 measuring	5 measuring
Poliester fabric (variant 1)	92,7	95,58	93,82	94,98	94,32
Arcelon fabric (variant 9)	98,81	99,21	99,76	99,13	98,89
Glass fabric (variant 10)	99,21	99,51	99,25	99,29	99,15
Nonwoven polyester material (variant 11)	95,64	94,32	91,95	94,17	95,59
Nonwoven arcelon material (variant 13)	98,66	99,07	99,23	97,88	99,11
Nonwoven material made of nomex fibers (variant 14)	98,47	98,62	99,01	99,06	99,26

Analyzing the data obtained, it was found out that the efficiency of dust capturing of filters made of polyester material (var.1 and var.11) after 12 months of operation was lower and amounted to 91.95 – 95.64 % than in units with arcelon material (var. 9 and var.13) – 98.66 – 99.76 %, accordingly.

The capture efficiency of output gases of the tested filtering nonwoven fabric made of nomex fibers (var.14) after 18 months of operation was between 98.47 – 99.26% during melting, and it was 99, 51% of glass fiber (var.10) for the entire melting period.

This indicates about the well-selected fibrous composition of the fabrics and their production method, which determine the structure of the material, as well as the efficiency of the pulse regeneration method for nonwoven filtering materials and back purge for woven filtering materials.

The main task during regeneration is to maintain an operation mode that provides the maximum reduction of the hydraulic resistance of the filter while maintaining high efficiency of the filtration process. It should also be noted that the intensity of regeneration of a dusty filtering material depends directly on the amount of dust adhesion, so, to reduce the hydraulic resistance one should be more concerned about the destruction of the dust layer than about its removal off the material.

Conclusions

1. It is proved that the dense structure of filtering fabrics leads to their rapid contamination with dust particles. Fine fractions of dust, filling the porous layers, are able to form dust formations on the surface and inside the fabrics, resulting in reducing their air permeability. It is higher in the materials made of thermo-resistant fibers than in polyester materials.

2. It is determined that the intensity of regeneration of dusty filtering material directly depends on the amount of dust adhesion, so, in order to reduce the hydraulic resistance one should be more concerned about the destruction of the dust layer than about its removal off the material.

3. It is proved that the filtering capacity of a hose filter is determined by the capture efficiency, which is the main indicator of the quality of its work. Dust capture efficiency was found out to be lower in filters made of polyester material than in the units using arcelon material after 12 months of operation.

References

1. Pelyk L.V. Innovative filters made of polyoxadiazole fibres for industrial gas and dust emissions treatment/ L. V. Pelyk, Volodymyr O. Vasylechko, Petro O. Kutsyk, Yuliya A. Peleh. Adsorption Science & Technology, 2017, Vol. 35 (9–10) 817–824.
2. Material studies and basics of goods production technologies: a textbook/ I. S. Policarpov, R.V. Kyrylchuk, A.M. Uska, L.V. Pelyk.– Lviv: Publishing house LAC, 2015.– 108 p.
3. Pelyk L.V. Scientific basics of formation of the range and quality of filtering textile materials: a monograph / L.V. Pelyk. Publishing house LAC. – Lviv, 2010. – 260 p.
4. Kornienko D. G. Technological standards of permissible emissions of pollutants and instrumental control over them / D. G. Kornienko, V. P. Prymiskyi, V. M. Ivasenko // Eastern European Journal of Advanced Technologies. – 2014. – № 3. – P. 8 – 15.
5. Zashchepkina N. M. Development and quality control of materials to protect people from dust/ N. M. Zashchepkina, N. R. Terenteva // Bulletin of KhNTU. – 2016. –. №3 (58). – P. 99 – 103.
6. Sheliukh Yu.Ye. Modern methods of air purification from industrial types of dust / Yu.Ye. Sheliukh // Bulletin of LSU LS, 2012, № 6, P. 214-218.

STUDY OF INFLUENCE OF THE COTTON KNITTED FABRIC WEAVE ON THE SURFACE GEOMETRY AND LIGHTFASTNESS OF COLOURS

Semeshko O., Asauliyuk T., Saribyckova Yu.

Kherson National Technical University, Ukraine

Introduction

The ability of fibrous materials to retain colour is one of the most important requirements for clothing by consumers. The stability and colour retention of fabrics depends on a number of factors both during the manufacture of the fibrous material and during the operation of the finished product. Considering that the effect of light is one of the significant factors affecting the appearance of clothing regardless of the season, the study of the effect of light on dyed cotton knitted fabric is relevant.

Unfortunately, the overwhelming majority of work in this direction concerns textile materials. So, in studies [1, 2] results are given on the influence of the type of weave, surface density, coverage coefficient, pore structure and colour of cotton fabric on the protection factor of textile material from UV radiation. It has been determined that it is the colour of the cotton fabric that most affects the UV protection factor, and recommendations are made for the design of cotton textiles with sufficient UV protection.

To date, relatively few works have been devoted to the study of the effect of light on knitted materials [3 – 6], and they are mainly aimed at studying the protective properties of knitted materials from UV radiation in relation to human skin. The work [5] is devoted to the determination of the protective properties against UV radiation, as well as the antibacterial activity of knitted cotton fabrics, depending on the type of structure, the method of preparation and final processing and the presence of heavy metal oxides on the knitted fabric. Known work [7], which investigated the effect of weaving cotton knitted fabric on its functional and hygienic properties.

Thus, the analysis of modern scientific works, which study the influence of the structure of fabrics and knitwear on the materials properties,

indicates the absence of systematic studies of the influence of knitwear weave on its lightfastness.

Methods

The main characteristics of cotton knitted fabrics of various weaves and surface density used in the work are given in Table 1.

Table 1. Characteristics of knitted fabrics

Style	Raw material	Weave	Surface density, g/m ²
3V1-67-TDK	100% cotton	Plain	150
76863		Rib 1×1	150
39936		Rib 1×1	280
399318		Pique	170

Cotton knitted fabric was prepared using a one-step combined technology [8] and dyed in a periodic way with bifunctional reactive dyes with monochlorotriazine / vinyl sulfone active groups of the Bezaktiv Cosmos brand (Rot S-C, Blue S-C, Gold S-C) using the technology presented in Table 2.

Table 2. Mode of preparation technology for cotton knitted fabric

Bath composition	Mode
Bath module M=50; A: Ultravon TC – 1 g/l; sodium chloride – 20 g/l; sodium carbonate – 10 g/l (20%); B: dye – 1–3% of material weight; C: sodium carbonate – 10 g/l (80%).	

After dyeing, knitted fabric samples were subject to washing, the mode of which is given in Table 3.

Table 3. Washing mode for cotton knitted fabric after dyeing with reactive dyes

Bath number	Composition	Mode
1	Acetic acid 30% – 0.5 ml/l	T = 50°C, τ = 10 min
2	Hot water	T = 70°C, τ = 10 min
3	Eriopon R – 1 g/l	T = 100°C, τ = 10 min
4	Hot water	T = 70°C, τ = 10 min
5	Cold water	T = 25°C, τ = 10 min

After washing according to the given mode, the knitted fabric samples were dried.

Insolation of dyed samples of knitted fabrics was carried out on a device with a mercury-tungsten lamp RF 1201 BS ("REFOND", China).

The determination of the lightfastness of the colours of knitted fabrics was carried out by establishing colour differences dE using a TCR-200 colorimeter (PCE Instruments, Germany).

The study of the surface roughness of knitted fabrics was carried out by obtaining the roughness profiles of the corresponding samples of knitted fabrics by the optical method by processing digital images of the knitted fabrics surface in the JMicroVision 1.3.2 software environment. Next, the main indicators of surface roughness were calculated: the height of the profile at ten points R_z and the arithmetic mean of the deviations of the profile R_a according to formulas (1), (2), in accordance with ISO 4287: 1997 "Geometrical Product Specifications (GPS) – Surface texture: Profile method – Terms, definitions and surface texture Parameters" [9].

$$R_z = \frac{\sum_{i=1}^5 y_{pmi} + \sum_{i=1}^5 |y_{vmi}|}{10}, \quad (1)$$

where y_{pmi} – height of i -th the highest profile ridge;

y_{vmi} – depth of i -th the largest valley of the profile.

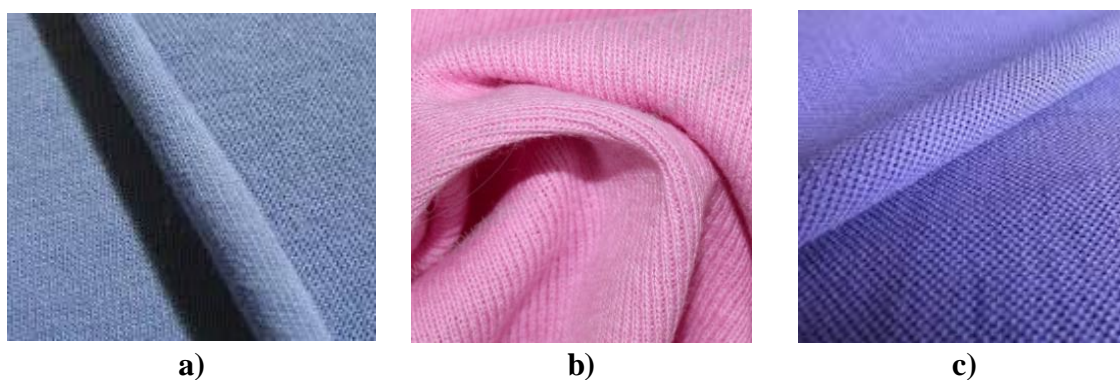
$$R_a = \frac{1}{2n} \sum_{i=1}^n y_{pmi} + \frac{1}{2n} \sum_{i=1}^n |y_{vmi}|, \quad (2)$$

where n – number of selected points at base length.

Experimental and Results

The structural properties of knitted fabrics, which affect the complex of characteristics of their wear resistance, include the properties that are formed at the stage of spinning and knitting of knitted fabrics – weave and surface density. Therefore, further in the work, the influence of the indicated structural properties of cotton knitted fabrics on their lightfastness will be investigated.

The study was carried out using samples of cotton knitted fabrics of various weaves, their appearance is shown in Fig. 1.



**Fig. 1. Appearance of cotton knitted fabric of different weave:
a) plain; b) rib 1×1; c) pique.**

The plain weave – single plain stitch – belongs to the class of the main cross-knitted single weaves and has a different character of the front and back sides (Fig. 1, a). On the front side there are tightly located vertical looped columns formed by loop sticks, and on the back side there are transverse rows (stripes) formed by arcs of loops. A distinctive feature of the surface is that the loops are the same in shape and size. The front side is smooth, shiny, the back is rough, matte with transverse stripes. The plain weave is the most common and simple cross-knitted weave, widely used for the manufacture of linens, sportswear, hosiery and outerwear. The positive properties of the plain weave are high extensibility, elasticity and strength. A negative property of the plain weave is a slight horizontal blooming. If the fabric is knitted with a strip, then it will bloom in the opposite direction to knitting, if it is knitted with a tube, then it will bloom

in two directions – from top to bottom and from bottom to top. The plain weave is twisted around the edges, which leads to inconveniences during processing and cutting of the fabric [10 – 12].

The rib weave is a double cross-knitted weave, in which the front and back sides are formed by vertical looped columns, which are arranged in a checkerboard pattern (Fig. 1, b). In the rib weave, the same thread sequentially forms loops on the adjacent needles of two sets of needles, which go either to the front side, then to the back side. The needles are arranged in a checkerboard pattern. In an unstretched form, the rib resembles the front side of the plain weave, and in the stretched one it is clearly visible that the looped columns alternate with looped arcs. Depending on the combination of front and back looped columns, you can get different types of rib weaves (weaving of different pattern area), which are indicated by numbers (1×1 , 2×1 , 2×3 , etc.). In this case, the first figure shows the number of front columns, the second – the number of back columns.

Compared to plain knitted fabric, the rib knitted fabric has increased extensibility, especially in width (about three times more than in length). That is why it is recommended to use it in those products that should have greater extensibility in width and shorter in length.

The rib knitted fabric, in addition to increased extensibility, is characterized by high elasticity, less ability to bloom, no curling of the edges. It is widely used for the manufacture of outerwear, underwear, sports knitwear, hosiery [10 – 12].

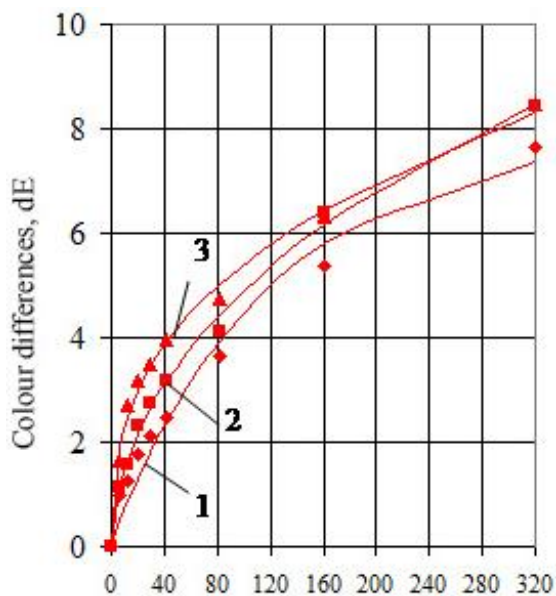
A single pique is a combined weave that combines cross and warp weaves of the main, derivative, and drawing classes (Fig. 1, c). It is obtained on the basis of joining the loop rows of the interlock with the rows of press weave, which contributes to a significant decrease in the stretchability of the fabric in width and increasing the dimensional stability. Fabrics of combined weaves, as the least stretchable and unraveling, have a high dimensional stability and are used in the production of knitted

outerwear. For their specific properties, these knitted fabrics are called fabric-like [10 – 12].

With this in mind, Fig. 2 shows the results of a study of the kinetics of colours photodegradation of cotton knitted fabric samples of different weaves which were dyed with reactive dyes of the Bezaktiv brand at a concentration of 1% by weight of the material.

With this in mind, Fig. 2 shows the results of a study of the kinetics of colours photodegradation of cotton knitted fabric samples of different weaves which were dyed with reactive dyes of the Bezaktiv brand at a concentration of 1% by weight of the material.

The results obtained (Fig. 2) indicate that the greatest photodestruction is observed for the Bezaktiv Cosmos Rot S-C dye, and the smallest for Bezaktiv Cosmos Blue S-C, regardless of the type of knit weave. In addition, the data obtained show that the weaving of cotton knitted fabric affects the lightfastness of dyes with reactive dyes. The greatest photodegradation of the colours is observed on the knitted fabric of the pique weave. Colours on the samples of rib 1×1 and plain knitted fabrics experience less photodegradation. This dependence is observed for all investigated reactive dyes.

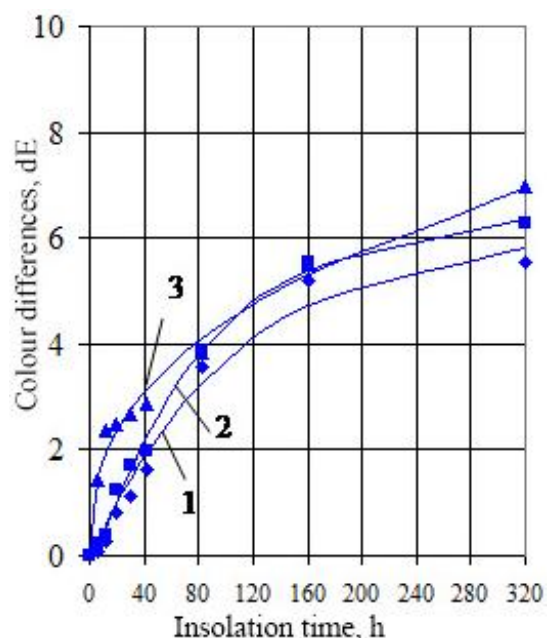


1) plain: $y = 7,840(1,018 - e^{-0,008x})$,
 $S=0,296$, $R=0,992$;

2) rib 1×1: $y = \frac{0,086+43,684 \cdot x^{0,553}}{101,029+x^{0,553}}$, $S=0,125$,
 $R=0,999$;

3) pique: $y = \frac{1,239+504,262 \cdot x^{0,375}}{519,541+x^{0,375}}$, $S=0,152$,
 $R=0,999$.

a)

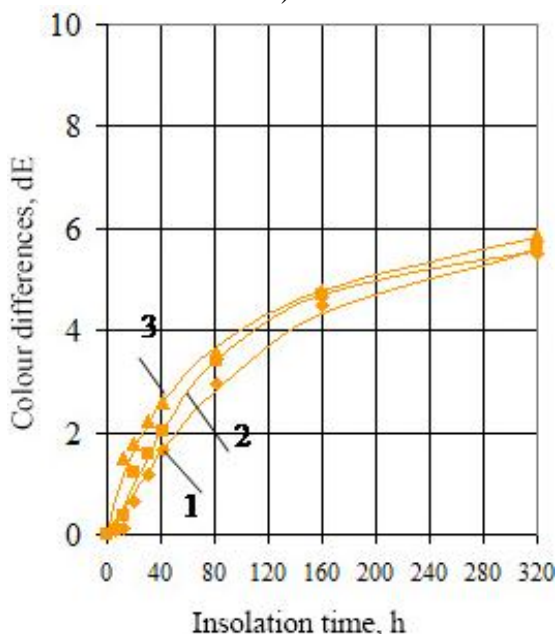


1) plain: $y = 6,215(0,986 - e^{-0,009x})$,
 $S=0,240$, $R=0,993$;

2) rib 1×1: $y = \frac{2,013+7,113 \cdot x^{1,438}}{467,716+x^{1,438}}$, $S=0,121$,
 $R=0,999$;

3) pique: $y = \frac{14,887+1347,483 \cdot x^{0,391}}{1842,803+x^{0,391}}$,
 $S=0,177$, $R=0,997$.

b)



c)

1) plain: $y = 6,183(0,989 - e^{-0,008x})$,
 $S=0,143$, $R=0,997$;

2) rib 1×1: $y = \frac{-4,007+6,407 \cdot x^{1,300}}{266,089+x^{1,300}}$, $S=0,094$,
 $R=0,999$;

3) pique: $y = \frac{-2,546+8,103 \cdot x^{0,819}}{43,681+x^{0,819}}$, $S=0,177$,
 $R=0,996$.

Fig. 2. Kinetics of photodestruction of cotton knitted fabrics of different weaves, dyed with reactive dyes: a) Bezaktiv Cosmos Rot S-C; b) Bezaktiv Cosmos Blue S-C; c) Bezaktiv Cosmos Gold S-C.

Thus, when studying the effect of weave on the lightfastness of dyed knitted fabrics made of natural fibers, the regularity was found, which made it possible to place the studied weaves in the order of increasing their lightfastness in the following row: pique < rib 1×1 < plain.

It is possible to quantify the unevenness of the surface of knitted fabrics, depending on their weave and surface density, by determining the roughness of the knitted fabric.

The roughness of fibrous materials is an important aspect of their quality and determines the surface properties and appearance of fabrics, knitwear and products from them [13 – 17].

The roughness of the material is characterized by the parameters given in ISO 4287: 1997 "Geometrical Product Specifications (GPS) – Surface texture: Profile method – Terms, definitions and surface texture Parameters" [9]. According to it, the surface roughness is a set of surface irregularities with a relatively small step, which is usually determined by its profile, which is formed in the section of this surface by a plane perpendicular to the nominal surface. In this case, the roughness profile is considered along the length of the baseline, which is used to highlight irregularities and quantify their parameters.

When evaluating the surface roughness, a reference system is taken as a basis, in which the midline of the profile serves as the baseline. This is the baseline, which has the shape of the nominal profile and is drawn so that within the base length the average deviation of the profile to this line is minimal. The midline of the profile is equidistant from the lines of the profile ridges and valleys, which respectively pass through the highest and lowest points of the profile within the base length.

The main characteristics of the roughness profile are the height of its ridges y_{pm} and the depth of its valleys y_{vm} . These are the distances from the midline of the profile to the highest point of the ridges and the lowest point of the valley, respectively.

To assess the surface roughness of fibrous materials, the altitude criterion R_z is widespread — the height of the profile at ten points [9]. It is

the sum of the average absolute values of the heights of the five largest profile ridges and the depths of the five largest profile valleys within the profile length. Also important in assessing the surface roughness is the criterion of the arithmetic mean deviation of the R_a profile. This is the arithmetic mean of the absolute values of the profile deviations within the base profile length [9, 18].

Thus, to calculate the roughness parameters of knitted fabrics, it is necessary to obtain their roughness profiles.

Studies aimed at measuring and assessing the profile characteristics of the roughness of textile materials using various devices are presented in [14, 15], where all methods are divided into contact and non-contact. Contact methods for determining roughness provide for direct measurement of the relief of textile material using a multidirectional tribometer [15], an optical multidirectional roughness meter [19], the so-called "vibrating blade" [20], etc. Non-contact roughness measurement is performed using various optical systems of profilometers: Talysurf CCI 6000 [21], Micro Measure 3D Station [22], MicroXAM-100 and MicroXAM-1200 [23], helium-neon laser [24, 25], atomic force microscopy and confocal microscopy [25], etc. However, these devices are expensive and not widely available. The method for determining the roughness of textile materials using software products for processing scanned images, proposed in [16], does not require additional equipment and is available. Therefore, in this work, the determination of the roughness indicators of knitted fabrics was carried out by a contactless optical method.

The obtained profiles of the surface roughness of the cotton knitted fabric samples of the investigated weaves and the surface density along the looped columns and along the looped rows are shown in Fig. 3.

According to the obtained profiles of the roughness of cotton knitwear (Fig. 3), it can be concluded that the investigated knitted fabrics have different roughness, which depends on their weave. Knitted fabric with plain weave has a uniform roughness of low values in both directions. For the rib weave, there is an increase in roughness along the looped rows.

Pique knitwear is characterized by high roughness values both along the looped columns and along the looped rows.

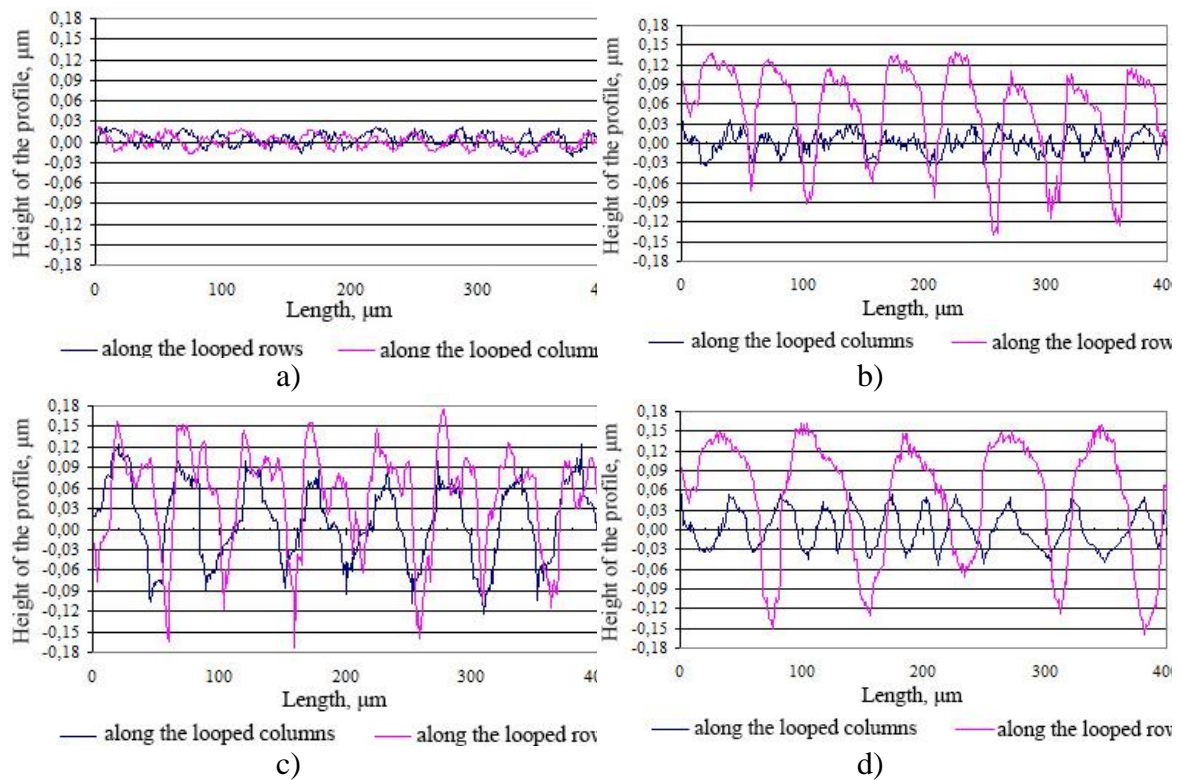


Fig. 3. Roughness profiles of cotton knitted fabric samples:
 a) plain; b) rib, 150 g/m²; c) pique; d) rib, 280 g/m².

On the basis of the obtained roughness profiles, the main roughness characteristics were calculated: the profile height at ten points R_z and the arithmetic mean of the profile deviations R_a . The research results are presented in Table 4.

Table 4. Influence of weave and surface density on surface roughness characteristics of cotton knitted fabrics

Weave and surface density	Profile height at ten points $R_z, \mu\text{m}$			Arithmetic mean of the profile deviations $R_a, \mu\text{m}$		
	Along the looped columns	Along the looped rows	Mean	Along the looped columns	Along the looped rows	Mean
Plain	0.018	0.018	0.018	3.09	4.08	3.58
Rib 150 g/m ²	0.029	0.122	0.076	6.39	6.36	6.38
Rib 280 g/m ²	0.044	0.142	0.093	6.62	7.11	6.86
Pique	0.152	0.139	0.146	8.57	7.75	8.16

The results of calculating the main roughness indices R_z and R_a (Table 4), which characterize the unevenness of the knitted fabric surface, indicate that the roughness of knitted fabrics made of natural fibers depends on the weave and increases in the row plain < rib < pique and with an increase in the surface density of knitwear.

The diagrams in Fig. 4 summarizes the results of the study of photodegradation of colours of knitted fabrics for 320 hours of insolation and roughness indicators depending on the weave of knitwear.

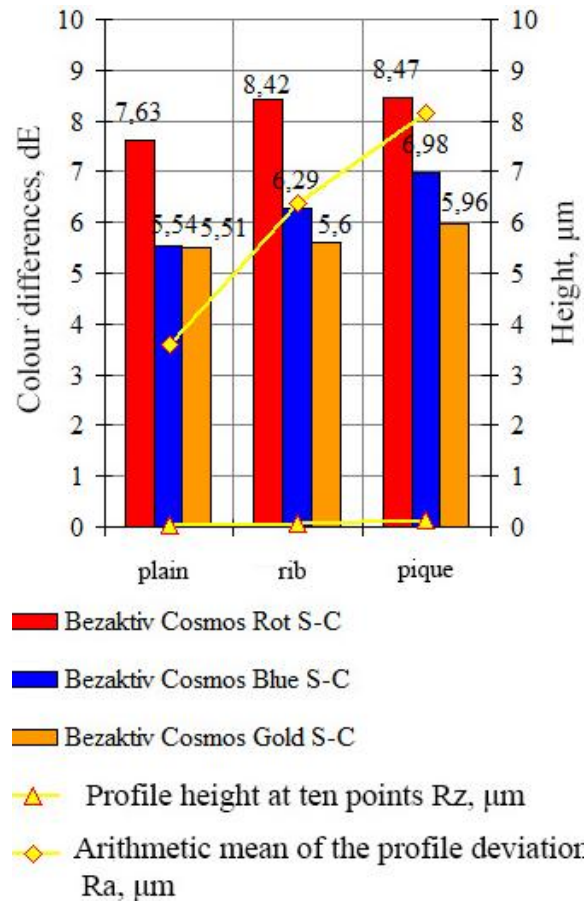


Fig. 4. Influence of weave on surface roughness and photodegradation of colours of cotton knitwear dyed with reactive dyes.

Results in Fig. 4 show that with an increase in the roughness of knitted fabrics, the photodegradation of colours with reactive dyes increases.

The results obtained confirm the effect of the surface structure of knitted fabrics, namely weave and surface density, on the process of

photodegradation of colours and show that the amount of dye that has undergone photodegradation increases with an increase in the surface roughness of the knitted fabric.

Taking into account the results of determining the surface roughness of knitted fabrics and the features of the process of photodegradation of colours, depending on the weave of material, the schematic representation of the investigated knitted fabrics and the mechanism of light action on them are presented in Fig. 5.

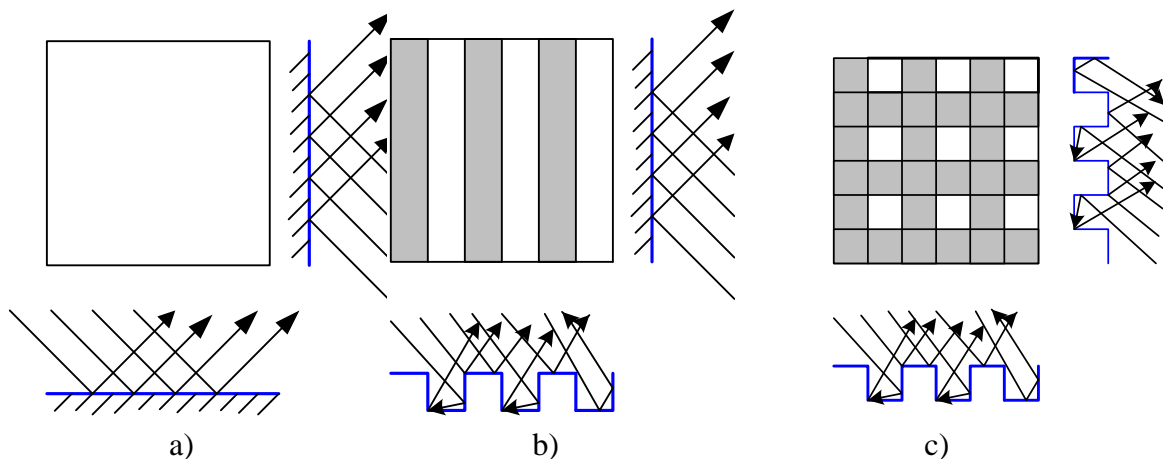


Fig. 5. Mechanism of light action on knitted fabric of different weaves: a) plain; b) rib 1×1; c) pique.

Thus, the conducted studies of the roughness of knitted fabrics make it possible to determine the relationship between the lightfastness of colours and the structural properties of knitwear. The relatively uniform surface of plain weave knitted fabrics evenly distributes energy and reflects more incident light than knitted fabrics with an uneven rough surface of rib 1×1 and pique weave. Knitted fabrics with a more uneven rough surface (rib 1×1 and pique) reflect less light, the incident rays are refracted and again fall on the surface of the knitwear, which leads to greater photodegradation of its colours.

Conclusions

On the basis of the obtained roughness profiles by calculating the main characteristics of roughness – the height of the profile at ten points R_z

and the arithmetic mean deviation of the profile R_a – it was found that for the investigated knitted fabrics the photodegradation of colours increases with an increase in the roughness in the row plain < rib 1×1 < pique and with an increase in the surface density of knitwear. Based on the studies carried out, it can be concluded that knitted fabrics, which have an uneven rough surface structure, necessarily require light-shielding treatment.

References

1. Dobnik Dubrovski P. Effects of Woven Fabric Construction and Color on Ultraviolet Protection / P. Dobnik Dubrovski, D. Golob // *Textile Research Journal*. – 2009. – Vol. 79. – P. 351-359. doi: 10.1177/0040517508090490.
2. Dobnik Dubrovski P. Prediction of the Ultraviolet Protection of Cotton Woven Fabrics Dyed with Reactive Dystuffs / P. Dobnik Dubrovski, M. Brezocnik // *Fibres & Textiles in Eastern Europe* – 2009. – Vol. 17, Issue 1 (72). – P. 55-59.
3. Çelik N. Effect of the particle size of fluorocarbon-based finishing agents on fastness and color properties of 100% cotton knitted fabrics / N. Çelik, H.İ. İçoğlu, P. Erdal // *Journal of the Textile Institute*. – 2011. – Vol. 102(6). – P. 483–490. doi:10.1080/00405000.2010.489743.
4. Sheshachala D. Comparative Study of Bamboo and Cotton Knitted Fabric / D. Sheshachala, D.N. Sandeep, S. Santosh, H. Chetan // *Man-Made Textiles in India*. – 2008. – Vol. 51, Issue 9. – P. 300-303.
5. Ibrahim N.A. UV-protecting and antibacterial finishing of cotton knits / N.A. Ibrahim, M. Gouda, S.M. Hussein, A.R. El-Gamal, F. Mahrous // *Journal of Applied Polymer Science*. – 2009. – Vol. 112(6). – P. 3589-3596. doi:10.1002/app.29669.
6. Wong W.-Y. Ultraviolet protection of weft-knitted fabrics / W.-Y. Wong, J.K.-C. Lam, C.-W. Kan, R. Postle // *Textile Progress*. – 2016. – Vol. 48(1). – P. 1-54. doi:10.1080/00405167.2015.1126952.
7. Ibrahim N.A. Effect of Knit Structure and Finishing Treatments on Functional and Comfort Properties of Cotton Knitted Fabrics / N.A. Ibrahim, T.F. Khalifa, M.B. El-Hossamy, T.M. Tawfik // *Journal of industrial textiles*. – 2010. – Vol. 40, Issue 1. – P. 49-64. doi: 10.1177/1528083709357975.
8. Skalozubova N. Designing a composition formulation of surface active substances for the pretreatment of knitted fabric / N. Skalozubova, A. Kunik, O. Semeshko, J. Saribyekova, S. Myasnikov // *Eastern-European Journal of Enterprise*

Technologies. Technology organic and inorganic substances. – 2016. – №4/6(82). – P. 29-36.

9. ISO 4287:1997. Geometrical Product Specifications (GPS) – Surface texture: Profile method – Terms, definitions and surface texture Parameters.

10. Halyk I.S. Tovaroznavstvo neprodovol'chykh tovariv. Chastyna 2. Tovaroznavstvo trykotazhnykh tovariv / I.S. Halyk, B.D. Semak. – K.: NMTS «Ukooposvita», 2001. – 292 c.

11. Voynash L.H. Tovaroznavstvo neprodovol'chykh tovariv / L.H. Voynash, I.O. Dudla, D.I. Koz'mych, N.V. Pavlovs'ka: [pid red. Voynasha L.H.]. – Kyiv: NMTS «Ukoopspilka», 2004. – 436 s.

12. Charkovskiy A.V. Stroyeniye i proizvodstvo trikotazha risunchatykh i kombinirovannykh perepleteniy / A.V. Charkovskiy. – Vitebsk: UO «VGTU», 2006. – 416 s.

13. Apurba D. A Study on Frictional Characteristics of Woven Fabrics / D. Apurba, V.K. Kothari, N. Vandana // Autex Research Journal – 2005. – Vol. 5, Issue 3. – P. 133-140.

14. Najeh M. Statistical analysis of surface roughness parameters for weft knitted fabrics measured by the Textile Surface Tester / M. Najeh, S. Mehdi, S. Faouzi // Journal of Engineered Fibers and Fabrics. – 2012. – Vol. 7. – P. 104-112.

15. Kolcavova Sirkova B. Description of fabric thickness and roughness on the basis of fabric structure parameters / B. Kolcavova Sirkova // Autex Research Journal. – 2012. – Vol. 12, No 2. – P. 40-43.

16. Kang T.J. Fabric surface roughness evaluation using wavelet-fractal method. Part I: Wrinkle, Smoothness and Seam Pucker / T.J. Kang, S.C. Kim, I.H. Sul, J.R. Youn, K. Chung // Textile Research Journal. – 2005. – Vol. 75 (11). – P. 751-760.

17. Sülar V. Roughness and Frictional Properties of Cotton and Polyester Woven Fabrics / V. Sülar, E. Öner, A. Okur // Indian Journal of Fibre & Textile Research. – 2013. – Vol. 38. – P. 349-356.

18. Parshev S.N. Issledovaniye parametrov sherokhovatosti poverkhnosti / S.N. Parshev, A.YU. Ivannikov. – Volgograd: IUNL VolgGTU, 2010. – 14 s.

19. Bueno M.A. Effect of grain size and abrasion duration on the state of textile fabric surfaces / M. A. Bueno, B. Lamy, M. Renner // Wear. – 2002. – Vol. 253. – P. 448-457.

20. Fontaine S. Development of a Sensor for Surface State Measurements Using Experimental and Numerical Modal Analysis / S. Fontaine, C. Marsiquet, N. Nicoletti, M. Renner, M. A. Bueno // Sensors and Actuators A. – 2005. – Vol. 120. – P. 507-517.

21. Ynterferentsyonnyy mykroskop SSI. [Elektronnyy resurs]. – Rezhym dostupu: <http://www.vniims.ru/nano/participation/cci.html>.
22. Trekhmernyy beskontaktnyy profylometr. [Elektronnyy resurs]. – Rezhym dostupu: <http://portal.main.tpu.ru/departments/centre/cism/prib/measure-3d>.
23. Opticheskiye profilometry MicroXAM – Opticheskiye i stilusnyye profilometry – INTERTECH Corporation. [Yelektronniy resurs]. – Rezhim dostupu: <http://www.intertech-corp.ru/aboutproduct.asp?gr=21&subgr=71&prid=195>.
24. Ezazshahabi N. Surface Roughness Assessment of Woven Fabrics Using Fringe Projection Moiré Techniques / N. Ezazshahabi, M.A. Tehran, M. Latif, K. Madanipour // FIBRES & TEXTILES in Eastern Europe. – 2015. – Vol. 23, Issue 3(111). – P. 76-84.
25. Romdhani Z. Surface Roughness Evaluation of Treated Woven Fabric by Using a Textile Surface Tester / Z. Romdhani, M. Hamdaoui, A. Baffoun, N. Maatoug, S. Roudesli // Research Journal of Textile and Apparel. – 2013. – Vol. 17, Issue 2. – P. 51-60.

DEVELOPMENT OF A DEVICE AND METHODS FOR ASSESSING THE FLAMMABILITY OF MATERIALS

Zasornov A., Zasornova I.
Khmelniyskyi National University, Ukraine

Introduction

When creating a heat-protective package of materials for uniform, it is necessary to perform preliminary tests of materials in order to assess their flammability. The essence of the technique is to determine the ability of materials not to support the combustion process after contact with an open flame of a gas burner. The test procedure complies with the international standard ISO 15025 [1].

Methods

The development of the device and methods is impossible without the theoretical foundations of the method of assessing the flammability of materials. There are a number of methods that are designed to assess the flammability of textile materials under the action of open flames [1-6]. The essence of these methods is that the samples of materials that are fixed in a certain position (vertically, horizontally or at an angle) are exposed to an open flame of a gas or alcohol burner. To increase the reliability and repeatability of the test results, the size and parameters of the burner flame are adjusted to give it certain characteristics (corresponding to the requirements of each method): temperature, height, duration of action on the sample.

To assess the flammability of materials, the following characteristics are used firstly: the speed of flame spreading, the time of final combustion, the time of final decay.

The main differences that distinguish these methods of testing the flammability of materials are the test parameters, as well as the method of recording the movement of the flame through the sample. Most methods involve visually observing the movement of the flame. The registration of

the position of its front, in a certain period of time, is usually carried out by the operator using mechanical or electrical time meters. Therefore, the test results largely depend on the operator's qualifications, skills and attention, which makes a subjective error in the study.

The closest in technical essence is the method described in the international standard [1]. In the method regulated by the standard, an attempt is made to reduce the influence of the operator on the test results. According to this document, to control the movement of the flame front, it is necessary to use cotton marking threads, which are located perpendicular to the sample material, at a certain distance from the gas burner, the beginning of the sample and from each other. The marking threads are in a taut state and are connected to timers. Under the action of heat, a certain marking thread is destroyed and the timer records the time during which this destruction occurred. It is believed that the moment of destruction of the cotton marking threads is the moment when the edge of the flame reaches this area of the sample.

Obviously a simple methodological error - the time of destruction of the cotton thread under the action of flame (or heat), and the time of reaching the edge of the flame of the sample at the location of the thread have different physical essence, characterize different processes and time values.

The first characteristic shows the time of reaching a certain temperature at the location of the thread. This temperature corresponds to the destruction temperature of cotton fiber materials and is approximately 180oC. As a result, the destruction of the marking thread may occur not when the front reaches the flame of the cotton thread, but from thermal exposure (convection, thermal radiation). Therefore, this characteristic is not objective in its use to determine the rate of combustion of materials. In addition, the thermophysical properties of the polymer from which the textile (or other) material is made may not coincide with the thermophysical properties of cotton thread (this happens most often), and therefore the results of the study are not correct for this reason.

The second characteristic shows the time of reaching the edge of the flame of the same place of the sample, where in the first case the marking thread should be located (the temperature in this area significantly exceeds the destruction temperature of cotton thread), respectively, the value will be different. It is the exponent of this second characteristic that determines the speed of flame propagation.

Therefore, the disadvantage of the method described in the international standard [1] is an inaccurate information about the flammability of materials by controlling the time of failure of cotton threads, which are located in certain areas of the material, rather than the time of reaching the flame front certain areas.

The essence of the proposed method is that the sample material is fixed in a holder mounted in a fixed position relative to the flame of the burner (vertically or at an angle). A burner with a flame that has certain parameters is installed in a given place and position. When the burner is installed, the timers are switched on. The open flame of the burner acts on the lower edge of the sample for a certain period, igniting it. The control and determination of the moments of passage of the flame front of a certain distance on the sample is carried out using photoelectric elements located at strictly fixed distances from the beginning of the sample (lower edge), along its length and from each other. When the front of the flame reaches a certain area of the sample, which is located opposite the working window of a certain photovoltaic cell, the latter generates an electrical signal. Each photovoltaic cell is connected to a corresponding timer, which at the moment of receiving a signal from the photovoltaic cell automatically records the time of passage of the flame front of a certain distance. It is equal to the distance from the beginning of the sample to a certain photovoltaic cell. The calculation of the flame propagation rate in a certain area of the sample is carried out according to the known formula:

$$V = S/T \quad (1)$$

where: S – the distance from the beginning of the sample to a specific photoelectric cell, mm;

T – the time during which the flame front passes the distance from the beginning of the sample to a certain photoelectric cell, sec.

On the “Fig. 1” a list of technical means for implementing the proposed method is schematically presented.

The scheme contains a sample of material - 1, burner - 2, photoelectric cells - 3, timers - 4.

The method of implementation of the proposed way of assessing the flammability of materials under the open flame is the following:

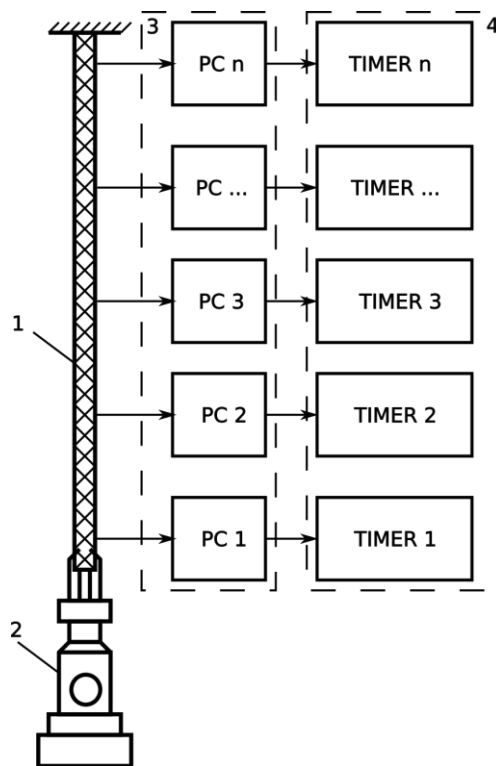


Fig. 1. The scheme of implementation of the method of assessing the flammability of materials

Sample 1 of the material is fixed in the sample holder. The burner 2 is installed and heated for 2 minutes. A certain height of the flame, with the vertical location of the burner 2 is adjusted and set. The height of the flame is set depending on the test conditions, but such that when the burner 2 is in the operating position, the upper limit of its flame is below the sample 1, from which the information about the presence or absence of flame in this area, the first (lower) photovoltaic cell (photovoltaic cell) (PC1) is

removed. The burner 2 is placed below the lower cut of the sample 1 (so that it is on the same axis with the center line passing along the sample 1), while simultaneously turning on the timers (timer) 4. The flame of the burner 2 is operated for a certain time (depending on the type of material and its operating conditions). As a result of the flame of the burner 2, the sample ignites. After some time, the first photovoltaic cell (PC1) enters the sampling area to ignite the sample. The photovoltaic cell (PC1) turns off the first timer, which shows the time the flame has passed the distance between the lower edge of sample 1 and the photoelectric cell (PC1). After the flame has passed the distance from the lower edge of sample 1 to the second photovoltaic cell (PC2), the latter switches off the second timer, which shows the time of the flame front of the distance from the beginning of sample 1 to the second photoelectric cell (PC2). In the future, the process of measuring the time of passage of the flame front of the distance from the beginning of the sample 1 to the next photovoltaic cells 4 is repeated. The obtained results (indicators of time meters) calculate the speed of flame propagation in a certain area of the sample (according to formula 1).

Thus, due to the fact that the measurement results are obtained without the subjective participation of the operator, the proposed method allows to obtain reliable data on the flammability of materials under the open flame, using an objective criterion - the speed of flame propagation.

Results

Using the theoretical foundations of the method of assessing the flammability of materials, which is given above, a device and techniques for assessing the flammability of materials AFM-1 (assessment of flammability of material) were developed. The developed AFM-1 device is intended for assessment and research of combustibility of materials under the open flame and can be used in laboratories and the organizations which are involved in creation of materials, means of personal protection and research of their properties.

The operation of the device is based on the fact that the flame with the specified parameters from the unified burner acts for a certain period of time on a vertically located (if necessary at a certain angle) sample of the material. The period of time of flame spreading is considered to be the time (in seconds) required for the front of the flame to travel the distance between certain areas of the sample. The moments of reaching these areas by flame are fixed with the help of photoelectric elements, which change the electrical resistance when the amount of light falling on their photodetector surface changes. The signals are sent to electronic timers, which automatically record the time of passage of the flame of certain areas.

The device is a complex electronic-mechanical device, which is conventionally divided into two units connected to each other: thermal unit 1 and control unit 2 (“Fig. 2”).

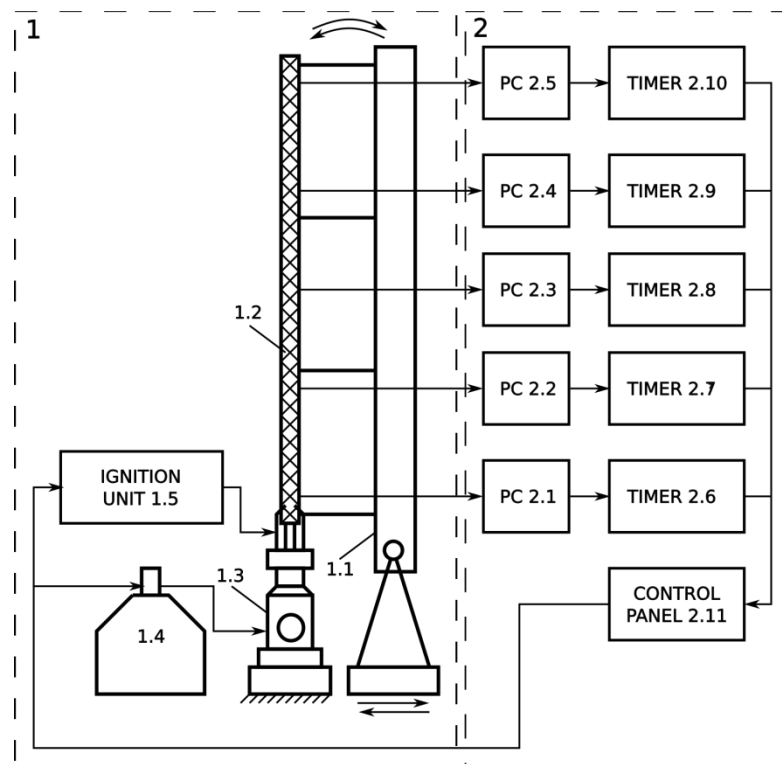


Fig. 2. The structured scheme of the device AFM-1

The heat unit 1 consists of a holder 1.1 of the sample 1.2, a gas burner 1.3 connected to the cylinder 1.4. The cylinder 1.4 is opened and the

gas burner 1.3 is ignited by means of the automatic ignition unit (ignition unit) 1.5, which in turn is controlled by the control unit 2.

The control unit 2 contains photovoltaic cells 2.1 - 2.5, which are located in a ruler (not shown on the diagram), which is fixed to the holder 1.1 at a certain distance from the longitudinal axis of the sample 1.2 and from the lower edge of the sample 1.2. Each photovoltaic cell 2.1 - 2.5 is connected to a corresponding timer 2.6 - 2.10.

The control unit 2 has a control panel (control panel) 2.11 through which the selection of operating modes and control of the device. Work on the device by means of the control panel consists in the following ("Fig. 3").

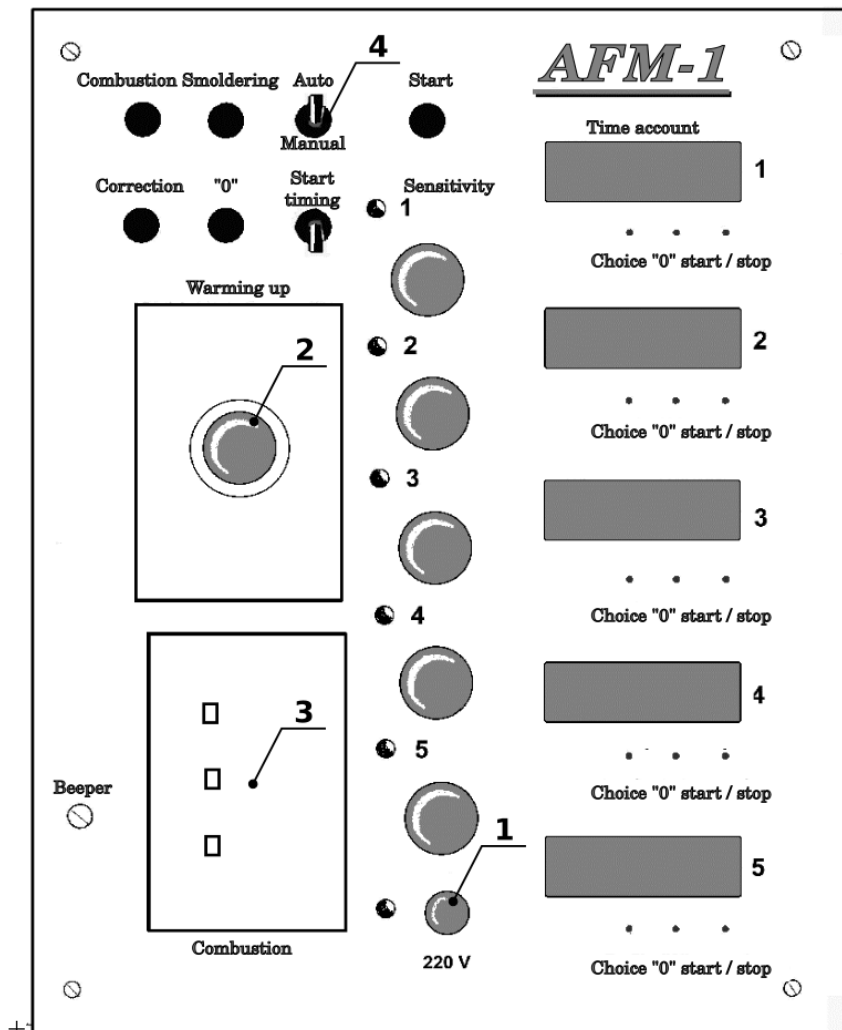


Fig. 3. The front panel of the control unit of the device AFM-1

Advanced technologies in education, industry and the environment

The device is turned on in the 220 V alternating current and press button 1 on the control panel. The power indicator next to button 1 should light up.

Use the small handle of the relay to select the 1 hour (warming up) 2, and use the large handle to set the period to the hour (2 hours), which is necessary for the burner program.

Push the "Start" button. When the signal from the control unit is turned on, the electromagnet valve of the gas cylinder 1.4 (gas is supplied to the gas fired gas cylinder 1.3) and immediately enters the institute fired up 1.5 of the heat block 1. Vuzol fired up 1.5 the gas fired up to 1.3.

When the program finishes 1.3 (at least 2 quills), just a sound signal (Beeper) relay to the hour of program 2, behind the aid of the handle for regulating the amount of gas supply, regulate the half of the gas burner 1.3. Gas fighter 1.3 is located in the vertical position. Dovzhina half from the stabilizer of the half shaft 1.3 to the tip of the cone of the second part of the half is (40 ± 2) mm.

Turning the screws for adjusting the position of the gas burner 1.3 relative to the vertical and horizontal axes have the burner 1.3 in a given position, which depends on the type of test (test with edge ignition, or test with surface ignition):

- when the edge ignition of the sample burner in relation to the sample holder is placed according to "Fig. 4";

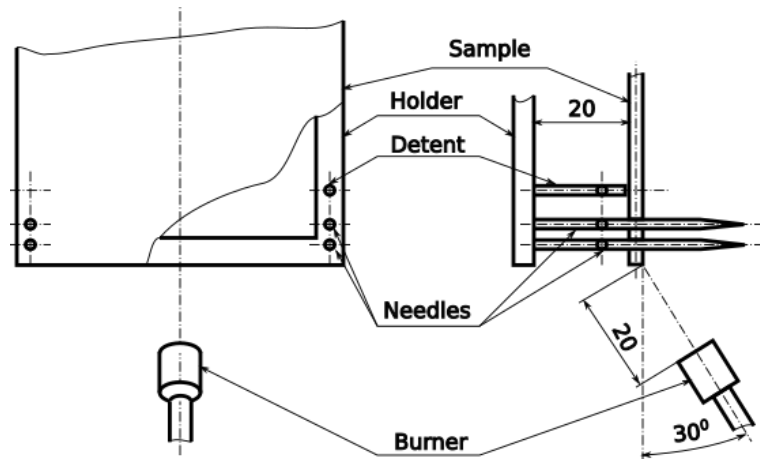


Fig. 4. Layout of the burner at the edge ignition of the sample

- at surface ignition the burner is set according to “Fig. 5”.

Fix the sample 1.2 on the pins (needles) of the holder of the sample 1.1 in such a way that the pins pass through the marked, using a template, place of the sample and that the latter was placed at a distance of 20 mm from the frame of the holder 1.1.

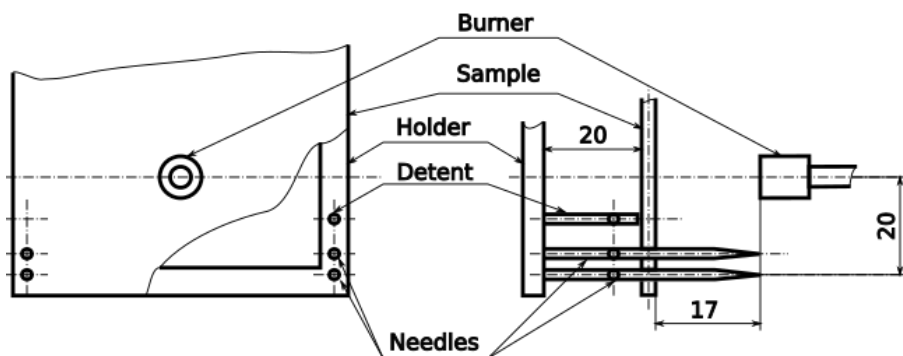


Fig. 5. Layout of the burner during surface ignition of the sample

The automatic mode of operation of the device is selected, for which the toggle switch 4 is moved to the position "Auto.", And the toggle switch "Start timing" to the upper position.

To make sure the device works, the "Sensitivity" is installed on the device. To do this, turn each “Sensitivity” knob on the control panel in the direction of the time arrow until the corresponding indicator lights up. After lighting the indicator, the handle is turned in the opposite direction

Advanced technologies in education, industry and the environment

until it goes out. In case of low light, the indicators may not light up. In this case, set the corresponding "Sensitivity" knobs to the maximum gain position.

Time switch 3 is used to set the burner burning time (flame effect on the test) to 5 seconds.

The indicators on the scoreboard are set to zero. To do this, the "Correction" button is pressed and hold it in this position for 3-5 seconds. If not all timers have reached zero, the pin is used to press the "0" buttons below the corresponding timers.

The holder 1.1 with the breakdown 1.2 is moved to the working position.

The operating position of the sample holder 1.1 is considered to be that at which 20 mm of flame from the burner 1.3 reaches the lower edge of the sample 1.2. The operating position is set by moving the carriage on which the holder 1.1 is fixed in the direction of the gas burner 1.3, to the stop of the starting rod in a stationary platform and pressing the microswitch mounted on the platform on which the gas burner 1.3 is placed.

When the holder 1.1 with breakdown 1.2 is moved to the working position, the "Combustion" relay is activated, which switches on the time meters 2.6-2.10 and starts counting the time of the flame action on the sample.

After 5 seconds of the burner flame on the test, the Combustion relay switches off the solenoid valve and stops the gas burning.

When the flame moving through the sample reaches the first photoelectric element 2.1, the latter switches off the first timer 2.6. If the flame front reaches other photovoltaic cells 2.2-2.5, they stop counting the time of the corresponding meters 2.7-2.10. Remove the carriage with the

Advanced technologies in education, industry and the environment

holder 1.1 of the sample from the working area. Record the results of time measurements in the log of experimental results. Clean the carriage with holder 1.1 from residues and combustion products. Similarly, tests of other samples of material.

If the sample does not ignite after the flame acts on the sample for 5 seconds, set the burner burning time to 15 seconds using relay 3 and repeat the test and data processing.

When testing materials that stop burning with a flame gradually or immediately after the burner has stopped working on the sample for 15 seconds (limited flammable or non-flammable), the manual mode of operation of the device is used.

When working in manual mode, there is a need to perform preparatory actions then to switch the toggle switch to select the operating mode to the "Manual" position, and the toggle switch "Start timing" to the lower position (photovoltaic cells 2.2-2.5 in this mode do not work).

The maximum "Sensitivity" of photovoltaic cells is set.

Using the time relay 3 the burner burning time of 15 seconds is set.

The indicators on the scoreboard are set to zero.

The holder 1.1 with the breakdown 1.2 is moved to the working position.

After 15 seconds of the burner flame on the test, the Combustion relay switches off the solenoid valve and stops the gas from burning. When the gas supply is stopped (burner stops burning), the first timer is switched on.

In the future, the combustion process is monitored by the operator. At the moment of the termination of independent burning of sample press the "Combustion" button. In this case, 1 time meter will record the time of

residual combustion of the sample. At the same time, the second timer will start counting down the decay time of the sample.

At the moment of cessation of decay of the sample press the "Smoldering" button. 2 the time meter records the decay time of the sample.

Table 1 shows the main technical characteristics of the developed device AFM-1.

Table 1. Technical characteristics of the AFM-1 device

Characteristic	Measurement units	The magnitude of the indicator
The size of the test sample	mm	560170
The thickness of the studied materials	mm	up to 7
Maximum measurement time of the burning process	sec	600
Accuracy of measurement of burning time of sample	sec	not lower than 0,1.
The supply voltage of the device	V	220
Power consumed by the device	W	50

Conclusions

The flammability of clothing materials cannot be determined without the use of objective control methods. With the help of the device and a technique developed by authors objective control of flammability becomes possible. The essence of the proposed method of assessing the flammability of materials is that the control and determination of the moments of passage of the flame front of a certain distance on the sample is carried out using photoelectric elements located at strictly fixed distances from the beginning of the sample along its length and from each other. Each photovoltaic cell is connected to a timer, which at the moment of receiving a signal from the photovoltaic cell automatically records the time of passage of the flame front of a certain distance. The proposed test method corresponds to the international standard ISO 15025 [1].

References

1. ISO 15025:2000, (2000), Protective clothing – Protection against heat and flame – Method of test for limited flame spread.
2. Song, G., Barker, R.L. (ed) (2004), Modeling the Thermal Protective Performance of Heat Resistant Garments in Flash Fire Exposures, Textile Res, Vol. 74, No. 12.
3. DIN EN 1102: 2016, (2016), Textiles and textile products – burning behaviour – curtains and drapes – detailed procedure to determine the flame spread of vertically oriented specimens.
4. Zasornov A.S. (2004), Development of the method and assessment of thermal power supply of materials for special equipment, Kiev National University of Technologies and Design.
5. Perepelkin, K.E. (2001), Flammability of textiles as one of its most important characteristics, Light industry, №. 8.
6. Zasornov, A.S. & Sarana O.M. (1999), Methodological aspects of the study design installation termozahysnyh properties for clothing, Measuring and computing in technological processes. № 3.

MOISTURE TRANSPORT INSIDE TEXTILE STRUCTURES AND LEATHER

Korycki R.¹, Szafrńska H.²

¹Lodz University of Technology, Lodz, Poland

²University of Technology and Humanities in Radom, Radom, Poland

Nomenclature

- A, B integration constants, -;
- D matrix of diffusion coefficients within the tested material (leather), $\text{m}^2 \text{s}^{-1}$;
- f_w moisture source capacity, $\text{mol m}^{-3} \text{s}^{-1}$;
- h_w mass convection coefficient; s^{-1} ;
- n unit vector normal to the external boundary of tested material leather, directed outwards to the bounded domain, -;
- q_w vector of the moisture flux density, $\text{mol m}^{-3} \text{s}^{-1}$;
- q_w^* vector of the initial moisture flux density, $\text{mol m}^{-3} \text{s}^{-1}$;
- $q_{nw} = n \cdot q_w$ moisture flux density normal to the external boundary, $\text{mol m}^{-3} \text{s}^{-1}$;
- t real time, s;
- w water vapor concentration (state variable), mol m^{-3} ;
- w^0 level of water vapor concentration during the steady transport (saturation conditions), mol m^{-3} ;
- w_∞ water vapor concentration in surrounding, mol m^{-3} ;
- x vector of coordinates, m;
- x coordinate of one-dimensional moisture transport, m;
- Γ external boundary of the sample, -;
- ∇ gradient operator, -.

Introduction

The moisture permeability is an important parameter to estimate the complex textile materials as well as the leather. It can be measured by means of different methods but the typical procedure consists in the application of steady moisture transport. The example of the test stand used

to determine the moisture permeability of the complex textile structures or leather is shown in Fig.1.

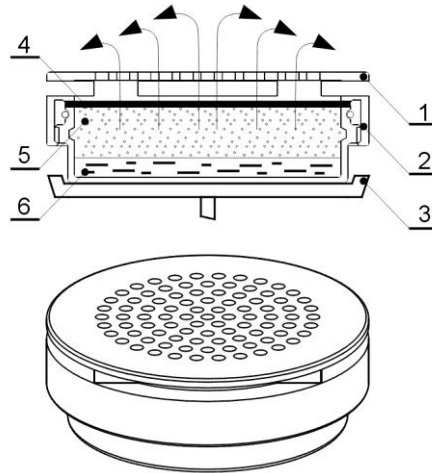


Fig.1. Test stand of moisture permeability for the complex textiles and leather [1]

1 – plate; 2 – housing; 3 – plate of weight-dryer; 4 – testing sample; 5 – water vapor;
6 – distilled water

Physically speaking, the water vapor is transported from the vessel with distilled water to the air layer above covered by the sample of tested textiles or leather. The only one lost mechanism is the transport through the sample material. The water vapor permeability is determined by means of moisture loss, i.e. evaporation through the leather sample [1]. The mass of lost water (that is the moisture) is precisely determined by the weight-dryer.

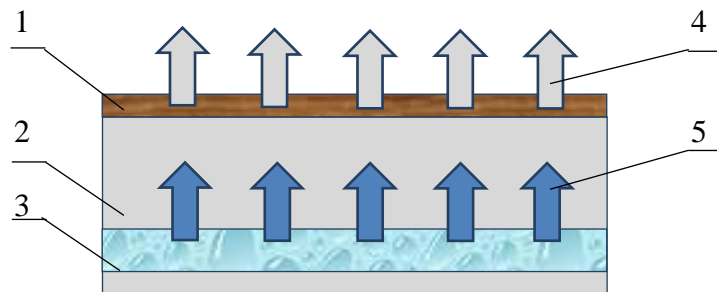


Fig.2. Scheme of transport process

1 – tested sample of textiles or leather; 2 – water vapor within vessel; 3 – distilled water;
4 – convection from leather surface to surrounding; 5 – evaporation from distilled water.

Let us next introduce the physical model of transport process and the state variable, cf. Fig.2. The state variable determines the physical state of system and can be in fact an optional parameter of the adequate physical description. This class of problems is usually defined using the distribution of water vapor concentration w (i.e. the moisture concentration w) inside the tested sample, which can be assumed as design variable.

The distilled water evaporates from the bottom of vessel into the air layer within the same container. The moisture concentration in air changes in time and space and can be determined generally in dynamic conditions as follows.

$$w = w(\mathbf{x}, t) \quad (1)$$

Formulation of moisture transport equation

Generally speaking, the problem is determined by the transient problem of moisture transport. Let us assume that after the prescribed time the water vapor within the air layer between the distilled water and the sample reach saturation conditions $w=w^0$. The water vapor is next transported through the tested structure to the surrounding. The transport equation can be expressed in general form by the second-order differential equation in respect to the coordinate z and the first-order equation in respect to time [2,3].

$$\begin{cases} -div \mathbf{q}_w + f_w = \frac{dw(\mathbf{x},t)}{dt} \\ \mathbf{q}_w = \mathbf{D} \cdot \nabla w + \mathbf{q}_w^* \end{cases} \quad (2)$$

Typical sample structure does not contain the moisture sources, i.e. the capacity of internal sources is negligible $f_w=0$. Additionally, the vector of the initial moisture flux density is also equal to zero $\mathbf{q}_w^*=0$. The transport correlation (2) can be consistently simplified to the following form.

$$\begin{cases} -div \mathbf{q}_w = \frac{dw(\mathbf{x},t)}{dt} \\ \mathbf{q}_w = \mathbf{D} \cdot \nabla w \end{cases} \quad (3)$$

Theoretically speaking, the problem can be described using two consecutive physical states.

At the beginning, the transport is characterized by the variable water vapor concentration within air and the dry tested structure/leather. There is the transient heat and moisture/mass transfer through the air and the sample. The problem is consequently space- and time-dependent. Physically speaking, the transient heat and mass transport has a complicated description. A part of heat is transported with mass whereas the transport of mass with heat is practically negligible. The problem is determined by the set of second-order differential equations: the heat transport equation and the moisture (the water vapor) transport equation. We have to introduce two state variables – the temperature T and the water vapor concentration w . Each of these equations is the second-order equation in respect to the corresponding design variable and the first-order differential equation in respect to time. The practical application of problem is unlimited (cf. for example the test measurements, the protective clothing, the medical care, the clothing technology etc.) and some aspects were discussed for example in [4-7]. The moisture permeability is tested in the insignificant temperature. Thus, the transport of heat with moisture is consequently negligible and we introduce the only mass/moisture transport through the sample.

The permanent evaporation causes that the water vapor in air layer reach the saturation conditions and the sample is subjected to stable moisture transfer of the same repeatable conditions. The problem is only space-dependent of the same description in time, i.e. there is the steady problem. Therefore, the moisture transport is determined in respect of Eq.(3) as follows.

$$\operatorname{div}(\mathbf{D} \cdot \nabla w) = 0 \quad (4)$$

The simple steady problems can be solved analytically whereas the complicated steady problems and the cases of transient transport should be solved numerically. Generally speaking, the matrix of diffusion coefficients in material can be time-; moisture- and place-dependent.

$$\mathbf{D} = \mathbf{D}(x, w, t) = 0 \quad (5)$$

The problem can be considerably simplified for the steady moisture transport because is time-independent $D=D(x,w)$. The diffusion coefficients can be constant in the limited measuring time $D=D(x)$. Let us assume that the matrix of diffusion coefficients is space-independent, i.e. $D=const$. Let us for simplicity assume that the material is isotropic of the single diffusion coefficient D . It follows immediately from Eq.(4).

$$\mathbf{D} \operatorname{div}(\nabla w) = 0 \rightarrow \operatorname{div}(\nabla w) = \mathbf{0} \quad (6)$$

The mechanism of moisture transport within vessel and sample shows that there is in fact the one dimensional transfer through the tested sample. The problem can be described by the only coordinate x . Equation (6) can be simplified to the following differential correlation in respect of the coordinate x .

$$\frac{d^2 w}{dx^2} = w_{,xx} = 0 \quad (7)$$

There is a simple differential equation in respect to the one variable which can be integrated analytically with the imposed boundary conditions. The problem is solved analytically by the simple integration in respect to the coordinate x .

Results and solution

To solve the above equation, we have to introduce the set of boundary conditions in order to determine the integration constants. Assuming the steady problem and the same dimensions in the plane perpendicular to the cutting plane, the conditions of water vapor transport are identical within an optional cross-section of the tested sample. Thus, the space 3D problem can be consistently reduced to the plane 2D analysis, i.e. an optional cross-section of the sample, cf. Fig.3.

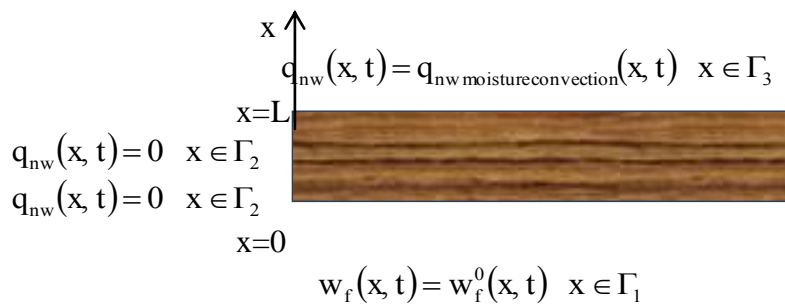


Fig.3. Scheme of boundary conditions of textile structure / leather

The physical state of air layer within the vessel is characterized by the water vapor concentration. Therefore the value of water vapor concentration in air layer and on the lower surface of tested sample is the boundary condition of moisture transport. The lower surface of leather is subjected to the prescribed moisture concentration. This part of external boundary can be defined as Γ_1 and is subjected to the first-kind condition.

The water vapor is transferred through the material to the upper surface of sample. The upper surface is subjected to moisture convection to surrounding. Thus, the convectonal mass flux is also the boundary condition on the upper surface of leather or textile material. The upper part of leather is subjected to mass convection to surrounding. We define also the third-kind conditions on this boundary portion Γ_3 .

The side boundaries have insignificant dimensions and are subjected to negligible moisture loss. The mass flux densities can be assumed as equal to zero on this boundary portion. It follows immediately that there is the one-dimensional diffusion of water vapor from the lower to the upper surface of leather along the coordinate x . The moisture transport is one-dimensional from the vessel through the sample to surrounding. Thus, both side boundaries can be characterized by the second-kind conditions and denoted as portions Γ_2 .

Summarizing, we have defined the first-, second- and third-kind boundary conditions on the appropriate parts of external boundary. The boundary conditions have the coherent form.

$$w(x, t) = w^0(x, t) \quad x \in \Gamma_1 \quad q_{nw}(x, t) = q_{nw}^0(x, t) \quad x \in \Gamma_2 \quad (8)$$

$$q_{nw}(x, t) = D \frac{dw}{dx} = h_w [w(x, t) - w_\infty(x, t)] \quad x \in \Gamma_3$$

The correlations can be reduced for the steady problem (i.e. for the time-independent parameters) as follows.

$$\begin{aligned} w|_{x=0} = w^0|_{x=0} \quad x \in \Gamma_1 \quad q_{nw}(x) = q_{nw}^0(x) \quad x \in \Gamma_2 \quad (9) \\ q_{nw}|_{x=L} = D \frac{dw}{dx} \Big|_{x=L} = h_w [w|_{x=L} - w_\infty] \quad x \in \Gamma_3 \end{aligned}$$

In order to determine the distribution of water vapor concentration, we integrate twice Eq.(7) in respect of the coordinate x. We can determine the general form of equation of moisture distribution.

$$\frac{dw}{dx} = w_{,x} = A \quad w = Ax + B \quad (10)$$

The integration constants A, B can be described using the boundary conditions. Water vapor concentrations on both lower and upper surfaces are determined respectively from Eq.(10) for the coordinates x=0 and x=L in the form.

$$w|_{x=0} = w^0|_{x=0} = B \quad w|_{x=L} = AL + B = AL + w^0 \quad (11)$$

Introducing next the Eqs.(11) and Eq.(10) into Eq.(9)₃ we can derive the following formula.

$$D \frac{dw}{dx} \Big|_{x=L} = h_w [w|_{x=L} - w_\infty] \quad \rightarrow \quad DA = h_w (AL + w^0 - w_\infty) \quad (12)$$

$$\rightarrow A = \frac{h_w (w^0 - w_\infty)}{D - h_w L}$$

The formula describing the moisture distribution has the final form in respect of Eq.(10), Eq.(11)₁ and Eq.(12).

$$w = \frac{h_w(w^0 - w_\infty)}{D - h_w L} x + w^0 \quad (13)$$

According to Eq.(13), the moisture distribution has the linear character along the sample, i.e. in respect of the coordinate x . The initial and final values obtained from Eq.(13) are the following.

$$\begin{aligned} x = 0 &\rightarrow w = w^0 \\ x = L &\rightarrow w = \frac{h_w(w^0 - w_\infty)}{D - h_w L} L + w^0 \end{aligned} \quad (14)$$

The problem can be visualized by means of Fig.4. The problem is linear and its illustration is the straight line.

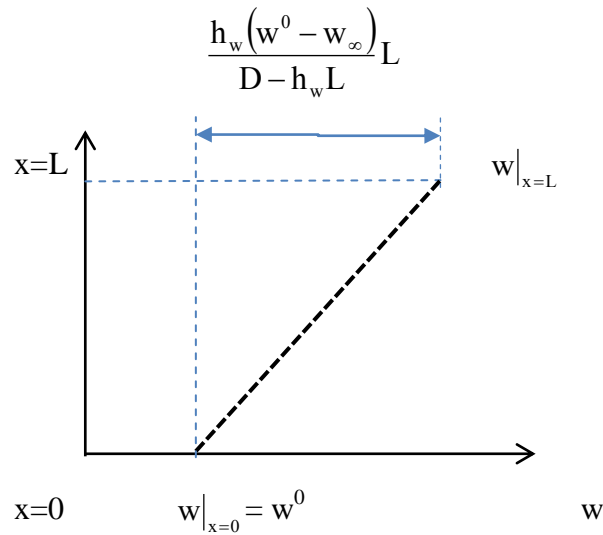


Fig.4. Distribution of water vapor concentration within sample

Description of multilayer structure

The problem is more complicated for the complex multilayer structure. The same description can be applied to determine the influence of finishing procedure. The obtained characteristics can be defined as the additional material layer. In this case we introduce the advanced model of internal structure. We have to introduce the multilayer internal structure of the same values of the state variable on the internal boundaries. Thus, we assume the

complete moisture transport through the internal layers without moisture loss, cf. Fig.5.

The mathematical model for the internal layer has the following form.

$$w_1(x, t) = w_2(x, t) \quad x \in \Gamma_4 \quad (15)$$

The problem can be simplified for the particular coordinate of the internal boundary $x=x_{in}$. as well as the steady transport conditions. We can denote.

$$w|_{x=x_{in}} = w^0|_{x=x_{in}} \quad (16)$$

The obtained characteristics are still the segments of straight lines. The only difference is now the description by means of two segments of the different angles of inclination to the axis x . There is a consequence of different material characteristics.

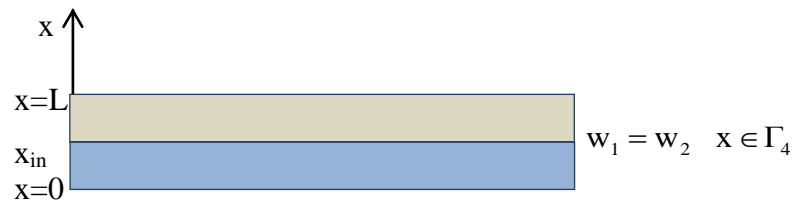


Fig.3. Scheme of boundary conditions inside textile structure / leather

Conclusions

The obtained correlation of moisture distribution is linear in respect of the coordinate x . However, the problem is complicated and the accurate results are determined for the simplified model.

The matrix of diffusion coefficients was assumed during the calculations as parameter-independent. In fact, the matrix can be time-; moisture- and place-dependent, cf. Eq.(5). However, the analysis of these problems is difficult and can be determined by numerical methods adequate for each particular case. It is time- and labor-consuming and beyond the scope of analysis presented.

The thickness of tested sample changes during the moisture transport irrespective of the material applied. The higher the moisture content, the

greater the volume of textile yarns and leather. It follows that the distance of moisture molecules grows inside the material which can change the moisture diffusion coefficient. The characteristics of transport can be time-dependent.

Typical sample (the textile material and leather) is subjected to the special finishing procedure by means of different chemicals. These substances can change the diffusion coefficients and the description of boundary conditions that is the characteristics of moisture transport.

The moisture diffusion is the complex process. A part of water vapor molecules can condense inside the material tested and create the molecules of liquid water. The analysis should introduce both transport of water vapor and liquid moisture. The transport equations are quite different and their solution can be troublesome. However, the problem needs additional studies and considerations.

References

1. Szafrńska, H., Pawłowa, M., Śmiechowski, K., Żarłok, J. (2015), The study of water vapor permeability of textiles and leather using the simplified method, *Materials of the Conference Clotech*
2. Korycki, R., (2009), Shape optimization in oppositely directed coupled diffusion within composite structures, *Structural and Multidisciplinary Optimization*, Vol.39, 283-296
3. Korycki, R., (2007), Shape optimization and shape identification for transient diffusion problems in textile structures, *Fibres and Textiles in Eastern Europe*, Vol.15 nr 1(60), 43 – 49
4. Korycki, R., Szafrńska, H., (2016), Optimisation of pad thicknesses in ironing machines during coupled heat and mass transport, *Fibres and Textiles in Eastern Europe*, Vol.24, No. 1(115), 128-135
5. Korycki, R., Szafranska, H., (2016), Thickness optimisation of textiles subjected to heat and mass transport during ironing, *Autex Research Journal*, Vol. 16, No. 3, 165-174
6. Korycki, R., Krucińska, I., (2016), Numerical Optimisation of Thickness of Composite Bonnet for Neonates, *Autex Research Journal*, Vol. 16, No. 4, 196-204
7. Korycki, R., (2018), Determination of Material Thicknesses in Protective Clothing for Firefighters, *Fibres and Textiles in Eastern Europe*, Vol. 26, No. 2(128), 93-99

INCREASE OF TEMPERATURE AND FIRE RESISTANCE FOR REINFORCED-CONCRETE STRUCTURES BY SURFACE TREATMENT WITH PROTECTIVE COATING

Demydchuk L., Sapozhnyk D.

Lviv University of Trade and Economics, Ukraine

Introduction

The normative documents of Ukraine (DBN V.1.1.7– 2016) [1] establish that the limit of fire resistance of reinforced-concrete building structures is determined by the calculation method or by fire tests, and shall be at least 45 minutes. Taking into account the modern construction technologies, namely, the reduction of the section of the main building reinforced-concrete structures, it is expedient to use fire-retardant coatings to provide the necessary fire resistance limit.

Under actual operating conditions, the reinforced-concrete structures are subjected to a comprehensive effect of aggressive factors, which are greatly enhanced in the conditions of high temperatures and fire. The main factor that affects the reinforced-concrete structures under the influence of the above factors is the loss of strength characteristics that results in the destruction.

The fire resistance of reinforced-concrete structures can be improved by their surface modification with protective materials of different chemical nature.

The currently developed compositions of coatings do not provide the necessary protection for such building structures under experimental conditions of the fire [2, 3]. Therefore, the fire resistance of reinforced-concrete structures can be improved by applying polysiloxanes filled with refractory components on their surface, as they have high thermostable properties in a wide range of temperatures. Under conditions of high temperatures during fire, the fire resistance of the protected reinforced-concrete structures is affected by the phase composition of the coating due to a significant difference in thermomechanical properties.

Polyfunctional protective coatings based on the filled polysiloxane compositions are producible and can be used to improve fire resistance of reinforced-concrete structural materials due to high thermomechanical properties, which are determined by stable structural and phase composition [3,4]. However, due to the heterophase structure and the effect of high temperatures of the fire, the formation of the protective heat-insulation layer is greatly influenced by the processes at the border of “coating-concrete” contact [3, 5].

At the same time, the issues of influence of the protective coating application method on the surface of reinforced concrete, its thickness, fire temperature and proportion of the original composition on the fire resistance of the treated material continue to be relevant. Therefore, this work is devoted to the investigation of these dependences.

Method

Mathematical treatment of the experimental results obtained during the study was carried out with a small number of direct measurements. It is based on methods of probability theory and mathematical statistics, which assume the random nature of the changes of the analyzed value. IR spectroscopic examination of the samples was carried out by spectrophotometer SPECORD-IR-75 and SPECORD-M-80, which record spectra in the range $4000 \dots 400 \text{ cm}^{-1}$. The microhardness was determined on the PMT-3 device by pressing a regular tetrahedral diamond pyramid with an angle at the vertex of 136° under a load in the flat sample surface. The adhesive strength of the coatings was determined by the method of cutting two concrete prisms of $10 \times 10 \times 40 \text{ cm}$ by the simultaneous normal displacement of the coating film they bind at the bursting machine MR-0-05 with an accuracy of $\pm 5\%$. The fire resistance of the coating was determined by the loss of thermal insulation capacity. The general scheme of fire resistance tests consists of one-sided heating of the sample in a fire furnace at a standard temperature heating regime. The size of the samples was $400 \times 400 \text{ mm}$, with a thickness of $20\text{-}40 \text{ mm}$.

The study was intended to investigate the effect of protective coating on the basis of polysiloxane filled with oxide components on the temperature and fire resistance of reinforced-concrete structures.

The basic proportions of the original compositions for fire-retardant coatings (Table 1) were chosen using the method of mathematical planning of the experiment.

Aggregation-resistant compositions of the same uniformity were obtained by a compatible mechanochemical dispersion of components in ball mills due to the destruction processes of the crystalline lattice of oxide filler and additive, physical adsorption and grafting of the fragments of polysiloxane film-former to the filler surface.

Table 1. Proportions of the original compositions for protective coatings

Coating composition number	Content of components, [wt %]					
	KO-08	AL ₂ O ₃	ZrO ₂	Kaolin	Kaolin fiber	Broken fireclay brick
1	20	40	35	-	5,0	-
2	40	20	38	-	2,0	-
3	25	40	10	20	5,0	-
4	35	35	18	10	2,0	-
5	30	30	22	12,5	3,5	2,0
6	35	25	25	10	2,0	3,0

The optimal dispersion period (100 – 125 h) and graft-polymer mass (5.7 – 6.3 wt %) were determined by IR spectroscopy.

Experimental

The conducted and published experimental studies demonstrated that the flow ability of the original composition depends only on the content of film-former (20 – 26 sec.), and the dry residue is 75 – 85 wt % [6].

The operational properties of protective coatings (adhesion strength, continuity, fire resistance, etc.) depend to a large extent on the processing

parameters of their application to the concrete surface and on hardening conditions. Previous studies [3, 5] have established that after application of the original composition for protective coating on the concrete surface, the evaporation of the organic solvent with complete polymerization of polysiloxane film-former takes place with the formation of a strong protective layer. In this case, polysiloxane acts as a matrix, the dispersion phase is aluminum particles, zirconium oxides, broken fireclay brick, kaolin and kaolin fibers. Depending on the proportion of the original composition, the microhardness of the protective coating generated on the concrete surface, which is the criterion for the degree of hardening, varies over a wide range.

Results

The influence of the hardening conditions of the protective coating on its microhardness was studied by modes:

- 1 - sustained for 2 hours at the temperature of 353 K;
- 2 - sustained for 1 hour at the temperature of 423 K;
- 3 - sustained for 0.1 hours at the temperature of 473 K;
- 4 - sustained for 24 hours at the temperature of 293 K.

The results of the studies are presented in Table 2.

Table 2. Change in the microhardness of protective coatings depending on the hardening mode

Coating composition number	Microhardness depending on the hardening mode, [MPa]			
	1	2	3	4
1	264,5	289,3	271,7	243,2
2	263,4	278,9	269,8	231,7
3	247,3	271,3	260,4	225,3
4	252,7	275,7	263,2	233,5
5	250,4	270,2	259,3	229,1
6	262,5	282,3	265,9	242,3

It was experimentally established that the highest values of microhardness (271.3 – 289.3 MPa) of protective coating were obtained in hardening mode 2. In this case, it correlates with the content of the filler and depends on the mass fraction of kaolin. Minimum parameters of

microhardness (225.3 – 243.2 MPa) are characteristic for protective coatings hardened by mode 4. Considering the process conditions of hardening and energy saving, satisfactory microhardness values, it is expedient to use a rather simple mode, namely 24 hours at room temperature (293 K), to obtain protective coatings.

The application of original compositions for protective coatings was carried out with the help of a spray gun on the dust-free concrete surface pre-dried to moisture value not more than 3 wt %. The thickness of the protective coating was 0.4 – 0.6 mm.

By the methods of physicochemical analysis, it was established that gaseous products generate in the process of heating, due to the thermo-oxidative degradation of the polysiloxane film-former, causing bulging of the coating and formation of a heat-insulating protective layer, the nature which depends on the thickness of the original coating, temperature and heating gradient.

The dependence of the bulging coefficient of the protective coating on the thickness, rate and temperature of heating (Table 3) was established, indicating its parameters in a wide range. Laboratory measurements were conducted by representatives of the Ministry of Emergency Situations. The measurement error is ± 1.5 %.

Table 3. Dependence of the bulging coefficient of coating on the thickness and rate of heating temperature

Coating composition number	Coating thickne, [μm]	Bulging coefficient [Kcn] at heating temperature [K]											
		573			673			773			873		
		Rate of temperature rise [degree/min]											
		20	60	120	20	60	120	20	60	120	20	60	120
2	400	1.14	1.82	3.12	2.87	5.14	6.21	3.02	7.12	8.14	3.07	8.12	10.41
	600	1.57	2.03	3.81	3.02	6.02	7.01	3.51	8.03	9.12	3.82	9.14	11.07
	800	1.92	2.87	4.03	3.41	7.93	8.14	3.91	9.02	10.14	4.03	10.10	11.97
5	400	1.16	1.91	3.08	2.91	5.27	6.31	3.09	7.51	8.27	3.12	8.47	10.37
	600	1.61	2.09	3.78	2.98	5.19	6.37	3.62	8.12	9.21	3.91	9.07	10.93
	800	2.01	2.17	4.18	3.31	7.12	8.21	4.01	8.93	10.02	3.98	10.12	11.37
6	400	1.21	2.01	3.17	3.01	5.21	6.37	3.87	7.14	8.93	3.93	8.53	10.87
	600	1.57	2.12	4.01	3.17	5.91	7.17	3.91	7.97	9.91	4.17	9.85	11.43
	800	2.07	2.37	4.33	3.53	6.95	8.29	4.02	8.91	10.14	4.83	10.19	11.87

So, on heating to a temperature of 573 K, the bulging coefficient depends on the thickness and the heating rate. An increase in the coating thickness leads to an increase in the bulging coefficient by a factor of 3 – 3.3, and an increase in the heating rate – by a factor of 1.35 – 1.9, depending on the thickness of coating.

It should be noted that the increase in the coating thickness less significantly affects the bulging coefficient. The increase in the heating temperature to 873 K leads to a significant increase in the bulging coefficient, especially on heating at a rate of 120 degrees/min, and an increase in the heating temperature to 873 K partially increases the bulging coefficient for coatings of different thickness values.

The high experimental bulging coefficient is characteristic for coating composition 1 and 5 at their thickness of 800 μm and heating rate of 120 degrees/min. The heating of protective coatings above the temperature of 873 K leads to a slight decrease in the bulging coefficient due to the sintering of the coatings and formation of a more dense structure.

The porosity of the surface is one of the parameters that must also be determined for the complete solution of the problem. That's why the influence of the thickness of protective coating on the total porosity index during the period of thermo-oxidative destruction of polysiloxane film-former (in the temperature range 573 – 873 K) also was studied. It was established (Fig. 1 pos. a) that an increase in the total porosity index by 6 – 16 % occurs on heating to a temperature of 573 K at a thickness of protective coating 400 – 600 μm .

Dependence of the total porosity index on the heating temperature (Fig. 1 pos. b) was determined for a protective coating 600 μm thick.

When heated to a temperature of 513 K, the total porosity index is 2 % due to evaporation of the residual solvent. The growth of the curves of the dependence of porosity index on heating above the temperature of 623 K is due to the processes of thermo-oxidative destruction of polysiloxane. The maximum total porosity index is on heating to a temperature of 753 K

(maximum of the destruction process). It should be noted that the minimum total porosity index (28.3) is characteristic for coating composition 6.

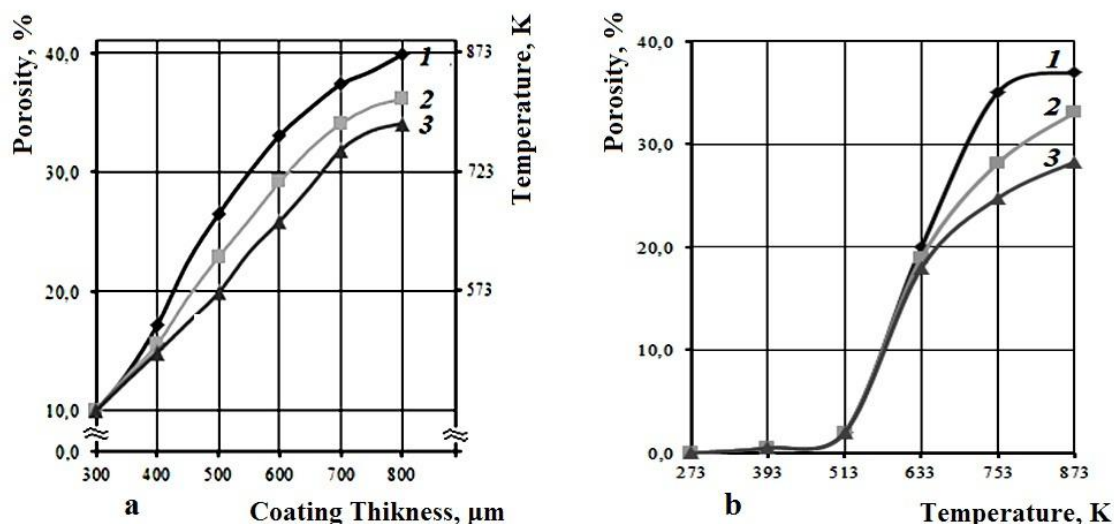


Fig. 1 Dependence of the total porosity index of protective coating on the thickness (a) and heating temperature (b):

1 – composition 2; 2 – composition 5; 3 – composition 6

An increase in the heating temperature above 753 K leads to a decrease in the porosity index due to the processes of interaction between the components, with the formation of new silicate phases, which consolidate the structure of the material due to sintering.

The important factors that determine the conditions for the formation of a qualitative coating for concrete and reinforced-concrete surfaces and provide a reliable protective effect are the physical and chemical processes that take place at the border of “coating – material” contact.

The quality of the coating providing a reliable protective effect, depends on the strength of adhesion bond of the coating with the material surface, and is a quantitative and qualitative assessment of these processes. Such properties of coatings as durability and protective ability under operating conditions greatly depend on the degree and stability of adhesion strength.

It is known that the adhesion of coatings is determined by the interaction between the contacting surface molecules. It is obvious that physical and chemical processes that occur in the compositions at heating in a wide range of temperatures cause a change in the adhesion strength.

The adhesion strength is significantly affected by the state, degree of machining, surface structure and volume shrinkage due to the difference in temperature coefficient of linear expansion of the coating and substrate, as well as the contact area between them. Therefore, a qualitative and quantitative assessment of these processes can be made by determining the adhesion strength between the coating and the material surface, which is achieved by determining the adhesion strength index.

Physical and chemical processes in the contact area depend, firstly, on the composition of coating, the operating conditions and the heating temperature. Therefore, the change in adhesion strength, depending on the specified conditions and the time of contact, is an indirect indicator of the processes that occur at the phase (contact) boundary.

It was established that under the influence of high temperatures, the thermo-oxidative degradation of film-former, with the formation of gaseous products and SiO_2 , takes place in the coatings based on the filled polymethylphenylsiloxane. The presence of the latter contributes to the synthesis of new phases, which positively influences on their properties. Therefore, phase transformations in the coating composition will affect the adhesion strength. It is also necessary to take into account the physical and chemical processes occurring in the material itself when heated. Consequently, the choice of the rational method for processing the material surface has a significant impact on the index of adhesion strength, and its surface should have the same finish quality.

The adhesion strength after hardening is within 1.9 MPa for steel 09Г2С and 3.6...3.8 for concrete. It was established that the increase of the adhesion strength index at heating to a temperature of 473 K depends on the initial coating composition and is 3.45...4.2 MPa for steel 09Г2С and 5.9...6.4 MPa for concrete, respectively, which is explained by the

formation of additional connections between the coating and the material surface. At this temperature, the adhesion strength is determined not only by the coating (adhesive) flowing conditions, but also by the change in the properties of polymethylphenylsiloxane and the structure of the material itself.

The adhesion strength index increases for both materials to a heating temperature of 573 K, and then decreases as a result of thermo-oxidative degradation of polymethylphenylsiloxane and increased porosity.

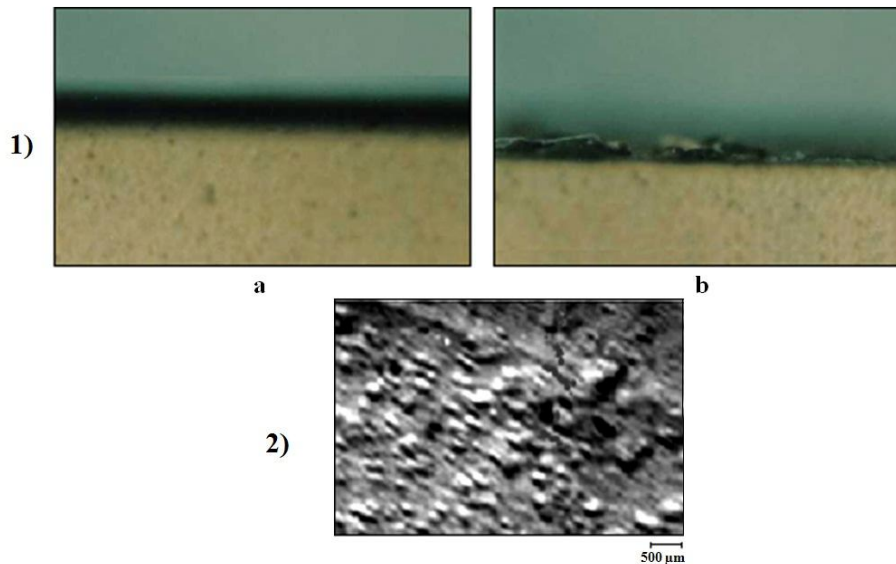
The heating of the material above 573 K leads to a significant reduction in the adhesion strength due to the partial degradation of the coating and the formation of pores and breaks. This process is most intensive at heating above 673 K due to the intensive loss of the mass of coating, which is due to the release of organic component and the destruction of the coating surface.

It should be noted that introduction of kaolin (composition 2) into the composition of the protective coatings increases the adhesion strength index by 0.5...0.6 MPa (12...15 %), kaolin fiber (composition 5 and 6) by 1.4...1.5 MPa for steel 09G2S and by 13...14% – for concrete due to the reduction of the porosity index in the temperature range 473...573 K and especially (by 1.8...2.0 MPa) at 673 K. Such an increase in the adhesion strength is partly influenced by the presence of kaolin the coating composition, which closes pores and significantly restricts the access of oxygen to the material and the proportion of its degradation products.

The maximum adhesive strength at a heating temperature of 523 K is explained by the presence of a strong transition layer from the newly formed phases and connections between the coating and the material (Fig. 2).

As indicated by Fig. 2, there are no cracks and detachments in the structure of the transition layer. Consequently, the improved protective effect can be achieved by introducing additives able of forming the vitreous phase in the “coating – substrate” contact area, into the composition of the coatings.

The presence of the transition layer in the “coating – substrate” contact area increases the adhesion strength of protective coatings and enables the improvement of the thermal stability of protective coatings of metal and concrete building structures. The micrograph of the transient process on the concrete surface wasn't made due to the difficulties in recognizing the coatings in the pores of the concrete.



**Fig. 2 Macro- (1) and microstructure (2) of the transition layer “coating – substrate“ at a heating temperature 523 K (x100):
a – steel 09Г2С; б – concrete**

It should be noted that the coating destruction nature during heating depends on the temperature and varies from cohesive to the mixed-adhesive and adhesive at a temperature of 773 K, which is explained by the stability of the polymethylphenylsiloxane binder.

The adhesion strength of protective coatings is closely related to their continuity, which changes with heating. Therefore, the fire protection of coated materials will depend on the state of the surface, which changes with heating due to the formation of pores and cracks in the physical and chemical processes that take place in the coatings.

It was established that when the coating is heated to a temperature of 573 K, the structuring of the film-former takes place in it, which positively influences on the density and continuity of the coating.

At higher temperatures, polymethylphenylsiloxane starts to degrade with the release of gaseous products, resulting in pore formation that adversely affects the continuity of the coating.

However, this is partially compensated by the silicon-oxygen frame already when heated to a temperature higher than 723 K. When the coating is heated, it is separated into a volatile part and a solid residue.

Decrease in the continuity of coatings by 10...12 % when heated above 473 K is due to the coke pyrolysis, which is significantly manifested at temperatures of 573 K and above and is usually accompanied by the release of CO and CO₂, which destroy the structure of the protective coating. Due to the loss of the coating mass at a heating temperature of 773 K, the coating partially collapses. The introduction of kaolin and kaolin fibers into the compositions of coatings increases their continuity when heated to a temperature of 873 K, and then practically does not affect its index (Fig. 3).

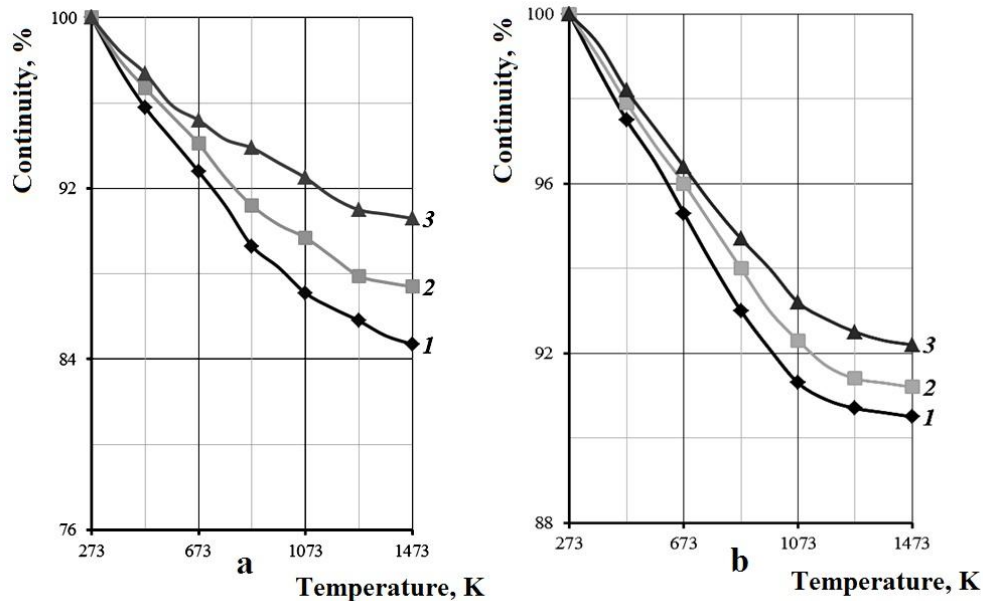
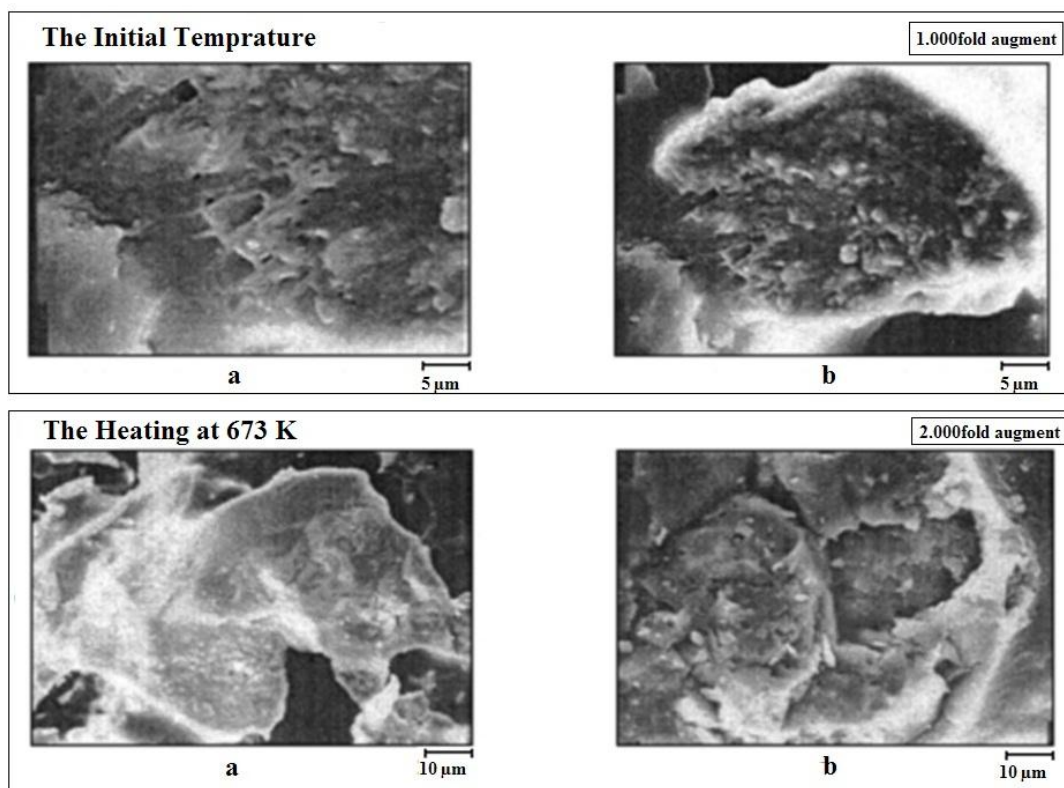


Fig. 3 Change in the continuity of the protective coating on steel 09G2S (a) and reinforced concrete (b) during heating:

1 – composition 2; 2 – composition 5; 3 – composition 6

The reduced continuity of coatings is confirmed by these changes of the microstructure of their surfaces during heating. As indicated by Fig. 4, the structure of the initial coating surface is continuous, without visible cracks and breaks. Further heating of the coating above 673 K, a certain amount of pores and breaks are present on the surface of the coating (Fig. 4), which significantly reduces its continuity and increases the volume of oxygen that passes to the surface of the material and contributes to its destruction.

Efficiency of fire protection of reinforced-concrete structures was determined in a fired furnace according to STU-H-P B V.1.1-29:2010 Fire protection. Fireproofing of building structures. General requirements and inspection methods. (Date of entry into force: 10/01/2011) (Table 4).



**Fig. 4 Microstructure of the surface of coating composition 5 at heating:
a – on steel 09Г2С, b – on reinforced concrete**

Table 4. Limit of fire resistance of reinforced-concrete samples by the loss of heat-insulating capacity

	Coating composition number						No coating
	1	2	3	4	5	6	
Fire resistance limit, [min]	108	115	126	122	120	112	60

The obtained results confirm the expediency of using the developed compositions of protective coatings on the basis of polysiloxane filled with oxide and silicate components for increasing the fire resistance limit of reinforced-concrete structures by a factor of 1.8 – 2.1 in terms of the loss of heat-insulating capacity.

Conclusions

The optimum hardening mode of the protective coating on the concrete surface, which is achieved on heating to 473 K or exposure to room temperature for 24 hours, was experimentally established. The porosity of the protective layer depends on the heating temperature, the thickness of the coating and the rate of temperature rise. It was proved that with the increase in the coating thickness from 300 to 800 μm , the porosity index increases by a factor of 5.0 – 7.5 due to the coating bulging, and with the increase in the temperature gradient from 20 to 60 degrees/min – by a factor of 8.2 – 9.4.

The effectiveness of fire protection of reinforced-concrete structures with the developed protective coating compositions has been proved. With their use, the fire resistances limit of reinforced-concrete structures increases 1.8 – 2.1 times in terms of heat-insulating capacity.

References

1. DBN V.1.1.7 (2016), State construction regulations of Ukraine. Fire safety of construction objects. – URL: http://www.mil.gov.ua/content/other/TO_tkanuna_watermark.

Advanced technologies in education, industry and the environment

2. Litovchenko, S. V., Maslova T. S., et al. (2005), Improvement of the stability of multiphase silicide coatings based on molybdenum, *Vysn. NTU “KhPI”*, Vol. 52, pp. 94-98.
3. Aguilar-Santillan Joaguin, Ricardo Cuenca-Alvarez, Heberto Balmori-Ramires (2002), Mechanical activation of the decomposition and sintering of kyanite. *J. Amer. Ceram. Soc.*, Vol. 10, pp. 2425-2431.
4. Demydchuk L. B., Hyvliud M. M., I. V. Margal (2012), Organosilicate temperature-resistant coatings for building materials. *Bulletin of Khmelnytskyi National University (scientific journal, technical sciences)*, Khmelnytskyi, Vol. 1, pp. 92 - 96.
5. Demydchuk L., Sapozhnyk D., (2020). The influence of the composition of protective coating of building material from reinforced concrete on its atmosphere resistance, *Herald of Khmelnytskyi national university*, Issue 1 (281). pp. 89 – 93.
6. Demydchuk L., Sapozhnyk D., (2018) Increase of temperature and fire resistance for reinforced-concrete structures by surface treatment with protective coating, *Key Engineering Materials*, Vol. 788, pp. 36-44.

IMPLEMENTATION OF EXPERT SYSTEM FOR CLOTHES STYLE SELECTION

Kuleshova S.

Khmelnytsky National University, Ukraine

Introduction

The clothing industry is quickly becoming a high-tech industry due to rapid advances in technology. High saturation of information environment and the risk of making wrong decisions increase the relevance of information technology as a means to support decision-making. Expert system is one of the most active and productive research in the artificial intelligence field now. Today, scientists in the world successfully implement elements of artificial intelligence and the expert system (ES) at various stages of designing clothes [1-6].

Methods

The aim of this study is to implement a prototype of the ES of the choice of clothes models based on the assessment of consumers' emotional impressions using the methodology of Kansei Engineering (KE) [1, 4, 7, 9].

Analysis of the emotional component of the garment on the basis of KE can be achieved through cluster analysis. Such an approach will identify models of clothes based on perception and emotional needs of the consumer.

To perform the procedure of cluster analysis as a function of the distance between clothing models $\rho(Xp, Xq)$ Euclidean distance is selected. Euclidean distance is usually represented by the formula of the traditional distance between two points, in this case, between two clothing models.

Then, if we take the notation of the set of clothing models – X , and each of the two clothing models – $Xp=(a_{p1}, a_{p2}, \dots, a_{pn})$ та $Xq=(a_{q1}, a_{q2}, \dots, a_{qn})$, where $a_1 = CS$ (Casual – Smart (clothes)), $a_2 = RS$ (Romantic – Sports (style)), $a_3 = CA$ (Classic – Avant-garde (style)), $a_4 = FM$ (Folk – Modern (clothes)), $a_5 = RO$ (Rectangular shape – Oval shape), $a_6 = TdTu$ (Trapezoid shape (long base down) – Trapezoid shape (long base up)), $a_7 = MP$ (Mono colour – Poly colours), $a_8 = BS$ (Bright – Soft (colour)), $a_9 = LD$ (Light – Deep (colour)), $a_{10} = WC$ (Warm – Cool (colour)), $a_{11} = MtPt$ (Mono texture clothes – Poly texture clothes), $a_{12} = MS$, $a_{13} = TN$ (Transparent – Non-transparent (texture)), $a_{14} = SA$ (Symmetry – Asymmetry).

The formula for calculating the Euclidean distance will take the form:

$$\rho(X_p, X_q) = \sqrt{\sum_{i=1}^n (a_{pi} - a_{qi})^2}, \quad (1)$$

where X_p, X_q – clothing models with conditional numbers p, q ;
 $a_{p1}, a_{p2}, \dots, a_{pn}$ ($a_{q1}, a_{q2}, \dots, a_{qn}$) – key design attributes of clothing models with conditional number p (q).

According to the formed bipolar scales [], the code of the each clothing models of the studied set should be represented as a tuple of 14 variables: $X=(CS, RS, CA, FM, RO, TdTu, MP, BS, LD, WC, MtPt, MS, TN, SA)$.

Accordingly, for further clustering, the set of X clothing models is represented as:

$$X=(f_1, f_2, f_3, f_4, f_5, f_6), \quad (2)$$

were $f_1=f(SA, CA)$; $f_2=f(BS, LD, WC)$; $f_3=f(CS, MS, RS)$; $f_4=f(TN, MtPt)$; $f_5=f(FM, MP)$; $f_6=f(TdTu, RO)$.

Then the formula (1) for determining the Euclidean distance between two clothing models of takes the form (3):

$$\rho(X_p, X_q) = \sqrt{(f_{p1} - f_{q1})^2 + (f_{p2} - f_{q2})^2 + (f_{p3} - f_{q3})^2 + (f_{p4} - f_{q4})^2 + (f_{p5} - f_{q5})^2 + (f_{p6} - f_{q6})^2}$$


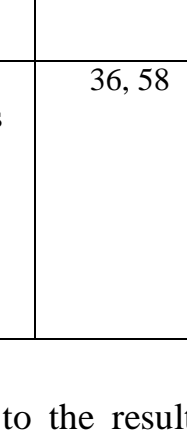




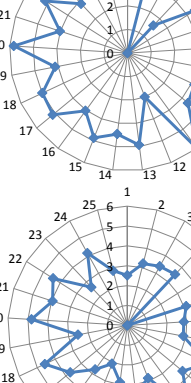
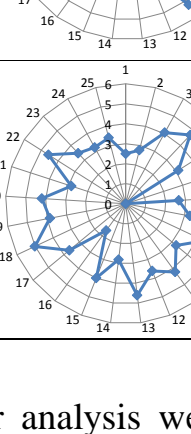
where X_p, X_q – clothing models with conditional numbers p, q ;
 $f_{p1}, f_{p2}, f_{p3}, f_{p4}, f_{p5}, f_{p6}$ ($f_{q1}, f_{q2}, f_{q3}, f_{q4}, f_{q5}, f_{q6}$) – set values of key design attributes of clothing models with conditional digits p (q), respectively.

Thus, according to the results of factor analysis, 6 factors (components) have been identified, in which all pairs of design attributes that reflect the consumer's impression from clothing can be combined, were f_1 –composition feature of clothes style; f_2 – characteristics of clothes colour; f_3 – style characteristics by the situation of use and functionality; f_4 – characteristics of clothes texture; f_5 – clothes colours; f_6 –geometric symbols of clothes shapes [8-11].

Visualization of differences in clothing models belonging to different clusters is presented in the form of spider diagrams. The analysis of the

diagrams indicates the adequacy of the performed cluster analysis, as all cluster centers differ from each other. As a result of the cluster analysis 25 conventional groups were selected [9]. In each cluster there are models of different colours that are in separate cells. This approach allows to detail the search for the desired models in a common database of images, the results are presented in table 1.

Table 1. Belonging of clothes' models to clusters (CI) (fragment)

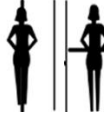

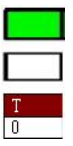
Cluster	Colour	Model number	Photo from database	Diagram
1	Red	1		
3	Black	51, 57		
5	White	41		
6	Poly colours	36, 58		


According to the results of factorial and cluster analysis we may form a productive ES models for choosing clothes considering the wishes (opinions) of a consumer. ES model of production presupposes knowledge

of the relationship between the concepts. The relationship between the concepts is presented in the form of ordered sequences $Cl_i=(f_{1i}, f_{2i}, f_{3i}, f_{4i}, f_{5i}, f_{6i})$ and $M = (Cl_i, colour)$, where i is a model number.

The ES illustrated in this paper is based on the expert rules. It can help customers selecting the most suitable clothes among the abundant apparel according to personal condition and increase customers' satisfaction. The structure of apparel recommended ES is shown in table 2.

Table 2. The structure of the expert system "Clothing model selection"

Entity	The answer number	Scale SD	Meaning	Comment	Figure
1	2	3	4	5	6
Evaluate the level of symmetry of the model of clothing that is under design, 1 - symmetry, 7 is not symmetric at all	1	-3	Vertical or horizontal symmetry	Garment consists of relatively equal parts. It displays an idea of the traditional forms of various types of clothing. It is associated with such words as follows: static, proportional, balanced, respectable, rigorous, and elegant.	
	2	-2
	3	-1
	4	0
	5	+1
	6	+2
	7	+3	Vertical or horizontal asymmetry	It is common for the avant-garde style. It strikes with its unusual appearance and reveals the fashion trends ahead of time. Garment that consists of no equal parts. It is associated with such words as follows: expressive, dynamic, exclusive, charming, creative, extravagant.	
Choose the characteristics of the required/fashionable colour palette	1	-3	Bright light warm colour	S=0÷50%, B=59÷100%, H=0÷75° It is associated with such words as follows: festive, refreshing, dynamic, easy, transparent, soft, dazzling, fun, cheerful.	

	7	+3	Soft dark cold colour	S=0÷100%, B=0÷13%, H=220÷290° It is associated with such words as follows: deep, matte, intellectual, heavy, classical, conservative, chic, official, reserved.	

Advanced technologies in education, industry and the environment

Continue of the table 2


1	2	3	4	5	6
What type of clothing do you prefer?	1	-3	Casual sports style clothes	Practical and comfortable clothes. It combines elements of the different clothing styles. It is associated with such words as follows: conservative, practical, classical, functional, comfortable, dynamic. The texture is matted. It is associated with such words as follows: cozy, elegant.	


	7	+3	Festive clothes for the special occasions such as weddings, anniversaries etc.	Clothing for the special occasions. It is distinguished by its brightness and uniqueness. It is associated with such words as follows: elegant, creative, and attractive. The texture of clothing is shiny. It is associated with such words as follows: smooth, polished, dazzling.	
Do you prefer a model of clothing with or without transparent elements?	1	-3	Transparent, mono textured	Fashion fabric is see-through and it is absolutely transparent. It is associated with such words as follows: seductive, sexy, spectacular. Garment consists of the fabric with only one texture. It is associated with such words as follows: concise, exquisite.	

	7	+3	Opaque, mono-textured or multi-textured	<p>Fashion fabric is not able to be seen through; not transparent. It is associated with such words as follows: strong, concise.</p> <p>The area of elements of the main fashion fabric is approximately $1/K_f < 1/6$, where K_f is the number of the different textures in the outfit. It is associated with such words as follows: luxurious, avant-garde.</p>	

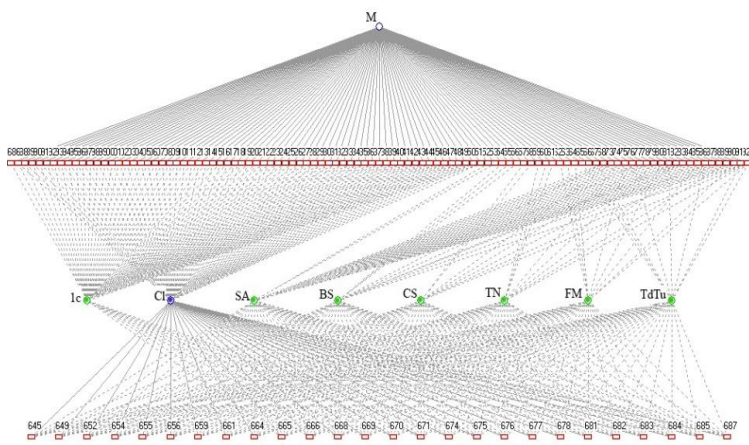
End of the table 2

1	2	3	4	5	6
Do you intend to have folk elements in the outfit?	1	-3	Folk clothing	It is formed under the influence of national costumes of different nations. It is associated with such words as follows: ethnic, natural, ecological. Complex colour range: two-tricolour, four-colour, five-colour and more. It is associated with such words as follows: sophisticated, fantasy, creative.	

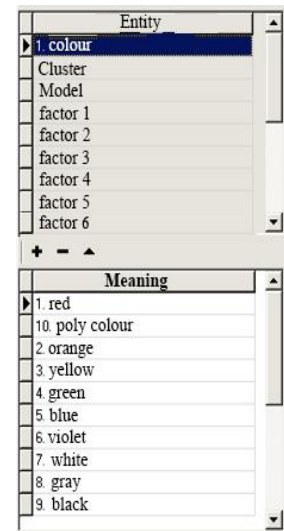
	7	+3	Modern clothes. One colour prevails	The style becomes fashionable, but it is not stable over a long period of time. It is associated with such words as follows: fashionable, modern, topical. Simple colour palette within a single tone of varying saturation. It is associated with such words as follows: monotonous, clean, stable	
What kind of clothing shape is fashionable and/or desirable for the time being?	1	-3	Trapezium with a base down	It is associated with such words as follows: creative, dreamy, impulsive.	

	7	+3	Trapezium with a base up	It is associated with such words as follows: pragmatic, decisive, energetic.	

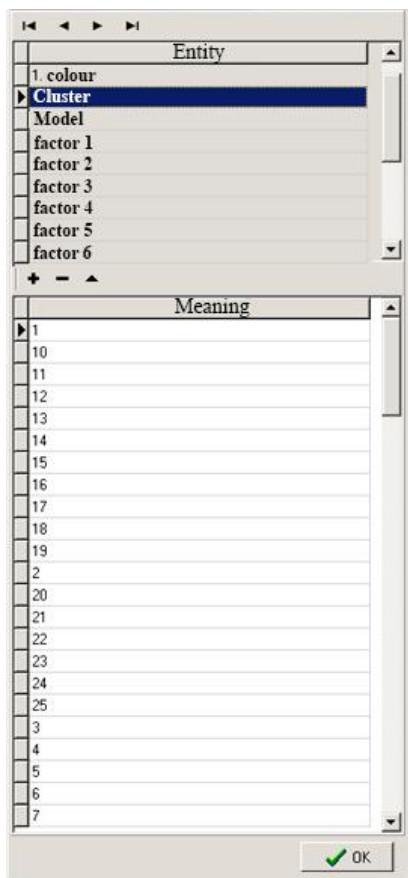
Prototype of ES of a subtask of models' selection based on the methodology of KE in the shell "Rapana" provides a dialogue with the user as a series of questions and answers of system's user. Examples of dialogues of the ES are shown in Fig. 1 [12].



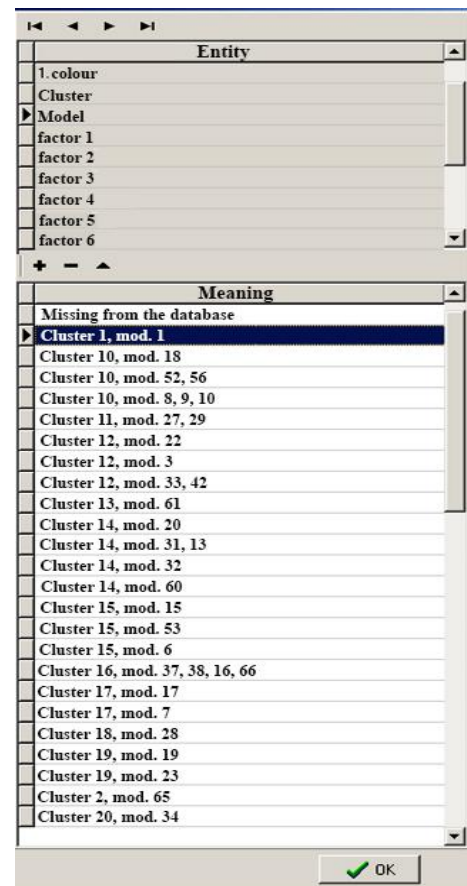
a



b



c



d

Fig. 1. Examples of dialogues of the ES: a) knowledge base in the form of a graph; b) colour; c) Cluster; d) Model

Experimental

The object of the study is the women's fashion dresses in spring-summer 2020 season. Thus, a general collection was formed which amounted to 66 photos of fashion dresses for subsequent questionnaire [13].

As a result of the dialogue of the address consumer with the ES 57 model of women's dresses was selected from the formed base of 66 images, Fig. 2.

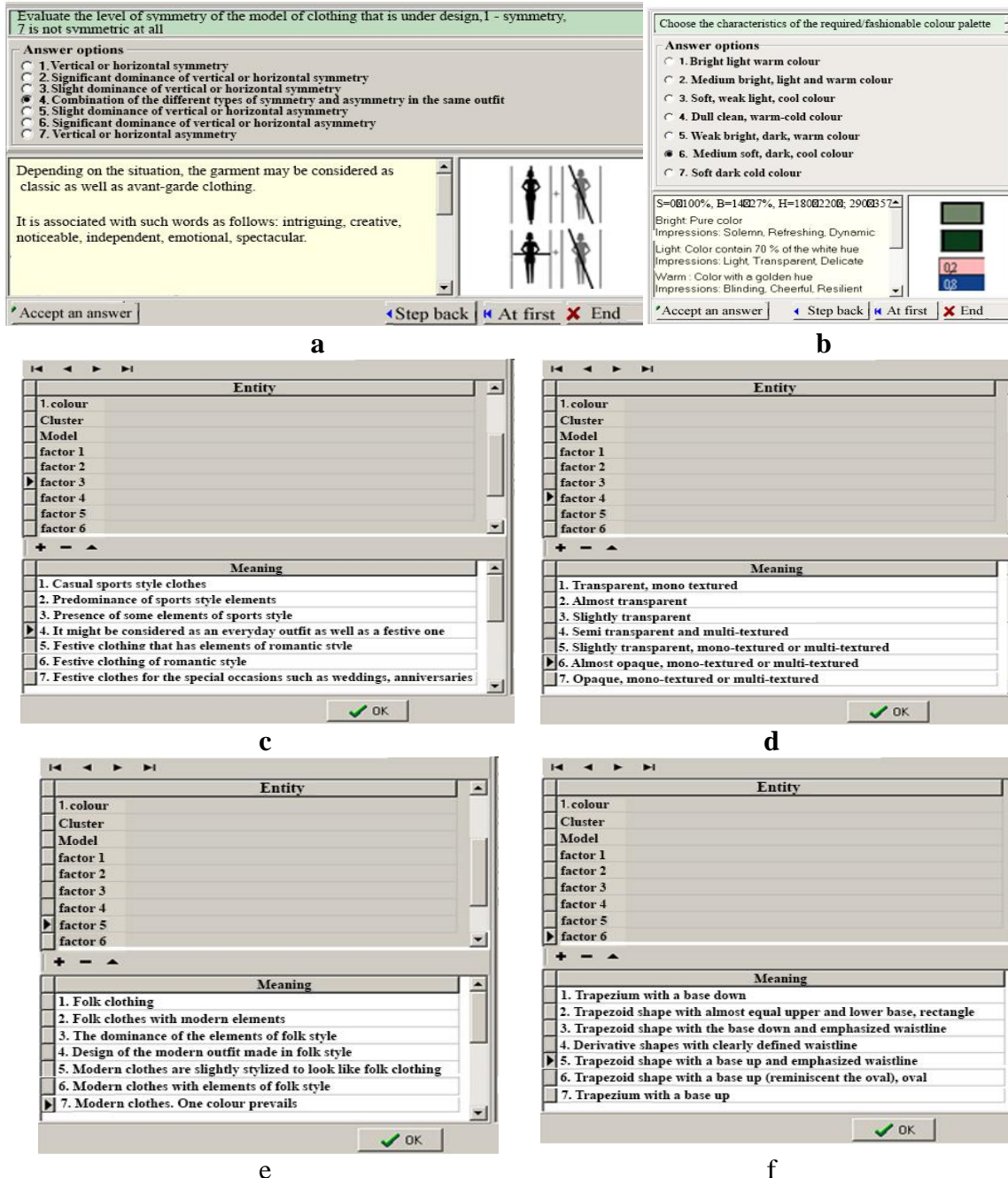


Fig. 2. Dialogues of ES prototype of subtask of readymade garments' selection based on the methodology of KE: a) the choice of the symmetry model of designed clothing; b) choice of outfit's colour characteristics; c) the choice of factor 3; d) the choice of factor 4; e) the choice of factor 5; f) the choice of factor 6

Advanced technologies in education, industry and the environment

Decision making (Fig. 3, 4) provides for the implementation of rules 637 and 659, which are involved in entities: *M* – model, *Ic* – colour, *Cl* – cluster, *SA* – symmetry-asymmetry clothes, *BS* – colour characteristics, *CS* – casual, elegant clothes, *TN* – tissue characteristics, *FM* – folk, modern clothes, *TdTu* – dress. The way how the decision is made is marked with a thick line.

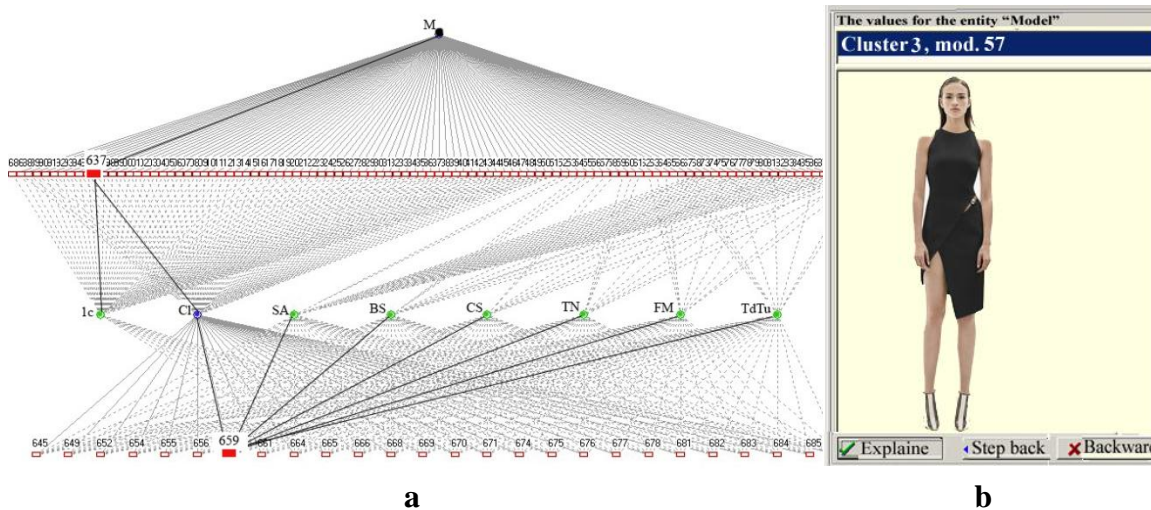


Fig. 3. The result of the dialogue: a) the way of the decision-making; b) the proposed clothes' model

Explanation of the dialog results

Question: "Choose color for the garment?"
 Answer: "10. black"

Question: "Evaluate the level of symmetry of the model of clothing that is under design, 1 - symmetry, 7 is not symmetric at all"
 Answer: "4. Combination of the different types of symmetry and asymmetry in the same outfit"

Question: "Choose the characteristics of the required/fashionable colour palette"
 Answer: "6. Medium soft, dark, cool colour"

Question: "What type of clothing do you prefer?"
 Answer: "4. It might be considered as an everyday outfit as well as a festive one"

Question: "Do you prefer a model of clothing with or without transparent elements?"
 Answer: "6. Almost opaque, mono-textured or multi-textured"

Question: "Do you intend to have folk elements in the outfit?"
 Answer: "7. Modern clothes. One colour prevails"

Question: "What kind of clothing shape is fashionable and/or desirable for the time being?"
 Answer: "5. Trapezoid shape with a base up and emphasized waistline"

- The rule 659 has worked. Subtask: Cluster, KD = "100"
 "Cluster" takes the value: "3"
 if "factor 1" is "4"
 and "factor 2" is "6"
 and "factor 3" is "4"
 and "factor 4" is "6"
 and "factor 5" is "7"
 and "factor 6" is "5"
 It is defined: "Cluster" takes the value: "3" KD = 100

- The rule 637 has worked. Subtask: Cluster, KD = "100"
 "Model" takes the value: "Cluster 3, mod. 57"
 if "1. color" is "10. black" and "Cluster" is "3"
 It is defined: "Model" takes the value: "Cluster 3, mod. 57" KD = 100

Fig. 4. Explanation of the dialogue result

Results

Photos of outfits, which are shown in the figure 3 b, were assessed by experts using the questionnaire, which was developed and submitted in [9].

The expert group consisted of 10 experts and 16 consumers. In a survey photos of clothes were valued using evaluation factors in bipolar scales defined by verbal antonyms of KW from each end of the scale (table 3).

Table 3. Results of the evaluation degree of coordination of expert opinions

№ Photo	Code	Professionals (10 experts)										Kf	Consumers (16 experts)																Kc	K
		1	2	3	4	5	6	7	8	9	10		1	2	3	4	5	6	7	8	9	10	11	12	13	14	15	16		
57	CS	1	0	1	3	3	1	2	2	2	3	1,80	1	3	3	2	2	1	2	2	2	2	3	1	1	2	2	2	1,94	1,87
	RS	1	1	0	1	1	2	0	0	1	3	1,00	1	1	0	1	0	1	1	1	2	0	0	1	1	2	1	1	0,88	0,94
	CA	2	3	3	3	3	3	3	3	3	3	2,90	2	3	3	3	3	3	3	3	2	3	3	3	2	3	3	3	2,81	2,86
	FM	3	3	3	3	3	3	3	3	3	3	3,00	3	3	3	3	3	3	3	3	3	3	3	3	3	3	3	3	3,00	3,00
	RO	0	2	2	0	3	1	3	1	0	3	1,50	0	2	2	1	3	1	3	2	2	1	3	0	0	2	2	2	1,63	1,56
	TdTu	0	0	0	0	0	0	0	0	0	0	0,00	0	0	0	0	0	0	0	0	0	0	0	0	0	0	0	0	0,00	0,00
	MP	2	2	1	1	1	1	1	1	1	1	1,20	2	2	1	1	1	1	1	1	2	2	1	1	1	1	1	1	1,25	1,23
	BS	-3	-3	-2	-2	-3	-3	-3	-2	-2	-3	-2,60	-3	-3	-2	-3	-3	-2	-3	-3	-3	-2	-3	-3	-2	-2	-3	-3	-2,69	-2,64
	LD	-1	-3	-3	-3	-3	-3	0	-2	0	-2,10	-1	-3	-2	-1	0	-1	-3	-3	-2	-3	-3	-2	-3	-2	-3	-2	-2,13	-2,11	
	WC	2	3	3	2	3	2	3	3	2	3	2,60	3	3	2	3	2	3	2	3	3	2	3	3	2	3	2	3	2,63	2,61
	MtPt	3	1	2	1	1	1	3	1	2	1	1,60	3	3	2	1	1	1	3	1	2	2	1	3	1	1	1	1	1,69	1,64
	MS	-2	-3	-3	-2	-3	-3	-3	-3	-3	-3	-2,80	-2	-3	-3	-3	-3	-2	-2	-3	-3	-2	-3	-3	-2	-2	-3	-3	-2,25	-2,53
	TN	3	3	3	3	3	3	3	3	3	3	3,00	3	3	3	3	3	3	3	3	3	3	3	3	3	3	3	3	3,00	3,00
	SA	3	3	3	3	3	3	3	3	3	3	3,00	3	3	3	3	3	3	3	3	3	3	3	3	3	3	3	3	3,00	3,00

The consistency degree of photo evaluation results by experts using SD scales is confirmed by concordance coefficients and Pearson criteria. Table 4 presents the consolidated results of the evaluation level coordination of expert opinions of the first five models.

Table 4. The consolidated results of the evaluation degree of coordination of expert opinions (fragment).

Number of an outfit	ω for the expert group		χ ² _p for the expert group	
	professionals (10 people)	consumers (16 people)	professionals	consumers
57	0.734	0.898	95.42	186.74

Therefore, it is possible to state with 95-percent probability that the frequency of evaluation ratios of KW pairs in different experts is coordinated in accordance with the calculated rate of concordance.

Since these evaluations are subjective, as a result of the survey psychographic profile of the dress 57 was constructed (Fig. 5). Each profile is a list of the average meanings of the estimated coefficients of semantic differential from table 3.

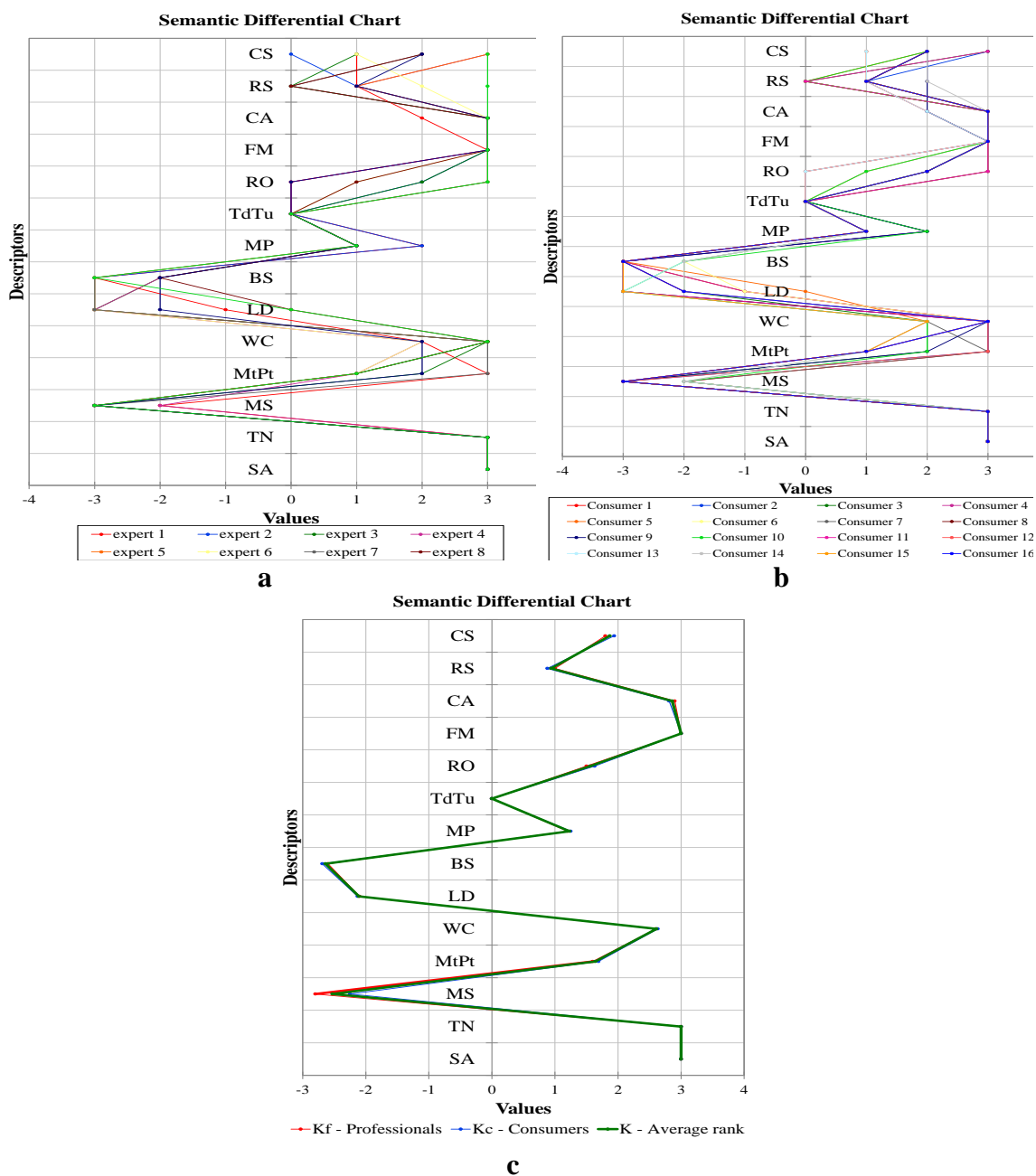


Fig. 5. Examples of psychographic profiles: a) experts are professionals; b) experts are consumers; c) total results

As shown in Fig. 5 psychographic profile of an outfit visually practically does not differ for different groups of experts. As a result, clothes' models that have roughly the same psychographic profiles present each of the 25 received clusters. Combinations of characteristics, which define each of clusters, are to be used in forming the productive model of ES under development.

Conclusion

This research is devoted to implementation of the expert systems for rapid change in production of women's outerwear. Factorial analysis and the cluster analysis are used for the structuring of the subject environment. Thus, the main objective of the study was achieved through the formation of rules of decision-making that intent to solve subtasks of rapid change in production of women's outerwear and choosing the models of readymade garments based on Kansei Engineering methodology, etc. In addition, the system can be used for the designing and for the selection of readymade garments that meets pre-defined customer's impressions (eg. in the shops, including online stores) and to select a prototype to develop new model of clothing that meets the wishes of the consumer.

The knowledge base has been developed in the empty shell "Rapana". It provides dialogue as a series of questions by the system and answers by the user. User can view the way decision making after getting results.

References

1. Nagamachi, M. (2011), *Kansei / Affective Engineering*. Taylor & Francis Group, United States of America.
2. Dong, A. H. Shan, D., Ruan, Z., Zhou, L. Y., & Zuo, F. (2013), The design and implementation of an intelligent apparel recommend expert system. *Mathematical Problems in Engineering*. Article ID 343171, 8 pages. Available at: <http://dx.doi.org/10.1155/2013/343171>
3. Shaari, N. (2013), Methods of analysing images based on Kansei Engineering. *International Journal of Computer Science and Electronics Engineering*, Vol. 1, No. 3.
4. Lu, H. Chen, Y., Du, J. (2013), An interactive system based on Kansei

Advanced technologies in education, industry and the environment

Engineering to support clothing design process. Research Journal of Applied Sciences, Engineering and Technology. Vol. 6, No. 24.

5. Nada, Y. A., Meshref, H. (2014), Analysis, design, and implementation of intelligent expert system for clothes style selection. International Journal of Computer Applications (0975 – 8887). Vol. 4.

6. Zakharkevich, O. V., & Pochuprin, A. V. (2014), Development of prototype of expert system for rapid change in production of women's outerwear, Easter-European Journal of Enterprise Technologies, Vol. 2/2 (68).

7. Rajasekera, J., & Karunasena, H. (2015), Apparel design optimization for global market: Kansei Engineering preference model, International Journal of Affective Engineering, vol. 14, , pp. 119-126. doi:10.5057/ijae.14.119

8. Kuleshova, S.G. & Kurochka, S. B. (2016), Emotional component in the clothing design with semantic differential. Resource-saving technologies of light, textile and food industry: proceedings of Ukrainian scientific-practical Internet-conference of young scientists and students, Khmelnytskyi: KhNU November 17-18 2016, pp. 56-57. [Online]. Available: http://tksv.khnu.km.ua/inetconf/2016/kuleshova_kurochka.pdf

9. Kuleshova, S. G., Zakharkevich, O. V., Koshevko, J. V. & Ditkovska, O. A. (2017), Development of Expert System Based on Kansei Engineering to Support Clothing Design Process. Vlakna a Textil, Vol. 24, No 3, September.

10. Kurochka, S. Sviruk, L., Kuleshova, S. & Zakharkevich, O. (2017), Method of analyzing images of clothes based on Kansei Engineering // International Conference on Technics, Technologies and Education ICTTE 2017, Yambol, Bulgaria, October 19-20st.

11. Kuleshova, S. G. (2017), Applications of Kansei Engineering in clothing design // Actual problems of modern science. Monograph : ed. by Musial Janusz, Polishchuk Oleh, Sorokatji Ruslan – Bydgoszcz, Poland.

12. Expert system “Rapana”. Retrieved 11. 16. 2016 Available at: <http://esrapana.narod.ru/>

13. VOGUE. URL: <https://vogue.ua/ua/gallery/collections/alexander-mcqueen-vesna-leto-2020.html>

OPTIMIZATION OF THE TECHNOLOGICAL PARAMETERS OF WET CLEANING PROCESS OF THE TEXTILE PRODUCTS

Paraska O.¹, Radek. N.²

¹Khmelniyskiy National University, Ukraine

² Kielce University of Technology, Poland

Introduction

The most textile chemicals and finishing compositions are multi-component mixtures composed of two or more surfactants. The effectiveness of their use depends on many factors, including multifunctional performance properties (homogeneity of the product, its viscosity and transparency). The components of such mixtures, especially surfactants, interact with each other and affect on these characteristics. This is displayed in the changes in surface activity, wetting, foaming and washing actions. In some cases, these properties are used to change the characteristics and properties of the textile materials and for the control of behavior of the technological processes. So for the most effective use it is necessary to study the processes of interaction of the surfactants in their mixtures, as well as how they influence on the properties of the final product [1, 2].

The main feature of the compositions for wet cleaning of garments is the washing ability, which provides a high degree of the cleaning of textile materials from pollutions, bright color, softness, lack of the stains on the treated fabrics.

The mathematical models is developed and the optimal parameters of the process of wet cleaning, which is characterized by the maximum removal of contaminations from textile products, high-quality cleaning products are determined.

Methods

The technological parameters (washing ability, anti-resorption capacity, composition concentration, treatment time) of the process of removal of contaminations from textile products made of cotton, polyester was analyzed. Characteristics of the fabrics are given in Table 1.

Table 1. Characteristics of the investigated fabrics

Name of fabric	Width, cm	Binding	Surface density, g/m ²
Cotton fabric	150	linen	180
Polyester fabric	150	linen	220

The fabrics used in the studies were in the prepared form – boiled and bleached.

Determination of the washing ability of the composition was carried out by an optical method based on measuring the reflection coefficients from the source, contaminated and treated fabric samples. For measurements of reflection coefficients, the FOU-42 (Belarus) device was used. By the Kubelka-Munch equation, the washing ability (WA, %) of the composition was determined [3, 4].

The optimization of the technological parameters of wet cleaning was performed with use the three-factor quadratic model according to the plan B₃ [5, 6]. The optimal conditions of using the mixtures of surfactants were determined for the most degree of the removal of pollutants and the selected criteria (Table 2): concentration (X₁), duration (X₂) and temperature (X₃).

Table 2. Initial data for a three-factor experiment

Selected criteria	Factors	Levels of variation			Interval of variation
		-1	0	+1	
Concentration, g/l	X ₁	1	2	3	1
Duration, min	X ₂	2	5	8	3
Temperature, °C	X ₃	20	35	50	15

After calculating the plan B_3 the significant coefficients of the regression equations were determined. The analysis of regression equations allows determining the factors that affect the process of removing pollutions from cotton and polyester fabrics. In the obtained equations the quadratic coefficients are significant, which confirms the right approach of choosing a plan of the second degree for research of the washing solutions. The calculation of the three-factor quadratic model (for cotton fabric) according to plan B_3 is shown in table 3.

Table 3. The calculation of the three-factor quadratic model for cotton fabric

№ _i experiment	№ _i implementation	Plan in natural values of factors				The output variable $Y_{\text{exper.}}$			$(Y_i - Y_c)^2$	S_i^2
		K_1	K_2	K_3	K_4	Y_{1i}	Y_{2i}	Y_c		
1	8	0,3	0,3	0,3	0,1	79,523	78,494	79,008	0,265	0,530
2	9	0,3	0,3	0,1	0,3	81,594	78,817	80,206	1,928	3,856
3	10	0,3	0,1	0,3	0,3	88,105	86,222	87,163	0,886	1,772
4	2	0,1	0,3	0,3	0,3	84,015	82,045	83,030	0,970	1,940
5	7	0,1	0,1	0,1	0,7	78,494	76,922	77,708	0,617	1,235
6	4	0,1	0,1	0,3	0,5	85,140	84,062	84,601	0,290	0,580
7	12	0,1	0,3	0,1	0,5	81,126	78,319	79,723	1,970	3,940
8	3	0,3	0,1	0,1	0,5	87,140	88,815	87,978	0,702	1,403
9	13	0,3	0,2	0,2	0,3	89,998	91,365	90,681	0,467	0,934
10	6	0,1	0,2	0,2	0,5	84,418	78,528	81,473	8,670	17,340
11	11	0,2	0,3	0,2	0,3	85,909	82,460	84,185	2,973	5,946
12	15	0,2	0,1	0,2	0,5	80,700	71,238	75,969	22,384	44,768
13	5	0,2	0,2	0,3	0,3	78,210	83,168	80,689	6,145	12,290
14	14	0,2	0,2	0,1	0,5	81,581	77,743	79,662	3,682	7,365
15	1	0,2	0,2	0,2	0,4	86,334	89,177	87,755	2,021	4,041
Total:									107,9421	

Cochrane's calculation criterion:

$$G_p = \frac{S_{i(\max)}^2}{\sum_{i=1}^N S_i^2}; G_T = \left\{ \begin{matrix} N = 15 \\ f = n - 1 = 2 - 1 = 1 \end{matrix} \right\} = 0,4709$$

$$G_p = 0,160645$$

Dispersion of playback:

$$S_{\hat{a}^2} = \frac{2 \sum_{i=1}^N (Y_{ij} - \bar{Y}_i)^2}{N} = 7,1961$$

$$S = 2,682562$$

The statistical analysis of the model (for cotton fabric) according to plan B₃ is shown in table 4

Table 4. Statistical analysis of the model for cotton fabric

№	Coded factor values												
	x ₀	x ₁	x ₂	x ₃	x ₁ ²	x ₂ ²	x ₃ ²	x ₁ x ₂	x ₁ x ₃	x ₂ x ₃	Y _p	(Y _c -Y _p)	(Y _c -Y _p) ²
1	1	1	1	1	1	1	1	1	1	1	80,15	-1,137	1,292432
2	1	1	1	-1	1	1	1	1	-1	-1	82,35	-2,142	4,586181
3	1	1	-1	1	1	1	1	-1	1	-1	86,68	0,480	0,230174
4	1	-1	1	1	1	1	1	-1	-1	1	83,59	-0,561	0,314227
5	1	-1	-1	-1	1	1	1	1	1	1	76,06	1,653	2,731675
6	1	-1	-1	1	1	1	1	1	-1	-1	81,94	2,657	7,062112
7	1	-1	1	-1	1	1	1	-1	1	-1	79,69	0,036	0,001308
8	1	1	-1	-1	1	1	1	-1	-1	1	86,90	1,076	1,158821
9	1	1	0	0	1	0	0	0	0	0	88,96	1,722	2,965761
10	1	-1	0	0	1	0	0	0	0	0	85,26	-3,786	14,33261
11	1	0	1	0	0	1	0	0	0	0	80,38	3,803	14,46119
12	1	0	-1	0	0	1	0	0	0	0	81,84	-5,866	34,41573
13	1	0	0	1	0	0	1	0	0	0	82,13	-1,440	2,073073
14	1	0	0	-1	0	0	1	0	0	0	80,29	-0,624	0,389236
15	1	0	0	0	0	0	0	0	0	0	83,63	4,127	17,03551
Total													103,05

Dispersion of model adequacy

$$S_{ad}^2 = \frac{\sum_{i=1}^N (\bar{Y}_i - \bar{Y}_i)^2}{N - \lambda} = 20,61001$$

where $f_{ad}=N-\lambda$ – number of degrees of freedom;

λ is the number of coefficients of the model;

number of experiments $N = 15$;

the number of repetitions of the experiment $n = 2$;

the number of coefficients of the model 10

The estimated value of the Fisher criterion $F_e = 2,864$. Tabular values of the Fisher criterion $F_t = \{f_{ad}=5; f_{rel}=N(n-1)=15\}=2,9$. If $F_e < F_t$, the model is adequate [6, 7].

The calculation of model coefficients (for cotton fabric) is shown in table 5.

Table 5. Calculation of model coefficients for cotton fabric

№	$Y_c \cdot x_0$	$Y_c \cdot x_1$	$Y_c \cdot x_2$	$Y_c \cdot x_3$	$Y_c \cdot x_1^2$	$Y_c \cdot x_2^2$	$Y_c \cdot x_3^2$	$Y_c \cdot x_1 x_2$	$Y_c \cdot x_1 x_3$	$Y_c \cdot x_2 x_3$
1	79,008	79,008	79,01	79,01	79,01	79,01	79,01	79,008	79,008	79,008
2	80,206	80,206	80,21	-80,21	80,21	80,21	80,21	80,206	-80,206	-80,21
3	87,163	87,163	-87,16	87,16	87,16	87,16	87,16	-87,163	87,163	-87,16
4	83,030	-83,030	83,03	83,03	83,03	83,03	83,03	-83,03	-83,03	83,030
5	77,708	-77,708	-77,71	-77,71	77,71	77,71	77,71	77,708	77,708	77,708
6	84,601	-84,601	-84,60	84,60	84,60	84,60	84,60	84,601	-84,601	-84,60
7	79,723	-79,723	79,72	-79,72	79,72	79,72	79,72	-79,723	79,723	-79,72
8	87,978	87,978	-87,98	-87,98	87,98	87,98	87,98	-87,978	-87,978	87,978
9	90,681	90,681	0,000	0,000	90,68	0,000	0,000	0,000	0,000	0,000
10	81,473	-81,473	0,000	0,000	81,47	0,000	0,000	0,000	0,000	0,000
11	84,185	0,000	84,19	0,000	0,000	84,19	0,000	0,000	0,000	0,000
12	75,969	0,000	-75,97	0,000	0,000	75,97	0,000	0,000	0,000	0,000
13	80,689	0,000	0,000	80,69	0,000	0,000	80,69	0,000	0,000	0,000
14	79,662	0,000	0,000	-79,66	0,000	0,000	79,66	0,000	0,000	0,000
15	87,755	0,000	0,000	0,000	0,000	0,000	0,000	0,000	0,000	0,000
Total:	79,008	79,008	79,01	79,01	79,01	79,01	79,01	79,008	79,008	79,008

Model coefficients for cotton fabric:

$$b_0=83,628$$

$$b_1=1,85011231$$

$$b_2=-0,72670557$$

$$b_3=0,9216477$$

$$b_{12} = -2,04638947$$

$$b_{13} = -1,52649292$$

$$b_{23} = -0,49608098$$

$$b_{11} = 3,481$$

$$b_{22} = -2,519$$

$$b_{33} = -2,421$$

Estimation of significance of model coefficients:

$$tp(b_0) = 58,0014$$

$$tp(b_1) = 2,180948$$

$$tp(b_2) = 0,856655$$

$$tp(b_3) = 1,086456$$

$$tp(b_{12}) = 2,157684$$

$$tp(b_{13}) = 1,609512$$

$$tp(b_{23}) = 0,856655$$

$$tp(b_{11}) = 1,660039$$

$$tp(b_{22}) = 1,201324$$

$$tp(b_{33}) = 1,154265$$

Error calculating model coefficients:

$$s(b_0) = 1,441823$$

$$s(b_i) = 0,848306$$

$$s(b_{ij}) = 0,94842$$

$$s(b_{ii}) = 2,097066$$

The calculation of the three-factor quadratic model (for polyester fabric) according to plan B_3 is shown in table 6.

Table 6. The calculation of the three-factor quadratic model for polyester fabric

№ experiment	№ implementation	Plan in natural values of factors				The output variable Y _{exper.}			(Y _i -Y _c) ²	S _i ²
		K ₁	K ₂	K ₃	K ₄	Y _{1i}	Y _{2i}	Y _c		
1	8	0,3	0,3	0,3	0,1	77,997	77,532	77,7644	0,054134	0,108268
2	9	0,3	0,3	0,1	0,3	74,422	73,880	74,15076	0,073301	0,146602
3	10	0,3	0,1	0,3	0,3	74,052	73,504	73,77812	0,075283	0,150566
4	2	0,1	0,3	0,3	0,3	79,521	77,576	78,54827	0,945372	1,890745
5	7	0,1	0,1	0,1	0,7	75,952	75,952	75,95218	0	0
6	4	0,1	0,1	0,3	0,5	76,388	75,207	75,79751	0,349123	0,698246
7	12	0,1	0,3	0,1	0,5	73,035	71,679	72,3571	0,459398	0,918797
8	3	0,3	0,1	0,1	0,5	69,629	69,629	69,62933	0	0
9	13	0,3	0,2	0,2	0,3	78,603	77,532	78,06719	0,286713	0,573426
10	6	0,1	0,2	0,2	0,5	75,643	75,643	75,64308	0	0
11	11	0,2	0,3	0,2	0,3	80,497	79,087	79,79218	0,496626	0,993252
12	15	0,2	0,1	0,2	0,5	60,200	73,880	67,04011	46,78442	93,56884
13	5	0,2	0,2	0,3	0,3	75,802	74,052	74,92713	0,764983	1,529965
14	14	0,2	0,2	0,1	0,5	79,438	78,408	78,9228	0,265474	0,530949
15	1	0,2	0,2	0,2	0,4	77,540	74,177	75,85843	2,828667	5,657334
Total:										106,767

Cochrane's calculation criterion:

$$G_p = \frac{S_{i(\max)}^2}{\sum_{i=1}^N S_i^2}; G_T = \left\{ \begin{matrix} N = 15 \\ f = n - 1 = 2 - 1 = 1 \end{matrix} \right\} = 0,4709$$

$$G_p = 0$$

Dispersion of playback:

$$S_{\hat{a}^2} = \frac{2 \sum_{i=1}^N (Y_{ij} - \bar{Y}_i)^2}{N} = 7,1178$$

$$S = 2,66792$$

The statistical analysis of the model (for polyester fabric) according to plan B₃ is shown in table 7

Table 7. Statistical analysis of the model for polyester fabric

№	Coded factor values												
	x ₀	x ₁	x ₂	x ₃	x ₁ ²	x ₂ ²	x ₃ ²	x ₁ x ₂	x ₁ x ₃	x ₂ x ₃	Y _p	(Y _c -Y _p)	(Y _c -Y _p) ²
1	2	3	4	5	6	7	8	9	10	11	12	13	14
1	1	1	1	1	1	1	1	1	1	1	79,406	-1,641	2,693539
2	1	1	1	-1	1	1	1	1	-1	-1	75,561	-1,410	1,988181
3	1	1	-1	1	1	1	1	-1	1	-1	71,532	2,246	5,045847
4	1	-1	1	1	1	1	1	-1	-1	1	77,618	0,930	0,865821
5	1	-1	-1	-1	1	1	1	1	1	1	74,344	1,609	2,587785
6	1	-1	-1	1	1	1	1	1	-1	-1	74,420	1,377	1,897472
7	1	-1	1	-1	1	1	1	-1	1	-1	74,636	-2,279	5,1931
8	1	1	-1	-1	1	1	1	-1	-1	1	70,592	-0,963	0,927438
9	1	1	0	0	1	0	0	0	0	0	76,299	1,768	3,125713
10	1	-1	0	0	1	0	0	0	0	0	77,281	-1,638	2,682405
11	1	0	1	0	0	1	0	0	0	0	75,393	4,400	19,35623
12	1	0	-1	0	0	1	0	0	0	0	71,310	-4,269	18,22784
13	1	0	0	1	0	0	1	0	0	0	77,840	-2,913	8,486027
14	1	0	0	-1	0	0	1	0	0	0	75,880	3,043	9,261325
15	1	0	0	0	0	0	0	0	0	0	76,119	-0,260	0,06777
Total													82,40649

Dispersion of model adequacy

$$S_{ad}^2 = \frac{\sum_{i=1}^N (\bar{Y}_i - \bar{Y})^2}{N - \lambda} = 16,4813$$

where $f_{ad} = N - \lambda$ – number of degrees of freedom;

λ is the number of coefficients of the model;

number of experiments $N = 15$;

the number of repetitions of the experiment $n = 2$;

the number of coefficients of the model 10

The estimated value of the Fisher criterion $F_e = 2,316$. Tabular values of the Fisher criterion $F_t = \{f_{ad}=5; f_{rel}=N(n-1)=15\}=2,9$. If $F_e < F_t$, the model is adequate.

The calculation of model coefficients (for polyester fabric) is shown in table 8.

Table 8. Calculation of model coefficients for polyester fabric

№	$Y_c \cdot x_0$	$Y_c \cdot x_1$	$Y_c \cdot x_2$	$Y_c \cdot x_3$	$Y_c \cdot x_1^2$	$Y_c \cdot x_2^2$	$Y_c \cdot x_3^2$	$Y_c \cdot x_1 x_2$	$Y_c \cdot x_1 x_3$	$Y_c \cdot x_2 x_3$
1	77,76	77,76	77,76	77,76	77,76	77,76	77,76	77,76	77,76	77,76
2	74,15	74,15	74,15	-74,15	74,15	74,15	74,151	74,151	-74,15	-74,151
3	73,78	73,78	-73,78	73,78	73,78	73,78	73,778	-73,78	73,78	-73,778
4	78,55	-78,55	78,55	78,55	78,55	78,55	78,548	-78,55	-78,55	78,548
5	75,95	-75,95	-75,95	-75,95	75,95	75,95	75,952	75,952	75,95	75,952
6	75,8	-75,8	-75,8	75,8	75,8	75,8	75,8	75,8	-75,8	-75,8
7	72,36	-72,36	72,36	-72,36	72,36	72,36	72,357	-72,36	72,36	-72,357
8	69,63	69,63	-69,63	-69,63	69,63	69,63	69,629	-69,63	-69,63	69,629
9	78,07	78,07	0,000	0,000	78,07	0,000	0,000	0,000	0,000	0,000
10	75,64	-75,64	0,000	0,000	75,64	0,000	0,000	0,000	0,000	0,000
11	79,79	0,000	79,79	0,000	0,000	79,79	0,000	0,000	0,000	0,000
12	67,04	0,000	-67,04	0,000	0,000	67,04	0,000	0,000	0,000	0,000
13	74,93	0,000	0,000	74,93	0,000	0,000	74,927	0,000	0,000	0,000
14	78,92	0,000	0,000	-78,92	0,000	0,000	78,923	0,000	0,000	0,000
15	75,86	0,000	0,000	0,000	0,000	0,000	0,000	0,000	0,000	0,000
Total	1128,2	-4,908	20,42	9,803	751,69	744,8	751,83	9,352	1,726	5,811

Model coefficients for polyester fabric:

$$b_0 = 76,119$$

$$b_1 = -0,49083465$$

$$b_2 = -2,04154696$$

$$b_3 = 0,9803259$$

$$b_{12} = -1,16900436$$

$$b_{13} = 0,21574115$$

$$b_{23} = 0,72633753$$

$$b_{11} = 0,671$$

$$b_{22} = -2,768$$

$$b_{33} = 0,741$$

Estimation of significance of model coefficients:

$$tp(b_0) = 53,08313$$

$$tp(b_1) = 0,581781$$

$$tp(b_2) = 2,419822$$

$$tp(b_3) = 1,161969$$

$$tp(b_{12}) = 1,239346$$

$$tp(b_{13}) = 0,228723$$

$$tp(b_{23}) = 0,770043$$

$$tp(b_{11}) = 0,321868$$

$$tp(b_{22}) = 1,327039$$

$$tp(b_{33}) = 0,355349$$

Error calculating model coefficients:

$$s(b_0) = 1,433954$$

$$s(b_i) = 0,843676$$

$$s(b_{ij}) = 0,943243$$

$$s(b_{ii}) = 2,08562$$

The process of removing pollutions from cotton fabrics depends on the surfactant concentration in the solution and temperature, and from polyester fabrics – washing duration and temperature. The sign "+" before the linear coefficients indicates that an increase of the values of these factors increases the washing ability of solutions. Since the values of the pair interaction effects are significant, it indicates the mutual varied influence of the factors and the complex nature of removal of the pollutions. Therefore, the consideration of these three factors is necessary for the optimization of the technological conditions of wet cleaning.

The research of the influence of factors on antiresorptional ability of the solutions shows that the process of redeposition of pollutants on cotton fabrics depends on surfactant concentration and duration of washing. In the case of polyester fabrics all coefficients of the equation were insignificant,

indicating the complex and varied effect of the studied factors on the resorption of pollutions.

The determination of the best conditions of material processing was realized by using the built-in functions for calculation of the maximum and minimum in MATHCAD [5 – 7], graphics optimizing the parameters for regression equations and constructing the appropriate sections of the surfaces of the response functions for fixed values of factors in Maple 14. Since the optimal value of the first factor corresponds to the level of variation -1, the value of this parameter was fixed as $X_1 = -1$ for graphics optimization and therefore the regression equations were obtained as follows:

Washing ability in relation to cotton fabrics at $X_1 = -1$:

$$WA_1 = 85,259 + 2,046X_2 + 2,448X_3 - 2,519X_2^2 - 2,421X_3^2$$

Washing ability in relation to polyester fabrics at $X_1 = -1$:

$$WA_1 = 76,119 + 0,873X_2 + 0,98X_3 - 2,768X_2^2$$

For these equations the response surfaces have the form of hyperbolic paraboloid (Fig. 1).

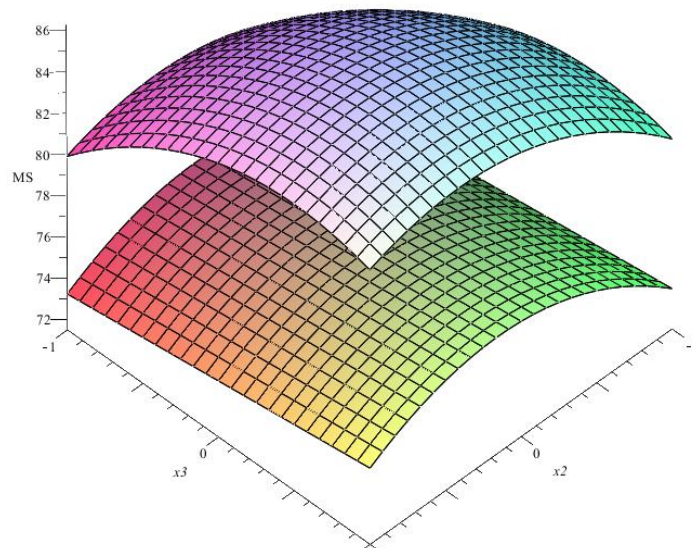


Fig. 1. The geometric form of the response surfaces of regression equations for cotton (top plot) and polyester (lower plot) fabrics

Projections of cross-sections of response surfaces for equations are show in figure 2.

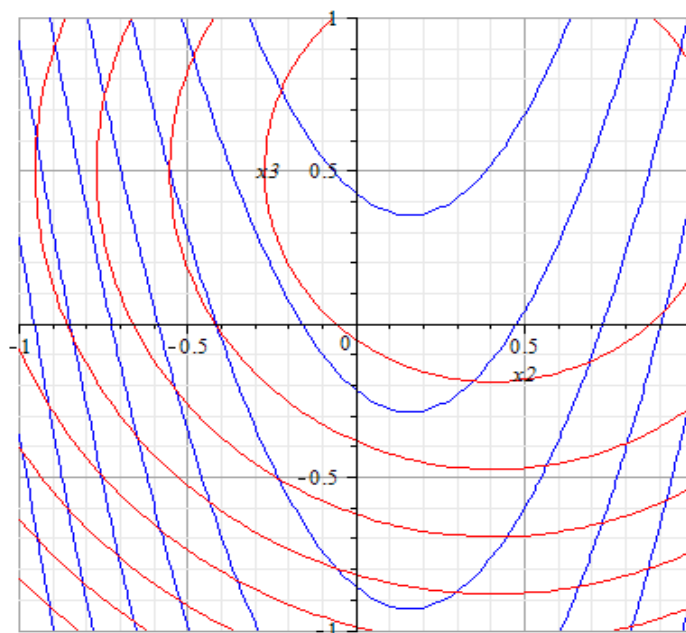


Fig. 2. Projections of cross-sections of response surfaces for equations: red lines – cotton fabric and blue lines – polyester fabric

Based on the calculations the optimum conditions of the processing materials were determined:

- for cotton fabrics: the concentration of the mixture of surfactant is 1 g/l, processing time is 6.2 min, temperature is 25⁰C, WA = 89.99%;
- for polyester fabrics: the concentration of the mixture of surfactant is 1 g/l, processing time is 6.7 min, temperature is 30⁰C, WA = 78.03%.

Conclusions

The mathematical models is developed and the optimal parameters of the process of wet cleaning, which is characterized by the maximum removal of contaminations from textile products, high-quality cleaning products are determined.

Summarizing the results of optimization we can recommend the following washing conditions for the treatment of materials from cotton and polyester blends: the concentration of surfactant is 1 g/l for 6 – 7

minutes at the temperature from 25 to 30⁰C. In these conditions, the degree of removal of the pollutants from textile materials is maximum (78 – 90 %).

References

1. Innovations in Clothing Design, Materials, Technology and Measurement Methods (2015): Monograph, ed. By Iwona Frydrych, Grazina Bartkowiak, & Maria Pavlowa. – Lodz. – 260 p.

2. Laundry Experience Event 2017. March 17-18th, 2017, Helmond, Netherlands.

3. Paraska, O. A., Kovalska, V.O., Karvan, S. A. (2016). Modern requirements for the production of detergents in Ukraine. Herald of Khmelnytskyi National University. №2. P. 273 – 277.

4. Yaroschuk O. V., Bokhonko O. P., Lepikash O. Yu. (2011). Structural approach to optimization of quality indicators of textile materials. Herald of Khmelnytskyi National University. №1. P. 209 – 213.

5. Paraska O., Karvan S. (2010). Mathematical modelling in scientific researches of chemical technology processes / Mechanics. Technical Transactions. – 2M/2010. – Issue 8. – Year 107. – P. 203 – 210. – Access mode: https://suw.biblos.pk.edu.pl/resources/i2/i4/i0/i2/r2402/ParaskaO_MathematicalModelling.pdf.

6. Karvan S., Chryashchevskiy V., Kulakov O., Golonzhka V. (2003). Application of Plaquet-Berman plan for optimization of dry cleaning processes // Measuring and computing technology in technological processes. – № 2. – P. 55 – 60.

7. Paraska O., Rak O. (2012). Optimization of technological parameters for improving energy efficiency laundry process // The XLIX session of the students scientific circles, Poland, Krakow, Maj 12st. – P. 64-65.

MATHEMATICAL MODELING OF HEAT PROTECTIVE PROPERTIES OF POLYMERIC MATERIALS FOR FOOTWEAR

Horiashchenko S., Horiashchenko K., Polishchuk O.
Khmelnyskyi National University, Ukraine

Introduction

According to physiological studies [1, 2, 3, 4], the duration of cooling of the human foot in shoes in the cold period of the year is clearly limited by the maximum allowable values of skin temperature in its various areas. Therefore, a long stay of a person in shoes during this period is possible only in shoes with appropriate heat-protective properties, i.e. for given climatic conditions of a certain length of stay will suit shoes with clearly defined heat-protective properties.

Methods and results

The proposed method for predicting the heat-protective properties of footwear, based on the equation of heat balance of the human foot [5]:

$$Q = Q_{m.n.} + Q_{\text{вип}} \pm D, \quad (1)$$

where Q – heat production of the human foot, W/m^2 which is determined according to the work [6];

$Q_{m.n.}$ - heat transfer from the surface of the foot to the environment through the details of the shoes, W/m^2 ;

$Q_{\text{вип}}$ - heat loss due to sweat evaporation, W/m^2 ; D – foot heat deficit, W/m^2 , that is, the change in the enthalpy of the foot relative to the comfort level.

If the heat production of the human foot is balanced by its heat loss, then $D = 0$; if the heat production of the human foot exceeds its heat loss, then $D > 0$ and heat accumulates in the foot; if the heat loss of the foot exceeds its heat production, then $D < 0$ and the foot is supercooled. Heat transfer from the surface of the foot to the environment through the details of the shoe is as follows:

$$\begin{aligned} Q_{m.n.} &= (Q_{m.n.})_B + (Q_{m.n.})_{H1} + (Q_{m.n.})_{H2} = \\ &= \frac{1}{S} \cdot \left[\left(\frac{S_B}{R_B} + \frac{S_{H1}}{R_{H1}} \right) \cdot (T_{CP.K} - T_0) + \frac{S_{H2}}{R_{H2}} (T_{CP.K} - T_{ГР}) \right], \end{aligned} \quad (2)$$

Advanced technologies in education, industry and the environment

where the indices "b", H1 and H2 show that the value refers to the parts of the upper of the shoe, to the parts of the bottom of the shoe that do not come into contact with the ground (snow, water) and to the parts of the bottom of the shoe in contact with the ground (snow, water);

$T_{CP,K}$ - weighted average temperature of the skin of the foot, °C;

$T_{ГП}$ - soil temperature (snow, water), °C;

T_0 - ambient temperature, °C;

S - full surface of the foot in contact with the details of the upper of the shoe, m^2 ;

S_b - the surface of the foot in contact with the details of the upper of the shoe, m^2 ;

S_{H1} - the surface of the foot in contact with the parts of the shoe bottom that do not have contact with the ground, m^2 ;

S_{H2} - the surface of the foot in contact with the parts of the bottom of the shoe that have contact with the ground, m^2 ;

R_{H1}, R_{H2}, R_B - the average total resistance of the heat transfer from the surface of the foot to the environment through the details of the shoes, $m^2 K/W$, which are complex characteristics for predicting the heat-protective properties of shoes.

$$\left\{ \begin{array}{l} \overline{R}_g = \left(\frac{\delta_{BH.}}{\lambda_{BH.}} \right)_g + \left(\frac{1}{\alpha_1} \right)_g + \sum_{i=1}^n \left(\frac{\delta_i}{\lambda_i} \right)_g + \left(\frac{1}{\alpha_2} \right)_g \\ \overline{R}_{H1} = \left(\frac{\delta_{BH.}}{\lambda_{BH.}} \right)_{H1} + \left(\frac{1}{\alpha_1} \right)_{H1} + \sum_{i=1}^n \left(\frac{\delta_i}{\lambda_i} \right)_{H1} + \left(\frac{1}{\alpha_2} \right)_{H1} \\ \overline{R}_{H2} = \left(\frac{\delta_{BH.}}{\lambda_{BH.}} \right)_{H2} + \left(\frac{1}{\alpha_1} \right)_{H2} + \sum_{i=1}^n \left(\frac{\delta_i}{\lambda_i} \right)_{H2} \end{array} \right. , \quad (3)$$

$\delta_{BH.}$ and $\lambda_{BH.}$ - respectively, the thickness of the layer of "inner shoes" (socks, stockings, etc.), m and the thermal conductivity of its material, W/(m K);

δ_i and λ_i - respectively, the thickness of the structural element of the shoe, m and the thermal conductivity of its material, W/(mK);

Advanced technologies in education, industry and the environment

α_1 - the average coefficient of heat transfer by convection and radiation from the outer surface of the "inner shoe" to the inner surface of the shoe, $W/(m^2 \cdot K)$;

α_2 - the average coefficient of heat transfer by convection and radiation from the outer surface of the shoe to the environment, $W/(m^2 \cdot K)$ (for areas of shoe bottoms that come into contact with the ground) $\alpha_1 = \infty$ ($1/\alpha_{H2} = 0$). Values of coefficients α_1 and α_2

are determined by the equations of the theory of heat transfer [7]. When determining the thermal resistance of thermal conductivity of structural elements of footwear $\sum_{i=1}^n \left(\frac{\delta_i}{\lambda_i} \right)$ also take into account the thermal resistance of adhesive joints and air layers. The selection of materials for the structural elements of footwear can vary the values R_{H1} , R_{H2} , R_B .

Heat loss due to sweat evaporation is defined as part of the heat production of the human foot:

$$Q_{\text{вип}} = \beta \cdot Q, \quad (4)$$

where $\beta = 0,25$ - for comfortable, $\beta = (0,16 \div 0,2)$ - for the cool and $\beta = (0,1 \div 0,16)$ - for cold climates [7, 8]. The heat deficit of the foot is determined by the formula:

$$D = \frac{m \cdot c}{S} \cdot \frac{d\theta}{d\tau}, \quad (5)$$

where m - foot mass, kg;

$c=3470$ J/kgK - the average heat capacity of human tissues,

$d\theta$ - changes in the average temperature of the foot over a period of time, K/m.

As shown in [5], for men $S/m=(0.038 \div 0.041)$. The average temperature of a human (Fig.1) foot is determined by the formula:

$$\theta = \mu \cdot T_{CP.K.} + (1 - \mu) \cdot T_p, \quad (6)$$

where T_p - temperature of internal tissues of the foot (rectal temperature), K.

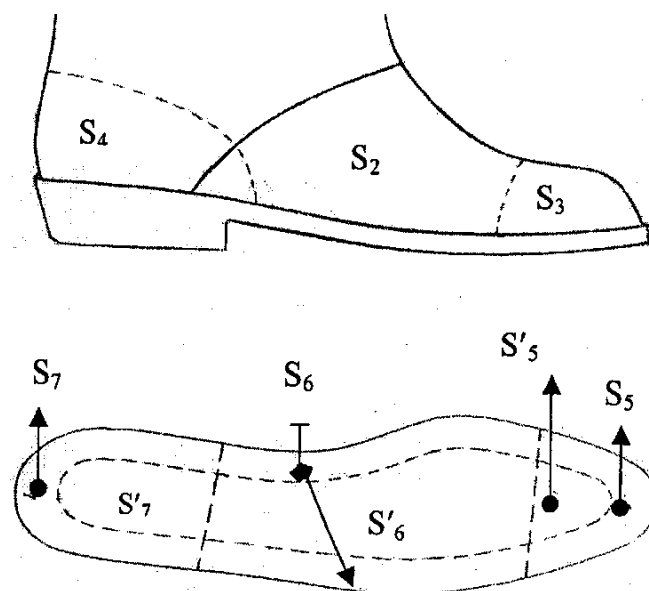


Fig.1. Zones on men's ankle boots

According to the research of A. Barton and O. Edholm [5, 7] $\mu = 0,3$. According to H. Bazetta [5, 8] - $\mu = 0,4$; E. Winslow and L. Herrington [5] - $\mu = 0,5$, at ambient temperatures below 23 °C and $\mu = 0,2$ at ambient temperatures from 23 to 35°C. Substituting expressions (2), (4), (5) and (6) into equation (1), and taking $d_{T_p} / d_{\tau} = -\gamma$, and taking into account the negative sign of D after some transformations, we obtain:

$$\frac{dT_{CP.K.}}{d\tau} = \frac{1}{\mu \cdot m \cdot c} \left\{ T_{CP.K.} \left(\frac{S_B}{R_B} + \frac{S_{H1}}{R_{H1}} + \frac{S_{H2}}{R_{H2}} \right) - T_0 \left(\frac{S_B}{R_B} + \frac{S_{H1}}{R_{H2}} \right) - T_{rp} \frac{S_{H2}}{R_{H2}} - Q \cdot S(1 - \beta) \right\} + \frac{(1-\mu)\gamma}{\mu} \quad (7)$$

The initial condition is written as when:

$$\tau = 0; T_{cp.k.} = T_{0cp.k.} \quad (8)$$

Solving the differential equation (7) with the initial condition (8) with respect to $T_{cp.k.}$, we will receive:

$$T_{CP.K} = T_{0CP.K} \cdot \exp \left[\frac{\tau}{\mu mc} \left(\frac{S_B}{R_B} + \frac{S_{H1}}{R_{H1}} + \frac{S_{H2}}{R_{H2}} \right) \right] + \left(\frac{S_B}{R_B} + \frac{S_{H1}}{R_{H1}} + \frac{S_{H2}}{R_{H2}} \right)^{-1} \times \times \left[T_0 \left(\frac{S_B}{R_B} + \frac{S_{H1}}{R_{H1}} \right) + T_{TP} \cdot \frac{S_{H2}}{R_{H2}} + Q \cdot S(1 - \beta) - mc(1 - \mu)\gamma \right] \times \times \left\{ 1 - \exp \left[\frac{\tau}{\mu mc} \left(\frac{S_B}{R_B} + \frac{S_{H1}}{R_{H1}} + \frac{S_{H2}}{R_{H2}} \right) \right] \right\} \quad (9)$$

and equation (9) is a mathematical model of the process of cooling the foot in shoes and allows you to determine the weighted average temperature of the skin of the foot TSRK. at any time τ according to the known design of the designed heat-shielding footwear (S_B , S_{H1} , S_{H2} , S), selected materials of its structural elements (R_{H1} , R_{H2} , R_B) and set temperatures T_0 , T_{TP} , $T_{0CP.K}$. values Q , m , c , γ and coefficients μ and β .

The obtained values $T_{CP.K}$ for different points of time τ are compared with the maximum allowable values of the temperature of the skin in different parts of the foot [8, 9] and determines the duration of the human foot in the designed shoes under specified climatic conditions. Structural elements of footwear i.e. change in the average total resistance of the heat transfer from the surface of the foot to the environment.

Thus, the polymer materials of the structural elements of the shoe i.e. the sizes R_{H1} , R_{H2} , R_B in formula (9), it is possible to predict the heat-protective properties of shoes.

The average forecasting of heat-protective properties of footwear is performed on the basis of expression of average complex forecasting characteristics, namely average total resistances of heat transfer from foot surface to external environment due to meteorological conditions of the region where the designed footwear will be operated. Properties of the human foot, the temperature of the internal tissues of the foot, as well as the maximum allowable values of the temperature of the skin in its various areas.

As known that during the operation of footwear in the system of foot - footwear - the external environment is observed as heat transfer and moisture transfer.

Thermal conductivity coefficients, which are determined taking into account humidity and porosity, are proposed to be used for local forecasting of heat-protective properties of footwear.

Advanced technologies in education, industry and the environment

In general, there is a formula for determining the weighted average temperature of the skin of the foot T_{cp} at any time τ for the average prediction of the heat-protective properties of shoes. Included in this formula are the surfaces S , S_B , S_{H1} , S_{H2} it is proposed to determine according to the method described in [12] taking into account the size range of shoes.

We introduce the following notation into formula (9):

$S_{H1} = S_B \cdot n_1$; $S_{H2} = S_B \cdot n_2$; $\overline{R_{H1}} = \overline{R_B} \cdot k_1$; $R_{H2} = \overline{R_B} \cdot k_2$ we will receive:

$$T_{CP.K} = T_{O.CP.K} \cdot \exp \cdot \left[\frac{\tau \cdot S_B}{\mu m c \overline{R_B}} \cdot \left(1 + \frac{n_1}{k_1} \right) \right] + \frac{\overline{R_B}}{S_B} \cdot \left(1 + \frac{n_1}{k_1} + \frac{n_2}{k_2} \right)^{-1} \cdot \left[T_0 \cdot \frac{S_B}{\overline{R_B}} \cdot \left(1 + \frac{n_1}{k_1} \right) + T_{\Gamma P} \cdot \frac{S_B}{\overline{R_B}} \cdot \frac{n_2}{k_2} + Q \cdot S(1 - \beta) - mc(1 - \mu) \right] \cdot \left\{ 1 - \exp \left[\frac{\tau \cdot S_B}{\mu m c \overline{R_B}} \cdot \left(1 + \frac{n_1}{k_1} + \frac{n_2}{k_2} \right) \right] \right\} \quad (10)$$

If instead of the weighted average temperature of the skin of the foot in the last formula to substitute the maximum allowable values of the temperature of the skin in its various parts $T_{cp.k.d.}$. According to works [3, 4], to approximate functions $y = 1 - \exp(B \cdot x)$ and $y = \exp(B \cdot x)$ by decomposing into a Taylor series. Then solving the resulting equation with respect to $\overline{R_B}$ and famous n_1 , n_2 , k_1 , k_2 already designed shoes and Q , m , c , γ , μ , β , T_0 , $T_{\Gamma P}$, determine the average total resistance of the heat transfer from the surface of the foot to the environment through the details of the upper of the shoe $\overline{R_B}$. Which provides the necessary duration of a person's stay in the shoes given metrological conditions:

$$\overline{R_B} = \frac{\tau \cdot S_B \left[T_{O.CP.K} \cdot \left(1 + \frac{n_1}{k_1} + \frac{n_2}{k_2} \right) - T_0 \cdot \left(1 + \frac{n_1}{k_1} \right) - T_{\Gamma P} \cdot \frac{n_2}{k_2} \right]}{\mu m c (T_{CP.K.d.} - T_{O.CP.K.}) + \tau [Q \cdot S(1 - \beta) + Q \cdot S(1 - \beta) - (1 - \mu) \gamma m c]} \quad (11)$$

The solution of equation (10) with respect to time τ gives the expression:

$$\tau = \frac{T_{CP.K.d.} - T_{O.CP.K.}}{\left\{ \frac{S_B}{\overline{R_B}} \left[T_{O.CP.K.} \cdot \left(1 + \frac{n_1}{k_1} + \frac{n_2}{k_2} \right) - T_0 \cdot \left(1 + \frac{n_2}{k_2} \right) - T_{\Gamma P} \cdot \frac{n_2}{k_2} \right] + Q S(1 - \beta) - (1 - \mu) \gamma m c \right\}} \quad (12)$$

Advanced technologies in education, industry and the environment

We use the equivalent - calm temperature $T_{\text{екв.шт.}}$ to obtain more accurate results instead of the ambient temperature (air) T_0 in expressions (10), (11) and (12), which is calculated by the formula:

$$T_{\text{екв.шт.}} = T_0 - \Delta T, \quad (13)$$

where ΔT - change in ambient temperature due to wind.

Mathematical processing of the results of our measurements gave for calculation ΔT such dependence:

$$\Delta T = 1,48044 - \ln v + 4,6488, \quad (14)$$

where V - wind speed in m/s.

Local forecasting of heat-protective properties of footwear is offered to be carried out in two ways.

In the first method in the design of shoes are allocated zones (packages), characterized by a constant composition of materials and calculated the total local resistance of the heat transfer from the human foot to the environment through the structural elements of these zones (packages) by the formula:

$$R_{XJ} = \left(\frac{\delta_{BH}}{\lambda_{BH}} \right)_x + \left(\frac{1}{\alpha_1} \right)_x + \sum_{i=1}^n \left(\frac{\delta_{IJ}}{\lambda_{IJ}} \right) + \left(\frac{1}{\alpha_2} \right)_x, \quad (15)$$

where α_1 - local heat transfer coefficients from the outer "surface of the inner shoe" to the inner surface of the shoe, $W/(m^2K)$;

α_2 - local heat transfer coefficients from the outer surface of the shoe to the environment;

λ_{BH} и δ_{BH} - respectively, the thickness of the layer of "inner shoes" (socks, stockings, etc.), m and the thermal conductivity of its material,

$W/(mK)$ $J = 1, 2, \dots, m$ - zone number (package); $I = 1, 2, \dots, n$ - the number of the material layer in the package, including adhesive seams and air layers;

δ_{IJ} и λ_{IJ} - respectively, the thickness, m and thermal conductivity, $W/(mK)$,

I - th material J- th packet; the index "x" shows the local conditions.

To recognize the heat transfer coefficient α_1 you can use the following criteria equations obtained for the air layers between two horizontal surfaces (foot and inner surface of the shoe) under conditions of free convection [5]:

$$\begin{aligned} Nu &= 0,195 \cdot Gr^{0,25} \text{ при } 10^4 < Gr < 4 \cdot 10^5; \\ Nu &= 0,068 \cdot Gr^{0,333} \text{ при } Gr > 4 \cdot 10^5; \end{aligned} \quad (16)$$

where $Nu = \frac{\alpha_1 \cdot \delta_{\text{поб}}}{\lambda_{\text{поб}}}$ Nusselt's criterion ;

$\delta_{\text{поб}}$ - the thickness of the air layer between the horizontal surfaces, m;

$Gr = \beta_m \cdot g \cdot \delta_{\text{поб}}^3 \cdot \Delta T / \nu^2$ - Grashof criterion;

$\beta_T = 1/T_{\text{поб}}$ - coefficient of volumetric expansion of air, 1/K;

g - acceleration of free fall, m/s²;

ΔT - the difference between the temperature of the heated horizontal surface (foot) and the average air temperature $T_{\text{боз}}$, K; $\lambda_{\text{поб}}$, Вт / м -K и $\nu_{\text{поб}}$, м/с - respectively, the coefficients of thermal conductivity and kinematic viscosity of air selected from the reference tables [5, 6] at its average temperature.

Heat transfer coefficient α_1 can also be determined by the following formula M.A. Mikheev [5]:

$$\alpha_1 = \frac{(\lambda_e)_{\text{поб}}}{\delta_{\text{поб}}} , \quad (17)$$

where the effective thermal conductivity of the air layer $(\lambda_e)_{\text{поб}}$, W/mK takes into account the intensification of heat transfer caused by free convection in the air layer between two horizontal or vertical surfaces under the influence of their temperature difference and is determined by the formula:

$$(\lambda_e)_{\text{поб}} = 0,165 \cdot \lambda_{\text{поб}} \cdot Gr^{0,25} . \quad (18)$$

Advanced technologies in education, industry and the environment

The values obtained by formula (12) R_{IJ} for each J-th packet are compared with the allowable values $[R]$. Obtained by numerous experimental studies of L.V. Kedrov adhering to the condition:

$$R_{xJ} \geq [R]. \quad (19)$$

In the second method, the values are determined R_{xJ} for each J -th packet by the following formula:

$$R_{xJ} = \frac{(T_{xJ}) - T_0}{g_{xJ}}, \quad (20)$$

$$R_{xJ} = \frac{(T_{KJ}) - T_{\Gamma P}}{g_{xJ}}, \quad (21)$$

where T_{xJ} - local skin temperatures in different parts of the human foot are measured using nichrome - constant thermocouples, °C; T_0 - ambient temperature, ° C; $T_{\Gamma P}$ - soil temperature , °C; g_{xJ} - local heat fluxes by radiation and convection, measured by heat measuring sensors, W/m [9]. Heat measuring sensors work by the method of an additional wall. Additional walls with the known thermal resistance of thermal conductivity are densely pressed to external surfaces of various zones of footwear.

$$R_{\text{доп}} = \frac{\delta_{\text{доп}}}{\lambda_{\text{доп}}}.$$

Measuring temperatures on the outer surfaces of the additional wall of nichrome - constants with thermocouples, and determining their difference $\Delta T_{\text{доп}}$, you can find local heat fluxes passing through the structural elements of the shoe according to the formula:

$$g_{xJ} = \lambda_{\text{доп}} \cdot \frac{\Delta T_{\text{доп}}}{\delta_{\text{доп}}}, \quad (22)$$

The values of R_{xJ} calculated by formulas (20) and (21) are compared with the admissible values of $[R]$, strictly adhering to condition (19). By selecting materials for

the top and bottom of shoes, as well as changing the thickness of the adhesive seams, you can achieve compliance with this condition.

The above engineering methods of averaged and local forecasting allow to determine at the stage of shoe design, the set of its heat-protective properties, which should have shoes designed for use in different climatic conditions.

The average heat transfer coefficient from the outer surface of the "inner shoe" to the inner surface of the shoe is taken $\bar{\alpha}_1 = \infty$, and the average heat transfer coefficient from the outer surface of the shoe to the external environment is equal to: $\bar{\alpha}_2 = 8 \text{ W} / \text{m}^2 \cdot \text{K}$.

For average forecasting of heat-protective properties of footwear, we use the formula (9). Which allows you to determine the weighted average temperature of the skin of the human foot $T_{\text{cp.k}}$ in men's shoes at different time τ .

The results of the average prediction of the heat-protective properties of men's ankle boots are shown in table 1.

Table 1. The results of the average prediction of the heat-protective properties of men's boots

$\tau, \text{ min}$	30	36	42	48	54	60	66	72	78	84	90
$T_{\text{cp.k}}, \text{ }^\circ\text{C}$	26	25	23	22,5	21	20	18	17	15,5	13,9	12,2

Analyzing the data in the table, we can conclude that in men's shoes this design at ambient temperature -18°C a person can be in a comfortable state, i.e. having a skin temperature of 24 to 26 $^\circ\text{C}$ [12], from about 30 to 40 minutes.

The presence of a person in men's shoes of this design is permissible only for 80 minutes, as according to the skin temperature of the foot 15°C is unacceptable.

Applying for men half-boots other more heat-protective materials, and changing thicknesses of glue seams, it is possible to achieve increase in time of stay of the person in the given footwear.

Conclusions

A mathematical model of the process of cooling a person's foot in shoes is obtained, which allows to determine the weighted average temperature of the foot skin at any time by known average total heat transfer resistances from the foot surface to the environment through shoe components, namely glue seams.

Advanced technologies in education, industry and the environment

The defined methods of forecasting heat-protective properties allow to define at a stage of designing of footwear that complex of its heat-protective properties which the footwear intended for operation in various climatic conditions should possess.

References

1. Dyeing of m-Aramid Fibers in Ionic Liquids/ Klaus Opwis, Bilal Celik, Rainer Benken, Dierk Knittel and Jochen Stefan Gutmann// *Polymers* 2020, 12(8), 1824; <https://doi.org/10.3390/polym12081824>
2. Reitz, R.D. and Bracco, F.V., "Mechanism of Atomization of Liquid Jets," *The Physics of Fluids*, Vol. 25, p. 1730, 1982. <https://doi.org/10.1063/1.863650>
3. Golinka, Є.O. Problems of applying protective coatings on rolled textile materials / Іe. Golinka // *Herald of Khmelnytsky National University. Technical sciences.* – 2017. – № 6. – С. 267-271.
4. Horiashchenko S. Research Spray and Device for Polymer Coatings on Fabric/ *Mechanika 2015 Proceedings Of The 20th International Scientific Conference, Kaunas - 2015*, p.101-104
5. Theory and practice of processes of gluing of details of clothes: the Textbook for students of higher educational institutions / V.E. Кузьвичев, Н.А. Gerasimov.-М.: Publishing Center "Academy», 2005.- 256 с
6. Astrita J., Marruchi J. Fundamentals of hydromechanics of non-Newtonian fluids. Y. Kazenin. М.: Publishing house. "World", 1978. – 310
7. Kovavich L. Bonding of metals and plastics. - М.: Chemistry, 1985. - 240 с.
8. Braslavsky V.A. Capillary processes in textile materials. - М.: Lightcombytizdat, 1987. - 112 с
9. Finite element modeling of porous polymer pipeline coating using X-ray micro computed tomography/Ole Vestrum Magnus Langseth Tore Børvik// *Composites Part B: Engineering* Volume 172, 1 September 2019, Pages 406-415, <https://doi.org/10.1016/j.compositesb.2019.04.028>
10. Harel, H., Marom, G. & Kenig, S, *Applied Composite Materials* 2002.
11. Horiashchenko, S.; Horiashchenko, K.; Musiał, J. Methodology of measuring spraying the droplet flow of polymers from nozzle. *Mechanika* 2020, 26, 82–86.
12. Betchelor Dzh. Vvedenie v dinamiku zhidkosti. Per. s angl./Pod red.. O. F. Vasil'eva. М., Mnr, 1973.
13. Modeling and research of polymer coating on clothing materials. S. Horiashchenko, G. Paraska, S. Petegerych. // *Innovation in textile materials&protective clothing. Monograph*, Warsaw, 2012, с.151-159.

DETERMINATION OF THE PARAMETERS OF RHEOLOGICAL LEATHER MODELS BY THE INDIRECT METHOD

Ihnatyshyn M., Rosul R.

Mukachevo State University, Ukraine

Introduction

There are materials, tissues, biological tissues, physical systems that have elastic-viscous properties, i.e. show elastic and viscous properties at the same time. Theoretical and experimental study of such systems is carried out using rheological models.

In [1], it has been indicated that theoretical and experimental studies of soil consolidation take into account the rheological properties of liquids in soil channels. In [2], rheological modeling was used in the study of the magnetostrictive transducer. Stupnytsky V.V. and Dolyniak Ya. V. [3] have considered the formation of surfaces of parts made of structural steels using a rheological picture of the influence of various factors on the process.

A number of authors study the influence of various factors on the behavior of rheological systems. Siromyatnikov V.G., Maslennikova L.D. and Anufriev V.A. consider the influence of molecular interactions in mixtures of polymers [5] on the rheological behavior of the system. Maslennikova L.D. and Fabuliak F.H. studied the effect of calcium carbonate on the rheological flow and molecular interactions with latex [6]. The rheological properties of adhesive mastic have been studied in [7]. Maslennikova L.D. has considered the rheological features of viscous aqueous systems [8] in the presence of calcium carbonate. Smachylo O.V. [9] has determined the effect of processing in organic solvents on the mechanical characteristics of clothing leather.

Researchers use different rheological schemes that transform into differential equations. The solutions of the corresponding differential

equations are functions of time and contain the parameters of the rheological scheme:

$$\begin{aligned}\varepsilon(t) &= \varepsilon(t, E_i, \eta_j) \\ \sigma(t) &= \sigma(t, E_i, \eta_j)\end{aligned}\quad (1)$$

where t - the time of the study of the process, ε - the relative deformation, σ - the stress, E_i - the modulus of elasticity i - i -th element of the model, η_j - the fluidity j - the element of the model.

The question of experimental determination of parameters of various rheological models is urgent. This question is relevant in various respects. For example, for the same system, you can build alternative rheological models and test them for adequacy of the object after experimental determination of relaxation characteristics. It would be interesting to determine the change in the relaxation characteristics of the rheological model, for example, clothing leather before and after treatment in organic solvents, and not only the integral modulus of elasticity, relative deformation and strength.

The aim of the study

To apply the mathematical apparatus for solving a system of nonlinear equations to determine the relaxation parameters of a rheological model by an indirect method.

Research methods

Construction of a rheological model of the object under study and determination of the model parameters by the numerical method used to solve the system of nonlinear equations.

Object, subject and research methods

The object of the study is a viscoelastic rheological model of clothing leather. The subject of research - relaxation parameters of the rheological model.

Formulation of the problem

We formulate the problem of finding the relaxation parameters of the rheological model in general. Let $1 \leq i \leq m$, where m - number of relaxation parameters α_i rheological model, c - parameter determined from the initial conditions. So, all the unknown parameters of the model $q = m + 1$. These unknown, α_i and c , can be found as a solution of a system of nonlinear equations:

$$\left\{ \begin{array}{l} \varepsilon(t_1, \alpha_i, c) = \varepsilon(t_1); \\ \dots\dots\dots; \\ \varepsilon(t_k, \alpha_i, c) = \varepsilon(t_k); \\ \dots\dots\dots; \\ \varepsilon(t_q, \alpha_i, c) = \varepsilon(t_q); \end{array} \right. \quad (2)$$

or

$$\left\{ \begin{array}{l} \sigma(t_1, \alpha_i, c) = \sigma(t_1); \\ \dots\dots\dots; \\ \sigma(t_k, \alpha_i, c) = \sigma(t_k); \\ \dots\dots\dots; \\ \sigma(t_q, \alpha_i, c) = \sigma(t_q); \end{array} \right. \quad (3)$$

where k - equation number $1 \leq k \leq q$.

In what follows we will consider a system of equations (2).

Results and their evaluation

The elastic properties of the leather are described by Hooke's law, fig.1:

$$\sigma = E \cdot \varepsilon, \quad (4)$$

and viscous properties - Newton's law, fig.2:

$$\sigma = \eta \cdot \dot{\varepsilon} \quad (5)$$

where $\dot{\varepsilon}$ - time derivatives of relative deformation ε .

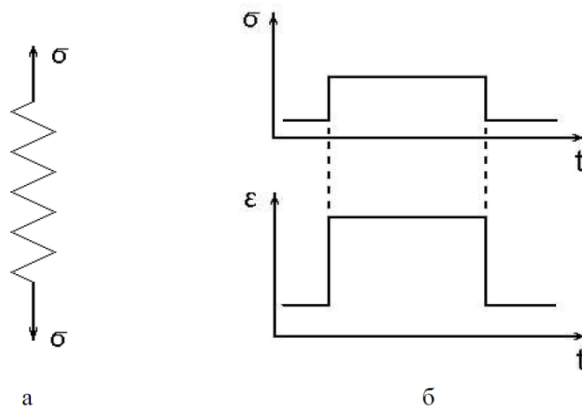


Fig. 1. Rheological model of the elastic element, a - the model of the elastic element, b - deformation of the elastic element by step load.

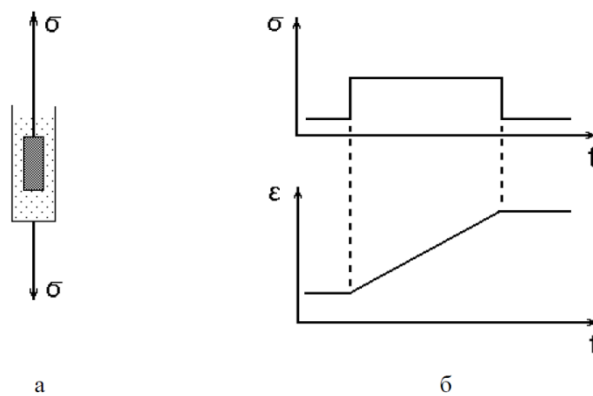


Fig. 2. Rheological model of a viscous element, a - model of a viscous element, b - deformation of the viscous element by step load.

Let's consider the following rheological model, Fig.3.

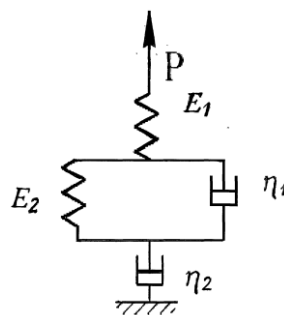


Fig. 3. Rheological model of the leather.

We transform the model, fig. 3., in the differential equation, given that when connected in parallel, Fig. 4, we have the ratio:

$$\begin{cases} \sigma = \sigma_1 + \sigma_2 ; \\ \sigma_1 = \eta \cdot \dot{\varepsilon} ; \\ \sigma_2 = E \cdot \varepsilon ; \end{cases} \quad (6)$$

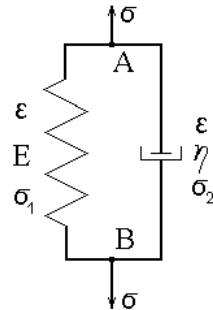


Fig. 4. Voigt's model.

and in series connection, fig. 5, we have the ratio:

$$\begin{cases} \varepsilon = \varepsilon_1 + \varepsilon_2 ; \\ \sigma = E \cdot \varepsilon_1 ; \\ \sigma = \eta \cdot \dot{\varepsilon}_2 ; \end{cases} \quad (7)$$

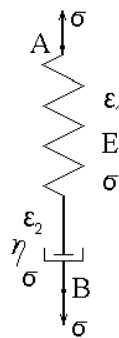


Fig. 5. Maxwell's model.

We introduce the notation describing the rheological model, fig. 3:

σ - stress arising under the action of force P ,

ε - relative deformation that occurs under the action of force P ,

σ_1 - the stress that occurs in the elastic element E_1 ,

ε_1 - the relative deformation that occurs in the elastic element E_1 ,

$\sigma_{x\sigma}$ - the stress that occurs in the elastic element E_2 ,

ε_x - the relative deformation that occurs in the elastic element E_2 ,

$\sigma_{x\eta}$ - the stress that occurs in the viscous element η_1 ,

ε_x - the relative deformation that occurs in the viscous element η_1 ,

σ_2 - the stress that occurs in the viscous element η_2 ,

ε_2 - the relative deformation that occurs in the viscous element η_2 ,

We construct the relations describing the rheological model, fig. 3:

$$\varepsilon = \varepsilon_1 + \varepsilon_x + \varepsilon_2 \quad (8)$$

$$\sigma = \sigma_1 = E_1 \cdot \varepsilon_1 \quad (9)$$

$$\sigma = \sigma_x = \sigma_{x\sigma} + \sigma_{x\eta} = E_2 \cdot \varepsilon_x + \eta_1 \cdot \dot{\varepsilon}_x \quad (10)$$

$$\sigma = \sigma_2 = \eta_2 \cdot \dot{\varepsilon}_2 \quad (11)$$

Let's exclude from formula (8) ε_1 , ε_x , ε_2 for this we find the first and second derivatives:

$$\dot{\varepsilon}_x = \dot{\varepsilon} - \dot{\varepsilon}_1 - \dot{\varepsilon}_2, \quad \ddot{\varepsilon}_x = \ddot{\varepsilon} - \ddot{\varepsilon}_1 - \ddot{\varepsilon}_2 \quad (12)$$

$$\dot{\varepsilon}_1 = \frac{1}{E_1} \cdot \dot{\sigma}, \quad \dot{\varepsilon}_2 = \frac{1}{\eta_2} \cdot \sigma \quad (13)$$

$$\ddot{\varepsilon}_1 = \frac{1}{E_1} \cdot \ddot{\sigma}, \quad \ddot{\varepsilon}_2 = \frac{1}{\eta_2} \cdot \dot{\sigma} \quad (14)$$

Let's find the first derivative of the relation (10):

$$\dot{\sigma} = E_2 \cdot \dot{\varepsilon}_x + \eta_1 \cdot \ddot{\varepsilon}_x \quad (15)$$

We substitute (13) and (14) in (12), and then (12) in (15), simplify and obtain the differential equation describing the rheological model, Fig.3.:

$$\eta_1 \cdot \ddot{\varepsilon} + E_2 \cdot \dot{\varepsilon} = \frac{\eta_1}{E_1} \cdot \ddot{\sigma} + \left(1 + \frac{\eta_1}{\eta_2} + \frac{E_2}{E_1}\right) \cdot \dot{\sigma} + \frac{E_2}{\eta_2} \cdot \sigma \quad (16)$$

In an isomeric experiment $\varepsilon = const$ equation (16) takes the form:

$$\frac{\eta_1}{E_1} \cdot \ddot{\sigma} + \left(1 + \frac{\eta_1}{\eta_2} + \frac{E_2}{E_1}\right) \cdot \dot{\sigma} + \frac{E_2}{\eta_2} \cdot \sigma = 0, \quad (17)$$

and in an isotonic experiment, equation (16) takes the form:

$$\ddot{\varepsilon} + \frac{E_2}{\eta_1} \cdot \dot{\varepsilon} - \frac{E_2}{\eta_1 \cdot \eta_2} \cdot \sigma_0 = 0. \quad (18)$$

Given the initial condition, we obtain the solution of a homogeneous second-order differential equation (18):

$$\varepsilon(t) = c \cdot [e^{\alpha_1 t} - e^{\alpha_2 t}], \quad (19)$$

where

$$\alpha_1 = \frac{E_2}{2\eta_1} \cdot \left(\sqrt{1 + 4 \cdot \frac{\eta_1}{\eta_2} \cdot \frac{\sigma_0}{E_2}} - 1 \right), \quad (20)$$

$$\alpha_2 = -\frac{E_2}{2\eta_1} \cdot \left(\sqrt{1 + 4 \cdot \frac{\eta_1}{\eta_2} \cdot \frac{\sigma_0}{E_2}} + 1 \right), \quad (21)$$

Relationships (18), (20) and (21) do not contain a parameter E_1 of the rheological model, so it is impossible to determine it in an isotonic experiment.

We have three unknown quantities, and, therefore, their experimental finding requires three nonlinear equations that form a system:

$$\begin{cases} c \cdot [e^{\alpha_1 t_1} - e^{\alpha_2 t_1}] = \varepsilon(t_1), \\ c \cdot [e^{\alpha_1 t_2} - e^{\alpha_2 t_2}] = \varepsilon(t_2), \\ c \cdot [e^{\alpha_1 t_3} - e^{\alpha_2 t_3}] = \varepsilon(t_3), \end{cases} \quad (22)$$

where t_1 , t_2 and t_3 moments of time at which the value of relative deformation is determined $\varepsilon(t_1)$, $\varepsilon(t_2)$ and $\varepsilon(t_3)$ at isotonic loading σ_0 .

Let's make the program for processing of experimental data and indirect definition of parameters of rheological model, fig. 3, namely, c , α_1 and α_2 , according to the results of an isotonic experiment. The program is compiled in the system MATHCAD.

Start of the program

Input data (conditional values)

$t_1 := 0.1$; $t_2 := 0.2$; $t_3 := 0.3$ (time in seconds),

$\varepsilon_1 := 0.391$; $\varepsilon_2 := 0.658$; $\varepsilon_3 := 0.846$ (relative deformation in particles)

Approximate values of the required parameters:

$$c := 2; \quad \alpha_1 := 3; \quad \alpha_2 := 4$$

Given

$$\begin{aligned} c \cdot (e^{\alpha_1 t_1} - e^{\alpha_2 t_1}) &= \varepsilon(t_1) \\ c \cdot (e^{\alpha_1 t_2} - e^{\alpha_2 t_2}) &= \varepsilon(t_2) \\ c \cdot (e^{\alpha_1 t_3} - e^{\alpha_2 t_3}) &= \varepsilon(t_3) \end{aligned} \quad \begin{pmatrix} c \\ \alpha_1 \\ \alpha_2 \end{pmatrix} := \text{Find}(c, \alpha_1, \alpha_2)$$

$$\begin{pmatrix} c \\ \alpha_1 \\ \alpha_2 \end{pmatrix} = \begin{pmatrix} 1 \\ 0.366 \\ 4.366 \end{pmatrix}$$

$$\varepsilon(t) = c \cdot (e^{\alpha_1 t} - e^{\alpha_2 t})$$

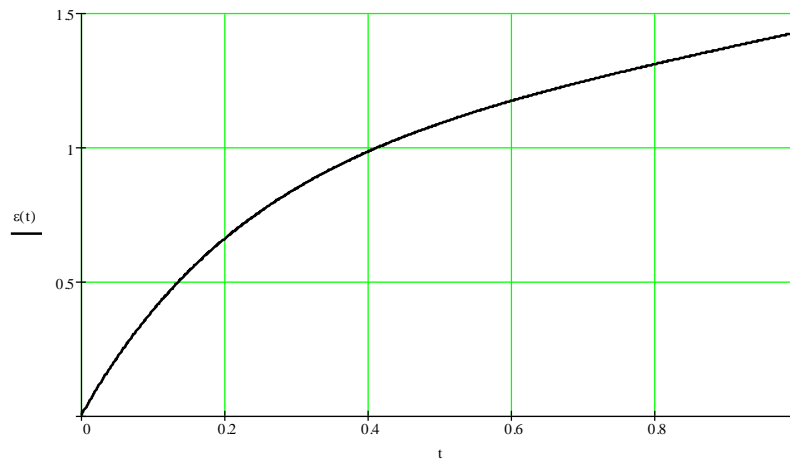


Fig. 6. Change in the relative deformation of the rheological model (Fig. 3) over time for the interval 0 - 1 sec.

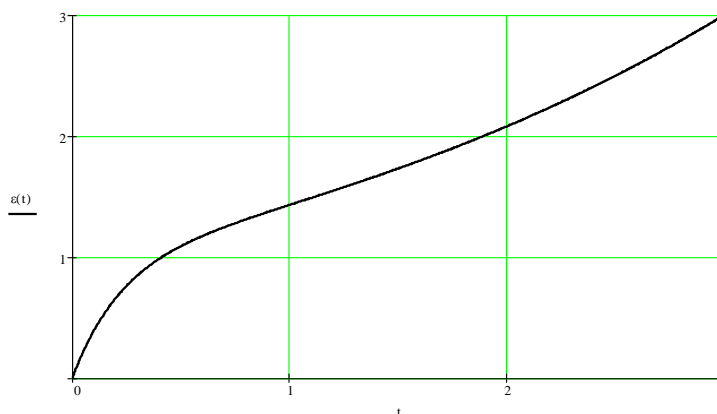


Fig. 6. Change in the relative deformation of the rheological model (Fig. 3) over time for the interval 0 - 3 sec.

Actual values of the required parameters: $c=1$; $\alpha_1=0.366$;
 $\alpha_2=4.366$

End of program.

Conclusions

The main result of this work is to verify the adequacy of the rheological model to the system being modeled. The check is carried out by calculating the relaxation parameters of the system, α_1 and α_2 according to conditional data. If in a given time interval the system of nonlinear equations (22) has a solution, then the model adequately describes the system, if not, the model must be changed.

The rheological model considered by us, fig. 3, adequately describes system in sites from 0 to 10 sec.

Further research involves the construction of an experimental setup to implement the mathematical model of the experiment described above.

References

1. Badiora N.P., Kots I.V. Analysis of theoretical and experimental studies of injection fixing of soil massifs. Bulletin of Khmelnytsky National University, №2, 2014 (211), p. 46.
2. Shapovalov O.I. Mathematical model of magnetodynamic flux in the zone of rheological transition of magnetostrictive transducer. Bulletin of Khmelnytsky National University, №2, 2014 (211), p. 240.

Advanced technologies in education, industry and the environment

3. Stupnytsky V.V., Dolyniak Ya.V. Simulation rheological modeling of the processes of forming the surfaces of parts made of structural steels. Lviv Polytechnic National University, Automation of Production Processes in Mechanical Engineering 98 and Instrument-Making. Vip. 49. 2015, p. 9.
4. Syromyatnikov V.G., Maslennikova L.D., Anufriev V.A. Influence of molecular interactions in mixtures of rubber polymers in latex-polyvinyl acetate in an aqueous medium on the rheological behavior of the studied systems // Chem. industry of Ukraine. - 2002. - № 1. - P. 24-26.
5. Osievska V.V., Fabuliak F.H., Maslennikova L.D. Rheological features of aqueous dispersions using calcium carbonate and aqueous solution of sodium silicate // Scientific Bulletin of the Nikolaev State Pedagogical University. - 2000. - Issue № 1. - P. 215-219.
6. Maslennikova L.D., Fabuliak F.H. Influence of calcium carbonate on rheological flow and molecular interactions with latex. // Scient. Bulletin of the Uzhhorod state. Univ. - 2001. - № 6. - P. 204-206.
7. V.V.Osievska, A.E. Miroshnikov, L.D. Maslennikova, F.H. Fabuliak. Rheological and IR spectroscopic studies of new adhesive mastic / V.V.Osievska, A.E. Miroshnikov, L.D. Maslennikova, F.H. Fabuliak // Physics of condensed macromolecular systems: Scientific notes of Rivne state. humanist. University.– 2000. - №8. - P. 9-16.
8. Maslennikova L.D. Rheological features of viscous water systems in the presence of calcium carbonate. // V All-Ukrainian Conference “Fundamental and Professional Training of Physics Specialists”: Abstracts. - K .: NPU. MP Dragomanova, 2000. - P.169.
9. Smachylo O.V. Material characteristics of clothing leather after treatment in organic solvents. Technology and Design, №4 (9), 2013, p. 7

APPLYING NONLINEAR APPROXIMATION METHODS IN EXPERIMENTAL DATA PROCESSING

Chesanovskyi I., Katerynychuk I.

B. Khmelnytskyi National Academy of the State
Borderguard Service of Ukraine, Ukraine

Introduction

A variety of electro-converting devices serves as the basis for instrumental measurements in technological processes. Such devices act as sensors with the characteristics that depend on the accuracy and information analysis quality about the entire technological process and its individual stages. This has been the case for a long time, until digital signal processing (DSP) has changed the approach. Particularly, the quantity and quality of primary data needed for effective information analysis. This became possible due to the application of mathematical methods, such as approximation, in the data analysis. These methods have convenient and efficient discrete forms both with fast digital implementation algorithms. Thus, their combination with an effective element base brought mathematical signal processing to a qualitatively new level.

Data approximation allows to build processing algorithms sensitive not only to the presence or absence of the signal in input mixture (detection task), or the presence of a separate signal implementation in the mixture (distinction task), but also to identify certain features (signs) of the signal. In the last case, signal features are the manifestations of expected or undesirable process trends. Therefore, the DSP algorithms are focused on them. In general, the theory of approximation studies the errors of different approximation systems on functional bases. Worth mentioning that for the problems of signal theory it focuses mainly on orthonormal bases. Linear approximation serves to make a signal projection (discrete sample set, function, etc.) on a system of a priori selected vectors in linear space. Such a linear approximation is particularly convenient for uniformly smooth

signals using Fourier, Hartley or various smooth wavelet bases. This is due to a compact reflection of monotonic processes. At the same time, described operation reacts sharply to local gaps. On the other hand, a number of discontinuous bases including Rademacher, Haar, etc., give valuable results in the approximation of discrete signals (stepped, pulsed, etc.). These two classes of bases for approximation are universal tools that give a satisfactory result for the analysis of signals of their class. It should be taken into consideration that for obtaining a good result it is always necessary to solve the problem of choosing the basis for each particular case. Truly, the best basis in one's task is the result of selection among all those that are most related to the approximation process. The optimal basis must be obtained in each specific case, which is the foundation of nonlinear approximation methods. The method of adaptive basis selection is much simpler, but in conditions of limited variation is no less effective. It depends on the characteristics of the signal and gives no less important result in the correct formation of the catalog of basic functions (vectors) for specific types of problems.

Methods and results

The signal in the orthonormal basis can be represented as the results of M scalar products with a priori given vectors (functions).

Assume $C = \{c_m\}_{m \in \mathbb{N}}$ orthonormal basis in the Hilbert space H , i.e.:

$$\begin{cases} \langle c_m, c_n \rangle = 0, \text{ at } m \neq n, \\ \langle c_m, c_n \rangle = 1, \text{ at } m = n, \end{cases} \quad (1)$$

where $\langle x, y \rangle$ – scalar product.

Any function that satisfies Dirichlet conditions can be decomposed by this basis

$$f = \sum_{m=0}^{+\infty} \langle f, c_m \rangle c_m. \quad (2)$$

If M projections are used, the approximation accuracy decreases as

$$f_M = \sum_{m=0}^{M-1} \langle f, c_m \rangle c_m, \quad (3)$$

because not all projections are taken into account.

The potential accuracy of real approximating systems is always limited by error

$$\varepsilon(M) = \|f - f_M\|^2 = \sum_{m=M}^{+\infty} |\langle f, c_m \rangle|^2, \quad (4)$$

which tends to zero with increasing value of M , $\lim_{M \rightarrow \infty} \varepsilon(M) = 0$, because $\|f\|^2 < +\infty$.

There are many approaches to solve the problem

$$\lim_{var(C), M \rightarrow 1} \sum_{m=M}^{+\infty} |\langle f, c_m \rangle|^2 \leq \varepsilon_{max} \rightarrow 0, \quad (5)$$

which in the vast majority agree that increasing the efficiency of the approximating system (increasing the accuracy of the approximation at $M \rightarrow 1$) is possible provided the following equation

$$c_m = G_m(f), \quad (6)$$

where $G(\cdot)$ – is a functional set, that forms an orthonormal basis from f , or serves as a criterion for the optimal selection and scaling of the existing basis for a given function f (f and C adjustment).

In signal processing tasks it is typical to use a Fourier approximation with its harmonic basis

$$c_m = e^{jm\omega t}, m \in \mathbb{Z}.$$

This is due to the fact that the harmonic process is the basis of almost all modulation methods, and a typical modulated signal is a narrowband process, i.e.

$$\delta_f = \frac{\Delta f}{f_0} \ll 1,$$

where Δf – the absolute width of the frequency spectrum of the signal ($f = \omega/2\pi$); f_0 – central frequency (in case of modulation signal – carrier frequency).

It should be noted that this type of signals are widely used in various technological processes, where as in radio applications, the value of Δf depends on the information capacity of the signal.

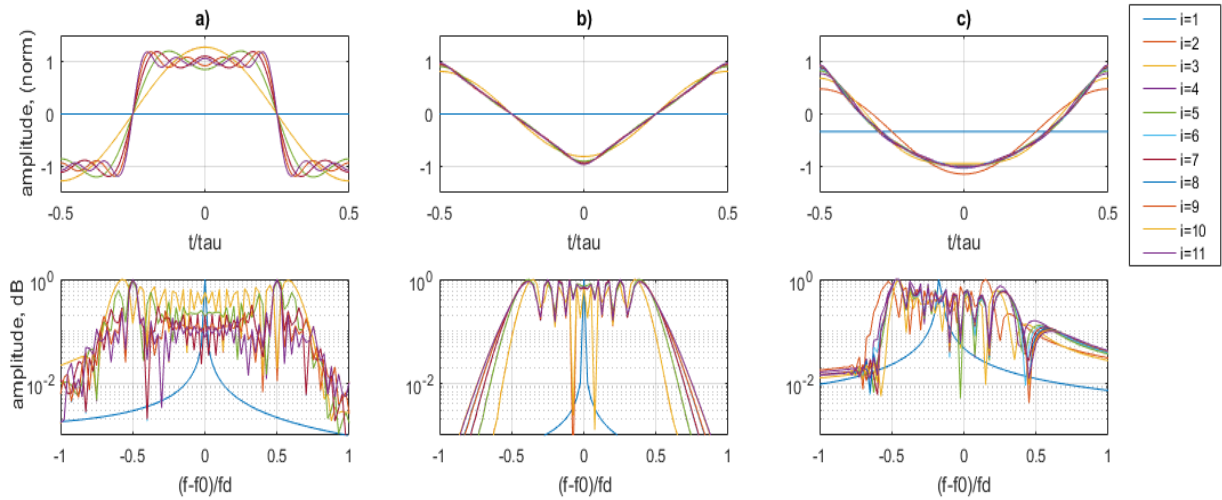


Fig. 1. Fourier approximation of different signal types

Fig. 1 shows an example of the application of the Fourier approximation for different types of narrowband signals (harmonic signal of duration τ (a), signal of the same duration but with a linear change of oscillation frequency (b), signal of the same duration but with quadratic change of oscillation frequency (c)).

As figure shows, this basis is better coordinated with smooth (monotonic) functions, and is extremely inconvenient for use in the approximation of functions with gaps. This can be clearly seen from the decreasing rate of the decomposition coefficients modules. The higher modulus value, the more monotonous function becomes. Aside, we can note the complete consistency of the basis with harmonic functions ($i = 1$), because the basis functions are harmonic ones.

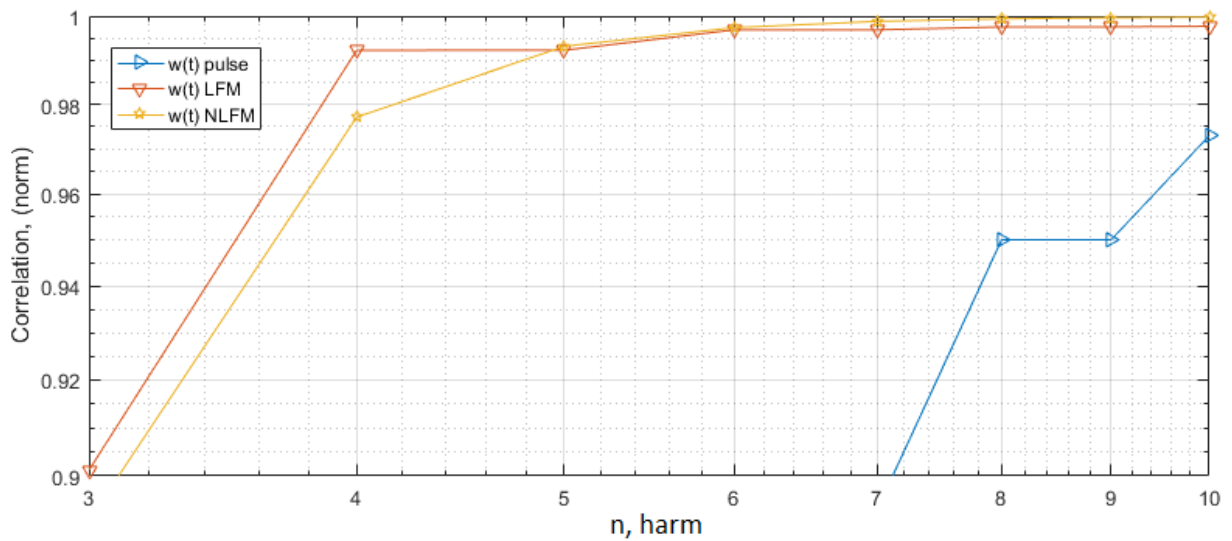


Fig. 2. The Fourier approximation accuracy of different signal types based on the number of decomposition coefficients

Depending on the number of projections in the harmonic basis, approximation accuracy can be estimated using the correlation coefficient (Fig. 2). It is obvious that the harmonic basis is quite suitable for this class of signals. Therewith, the situation will change along with Δf increasing, especially due to the discreteness of the modulating functions.

Despite the compactness of the harmonic basis, it is inefficient for the detection and distinguishing tasks. The kind of tasks that form the signal processing foundation.

As follows, applying the Fourier transform in the case of non-stationary modulating signals, results in complete loss of information about their internal dynamics. Thus, it makes it impossible to solve the problem of distinguishing the same type of signals. In [1], to avoid this, it is proposed to match the basis with the signal using weight windows, or to use the basis with a localized core that matches the signal. These are different variants of nonlinear approximation in signal processing tasks, the implementation mechanisms of which are similar.

As an example, consider two different narrowband signals formed by angular modulation of the polyharmonic functions (Fig. 3).

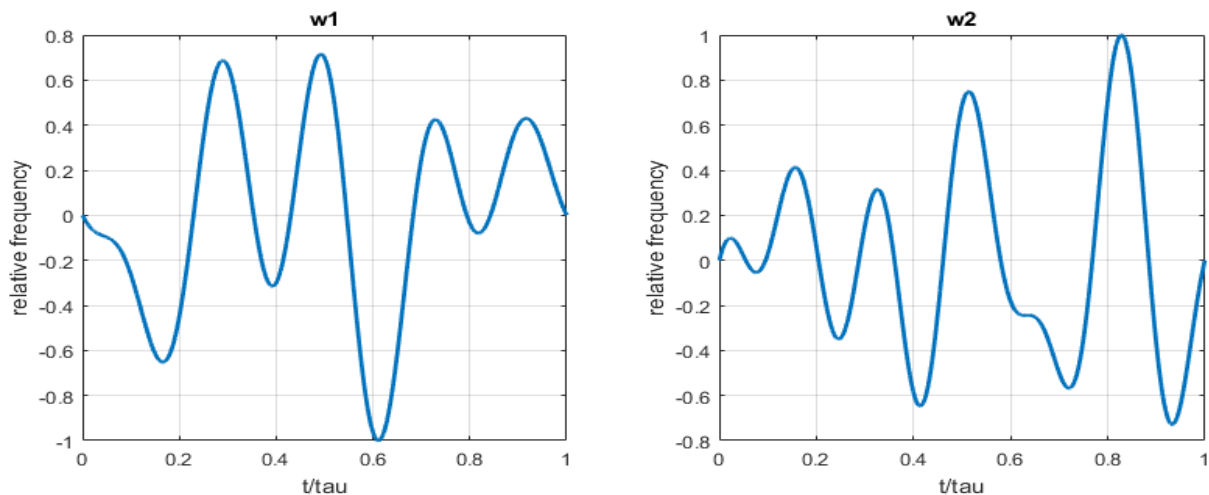


Fig. 3. Randomly generated modulating polyharmonic oscillations

This form of modulating signal is typical for many practical challenges that deals with narrowband signals. The amplitude-frequency spectrum of these signals obtained using the Fourier transform are presented in Fig. 4.

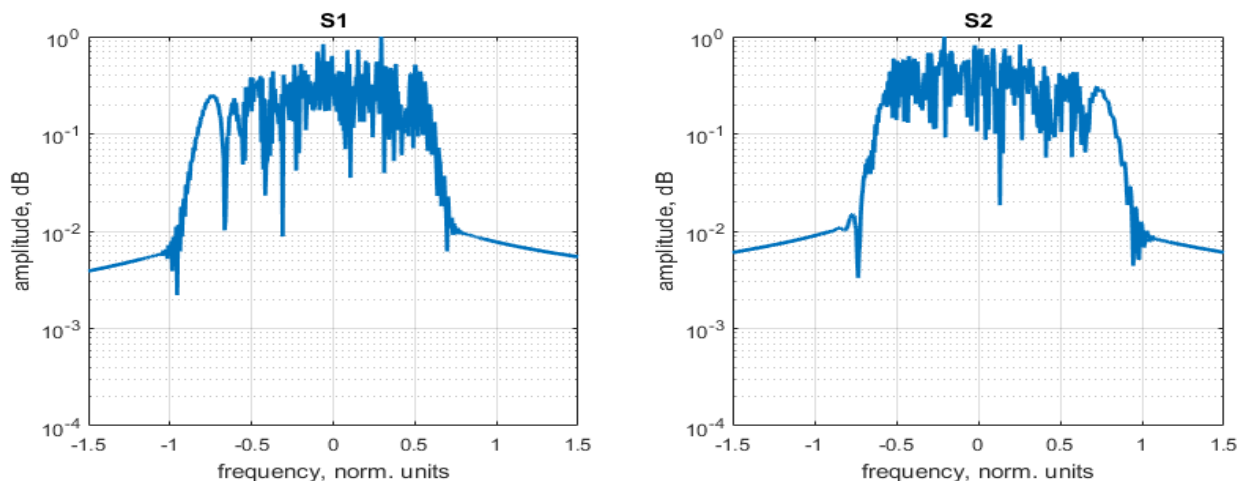


Fig. 4. Two implementations of frequency-modulated narrowband signals in the amplitude-frequency domain (spectrum)

As expected, the frequency spectrums are concentrated in a small area and have almost identical shape. Obviously, it is almost impossible to distinguish signals based on this representation. The reason is that they are completely identical.

In turn, applying windowed Fourier transform, with the correct choice of weight window filters and their scaling (relatively to their

modulating function dynamics in time domain), the result may be radically different. Fig. 5 demonstrates given statement.

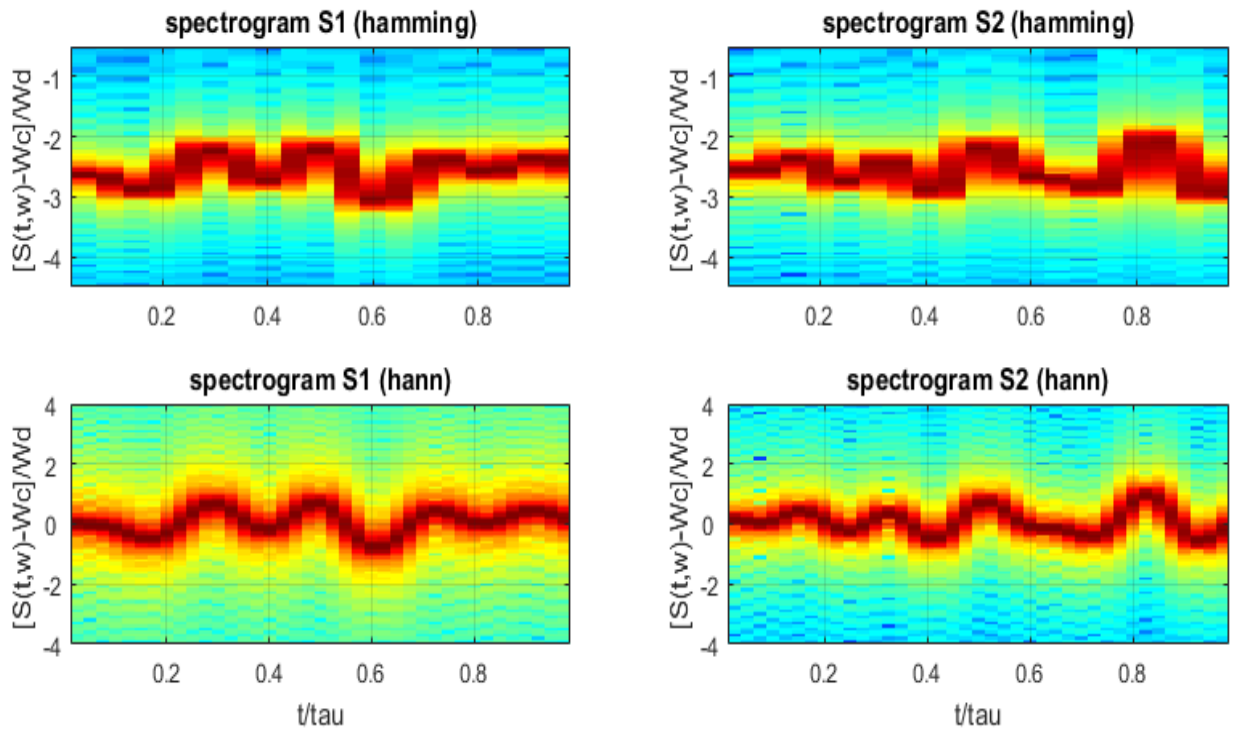


Fig. 5. Two implementations of frequency-modulated narrowband signals in time-frequency domain (spectrogram)

These spectrograms weighted by the Hamming window and the Khan window have different localization of signal energy on areas with the same dynamics of the modulating function. It indicates a direct dependence of the approximation efficiency on the choice of type and scale of the weight window filter.

Obviously, the variation in the shape and duration of the weight window filters is not a complete set of tools for obtaining an optimally compact and maximum contrast image of the studied signals. The main tool for solving this problem is a special design of the basis obtained directly from the signal shape, or adaptation of the existing basis. Last one is a typical approach of nonlinear approximation and can be implemented by means of the wavelet analysis theory.

Summarizing the above expressions of basic transformations, use the expression [1,3]:

$$S(t) = \sum_D \lambda_{S,D} C_D(t), \quad (7)$$

where D - basis dimensions vector; $C_D(t)$ – transformation basis (core functions); $\lambda_{S,D}$ – transformation coefficients (projections).

For the case of wavelet transform $D = \{a, b\}$:

$$\lambda_{S,D} = \int_D S(t) C_D(t) dt. \quad (8)$$

In wavelet transform theory, accepted the following statement $C_D(t) = \Psi_{a,b}^*(t)$, accordingly

$$\lambda_{S,D} = S(a, b) = \int_{-\infty}^{+\infty} S(t) \Psi_{a,b}^*(t) dt, \quad (9)$$

where $\Psi_{a,b}^*(t)$ – set of approximating functions (mother wavelet at $a = 1, b = 0$)

Fig. 6 shows the result of applying of local-basis transform (wavelet in particular) to approximate narrowband signals $w1(t), w2(t)$. The transformation which uncover zones with maximum energy concentration, or there is a possibility of skeletons allocation (analog of a gradient map of a vector field) is considered optimum. Continuous wavelet transforms (CWT) on the figures were obtained using Mexican hat wavelets (mexh) [2] and the first function of the coiflet family (coif1) [2].

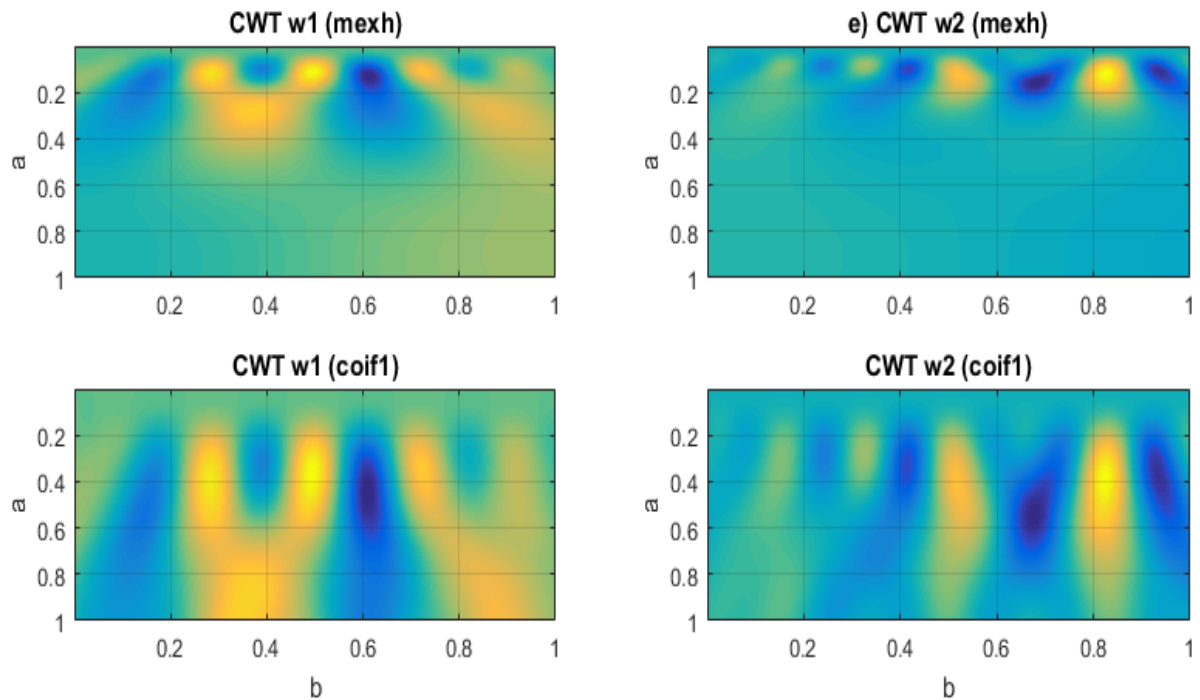


Fig. 6. Two implementations of frequency-modulated narrowband signals in wavelet domain

Obtained distributions show that the choice of the mother wavelet is a key task that requires special attention. To select the mother wavelet $\Psi_{a,b}$ from the library, we propose the criterion of minimum number of significant decomposition coefficients. Proposed criterion is analogous to (5) and lays in searching a wavelet with the minimum number of its decomposition coefficients whose absolute values exceed a threshold. At the same time, the approximation error does not exceed the allowable value. Fig. 7 shows the results of applying the optimal mother wavelet.

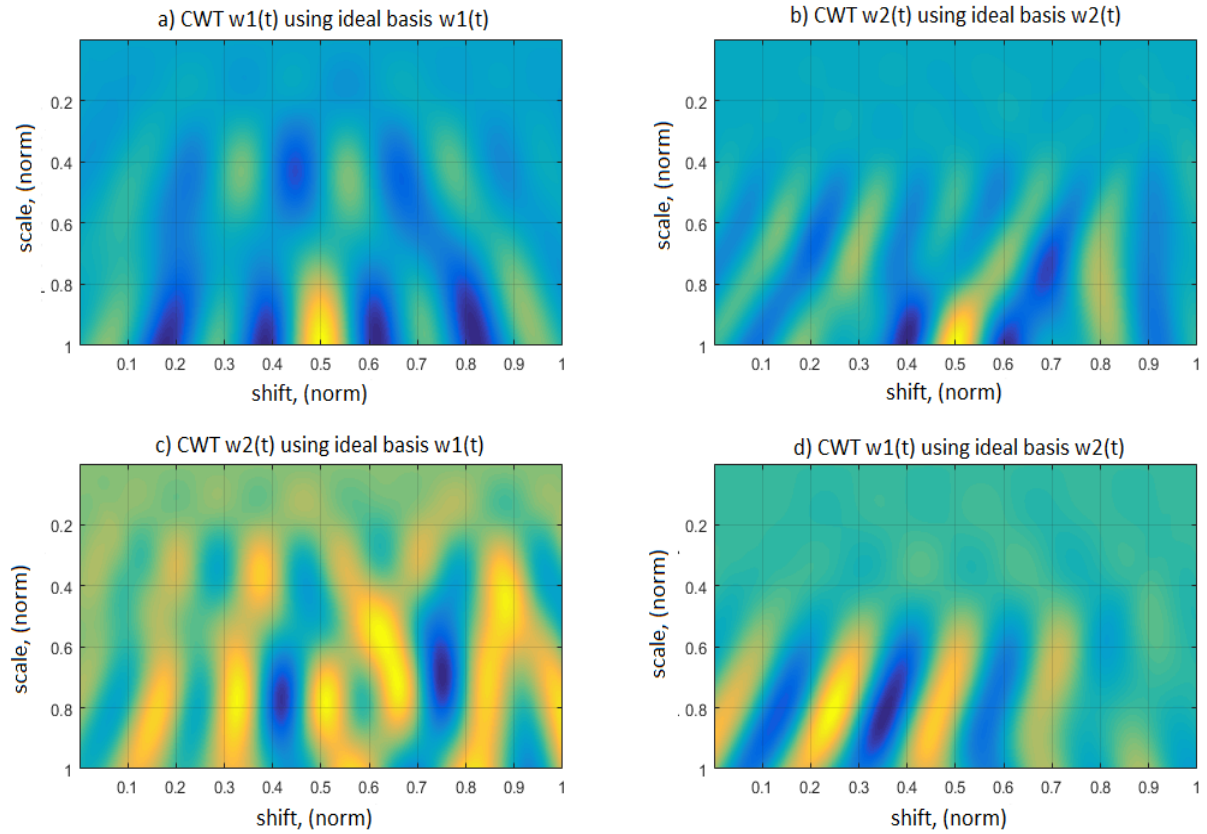


Fig. 7. Two implementations of frequency-modulated narrowband signals in wavelet domain applying optimal mother wavelet

From the above distributions it is obvious that the approximating algorithm, at the optimal basis becomes extremely sensitive to the matched signal implementation. It allows to concentrate energy in a small area and vice versa, becomes insensitive to the signal with another implementation of the modulating function.

Fig. 8 shows the dependence of wavelet transform energy concentration for the different types of mother wavelets. Dependence have agreed scale on the normalized number of the considered decomposition coefficients.

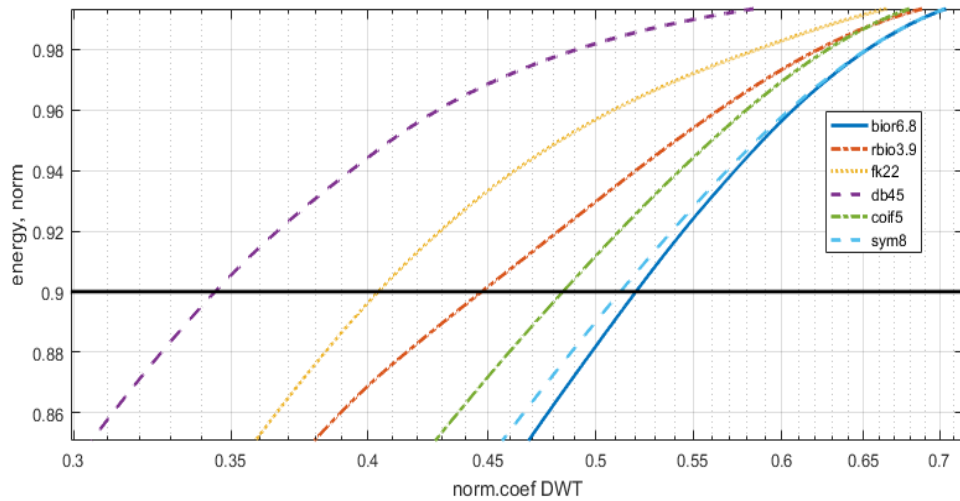


Fig. 8. Dependence of wavelet transform energy concentration on the normalized number of coefficients

Wavelet decomposition of signals w1 and w2 allows to concentrate the signal energy in a small number of significant coefficients when using the appropriate basis. In addition, the wavelet skeletons formed this way are overly informative and can be filtered. Quantitative data are given in table. 1.

Table 1. Quantitative data of signals wavelet decomposition using an ideal basis

Normalized amplitude, %	Number of coefficients, %		Energy, %	
	w1	w2	w1	w2
[100, 90]	0,2653	0,1476	1,8169	1,1371
(90, 75]	0,4328	0,2541	2,5709	1,6986
(75, 50]	0,8750	0,5562	3,9073	2,7835
(50, 25]	7,7230	7,5601	17,9843	21,3351
(25, 0]	42,3657	41,3714	27,6885	22,8185
[-25, 0)	39,4557	41,6608	22,0153	24,9476
[-50, -25)	7,7105	7,3028	19,5070	20,0140
[-75, -50)	1,1719	1,1470	4,5099	5,2656
[-100, -75)	0,0000	0,0000	0,0000	0,0000

It is important to note that real measurements in technological processes are always accompanied by noise and various interferences. Therefore, nonlinear approximation methods, the basis of which is matched with a certain modulating function, will always give a better result than linear ones. In the case of noise, with the expansion of its frequency

spectrum (from the standpoint of Fourier frequency analysis), it is quite appropriate to expect that the intensity distribution of its decomposition coefficients will approach uniform. It is also true for linear methods. However, in case of interference, the situation will be completely different. As shown in Fig. 7, the basis for nonlinear approximation (i.e. mother wavelet) is "sensitive" to a certain implementation of the function. Therefore, the energy of other implementations, including interference, will be distributed over all of the coefficients.

Conclusions

Approximation in signal processing tasks is the foundation of all digital filtering, detection and differentiation methods. Wherein, although the implementation of linear approximation methods is much simpler from a practical point of view and gives good results, in many practical cases this is not enough. In modern technological processes there are cases that cannot be solved by linear methods, so more and more attention is paid to nonlinear ones (adaptive, dynamically coordinated, etc.). The main challenge of nonlinear approximation methods from practical application prospective is the need in dynamical search for optimal bases among known variety. It can be partially solved by systematizing them according to certain criteria in libraries, although this does not solve the problem of their matching. As shown in the example of narrowband signals with frequency modulation, the efficiency of nonlinear approximation allows to achieve significant gains in their processing, using sufficient a priori information amount. It fully justifies their application in practice, especially given the capabilities of modern systems and computational performance.

References

1. Stephane M., (1999) A Wavelet Tour of Signal Processing (Wavelet Analysis & Its Applications) 2nd Edition, Academic Press., 664 pp.
2. Daubechies I., (1992) Ten lectures on wavelets. Philadelphia: SIAM., 437 pp.
3. Fugal L., (2009) Conceptual Wavelets, Space & Signals Technical Publishing, 374 pp.

FORMATION OF THE MODEL OF THE POLYMER MATERIAL STRUCTURE DURING ORIENTATIONAL DRAWING

Synyuk O.

Khmelnytskyi National University

Introduction

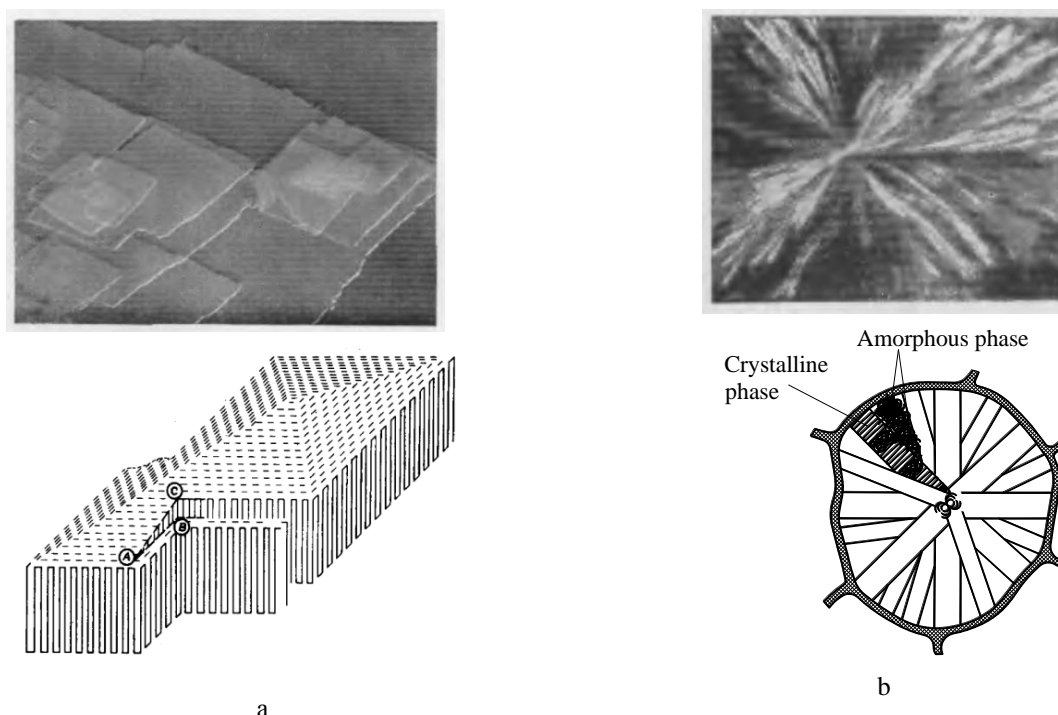
As a result of the structural analysis conducted by various physical methods [1..9], it was established that there are two main levels of SMS in the non-oriented state of amorphous crystalline polymers of the spheruline structure – spherulites of geometric shape close to the distorted sphere, possessing a microheterogeneous crystalline structure, and a homogeneous amorphous part of a medium with a disordered structure. In [10], a model of an non-oriented structure of amorphous-crystalline polymers was proposed, which satisfactorily linked the indices of their elastic properties with the parameters of the structure and the experimental data of the author and other researchers.

Taking the characteristics of structural elements – spherulite and amorphous phase [5, 7] as initial data, and neglecting the dissipative phenomena in the isolated elements, in the first approximation we break the entire drawing process of the polymer into a finite number of states with a fixed degree of deformation of the spherulites. It was established earlier [3...5] that up to the values of the degree of drawing equal to the natural $1 \leq \lambda \leq 9$, a direct genetic connection is maintained between the initial spherulitic order and the orientation one, and also that with An increase in the degree of drawing of λ also increases the degree of anisotropy of the material. These facts are the basis for the hypothesis of the existence of a quantitative relationship between the parameters of the drawing of spherulites and the indices of the mechanical characteristics of the medium in each of these states.

Many different supramolecular structures, occurring depending on the conditions of obtaining and processing of polymers, cannot now be described in one model of the mechanical properties of amorphous-

crystalline polymers. The main idea of this work is model fixation of a polymer of supramolecular structure that changes with deformation.

Undoubtedly the most convenient object for studying the structural changes taking place in polymers during deformation is monocrystals (Fig. 1a). However, the main and the most common structural form is spherulite structure (Fig. 1 b), which is formed during crystallization of amorphous crystalline polymers.



**Fig. 1. The structural model of the structure of the polymer material:
a – the monocrystal; b – spherulite.**

The structural model of spheruline structure of a polymer (see. Figure 1 b) consists of two interconnected models that describe two states of supramolecular structure of polymers: before deformation – a model of spherulite structure of polymers in non-oriented state; after deformation – a model of spheruline structure of polymers in oriented state.

Methods and results

A model of spheruline structure of a polymer can be represented as infinite elastic isotropic medium [11], consisting of spheruline structure placed in a homogeneous amorphous matrix. Following assumptions were

adopted during the construction of the model: spherulites have the same shape (spherical) and dimensions; spherulites are located in the corners of the spatial lattice [11]; the crystalline polymer medium is concentrated in spherulites (Fig. 2).

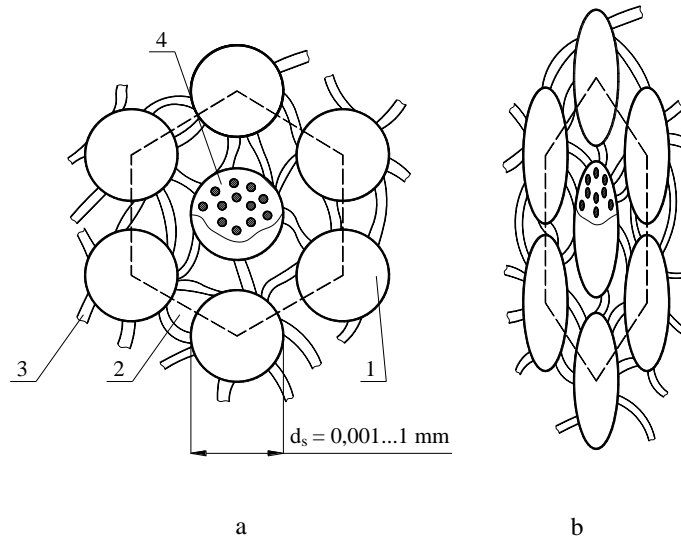


Fig. 2. A model of supermolecular spheruline structure of amorphous crystalline polymers in non-oriented (a) and oriented (b) state: 1 – an amorphous phase; 2 – spherulites (a crystalline phase); 3 – penetrating microfibrills; 4 – a model of internal structure of the spherulite

As a result of the orientation drawing, occurs uniform [6] in the direction of the x_1 axis and with an unchanged volume of spherulites [7, 8] ($\rho_s = const$), we will model the orientational drawing as a uniform compression (stretching) of the space with a coefficient η numerically equal to the stretching degree λ of the polymer: $\eta = \lambda$. In this case, a uniform compression (stretching) of the spherulite actually occurs in the direction from the plane $x_2 0 x_3$, taken as the main one (Fig. 2). The formulas for transforming the coordinates taking into account the invariance of the volume of the spherulite will have the form $x_1^* = x_1 \lambda$, $x_2^* = x_3^* = x_2 \lambda^{-1/2}$. Two cases can occur: for $\lambda > 1$, uniaxial stretching of the space takes place (obtaining fibers and films by drawing); when $\lambda < 1$, uniaxial compression of the space takes place (obtaining fibers and films by rolling or calendering).

The equation of spherulites with a radius r ($x_1^2 + x_2^2 + x_3^2 = r^2$), undergoing uniform stretching with the drawing coefficient λ , as a result of substituting the formulas for the transformation of coordinates and bringing it to the canonical form has the form

$$\frac{(x_1^*)^2}{\lambda^2 r^2} + \lambda \frac{(x_2^*)^2 + (x_3^*)^2}{r^2} = 1. \quad (1)$$

The determining of relative volumetric medium filling with spherulites ξ , sizes of spherulites in the shape of a sphere with a diameter d_s ; type of packaging μ and cyclic symmetry in its structure have paramount value in building of a theory of effective modules of spheruline structure in the first approximation

As characteristic that determines probable spatial lattice type, shape and type of spherulites, we will use the exponent of bulk crystalline polymer material [12].

$$\chi = \frac{\rho - \rho_a}{\rho_s - \rho_a}, \quad (2)$$

where ρ – density of a sample; ρ_a , ρ_s – density of amorphous and crystalline phase of a polymer, found by X-ray diffraction data.

Considering the assumption that all crystalline part of the polymer is concentrated in spherulites that consist of alternating lamellar crystalline regions and interlamellar amorphous layers [13], we can say that the degree of crystallinity χ is associated with the relative volume of spherulite in a spatial lattice, filling the medium with spherulites ξ and compactness coefficient of a spatial lattice μ [11].

$$\xi = \chi^2 = k^2 \cdot \mu, \quad (3)$$

where $k = d_s/L_s$ – a density coefficient of spherulites packing ($0 \leq k \leq 1$); L_s – the distance between the centers of spherulites.

Coefficient of compactness of the spatial lattice, in the corners of which spherulites are located, is determined by its type. The expression $\mu = \pi/6$ – corresponds the simplest cubic lattice; $\mu = \pi/3$ – body-centered cubic

lattice; $\mu = 2\pi/3$ – face-centered cubic lattice; $\mu = \sqrt{2}\pi/6$ – hexagonal structure of cubic lattice.

Clearly, the most densely packed spheres with a radius $d_s/2$, and boundary filling of the spatial lattice, accord to this structure, when the spheres touch one another, i.e. in $d_s = L_s$. In this case $k=1$, and $\xi = \chi^2 = \mu$.

The task of this modeling of the spheruline supramolecular structure of a polymer material is to determine the degree of influence of the polymer elastic properties and its stress-strain state on the form of the spatial lattice, the shape and the size of spherulites that will help to predict the change in the form of spatial lattice in the corners of which spherulites are located, and the shape and size of the spherulites themselves under any deformation of spheruline polymer structure. The models of regularities of elastic constants influence on the shape and size of spherulites and on kind of their mutual arrangement can be used in the modeling of spheruline structures formed during the drawing of polymers.

In connection with the foregoing, we consider the mode of deformation of the spherical crystalline phase, which is located in unlimited amorphous isotropic environment that is exposed to stretching along the axis x_3 (Fig. 3).

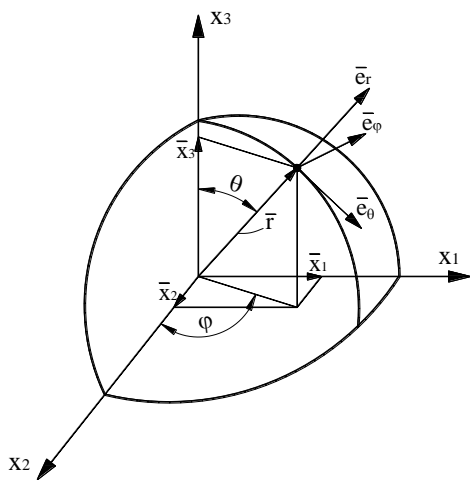


Fig. 3. Scheme of the stress-strain state of spherulites in the polymer structure

Assuming that the structure of amorphous and crystalline phase of the polymer is isotropic medium, as well as that spherulites are packed in a hexagonal lattice and between them there are homogeneous strain interaction, we will solve the problem in a curvilinear coordinate system (q^1, q^2, q^3) , which is associated with the interface environment and the origin is at the center of a spherulite.

As known from [14], the main local basis vectors of curvilinear coordinate system are defined by the formula:

$$\bar{e}_i = \partial \bar{r} / \partial q^i, \quad i = 1, 2, 3 \quad (4)$$

and is tangent to coordinate lines q^i , that pass through the point $\bar{r} = \bar{r}(q^1, q^2, q^3)$. Coordinates q^1, q^2, q^3 uniquely determine the vector \bar{r} in a curvilinear coordinate system, and coordinates x_1, x_2, x_3 uniquely determine this vector in the Cartesian coordinate system (Fig. 2). Cartesian coordinates x_i and curvilinear coordinates q^i can have different dimensions, ie curvilinear base components and Cartesian coordinate systems can be different. To take account of this, we need to determine the appropriate length of the main vectors of the local coordinate system curvilinear basis:

$$H_v = \sqrt{\left(\frac{\partial x_1}{\partial q^v}\right)^2 + \left(\frac{\partial x_2}{\partial q^v}\right)^2 + \left(\frac{\partial x_3}{\partial q^v}\right)^2}, \quad v = 1, 2, 3 \quad (5)$$

and divide them by these vectors, ie:

$$\bar{e}_{(v)} = \frac{\bar{e}_v}{H_v}. \quad (6)$$

Local basis of the unit vectors $\bar{e}_{(v)}$ is called "physical" basis in the scientific literature, and its use is very convenient for solving physical problems.

Since the spherulite has the shape of a sphere, we will use a spherical coordinate system, which is a particular case of curvilinear coordinate system. Then, the position of the vector \bar{r} will be determined by spherical coordinates r, θ, φ . From Fig. 2, we define the Cartesian coordinates x_1, x_2, x_3 through spherical coordinates r, θ, φ .

$$x_1 = r \cdot \sin \theta \cdot \sin \varphi, \quad x_2 = r \cdot \sin \theta \cdot \cos \varphi, \quad x_3 = r \cdot \cos \theta, \quad (7)$$

herewith $0 \leq r < \infty, 0 \leq \theta \leq \pi, 0 \leq \varphi \leq 2\pi$.

Using equation (4) and expressions (7), we decompose unit vectors of the spherical coordinate system by unit vectors of the Cartesian coordinate system.

$$\begin{aligned}
 \vec{e}_r &= \sin\theta \sin\varphi \cdot \vec{e}_1 + \sin\theta \cos\varphi \cdot \vec{e}_2 + \cos\theta \cdot \vec{e}_3, \\
 \vec{e}_\theta &= r \cdot \cos\theta \sin\varphi \cdot \vec{e}_1 + r \cdot \cos\theta \cos\varphi \cdot \vec{e}_2 - r \sin\theta \cdot \vec{e}_3, \\
 \vec{e}_\varphi &= r \cdot \sin\theta \cos\varphi \cdot \vec{e}_1 - r \cdot \sin\theta \sin\varphi \cdot \vec{e}_2 + 0 \cdot \vec{e}_3.
 \end{aligned}
 \tag{8}$$

We put component dimensions of the basis of a curvilinear coordinate system to the dimension of the vector \vec{r} (or basis dimensions of Cartesian coordinates), ie the unit. To do this, we divide the unit vectors of the spherical coordinate system by their lengths (Lame parameters $H_v (v=1,2,3)$) that are determined from equation (5). As a result, the system (8) can be rewritten as follows:

$$\begin{aligned}
 \vec{e}_{(r)} &= \sin\theta \sin\varphi \cdot \vec{e}_1 + \sin\theta \cos\varphi \cdot \vec{e}_2 + \cos\theta \cdot \vec{e}_3, \\
 \vec{e}_{(\theta)} &= \cos\theta \sin\varphi \cdot \vec{e}_1 + \cos\theta \cos\varphi \cdot \vec{e}_2 - \sin\theta \cdot \vec{e}_3, \\
 \vec{e}_{(\varphi)} &= \cos\varphi \cdot \vec{e}_1 - \sin\varphi \cdot \vec{e}_2 + 0 \cdot \vec{e}_3,
 \end{aligned}
 \tag{9}$$

where $e_{(v)} (v=1,2,3)$ – adjusted or "physical" basis. Later braces, standing at the index, will be dropped.

So orthogonal matrix of transition from Cartesian to spherical basis is written as follows:

$$\begin{aligned}
 \vec{e}_r &= a_{11} \cdot \vec{e}_1 + a_{12} \cdot \vec{e}_2 + a_{13} \cdot \vec{e}_3, \\
 \vec{e}_\theta &= a_{21} \cdot \vec{e}_1 + a_{22} \cdot \vec{e}_2 + a_{23} \cdot \vec{e}_3, \\
 \vec{e}_\varphi &= a_{31} \cdot \vec{e}_1 + a_{32} \cdot \vec{e}_2 + a_{33} \cdot \vec{e}_3,
 \end{aligned}
 \tag{10}$$

where a_{ij} – components of orthogonal matrix of transition from Cartesian to spherical basis:

$$\begin{aligned}
 a_{11} &= \sin\theta \sin\varphi, & a_{12} &= \sin\theta \cos\varphi, & a_{13} &= \cos\theta, \\
 a_{21} &= \cos\theta \sin\varphi, & a_{22} &= \cos\theta \cos\varphi, & a_{23} &= -\sin\theta, \\
 a_{31} &= \cos\varphi, & a_{32} &= -\sin\varphi, & a_{33} &= 0.
 \end{aligned}
 \tag{11}$$

The reverse transformation implemented by the following equations:

$$\begin{aligned}
 \vec{e}_1 &= a_{11} \cdot \vec{e}_r + a_{21} \cdot \vec{e}_\theta + a_{31} \cdot \vec{e}_\varphi, \\
 \vec{e}_2 &= a_{12} \cdot \vec{e}_r + a_{22} \cdot \vec{e}_\theta + a_{32} \cdot \vec{e}_\varphi, \\
 \vec{e}_3 &= a_{13} \cdot \vec{e}_r + a_{23} \cdot \vec{e}_\theta + a_{33} \cdot \vec{e}_\varphi.
 \end{aligned}
 \tag{12}$$

To determine the elastic properties (elastic modulus and Poisson coefficient) in the direction of the axis of polymer stretching (axis x_3) we consider the case of longitudinal tensile of non-oriented spheruline structure.

During the stretching, a stress state occurs in spherulites, that, according to the diadic presentation [11, 15], can be written as follows:

$$\mathbf{T} = \bar{e}_x \bar{e}_x \sigma_{xx} + \bar{e}_y \bar{e}_y \sigma_{yy} + \bar{e}_z \bar{e}_z \sigma_{zz} + (\bar{e}_x \bar{e}_y + \bar{e}_y \bar{e}_x) \cdot \sigma_{xy} + (\bar{e}_y \bar{e}_z + \bar{e}_z \bar{e}_y) \cdot \sigma_{yz} + (\bar{e}_z \bar{e}_x + \bar{e}_x \bar{e}_z) \cdot \sigma_{zx}, \quad (13)$$

where $\bar{e}_x, \bar{e}_y, \bar{e}_z$ – single orts of Cartesian coordinate system;

$\sigma_{xx}, \sigma_{yy}, \sigma_{zz}$ – normal stresses occurring on the perpendicular to the corresponding axes of the coordinate system;

$\sigma_{xy}, \sigma_{yz}, \sigma_{zx}$ – tangential tension occurring on the same fields.

If we orient the axes in a way that on platforms of elementary volume, bounded by spherical surface, tangential tensions are not present. Then equation (13) can be rewritten as follows:

$$\mathbf{T} = \bar{e}_1 \bar{e}_1 \sigma_1 + \bar{e}_2 \bar{e}_2 \sigma_2 + \bar{e}_3 \bar{e}_3 \sigma_3, \quad (14)$$

where $\bar{e}_1, \bar{e}_2, \bar{e}_3$ – unit orts of the Cartesian coordinate system, x_1, x_2, x_3 ; $\sigma_1, \sigma_2, \sigma_3$ – tensions in major fields, perpendicular to the corresponding axes of the coordinate system x_1, x_2, x_3 .

Submitting each of main tensions as the product of the average tension $\bar{\sigma}_1$ that influences spherulites along the axis x_3 , and unknown constants σ° characterizing the tension level of homogeneous interaction and the level of tension on the main fields, we get the following:

$$\mathbf{T}^c = (\bar{e}_1 \bar{e}_1 \sigma_1^\circ + \bar{e}_2 \bar{e}_2 \sigma_2^\circ + \bar{e}_3 \bar{e}_3 \sigma_3^\circ) \bar{\sigma}_1, \quad (15)$$

Tension of homogeneous interaction between the spherulites result from changes in stress-strain state of spherulites.

Tension tensor (15) in spherical coordinates (7) can be expressed as follows [11]:

$$\mathbf{T}^c = (\bar{e}_r \bar{e}_r \sigma_r^\circ + \bar{e}_\theta \bar{e}_\theta \sigma_\theta^\circ + \bar{e}_\phi \bar{e}_\phi \sigma_\phi^\circ + (\bar{e}_r \bar{e}_\theta + \bar{e}_\theta \bar{e}_r) \cdot \sigma_{r\theta}^\circ) \bar{\sigma}_1, \quad (16)$$

The unknown constants σ° in spherical coordinates are expressed through Cartesian by substitution of expressions (12) in equation (15)

$$\begin{aligned} \mathbf{T}^c = & \left[\bar{e}_r \bar{e}_r (a_{11}^2 \sigma_1^\circ + a_{12}^2 \sigma_2^\circ + a_{13}^2 \sigma_3^\circ) + \bar{e}_\theta \bar{e}_\theta (a_{21}^2 \sigma_1^\circ + a_{22}^2 \sigma_2^\circ + a_{23}^2 \sigma_3^\circ) + \bar{e}_\phi \bar{e}_\phi (a_{31}^2 \sigma_1^\circ + a_{32}^2 \sigma_2^\circ + a_{33}^2 \sigma_3^\circ) + \right. \\ & + (\bar{e}_r \bar{e}_\theta + \bar{e}_\theta \bar{e}_r) \cdot (a_{11} a_{21} \sigma_1^\circ + a_{12} a_{22} \sigma_2^\circ + a_{13} a_{23} \sigma_3^\circ) + (\bar{e}_r \bar{e}_\phi + \bar{e}_\phi \bar{e}_r) \cdot (a_{11} a_{31} \sigma_1^\circ + a_{12} a_{32} \sigma_2^\circ + a_{13} a_{33} \sigma_3^\circ) + \\ & \left. + (\bar{e}_\theta \bar{e}_\phi + \bar{e}_\phi \bar{e}_\theta) \cdot (a_{21} a_{31} \sigma_1^\circ + a_{22} a_{32} \sigma_2^\circ + a_{23} a_{33} \sigma_3^\circ) \right] \bar{\sigma}_1 \end{aligned} \quad (17)$$

It was assumed above that the spherulites form a hexagonal lattice. In the microstructure corresponding to hexagonal packing, elastic properties do not depend on the chosen direction (isotropic), that is why in the adopted approach we will direct axis x_3 so that the stress state of spherulites is independent of the angle φ . In this case, we assume that angle $\varphi=0$, and taking into account the expressions (11) we get:

$$\mathbf{T}^c = [\bar{e}_r \bar{e}_r (a_{23}^2 \sigma_2^0 + a_{22}^2 \sigma_3^0) + \bar{e}_\theta \bar{e}_\theta (a_{22}^2 \sigma_2^0 + a_{23}^2 \sigma_3^0) + \bar{e}_\varphi \bar{e}_\varphi \sigma_1^0 + (\bar{e}_r \bar{e}_\theta + \bar{e}_\theta \bar{e}_r) \cdot (\sigma_3^0 - \sigma_2^0) \cdot a_{22} a_{23}] \cdot \bar{\sigma}_1. \quad (18)$$

Comparing the obtained expression (18) to the equation (16), we determine the unknown components of the stress tensor of spherulites:

$$\sigma_r^s = (a_{23}^2 \sigma_2^0 + a_{22}^2 \sigma_3^0) \cdot \bar{\sigma}_1, \quad \sigma_\theta^s = (a_{22}^2 \sigma_2^0 + a_{23}^2 \sigma_3^0) \cdot \bar{\sigma}_1, \quad \sigma_\varphi^s = \sigma_1^0 \cdot \bar{\sigma}_1, \quad \sigma_{r\theta}^s = (\sigma_3^0 - \sigma_2^0) \cdot a_{22} a_{23} \cdot \bar{\sigma}_1. \quad (19)$$

According to solving the problem of elasticity of the axially symmetric mode of deformation field [11, 15], we define unknown components of the stress tensor of spherulites as follows:

$$\begin{aligned} \sigma_r^s &= -2 \cdot E_s \cdot A_0 - \frac{2 \cdot E_s}{1 + \nu_s} \cdot (3 \cdot A_2 \cdot \nu_s \cdot r^2 - B_2) \cdot P_2(\cos \theta), \\ \sigma_{r\theta}^s &= \left(\frac{E_s}{1 + \nu_s} \cdot (A_2 \cdot (2\nu_s + 7) \cdot r^2 + B_2) \right) \cdot \frac{dP_2(\cos \theta)}{d\theta}, \\ \sigma_\theta^s &= -2E_s \cdot A_0 - \frac{2E_s}{1 + \nu_s} (3A_2 \cdot r^2 (7 + \nu_s) + 2B_2) \cdot P_2(\cos \theta) - \frac{E_s}{1 + \nu_s} (A_2 \cdot r^2 (7 - 4\nu_s) + B_2) \cdot \frac{dP_2(\cos \theta)}{d\theta} \operatorname{ctg} \theta, \\ \sigma_\varphi^s &= -2E_s \cdot A_0 - \frac{E_s}{1 + \nu_s} (30 \cdot A_2 \cdot \nu_s \cdot r^2 - 2B_2) \cdot P_2(\cos \theta) + \frac{E_s}{1 + \nu_s} (A_2 \cdot r^2 (7 - 4\nu_s) + B_2) \cdot \frac{dP_2(\cos \theta)}{d\theta} \operatorname{ctg} \theta. \end{aligned} \quad (20)$$

where E_s – elasticity modulus of a spherulite; ν_s – Poisson coefficient of spherulites; $P_0(\cos \theta)$, $P_1(\cos \theta)$, $P_2(\cos \theta)$ – Legendre polynomials of the first kind of zero, first and second order; A_0 , A_1 , A_2 , B_2 – unknown constants that are of marginal conditions; r – the radius vector of volume of the spherulites.

We will express the components of the displacement vector in the spherulite in a spherical coordinate system:

$$\mathbf{u}^s = \bar{e}_r u_r^s + \bar{e}_\theta u_\theta^s + \bar{e}_\varphi u_\varphi^s. \quad (21)$$

The unknown components of displacement vector in the spherulite are defined as follows:

$$\begin{aligned}
 u_r^s &= A_0 \cdot r \cdot (-2)(1 - 2\nu_s) \cdot P_0(\cos \theta) + (A_1 \cdot r^2 \cdot 2 \cdot (-1 + 4\nu_s) + B_1) \cdot P_1(\cos \theta) + \\
 &+ (A_2 \cdot r^3 \cdot 3 \cdot 4\nu_s + 2B_2 \cdot r) \cdot P_2(\cos \theta) = -2 \cdot (1 - 2\nu_s) \cdot A_0 \cdot r + 2 \cdot (A_2 \cdot r^3 \cdot 6\nu_s + B_2 \cdot r) \cdot P_2(\cos \theta), \\
 u_\theta^s &= (A_0 \cdot r \cdot (5 - 4\nu_s) + B_0 \cdot r^{-1}) \cdot \frac{dP_0(\cos \theta)}{d\theta} + (A_1 \cdot r^2 \cdot (6 - 4\nu_s) + B_1) \cdot \frac{dP_1(\cos \theta)}{d\theta} + \\
 &+ (A_2 \cdot r^3 \cdot (7 - 4\nu_s) + B_2 \cdot r) \cdot \frac{dP_2(\cos \theta)}{d\theta} = (A_2 \cdot r^3 \cdot (7 - 4\nu_s) + B_2 \cdot r) \cdot \frac{dP_2(\cos \theta)}{d\theta}, \\
 u_\varphi^s &= 0.
 \end{aligned} \tag{22}$$

According to [11, 15] tension components at each point of the amorphous phase of polymer material can be represented as follows:

$$\begin{aligned}
 \sigma_r^m &= \frac{1}{3} \cdot Q + \frac{2 \cdot E_m}{1 + \nu_m} \cdot \frac{D_0}{r^3} + \left(\frac{2 \cdot E_m}{1 + \nu_m} \cdot \left(\frac{6 \cdot D_2}{r^5} - \frac{C_2}{r^3} \cdot (10 - 2\nu_m) \right) + \frac{2}{3} \cdot Q \right) \cdot P_2(\cos \theta), \\
 \sigma_{r\theta}^m &= \left(\frac{2 \cdot E_m}{r^3} \cdot C_2 - \frac{4 \cdot E_m}{1 + \nu_m} \cdot \frac{D_2}{r^5} + \frac{1}{3} Q \right) \cdot \frac{dP_2(\cos \theta)}{d\theta}, \\
 \sigma_\theta^m &= \frac{2}{3} Q - \frac{E_m}{1 + \nu_m} \frac{D_0}{r^3} - \left(\frac{2E_m}{1 + \nu_m} \frac{C_2}{r^3} (1 - 2\nu_m) - \frac{9E_m}{1 + \nu_m} \frac{D_2}{r^5} - \frac{2}{3} Q \right) \cdot P_2(\cos \theta) - \\
 &- \left(2E_m \cdot \frac{C_2}{r^3} \cdot \frac{1 - 2\nu_m}{1 + \nu_m} + \frac{E_m}{1 + \nu_m} \cdot \frac{D_2}{r^5} \right) \cdot \frac{dP_2(\cos \theta)}{d\theta} \cdot \text{ctg } \theta, \\
 \sigma_\varphi^m &= -\frac{E_m}{1 + \nu_m} \frac{D_0}{r^3} + \frac{E_m}{1 + \nu_m} \left(\frac{C_2}{r^3} (10 - 20\nu_m) - \frac{3D_2}{r^5} \right) \cdot P_2(\cos \theta) + \\
 &+ \frac{E_m}{1 + \nu_m} \left(\frac{C_2}{r^3} \cdot (2 - 4\nu_m) + \frac{D_2}{r^5} \right) \cdot \frac{dP_2(\cos \theta)}{d\theta} \cdot \text{ctg } \theta.
 \end{aligned} \tag{23}$$

where E_m – elasticity modulus of amorphous matrix; ν_m – Poisson coefficient of the amorphous matrix; Q – uniform tension of spherulites interaction; $P_0(\cos \theta)$, $P_2(\cos \theta)$ – Legendre polynomials of the first kind of zero second order; D_0 , D_2 , C_2 – unknown constants that are of marginal conditions; r – the radius vector of volume of the spherulites.

Equations (23) show that the tension, arising at some point in the amorphous matrix, decrease with distance from the beginning of the coordinate system. This is because the deformed spherulite has some influence on the amorphous phase of polymer that consists of microfibrils that connect spherulites. And the greater is the distance from the spherulite to the point of amorphous phase of a polymer, the less impact it has on the deformation of the spherulites.

Components of displacement vector for amorphous phase are represented as follows:

$$\mathbf{u}^M = \bar{\mathbf{e}}_r u_r^M + \bar{\mathbf{e}}_\theta u_\theta^M + \bar{\mathbf{e}}_\varphi u_\varphi^M. \quad (24)$$

Components of displacement at each point of amorphous phase of polymer material can be represented as follows:

$$\begin{aligned} u_r^M &= \frac{1-2\nu_M}{E_M} \cdot \frac{Q \cdot r}{3} - \frac{D_0}{r^2} + \left(\frac{C_2}{r^2} \cdot (10-8\nu_M) + \frac{2(1+\nu_M)}{E_M} \cdot \frac{Q \cdot r}{3} - \frac{3D_2}{r^4} \right) \cdot P_2(\cos \theta), \\ u_\theta^M &= \left((1-2\nu_M) \cdot \frac{2C_2}{r^2} + \frac{1+\nu_M}{E_M} \cdot \frac{Q \cdot r}{3} + \frac{D_2}{r^4} \right) \cdot \frac{dP_2(\cos \theta)}{d\theta}, \\ u_\varphi^M &= 0. \end{aligned} \quad (26)$$

The unknown constants A_0 , A_2 , B_2 , D_0 , D_2 , C_2 can be determined from the conditions of perfect contact of spherulites and amorphous matrix surfaces, which take place in case of contact of spherulites, ie when: $r = L_s/2 = a$:

$$u_\theta^M = u_\theta^S; \quad u_r^M = u_r^S; \quad \sigma_r^M = \sigma_r^S; \quad \sigma_\theta^M = \sigma_\theta^S; \quad \sigma_{r\theta}^M = \sigma_{r\theta}^S. \quad (27)$$

Therefore, solving the system of equations (22)-(25), we can indicate the field of stress and strain of spherulites at any moment during uniaxial stretching of polymeric material.

There is the uniform tension of spherulites interaction Q in the systems of equations (23) and (25), that is not there in systems of equations (22) and (24). This can be explained as follows: the spherulites are influencing one another through the amorphous phase that surrounds them. As a result, in the amorphous matrix there is an additional stress that is caused by the interaction between the spherulites, because of the impact of specific load on polymeric material.

Satisfying the conditions for an ideal contact (27) at $r = d_s/2 = a$ and equating the coefficients of the Legendre polynomials, we obtain expressions for the unknown constants A_0 , A_2 , B_2 , D_0 , D_2 , C_2 through the homogeneous stress interaction Q :

$$\begin{aligned}
 A_0 &= Q \cdot \frac{-(1-v_M)}{2(E_S(1+v_M)+E_M(1-2v_S))}, \\
 A_2 &= 0, \\
 B_2 &= Q \cdot \frac{5(1-v_M)(1+v_M)(1+v_S)}{E_S(1+v_M)(8-10v_M)+E_M(7-5v_M)(1+v_S)}, \\
 C_2 &= Q \cdot \frac{5r^3(1+v_M)(E_M(1+v_S)-E_S(1+v_M))}{6E_M(E_S(1+v_M)(8-10v_M)+E_M(7-5v_M)(1+v_S))}, \\
 D_0 &= Q \cdot \frac{r^3(1+v_M)(E_S(1-2v_M)-E_M(1-2v_S))}{3E_M(E_S(1+v_M)+2E_M(1-2v_S))}, \\
 D_2 &= Q \cdot \frac{r^5(1+v_M)(E_M(1+v_S)-E_S(1+v_M))}{E_M(E_S(1+v_M)(8-10v_M)+E_M(7-5v_M)(1+v_S))}.
 \end{aligned} \tag{28}$$

Substituting the meaning of the coefficients from (28) for Eqs. (20), (21), (23) and (26), we obtain a solution of the boundary problem of uniaxial stretching of an isotropic unbounded amorphous medium containing spherulite. As a result, we will have the expressions for the components of the displacement vector \mathbf{u} and the stress tensor \mathbf{T}_σ :

– for a spherulite

$$\begin{aligned}
 \sigma_r^s &= E_S \cdot Q \cdot \left(\frac{1-v_M}{E_S(1+v_M)+E_M(1-2v_S)} + \frac{10(1-v_M^2)}{E_S(1+v_M)(8-10v_M)+E_M(7-5v_M)(1+v_S)} \cdot P_2(\cos \theta) \right), \\
 \sigma_{r\theta}^s &= E_S \cdot Q \cdot \left(\frac{5(1-v_M^2)}{E_S(1+v_M)(8-10v_M)+E_M(7-5v_M)(1+v_S)} \right) \cdot \frac{dP_2(\cos \theta)}{d\theta}, \\
 \sigma_\theta^s &= E_S \cdot Q \cdot \left(\frac{1-v_M}{E_S(1+v_M)+E_M(1-2v_S)} - \frac{5(1-v_M^2)}{E_S(1+v_M)(8-10v_M)+E_M(7-5v_M)(1+v_S)} \cdot \left(4P_2(\cos \theta) + \frac{dP_2(\cos \theta)}{d\theta} \operatorname{ctg} \theta \right) \right), \\
 \sigma_\phi^s &= E_S \cdot Q \cdot \left(\frac{1-v_M}{E_S(1+v_M)+E_M(1-2v_S)} + \frac{5(1-v_M^2)}{E_S(1+v_M)(8-10v_M)+E_M(7-5v_M)(1+v_S)} \cdot \left(2P_2(\cos \theta) + \frac{dP_2(\cos \theta)}{d\theta} \operatorname{ctg} \theta \right) \right), \\
 u_r^s &= Q \cdot r \cdot (1-v_M) \left(\frac{1-2v_S}{E_S(1+v_M)+E_M(1-2v_S)} + \frac{10(1+v_M)(1+v_S)}{E_S(1+v_M)(8-10v_M)+E_M(7-5v_M)(1+v_S)} \cdot P_2(\cos \theta) \right), \\
 u_\theta^s &= Q \cdot r \cdot \frac{5(1-v_M^2)(1+v_S)}{E_S(1+v_M)(8-10v_M)+E_M(7-5v_M)(1+v_S)} \cdot \frac{dP_2(\cos \theta)}{d\theta}, \\
 u_\phi^s &= 0.
 \end{aligned} \tag{29}$$

– for an amorphous matrix

$$\begin{aligned}
 \sigma_r^m &= Q \cdot \left(\frac{1}{3} + \frac{2}{3} r \left(\frac{E_s(1-2\nu_m) - E_m(1-2\nu_s)}{E_s(1+\nu_m) + 2E_m(1-2\nu_s)} \right) + \left(\frac{1}{3} + \frac{E_s(1+\nu_m) - E_m(1+\nu_s)}{E_s(1+\nu_m)(8-10\nu_m) + E_m(7-5\nu_m)(1+\nu_s)} \cdot \left(\frac{5}{3}(10-2\nu_m) - 12 \right) \right) \cdot P_2(\cos \theta) \right), \\
 \sigma_\theta^m &= -Q \cdot \left(\frac{E_s(1-2\nu_m) - E_m(1-2\nu_s)}{3[E_s(1+\nu_m) + 2E_m(1-2\nu_s)]} - \frac{E_s(1+\nu_m) - E_m(1+\nu_s)}{E_s(1+\nu_m)(8-10\nu_m) + E_m(7-5\nu_m)(1+\nu_s)} \times \right. \\
 &\quad \left. \times \left[\left(\frac{25}{3}(1-2\nu_m) + 3 \right) \cdot P_2(\cos \theta) - \left(\frac{5}{3}(1-2\nu_m) + 1 \right) \frac{dP_2(\cos \theta)}{d\theta} \operatorname{ctg} \theta \right] \right), \\
 \sigma_\phi^m &= Q \cdot \left(\frac{2}{3} - \frac{E_s(1-2\nu_m) - E_m(1-2\nu_s)}{E_s(1+\nu_m) + 2E_m(1-2\nu_s)} - \frac{2}{3} P_2(\cos \theta) - \frac{E_s(1+\nu_m) - E_m(1+\nu_s)}{E_s(1+\nu_m)(8-10\nu_m) + E_m(7-5\nu_m)(1+\nu_s)} \left(\frac{113}{12} P_2(\cos \theta) - \frac{8}{3} \frac{dP_2(\cos \theta)}{d\theta} \operatorname{ctg} \theta \right) \right), \\
 \sigma_{r\theta}^m &= Q \cdot \left[\frac{1}{3} \frac{dP_2(\cos \theta)}{d\theta} - \frac{E_s(1+\nu_m) - E_m(1+\nu_s)}{E_s(1+\nu_m)(8-10\nu_m) + E_m(7-5\nu_m)(1+\nu_s)} \cdot \left(\frac{5}{6}(1+\nu_m) - 4 \right) \cdot \frac{dP_2(\cos \theta)}{d\theta} \right].
 \end{aligned} \tag{31}$$

$$\begin{aligned}
 u_r^m &= Q \cdot r \cdot \left[\frac{1-2\nu_m}{3E_m} - \frac{(1+\nu_m)(E_s(1-2\nu_m) - E_m(1-2\nu_s))}{3 \cdot r \cdot E_m(E_s(1+\nu_m) + 2E_m(1-2\nu_s))} + \frac{2(1+\nu_m)}{3E_m} \cdot P_2(\cos \theta) - \right. \\
 &\quad \left. - \frac{(1+\nu_m)(E_s(1+\nu_m) - E_m(1+\nu_s))}{E_m(E_s(1+\nu_m)(8-10\nu_m) + E_m(7-5\nu_m)(1+\nu_s))} \cdot \left(\frac{5}{6}(1-8\nu_m) - 3 \right) P_2(\cos \theta) \right], \\
 u_\theta^m &= Q \cdot r \cdot \left[\frac{1+2\nu_m}{3E_m} - \frac{(1+\nu_m)(E_s(1+\nu_m) - E_m(1-2\nu_s))}{E_m(E_s(8-10\nu_m)(1+\nu_m) + E_m(7-5\nu_m)(1+\nu_s))} \left(\frac{5}{3}(1-2\nu_m) + 1 \right) \right] \cdot \frac{dP_2(\cos \theta)}{d\theta}, \\
 u_\phi^m &= 0.
 \end{aligned} \tag{32}$$

To determine the homogeneous interaction stress Q , we use the method of successive regularization [11], which allows us express the potential energy of the elastic deformation U through the surface integral:

$$U = \frac{1}{2V} \sum_{k=1} \int_{V_k} \sigma_{ik} \varepsilon_{ik} dV = \frac{1}{2V} \sum_{S_0} \int \sigma_{in} u_i df_n, \tag{33}$$

where df_n is an element with normal n to the surface s_0 , bounding the volume V ; σ_{in} , u_i – the components of the stress tensor \mathbf{T}_e and the displacement vector \mathbf{u} , acting on the surface s_0 . Using the first representation of elastic energy through the average stress meanings $\bar{\sigma}_i$ and deformations $\bar{\varepsilon}_i$

$$U = \frac{1}{2} \bar{\sigma}_i \bar{\varepsilon}_i. \tag{34}$$

and expressing the components of the displacement vector \mathbf{u}^m in the spherical coordinate system through the average meaning of the deformation $\bar{\varepsilon}_i$, we find the elastic potential for the amorphous-crystalline body of the spherulite structure

$$\frac{1}{2V} \iint_{(S)} \left[\sigma_r^m \bar{\varepsilon}_1 r (\cos^2 \theta - \nu_m \sin^2 \theta) - \sigma_{r\theta}^m \bar{\varepsilon}_1 r (1+\nu_m) \sin \theta \cos \theta \right] r^2 \sin \theta d\theta d\varphi = \frac{1}{2} \bar{\sigma}_1 \bar{\varepsilon}_1. \tag{35}$$

Substituting into the formula obtained the meaning of the stresses σ_r^M and $\sigma_{r\theta}^M$ from equation (31), integrating (35) on φ in the interval $0 \leq \varphi \leq 2\pi$, and on θ in the interval $0 \leq \theta \leq \pi$ (thus reducing the unit cell to the concentric with the spherulite sphere with the radius r), we determine the homogeneous stress interaction Q between the spherulites through the given average stretching stresses $\bar{\sigma}_1$:

$$Q = \frac{\bar{\sigma}_1}{1 + \frac{2}{3}\chi^2 \left(\frac{(1-2\nu_M)(E_S(1-2\nu_M) - E_M(1-2\nu_S))}{E_S(1+\nu_M) + 2E_M(1-2\nu_S)} + \frac{(7-5\nu_M)(1+\nu_M)(E_S(1+\nu_M) - E_M(1+\nu_S))}{E_S(1+\nu_M)(8-10\nu_M) + E_M(7-5\nu_M)(1+\nu_S)} \right)}. \quad (36)$$

The components of the stress tensor \mathbf{T}_e and the displacement vector \mathbf{u} can be found from Eqs. (29), (30), (31) and (32) by substituting for them the meaning of the interaction stress from Eq. (36). The components of the strain tensor \mathbf{T}_e are obtained from the following equation:

$$\varepsilon_r = \frac{\partial u_r}{\partial r}; \quad \varepsilon_\theta = \frac{1}{r} \frac{\partial u_\theta}{\partial \theta} + \frac{u_r}{r}; \quad \varepsilon_\varphi = \frac{u_\theta}{r} \operatorname{ctg} \theta + \frac{u_r}{r}; \quad \varepsilon_{r\theta} = \frac{1}{r} \frac{\partial u_r}{\partial \theta} + \frac{\partial u_\theta}{\partial r} - \frac{u_\theta}{r}; \quad \varepsilon_{\theta\varphi} = \varepsilon_{\varphi r} = 0 \quad (37)$$

In the structure of a spherulite E , we replace the right side of equation (35) with the second energy representation [11], and the stresses σ_r^M and $\sigma_{r\theta}^M$ in the integrand function with the average stresses $\bar{\sigma}_1$:

$$\sigma_r^M = \bar{\sigma}_1 \cos^2 \theta, \quad \sigma_{r\theta}^M = -\bar{\sigma}_1 \sin \theta \cos \theta.$$

As a result, we get

$$U = \frac{\bar{\sigma}_1}{2V} \iint_{(S)} (u_r^M \cos^2 \theta - u_{r\theta}^M \sin \theta \cos \theta) r^2 \sin \theta d\theta d\varphi = \frac{\bar{\sigma}_1^2}{2E}. \quad (38)$$

Substituting for (38) the values of the displacements u_r^M and u_θ^M from (32), the value of the homogeneous interaction stress Q from (36) and solving expression (38) in relation to E , we find the elastic modulus of the amorphous crystal environment of the spherulite structure:

$$E = E_M \frac{1 + \frac{2}{3}\chi^2 \left(\frac{(1-2\nu_M)(E_S(1-2\nu_M) - E_M(1-2\nu_S))}{E_S(1+\nu_M) + 2E_M(1-2\nu_S)} + \frac{(7-5\nu_M)(1+\nu_M)(E_S(1+\nu_M) - E_M(1+\nu_S))}{E_S(1+\nu_M)(8-10\nu_M) + E_M(7-5\nu_M)(1+\nu_S)} \right)}{1 - \frac{1}{3}\chi^2 \left(\frac{(1+\nu_M)(E_S(1-2\nu_M) - E_M(1-2\nu_S))}{E_S(1+\nu_M) + 2E_M(1-2\nu_S)} - \frac{4(4-5\nu_M)(1+\nu_M)(E_S(1+\nu_M) - E_M(1+\nu_S))}{E_S(1+\nu_M)(8-10\nu_M) + E_M(7-5\nu_M)(1+\nu_S)} \right)}. \quad (39)$$

and for the bulk modulus of elasticity:

$$E_V = E_M \frac{E_S(1+\nu_M) + 2\chi^2 E_S(1-2\nu_M) + 2E_M(1-\chi^2)(1-2\nu_S)}{3[E_S(1-\chi^2)(1-2\nu_M)(1+\nu_M) + \chi^2 E_M(1+\nu_M)(1-2\nu_S) + 2E_M(1-2\nu_M)(1-2\nu_S)]}. \quad (40)$$

The elastic properties of any isotropic material are due to two independent constants. The second constant, the bulk modulus E_V , is determined from the consideration of uniform expansion ($\sigma_x = \sigma_y = \sigma_z = \bar{\sigma}$) of an amorphous crystalline isotropic medium of a spheruline structure. Repeating the reasoning mentioned above, we obtain expressions for the stress characterizing the homogeneous interaction between spherulites Q :

$$Q = \frac{(1-2\nu_s)(1+\nu_m)[E_s(1+\nu_m)+2E_m(1-2\nu_s)]}{E_s(1+\nu_m)+2\chi^2 E_s(1-2\nu_m)+2E_m(1-\chi^2)(1-2\nu_s)} \quad (41)$$

The effective constants E_V and E make it possible to determine other elastic constants of the amorphous crystalline polymer – the Poisson coefficient ν and the shear modulus G :

$$\nu = \frac{3E_V - E}{6E_V}; \quad G = \frac{3E_V E}{9E_V - E}. \quad (42)$$

Expressions (39)...(42) make it possible to predict the elastic properties of amorphous crystalline polymers depending on the degree of crystallinity χ , and require in the first approximation the knowledge of the elastic properties of the amorphous phase E_m , ν_m and spherulites E_s , ν_s . If the elastic constants of different polymers in the amorphous state can be measured or taken from reference literature, then the use of the elasticity modulus of the crystal lattice of polymers E_c as the constant of the crystalline phase, as is done in most papers [14...16], in our opinion, is not entirely correct. Firstly, this is associated with the complex structure of spherulites [7], which is the third level of SMS, after crystallites and lamellas, in which both crystallites and lamellas, having a different orientation in space, are in the inter-amorphous interlayers, which makes it impossible to examine neither spherulites nor other structural formations as single crystalline morphoses. Secondly, in some works, for example [10, 11, 14, 16], it has been established that the spherulites deform with the rest of the polymer mass as a single unit (Fig.2) [16], even in the case of large final deformations, stretching in the direction of the load and only slightly lagging behind the deformation of the macro sample. When the ratio between the elastic constants of crystallites E_c and the amorphous phase E_m

is, for example, for polyethylene $\sim 5 \cdot 10^3$ ($E_c/E_m = 250 \cdot 10^3 / 0,05 \cdot 10^3$ MPa) [16], this phenomenon would not be observed.

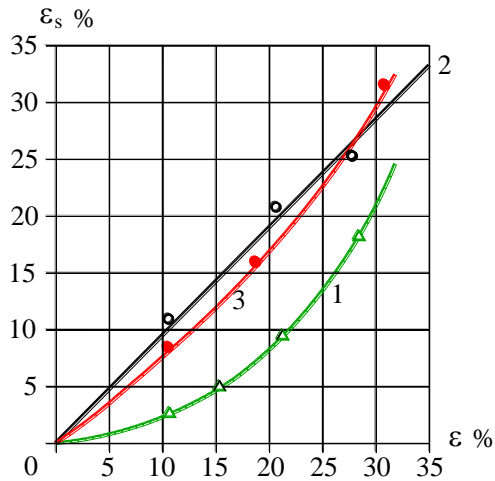


Fig. 4. Dependence of deformation of spherulites ϵ_s on the deformation ϵ of polypropylene film (curves 1, 3) and polyethylene film (curve 2) at temperature $T = 20$ (Δ , 1; \circ , 2) and $T = 90$ (\bullet , 3)

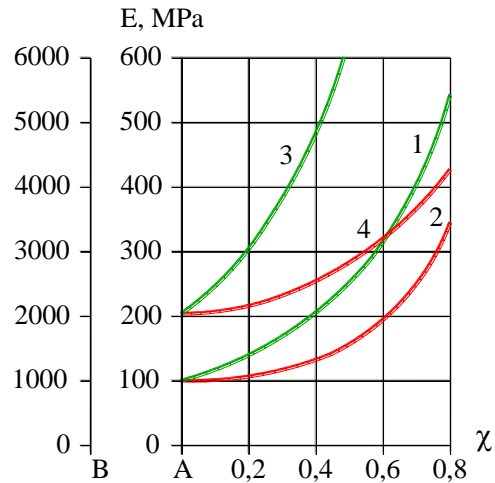


Fig. 5. Dependences of the elastic modulus E of polyethylene (scale of values of A) and polypropylene (scale of meanings of B) on the degree of crystallinity χ

As elastic constants of spherulites E_s , it is proposed to use the values of the elastic constants determined from Eqs. (39) ... (42) for the degree of crystallinity of χ_{\max} , corresponding to the maximum possible for a given polymer, under the assumption of the ideal structure of the spherulites, When substituting, for example, in Eq. (39) the quantities E_c as E_s^* . The obtained meanings of the elasticity modulus E^* was subsequently used as the elasticity modulus of spherulites E_s in the prediction of elastic properties.

Conclusions

The verification of the model described above was carried out on polyethylene and polypropylene, which are representatives of highly crystalline and intermediate crystalline polymers. The dependence of the polyethylene modulus of elasticity (curves 1 and 2, the scale of meanings A) and polypropylene (curves 3 and 4, the scale of meanings of B) on the

degree of crystallinity of χ , were shown in Fig. 5. Curves 1 and 3 were obtained in the approximation of the ideal structure of spherulites ($E_c = E_s^*$), and curves 2 and 4 were obtained using the results of the first approximation ($E_s = E^*$) as E_s and ν_s . The initial data for the construction of curves 2 and 4: for polyethylene $E_s = 1020$ MPa, $\nu_s = 0,2$, $E_M = 77$ MPa, $\nu_M = 0,39$; for polypropylene $E_s = 8239$ MPa, $\nu_s = 0,2$, $E_M = 2000$ MPa, $\nu_M = 0,39$.

The analysis of data in Fig. 4 showed a satisfactory coincidence of the predicted and measured meaning of the Young's modulus, the largest spread of meaning does not exceeded 12% for polypropylene and 15% for polyethylene.

Thus, the presented model satisfactorily reflects the spheruline structure of amorphous-crystalline polymers, even in the approximation of homogeneous interaction. The elastic constants E , K , obtained as a result of the construction of the model, are used as input data for the construction of the SMS mode, formed in the process of orientational drawing of amorphous crystalline polymers of the spheruline structure.

References

1. Akay M. (2012). Introduction to Polymer Science and Technology. New York : Publishing ApS, 269 p. (in English).
2. Argon, A. S. (2013). The Physics of Deformation and Fracture of Polymers. New York : Cambridge University Pres, 511 p. (in English).
3. Isayev, Avraam I. (Eds.). (2016). Encyclopedia of Polymer Blends. Volume 3: Structure. New York : John Wiley & Sons, 528 p. (in English).
4. Koseki, Yu., Keitaro, A., Shinji, A. (2012). Crystalline structure and molecular mobility of PVDF chains in PVDF/PMMA blend films analyzed by solid-state F MAS NMR spectroscopy. Polymer Journal, no. 44, pp. 757–763 (in English).
5. Stoclet, G., Seguela, R., Vanmansart, C., Rochas, C., Lefebvre, J.-M. (2012). WAXS study of the structural reorganization of semi-crystalline polylactide under tensile drawing. Polymer Journal, Vol. 53, Iss. 2, pp. 519-528 (in English).
6. Kireev, V. V. (2019). Vyisokomolekulyarnye soedineniya [High-molecular compounds]. M. : Yurayt, 602 p. (in Russian).

7. James, E., Kenneth, S., Watkins, B., Watkins, J., Hesse, M., Miller, N. (2012). Compositional gradients surrounding spherulites in obsidian and their relationship to spherulite growth and lava cooling. Springer, no. 4, pp. 229-243 (in English).
8. Ohlopkova, T. A., Borisov, R. V., Ohlopkova, A. A., Dyakonov, A. A., Vasilev, A. P., Mironova, S. N. (2015). Mikroskopicheskie issledovaniya deformatsii rastyazheniya sferolitnykh struktur v polimernykh kompozitsionnykh materialakh [Microscopic studies of deformation of stretching of spherulitic structures in polymeric composite materials]. Vestnik Severo-Vostochnogo federalnogo universiteta imeni M. K. Ammosova – Bulletin of the North-Eastern Federal University named after M. K. Ammosov, no 3 (47), pp. 75-87 (in Russian).
9. Synyuk, O.M. (2017). Model budovy nedeforovanykh polimeriv sferolitnoi struktury [Model structure undeformed polymer spherulitic structure]. Visnyk Khmelnytskoho natsionalnoho universytetu. – Bulletin of Khmelnytsky National University. Series “Technical sciences”, no. 3 (237), pp. 181-188 (in Ukrainian).
10. Synyuk, O.M. (2016). Vyznachennia pruzhnykh vlastyvostei amorfno-krystalichnykh polimeriv sferolitnoi struktury [Determination of the elastic properties of amorphous-crystalline polymer of spherulites structure]. Visnyk Vinnytskoho natsionalnoho tekhnichnoho universytetu. – Bulletin of Vinnitsa National Technical University. Series “Technical sciences”, no. 6, pp. 77-86 (in Ukrainian).
11. Abdikarimov, M. N., Turgumbaeva, R. H. Fiziko-mehaniicheskie svoystva polimernykh kompozitsionnykh materialov, vklyuchayuschih othodyi proizvodstv [Physico-mechanical properties of polymer composite materials, including waste products]. Sovremennyye naukoemkie tehnologii – Modern high technologies, no. 5, pp. 7-11 (in Russian).
12. Wen, T., Zhou, Y., Liu, G., Wang, F., Zhang, X., Wang, D., Chen, H., Walton, K., Marchand, G., Loos, J. (2012). Epitaxial crystallization of olefin block copolymers (OBCs) on uniaxially oriented isotactic polypropylene and high-density polyethylene films. Polymer Journal, Vol. 53, Iss. 2, pp. 529-535 (in English).
13. Utracki, L. A., Wilkie, C. A. (2020). Polymer Blends Handbook. Netherlands : Springer, 2378 p. (in English).
14. Bailey, J. (Eds.). (2019). Properties and Behavior of Polymers. Volume 2. New Jersey : John Wiley & Sons, 1591 p. (in English).
15. Brazel, Christopher S., Rosen, Stephen L. (2012). Fundamental principles of polymeric materials. New Jersey : John Wiley & Sons, 407 p. (in English).
16. Fakirov, S. (2018). Fundamentals of Polymer Science for Engineers. Weinheim (Germany) : Wiley-VCH Verlag GmbH & Co. KGaA, 385 p. (in English).

**PHYSICAL AND MECHANICAL CHARACTERISTICS
OF LEATHER FOR THE UPPER OF SHOES, FILLED WITH
NATURAL MINERALS**

Kozar O¹, Wozniak B.², Zhiguts Yu.³

¹Mukachevo State University, Ukraine

²Institute of Leather Industry, Poland

³Uzhhorod National University, Ukraine

Introduction

A promising direction in the tanning industry is the use of natural minerals as environmentally friendly technologically efficient materials that are able to adjust and regulate the efficiency of formation of the dermis structure and the properties of finished leather. The use of finely-dispersed minerals promotes alignment of topographic areas in thickness, increases the yield of leather on the area by avoiding bonding structural elements of the dermis. Changes in the microstructure of the dermis, as a result of mineral filling, contribute to improvement of performance and hygienic properties of finished leather. And the study of the properties of the specified skins should be consistent with the features of operations on their cutting, shoe molding and shoe upper fixing preparations.

The most important properties of leather materials, which largely determine the quality of basic technological operations of shoe manufacturing are the deformation properties. Lack of information about relaxation and deformation properties of the leather produced by the new technologies do not allow to predict their ability to form shapes and save it - indicates the relevance of this study.

This paper analyzes relaxation and deformation characteristics of natural leather for shoe uppers, filled with natural minerals montmorillonite and zeolite, and the ability to predict their formation and preservation of shape in service.

Features of deformation of the skin with mineral content were assessed by determining single-cycle characteristics when attaching to a complete test cycle "loading - unloading - rest" sample. Correlations of elastic and plastic (permanent) deformation have been established, kinetics of changes in linear characteristics of the samples after removal of the load has been investigated. Introduction of dispersions of mineral to the structure of the dermis contributes to the strength of semi-finished leather, increase of the uniformity of mechanical properties in the longitudinal and transverse directions and rise of shape stability index.

It is shown that the direction of this study allows us to offer new competitive ecologically friendly materials to produce shoes.

Increasing consumer demands for quality of shoes and high competition pose the problem of finding and application of new materials, resource-saving technologies, methods of improving the performance and aesthetic properties of products [1].

Expanding the range of natural leathers manufactured with the help of new technologies creates some prospects for making shoes with improved functional properties.

A promising direction in the tanning industry is the use of technologically efficient ecologically friendly materials based on naturally occurring minerals. There is a lot of information on the use of natural minerals as ion exchangers, sorbents, catalysts for solving environmental problems, wastewater treatment in the literature. This is due to their unlimited quantity, low cost, wide range of structural and sorption properties and ease of use. There is much less information about the use of naturally occurring minerals in the tanning industry as materials that can affect the efficiency of formation properties of the finished leather. In papers [2-6] the information is submitted about the modern methods of use of minerals for manufacture of leather that indicate the possibility of creating a high-performance structure of the dermis with predictable performance and hygienic parameters by complex selection of technologically efficient materials based on minerals.

In the papers [7-11] new ecologically friendly leather materials and modern advanced technology of re-tanning processes of leather production that provide the necessary performance properties of finished leather according to their purpose are presented. Applied fine minerals of natural origin are able to adjust and regulate the efficiency of formation of the dermis structure and relevant performance properties. In addition, the use of finely-dispersed minerals for semi-finished leather promotes alignment of topographic areas in thickness, increases the yield of leather on the area by avoiding bonding structural elements of the dermis.

However, relaxation and deformation properties of new leather materials are not covered in these works which does not allow to predict their ability to form and retain shape. The study of properties of these skins should be linked to the peculiarities of the process of manufacturing shoes - cutting operations, shaping and fixing shoe uppers, which indicates the urgency of the study.

Problem

Deformation properties are the most important properties of leather materials, because they largely determine the quality of basic technological operations of shoes, which in its turn determines the convenience of the product and shape retention during operation. The magnitude and nature of the deformation of the uppers depends not only on the way of shaping, equipment and instruments used, but also on the physical and mechanical properties of materials.

The aim of this research is to establish and analyze relaxation and deformation characteristics of leather, filled with fine naturally occurring minerals during re-tanning processes and to predict their ability of shaping and shape stability.

Objects and methods of research

Natural leather for shoe uppers, modified at the stage of liquid finishing with organic mineral compositions (OMC) has been studied. Instead of expensive synthetic polymer- mineral material Tanikor FTG

(3 % by weight of sliced semi-finished product) modified dispersions of natural minerals - montmorillonite (MDM) and zeolite (MDZ) in quantities of 3 and 4 % by weight of sliced semi-finished product respectively were used. Modification of montmorillonite and zeolite was performed with sodium polyphosphate in the amount of 10 % by weight of dry mineral. As a compared (control) sample natural leather for shoe uppers, obtained by the functioning technology of tannery JSC "Chinbar " (Kyiv) was used. All processes and operations that precede the process of filling and all subsequent ones were conducted in accordance with the current technology in production, and confirmed by corresponding acts of production testing and implementations.

The influence of the time factor, peculiarities of materials deformation, their ability to take shape and keep it fully characterize one cycle characteristics. These tensile properties were obtained by applying the complete test cycle "loading - unloading - rest" to sample material. Identification of the components of strain of modified skins was performed according to the method of study relaxation phenomena with the help of relaxometer "Rack" with accuracy $\pm 0,1\text{mm}$, scheme is shown in Figure 1, 2 [12].

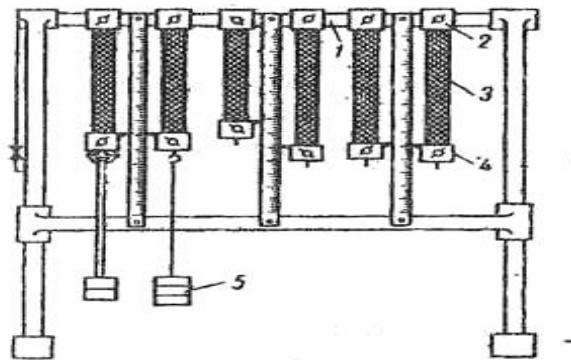


Fig.1. Scheme of relaxometer type "Rack" at constant load: 1- bracket for fixing clamps, 2, 4 - clamps, 3 skin samples, 5- load.

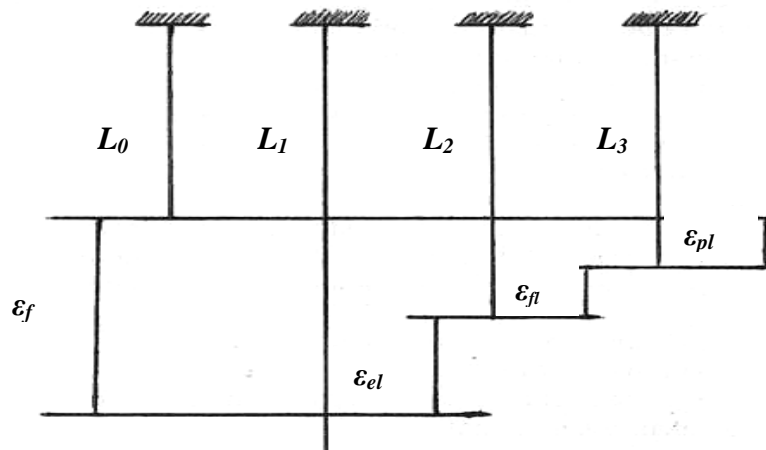


Fig.2. The scheme of materials samples testing on relaxometer "Rack»: L_0 -the initial length of the sample, mm; L_1 -length of the working section of the sample at the final measuring under load, mm; L_2 -length of working area immediately after unloading, mm; L_3 -length of the sample after rest for a certain time, mm.

Tests were conducted in Analytical and Experimental Testing Laboratory in Institute of Leather Industry, Lodz (Poland). 3 groups of samples were formed for research. Each group consisted of 10 samples of semi-finished products, of which 5 samples were cut (shaped) in a longitudinal direction relative to the back bone of hide and 5 - to cross.

To estimate the degree of anisotropy in the skin according to relaxation and deformation properties, uniformity coefficient $K_{unif.}$ of properties of leather in the area was determined - the ratio of the average values of relative elongations in a transverse direction relative to the backbone line, to the average value in the longitudinal direction by the formula

$$K_{unif.} = \frac{\epsilon_{transverse}}{\epsilon_{longitudinal}} \quad (1)$$

It is known [1,12], if the test material is mechanically stressed, the full strain caused by it ϵ_f at time t consists of three components:

$$\epsilon_f = \epsilon_{el} + \epsilon_{fl} + \epsilon_{pl} \quad (2)$$

where ε_{el} - instantly caused elastic deformation, ε_{fl} – highly flexible, due to the relaxation process of rearrangement of the structural elements of the polymer, which leads to the appropriate tension of their new equilibrium position and ε_{pl} - plastic, which occurs in case when the structural elements are capable of unlimited displacement.

Calculations of one cycle characteristics of new ecologically friendly leather materials with mineral content were carried out according to methods presented in [9]. The width and thickness of the standard sample of skin for tensile were measured in five areas and according to mean data its average cross-sectional area was calculated. Cross-sectional area was multiplied on the voltage value of 10MPa and received steady current load which is necessary to hang on the sample. With set screws relaxometer was installed by level and the samples were inserted so that the distance between the two clamps was $L_0 = 50$ mm. Then rated load was hung to the lower clamp. After 60 min. length of the sample between the clamps increased to L_1 and by Eg.(3), full (general) deformation was determined.

$$\varepsilon_f = \frac{L_1 - L_0}{L_0} \times 100\% \quad (3)$$

In 5 sec load was removed, sample length L_2 was measured and elastic deformation $\varepsilon_{elastic}$ was calculated using Eg.(4):

$$\varepsilon_{el} = \frac{L_1 - L_2}{L_0} \times 100\% \quad (4)$$

Then the working length of the sample was measured in 2 , 30, 60, 120, 1440 and 20160 min after removing the load from the lower clamp and measurements $L_{3(2)}$, $L_{3(30)}$, $L_{3(60)}$, $L_{3(120)}$, $L_{3(1440)}$ and $L_{3(20160)}$ were used to calculate the conditional relative flexible deformation $\varepsilon_{flexible}$, which manifests itself in 2 , 30, 60, 120, 1440 and 20160 min as follows:

$$\varepsilon_{fl} = \frac{L_2 - L_3}{L_0} \times 100\% \quad (5)$$

Conditional relative plastic deformation $\varepsilon_{plastic}$ was calculated by Eg.(6) in 2 hours rest of the sample

$$\varepsilon_{pl} = \frac{L_{3(120)} - L_0}{L_0} \times 100\% \quad (6)$$

To predict the ability of materials to shaping and form stability of products made of them, the share components of strain - a strain ratio to total deformation - were determined:

$$\Delta\varepsilon_{el} = \frac{\varepsilon_{el}}{\varepsilon_f} ; \quad \Delta\varepsilon_{fl} = \frac{\varepsilon_{fl}}{\varepsilon_f} ; \quad \Delta\varepsilon_{pl} = \frac{\varepsilon_{pl}}{\varepsilon_f} \quad (7-9)$$

Shape stability of skins modified with natural minerals was determined by Eg.(10):

$$S = \frac{L_{\text{permanent}}}{L_{\text{full}}} \times 100\% \quad (10)$$

The reliability of experimental results were measured by traditional methods of mathematical statistics. The standard deviation, the coefficient of variation and parameters that reflect the closeness of the research results - testing accuracy were determined [12].

Results and Discussion

Formation of upper is one of the most important phases of shoe production because its appearance and performance depend on shape stability of shoes. In the process of forming it is necessary to create conditions that ensure: 1) providing shoe upper with shape and body size that match the shape and size of shoe last, 2) shape retention while wearing, given to a shoe in the production process [1].

In the process of shaping materials undergo deformation that changes shape. With reticulate structure filled skins may exhibit different properties. They may be elastic or flexible (fully recover its original shape and size after removal of loads) and not elastic or plastic (keep the shape and size of shoes after removal of all or part of loads). Due to this materials take the

form of shoe last (plastic properties) and keep it in the process of shoe wear (elastic properties).

In work [13] a set of physical and mechanical, including deformation, properties of semi-finished leather with mineral filling was identified in the test for uniaxial tensile and bursting ball. It has been found that the physical and mechanical properties of skin are formed on macro level of collagen structure and depend on the type of mineral filler. Changes in the microstructure of the dermis as a result of mineral filling lead to increased strength, reduced elongation of the dermis and increase the coefficient of uniformity of mechanical properties in the longitudinal and transverse directions (Table 1).

Table 1. Characteristics of the mechanical properties of semi-finished leather under uniaxial tension

Indicator	Semi-finished material, filled		
	MDM	MDZ	Tanikor FTG (control)
Breaking load, H	487 $K_p=0,91$	428 $K_p=0,94$	396 $K_p=0,90$
Tensile strength at break, MPa	29 $K_p=0,79$	27 $K_p=0,78$	26 $K_p=0,77$
Relative elongation, %, at 10 MPa	22,3 $K_p=0,87$	23,4 $K_p=0,9$	24,95 $K_p=0,73$
Relative elongation, %, at break	67,3 $K_p=0,91$	65,6 $K_p=0,95$	65,3 $K_p=0,90$
Conditional modulus of elasticity, MPa	34,4	32,8	32,3
Stiffness, H	468	492	484
Hygroscopicity, %	10,25	9,93	8,09
Water yielding capacity, %	8,24	9,03	7,55

In most cases, the nature of the deformation of the material is not determined by the deformation properties of the elements of its "fine" structure, but properties of "large" structure of bundles of skin fibers. In general, the mechanical relaxation phenomena are caused by moving and rotating of the structure elements, while there are mechanical and chemical

transformations of macromolecules, destruction and the emergence of supramolecular structures. At the same time there is a transition of the polymer from the original isotropic state to an anisotropic (approximate condition), or a change in an input indicative state.

In terms of footwear manufacturing technology elastic and plastic components of filled skins strain are of interest, as they are responsible for the softness, flexibility, elasticity.

The process of elongation of materials under the action of external forces and their reduction after unloading and relaxation (Fig.2) occur as relaxation processes - processes of change of polymer bodies at the time that are caused by static equilibrium. Relaxation phenomena occur in any static disequilibrium caused by external actions.

The ability of the skin to the shaping and shape retention depends on its ability to stretch and balance of the elastic and plastic (permanent) deformation. The proportion of the components of strain, showing the relationship between strain relaxation processes that occur during stretching of the skin was determined. The magnitude of the components of deformation in the mode of loading and unloading are presented in Table 2.

Table 2. Relaxation and deformation characteristics of modified skins

Filler	Full deformation ε_f , %	Components of deformation, %			Share parts of deformation			Plasticity P, %	Elasticity E, %
		ε_{el}	ε_{fl}	ε_{pl}	$\Delta\varepsilon_{el}$	$\Delta\varepsilon_{fl}$	$\Delta\varepsilon_{pl}$		
MDM	31,5	6,5	8,7	16,3	0,20	0,28	0,52	52	48
MDZ	30,0	5,1	7,0	17,9	0,16	0,24	0,60	60	40
Tanikor FTG (control)	29,0	4,6	7,4	17,0	0,17	0,26	0,57	57	43

The emergence of adsorption centers in the form of mineral dispersion particles with high sorption surface promotes deeper diffusion and more uniform distribution of them in the structure of semi-finished leather, as evidenced by the increase in the coefficient of uniformity.

Interacting with the functional groups of the dermis collagen modified dispersions of montmorillonite and zeolite contribute to its formation and the formation of spatial structures. Penetration of minerals nanoparticles into between fibrillar intervals reduces the ability of the collagen structure to bonding when semi-finished product is dried, promotes the ordering of the elements of the dermis structure and provides the formation of oriented macromolecules and supramolecular structures. So we believe that elastic-plastic properties of experimental skins are characterized by a pronounced deformation compared with unfilled skins.

Figure 3 presents the chart of impact of the type of mineral filler on the value and size of semi-finished leather components of strain. As it can be seen from the chart, montmorillonite dispersion help to reduce the residual and increase elastic strain of semi-finished leather, and therefore increase the softness, flexibility of the skin. Although the magnitude of the residual strain decreases, the absolute value of the index at 5% provides sufficient shape stability.

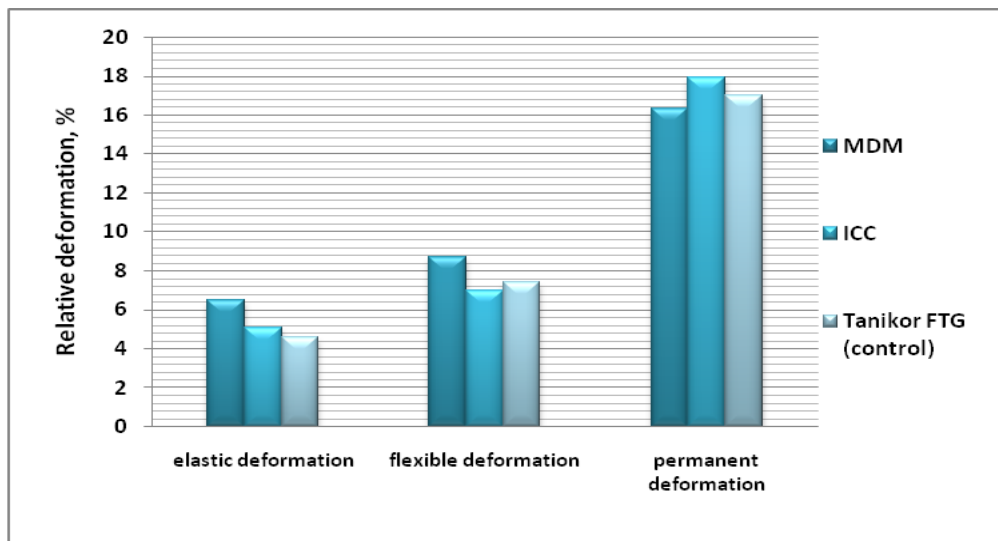


Fig. 3. The ratio of the components of leather deformations filled with variances of natural minerals

When zeolite dispersions are used as a filler, an increase of particles and residual elastic strain is observed, indicating a high ability of skin to shaping and retaining shape during operation, elastic modulus reduced and

hardness increased slightly. It can be positively used in the manufacture of footwear with high durable performance.

Curve of linear characteristics of modified skin samples after removal of the load over time and the rate of skins shape stability (Figure 4) show a positive effect of the mineral content of semi-finished leather on

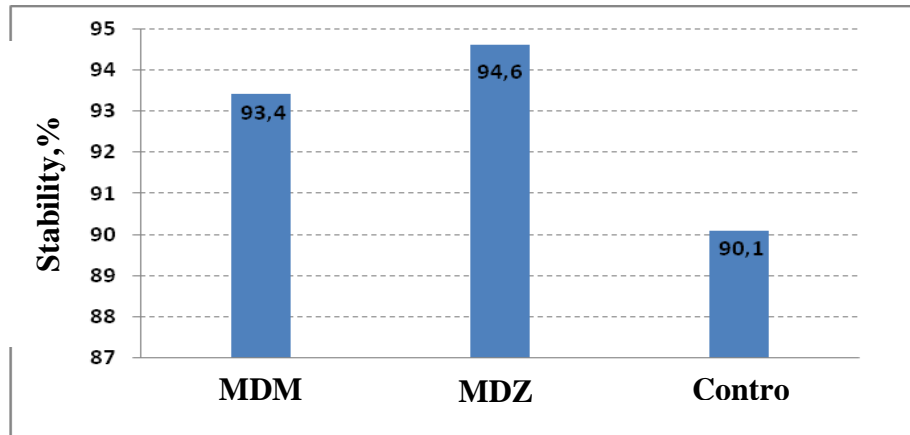


Fig. 4. The dependence of the shape stability of leather on the type of mineral filler.

the relaxation and deformation characteristics of the leather for shoe upper.

Conclusion

Thus, as a result of the research:

1) relaxation and deformation characteristics of leather, filled with fine- naturally occurring minerals and their impact on the performance properties of finished leather have been analyzed ;

2) it has been found that the introduction of dispersions of montmorillonite and zeolite to the structure of the dermis improves the durability of semi-finished leather products , the growth rate uniformity of mechanical properties in the longitudinal and transverse directions and higher rate of shape stability;

3) some particle components of deformations that show the relationship between the relaxation processes occurring during the stretching of the skin in full testing cycle "loading - unloading - rest" have been identified;

4) the results of research can offer new competitive materials for the production of leather shoes for special purpose.

References

1. Shcherbakov V.V., Rukhadze G.K., Kalita A.N. Polischuk V.A. (1989). *Leather and footwear Industries*, **12**, 19.
2. Danylkovych A.G., Lischuk V. I., Plavan V. P. [ta in.]; za red. A. G. Danylkovycha. (2011). *Ecolohichno orientovani tekhnolohii vyrobnytstva shkirianykh ta khutrovykh materialiv dlia stvorennia konkurentnospromozhnykh tovariv*. Ch.I K. : Fenix,
3. Mokrousova O.R., Danilkovich A.G. (2007). Formation of Collagen Structure of Derma by Mineral Dispersions. *Scientific proceedings of Riga Technical University. Series I(4)*, 83.
4. Chen Yi., Fan and Bi Shi. (2011). Nanotechnologies for leather manufacturing: A review. *JALCA*, Vol. 106 (8), 261–273.
5. Bao Yan, Ma Jianzhong, Wangi Yan-Li. (2009). Preparation of acrylic resin/montmorillonite nanocomposite for leather tanning agent. *JALCA*, Vol. 104 (10), 352-358.
6. Zhang Xiaolei, Liu Qinglan, Zhang Weiping (2006)/ Nanocomposites of Acrylate-Organsilicon Resin/Layered Silicate for Keather Finishing. *JSLTC*, Vol. 90 (6), 250-254.
7. Mokrousova O. (2010). The organo-mineral composition for retanning – filling of leather semi-finished item / *Proceedings of the 3rd Internatioal conference on advanced materials and systems. Bucharest, Romania*, 85.
8. Mokrousova O. R., Moraru V. N. (2010). In The Effect of Montmorillonite Modification by Cr(III)–Compounds on Its Microcrystalline Structure and Electrjsurface Properties. *Proceedings of XIX congress of the Carpatian-Balkan Geological Association by editors Christofides G., Kantiranis N., Kostopoulos D., Chatzipetros A. Thessaloniki, Greece*. **99**, 281.
9. Mokrousova O., Dzyazko Y., Volfcovich Y., Sosenkin V., Nikolskaya N.: (2011). *Proceedings of 1st International conference [“Nanomaterials: Applocations and properties”], (Alushta-Crimea, Ukraine, 2011) / A. Pogrebnyak, T. Lyuty, S. Protsenko. - Sumy: Sumy State University, , Vol. 1, Part II, 264.*
10. Mokrousova O.R., Kovtunenکو O.V., Kasian E.Ye. (2012) Environmentally Friendly Materials for the Leather Industry. *Ecolohichna bezpeka*, **2**, 93.
11. Mokrousova O.R., Danylkovych A.G. and Okhmat O.A.: Method of Semi-finished Leather Processing. Ukraina Patent U200607906, Publ. 10.05.2007.
12. Rybalchenko V.V., Konoval V.P., Drehulias E.P. (2010). Materialoznavstvo vyrobiv lehkoi promyslovosti. Metody vyprobuvan: *Navchalny posibnyk*. K.:KNUTD
13. Kozar O.P., Mokrousova O.R., Viktor T.M. (2013). Performance Evaluation of Scins Formstability Modified with Organic Mineral Compositions. *Mizhvuzivsky zbirnyk «Naukovi notatky» Lutskoho natsionalnoho tekhnichnoho universytetu*, - Lutsk, **41**,135.

THE ASSESSMENT OF THE IMPACT OF SHOE MATERIALS ON HUMAN HEALTH ON THE BASIS OF LCA-ANALYSIS

Ivanishena T., Ivanishena O.
Khmelnitskyi National University, Ukraine

Introduction

A characteristic feature of the third millennium is the growing importance of global processes and problems associated with the development of society. One of such problems is anthropogenic pollution of the environment, deterioration of product quality and depletion of natural resources [1].

With the transition of Ukraine to a market economy, there is a rapid increase in the production of new materials. New products from substances whose ecological properties have not been studied enough are appearing on the world and Ukrainian markets.

The introduction of research methods by means of which various materials can influence a person becomes relevant. This is especially true of shoes that have direct contact with human skin.

One of the methods aimed at analyzing and reducing the impact of products on humans, the environment is life cycle assessment (LCA).

The LCA method assesses the environmental safety of products or the impact of any activity on the environment during its life cycle [2].

Analysis of the life cycle of footwear shows that the materials used to make it are dangerous to human health. It should be noted that about 70% of shoes are made using polymeric materials. The main raw materials for this are rubbers, latexes, plastics, synthetic resins, film-forming and binders, solvents, dyes, synthetic and artificial fibers and fabrics, as well as various ingredients (pore-forming substances, plasticizers, fillers, activators, stabilizers).

Chemicals released from polymeric materials can be absorbed by human skin and cause skin damage.

Therefore, to prevent the occurrence of various human diseases, it is necessary to determine the degree of exposure to harmful substances.

Environmental impact in life cycle assessment is often taken into account the following basic classes:

- 1) use of natural resources, territory and energy;
- 2) impact on human health;
- 3) environmental impact.

The scheme of assessment of the life cycle of shoes is shown in Figure 1.

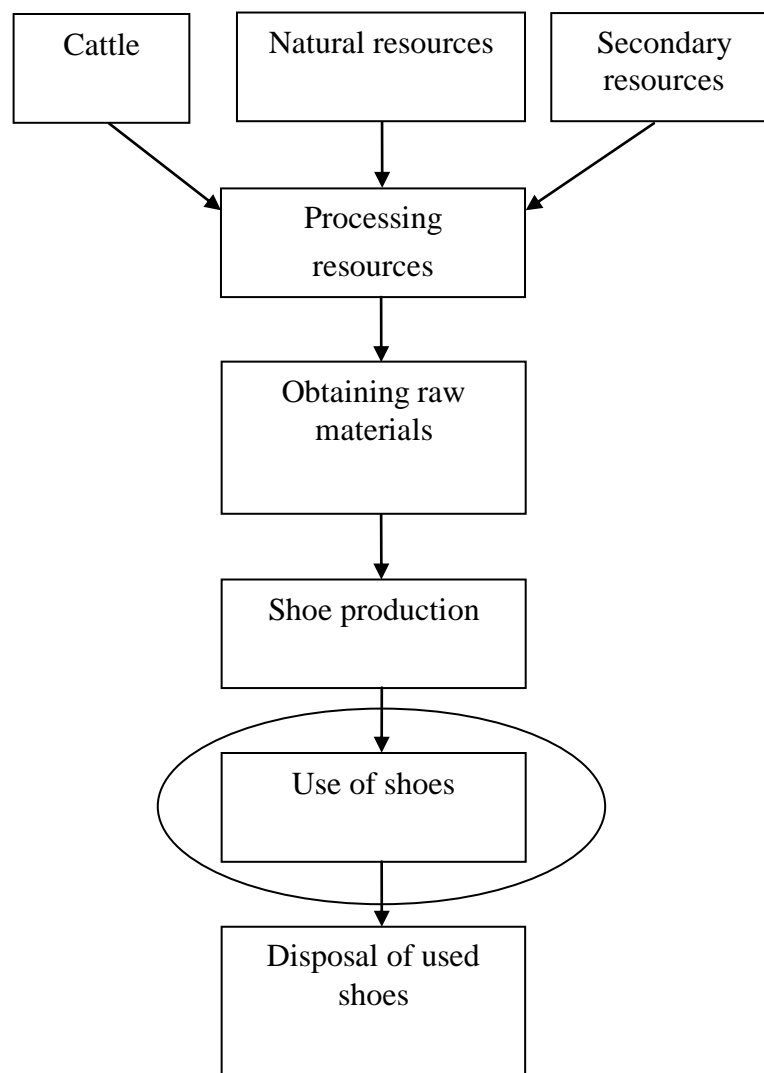


Fig. 1. Scheme of shoe life cycle assessment

The materials used to make shoes have a significant impact on the

Advanced technologies in education, industry and the environment

environment, namely global warming, ozone depletion, affecting aquatic organisms, and directly to humans.

The greatest impact on a person occurs at the stage of using shoes. Determining the impact on human health is not sufficiently studied for this stage.

As part of the LCA, we will investigate one of the most important and least studied subclasses of environmental impacts - toxicity of humans.

The purpose of the work to assessment the impact on human health of shoe materials in the study of their life cycle.

The problems of the study included:

- analysis of models for assessing the impact of harmful substances on the human body by different routes of entry;
- selection of methods and appropriate indicators for assessing the impact of harmful substances on the human body;
- development of an algorithm for extrapolation of data obtained on microorganisms to warm-blooded animals and humans;
- establishment of toxicological properties for various substances and calculation of human toxicity potential (HTP).

Materials for footwear production and their toxicological properties were chosen as objects of research.

Methods

Biotesting methods, mathematical models for calculating human toxicity potential - IMPACT 2002+, CalTOX, USEtox and a method for calculating the probability using a logistic curve were used.

Toxicity to humans is usually determined by the indicator of human toxicity potential.

HTP is a calculated indicator that reflects the potential damage chemical that entering the environment. It is based on specific signs of toxicity and its potential dose. Human toxicity potential estimated at equivalents of dichlorobenzene or chloroethylene [3].

There are many routes of exposure to chemicals in humans, namely

through inhalation, food intake and skin contact.

To calculate the human toxicity potential, the following models were selected: IMPACT 2002+ [4]., CalTOX [5], USEtox [6].

The main criterion of toxicity on which the calculation is based is NOAEL - this is the highest dose that has no effect. This dose is often extrapolated to humans. Interpretation of experimental data is very important to determine the negative impact. NOAEL (or LOAEL) can be divided into extrapolation factors to compare differences in sensitivity between humans and animals, between humans, and between periods of study of periods of human exposure According to the methodology LCA - IMPACT 2002+ human toxicological potential (HTPi) is determined by the formula:

$$HTP_i = \frac{HDF_i}{HDF_{ethylenechlorine}} \quad (1)$$

where HDF_i - the human factor of damage by the i -th pollutant;

$HDF_{ethylene\ chlorine}$ - human damage factor for ethylene chlorine ($1,45 \cdot 10^{-6}$ kg-eq / kg).

The human damage factor (HDF) at the level of damage provides an assessment of the cumulative toxicological risk and potential effects associated with the mass (kg) of the chemical entering the environment. According to this methodology, the Human Damage Factor is calculated as follows:

$$HDF_i = iF_i \cdot \beta_i \cdot D_i \quad (2)$$

$$EF_i = \beta_i \cdot D_i \quad (3)$$

where HDF - human damage factor, DALY;

Advanced technologies in education, industry and the environment

iF - fraction of use, $\text{kg}_{\text{consumption}} / \text{kg}_{\text{supply}}$;

EF - effect factor, mg / kg ;

β - factor of human health effect, $\text{risk} / \text{kg}_{\text{of use}}$;

D - efficiency, DALY

$$\beta = \frac{0,1}{ED_{10}} \cdot \frac{1}{BW \cdot LT_h \cdot N_{365}} \quad (4)$$

where ED_{10} - reference dose, which leads to a 10% effect, $\text{mg} / (\text{kg} / \text{day})$;

BW - average body weight, kg ;

LT_h - average life expectancy, years;

N_{365} - number of days in the year, day / year

The effect factor (EF) is the value of the slope of the dose-response curve (β , level of risk / kg use) and effectiveness (D, DALY / level).

The effectiveness of this methodology is in the form of DALY (non-viable years), which has a value of 6.7 (years / level) for carcinogens and 0,67 (years / level) - for non-carcinogens.

The damage factor of any substance can be obtained by multiplying the characteristic potentials by the damage factor factor for reference substances. With regard to human toxicity, all characterization factors can be expressed in DALY / kg .

Consider a block in which substances migrate from a product (such as clothing or footwear). The calculation of the effect will include an estimate of the amount of substance that will migrate from the part of the product in contact with the skin during the time of contact.

The amount of harmful substance A_{der} that gets on the skin can be calculated by the formula:

$$A_{der} = W_{der} \cdot ARE A_{der} \quad (5)$$

$$W_{der} = C_{der} \cdot TH_{der} \quad (6)$$

where W_{der} - mass of harmful substance on the skin, kg/ m²;

$AREA_{der}$ - area of contact between the product and the skin, m² [7];

C_{der} - concentration of harmful substance, kg / m³;

TH_{der} - thickness of the product, m.

When substances migrate, only a portion of the total ader is able to reach the skin. The amount of harmful substance that will migrate is calculated by the formula:

$$A_{migr,der} = A_{der} \cdot Fc_{migr} \cdot T_{contact} \quad (7)$$

where Fc_{migr} is the proportion of the substance that migrates per unit time, kg_s/ kg / day;

$T_{contact}$ - duration of contact, day.

Product of two numbers $Fc_{migr} \cdot T_{contact}$ must be much smaller than 1.

Potential absorption of harmful substances per kilogram of human weight per day, determined by the formula:

$$U_{der,pot} = \frac{A_{migr,der} \cdot n}{BW} \quad (8)$$

where $U_{der,pot}$ - absorption potential, kg_s / kg / day;

n - the average number of events per day, day⁻¹;

BW - human body weight, kg.

To calculate the HTP at the contact of materials with the skin, it is first necessary to calculate the concentration of $NOAEL_{der}$. This concentration can be obtained by extrapolating the value of $NOAEL_{oral}$ orally to $NOAEL_{der}$ under the skin, according to the following formula:

$$NOAEL_{der} = NOAEL_{oral} \cdot \frac{BIO_{oral}}{BIO} \quad (9)$$

where $NOAEL_{oral}$ - the highest dose level that does not cause a significant increase in adverse effects compared to the control group, mg / kg.

BIO_{oral} , BIO - bioavailability for the oral route and the route through the skin, respectively.

Default for extrapolation from oral exposure to skin exposure values $BIO_{oral} = 1$. Value BIO depends on the molecular weight of the substance [7].

According to the USEtox method, which calculates the HTP in oral exposure, you can calculate the HTP in contact of the product with the skin. But when determining the indicator $ED_{50,h}$, instead of the mass of the human body use the value of the area of the parts of the human body $AREA_{der}$ with which the shoe materials come into contact, namely the shin and foot. Also, the value of ED_{50i} is given in mg / m², which is obtained by multiplying the concentration of NOAEL by a factor of K_m [7]. After which the formula will look like this:

$$ED_{50,h} = \frac{ED_{50,a} \cdot AREA_{der} \cdot LT \cdot N}{AF_a \cdot AF_t \cdot 10^6} \quad (10)$$

For mathematical processing of research results the method of construction of a logistic curve was used [8].

Results

Studies of human toxicity potential were performed by extrapolation of biotesting data (D. Magna, Lemna minor L, Sinapis alba).

According to the method described above the amount of harmful substances that migrate into the skin A_{migr} . To do this, we used the maximum concentrations of extracts of materials (table 1), the potential absorption of the harmful substance by the skin of U_{der} and the concentration of $NOAEL_{der}$ (formula 9). Using the USEtox method, the

main indicators of human toxicity potential and according to the IMPACT 2002 method (formulas 1, 2) human toxicity potential (HTP) and human damage factor (HDF) were established. The results of calculations for each material are shown in tables 2 - 4.

Table 1. The maximum concentration of extracts of materials

Material	Maximum concentration, mg/l
Leather for uppers of footwear	1100
Leather lining	4000
Leather cardboard	1370
Material for the bottom of EVA shoes.	400
Cellulose cardboard Kariboard	1270
Rubber for the bottom of VSh footwear	1050
Polyurethane material	160
Vinyl leather-NT shoe	1470

Table 2. The results of the obtained values for the test object D. Magna

Material	A _{migr} , kg, 10 ⁻⁶	U _{der} , kg / kg, 10 ⁻⁶	NOAEL _{der} , mg m ²	ED _{50h} , kg	HDF		HTP, mg-eq of chloroethylene
					DALY / kg	DALY / person / year, 10 ⁻⁶	
Leather for uppers of footwear	550	7,8	12,48	0,045	0,068	13651	46896,5
Leather lining	2000	28,5	44,19	0,16	0,019	13870	13103,4
Leather cardboard	685	9,8	51,84	0,065	0,047	11751	32413,8

Table 3. Results of the obtained values for the test object Lemna minor L

Material	A_{migr} , kg, 10^{-6}	U_{der} , kg / kg, 10^{-6}	$NOAEL_{der}$, mg / m ²	ED_{50h} , kg	HDF		HTP, mg- eq of chloroethylene
					DALY/ kg	DALY/ person/ year, 10^{-6}	
Leather for uppers of footwear	550	7,8	235,02	0,84	0,00366	735	2530,4
Leather lining	2000	28,5	333,6	1,19	0,0026	1898	1793,1
Leather cardboard	685	9,8	336,9	0,42	0,0073	1825	5034,5
Material for the bottom of EVA shoes	200	2,8	138,3	0,17	0,0178	1299	12275,9
Cellulose cardboard Kariboard	635	9,07	281,34	0,35	0,0088	2039	6072,9
Rubber for the bottom of shoes	525	7,5	198,2	0,25	0,012	2299	8275,9
Polyurethane material	80	1,1	658,69	0,83	0,0037	108	2551,72
Vinyl leather- NT shoe	735	10,5	256,8	0,92	0,0033	885	2275,8

Table 4. Results of the obtained values for the test object *Sinapis alba*

Material	A_{migr} , kg, 10^{-6}	U_{der} , kg / kg, 10^{-6}	NOAEL _{der} , mg / m ²	ED _{50h} , kg	HDF		HTP, mg- eq of chloroethylene
					DALY/ kg	DALY/ person / year, 10^{-6}	
Leather for uppers of footwear	550	7,8	788,7	2,82	0,0011	221	758,6
Leather lining	2000	28,5	953,4	3,41	0,0009	657	620,7
Leather cardboard	685	9,8	889,2	1,12	0,0027	675	1862,07
Material for the bottom of EVA shoes	200	2,8	304,8	0,38	0,0081	591	5587,2
Cellulose cardboard Kariboard	635	9,07	863	1,08	0,0028	649	1931,03
Rubber for the bottom of shoes	525	7,5	639,2	0,8	0,0038	728	2620,7
Polyurethane material	80	1,1	434,8	0,55	0,0055	161	3793,1
Vinyl leather-NT shoe	735	10,5	871,7	3,12	0,00098	263	675,8
Recycled hot melt	1250	17,8	934,9	1,17	0,0026	1199	1813,79

According to the obtained results, comparing the values of human damage factor HDF (DALY / person / year), the highest values are typical for materials such as EVA, rubber, cardboard and leather. These materials, namely EVA material and rubber, are used for the bottom of shoes, and cardboard and leather as materials for insoles. Therefore, when sweating,

toxic substances contained in the materials penetrate through the skin pores and deplete the biologically active points of the foot, resulting in direct poisoning of the body.

Comparison of human toxicity potential for materials is shown in the diagrams for each test object (Figures 2, 3)

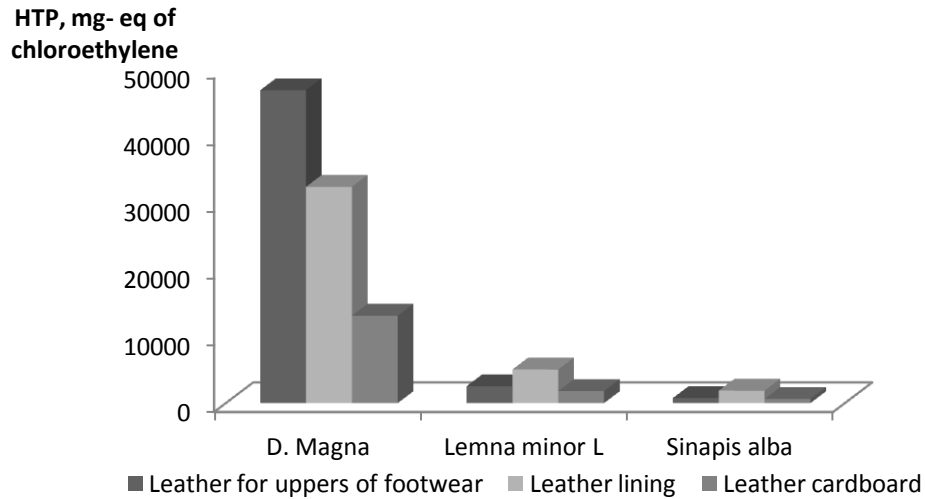


Fig. 2. Results of human skin toxicity potential for shoe uppers, cardboard and leather linings

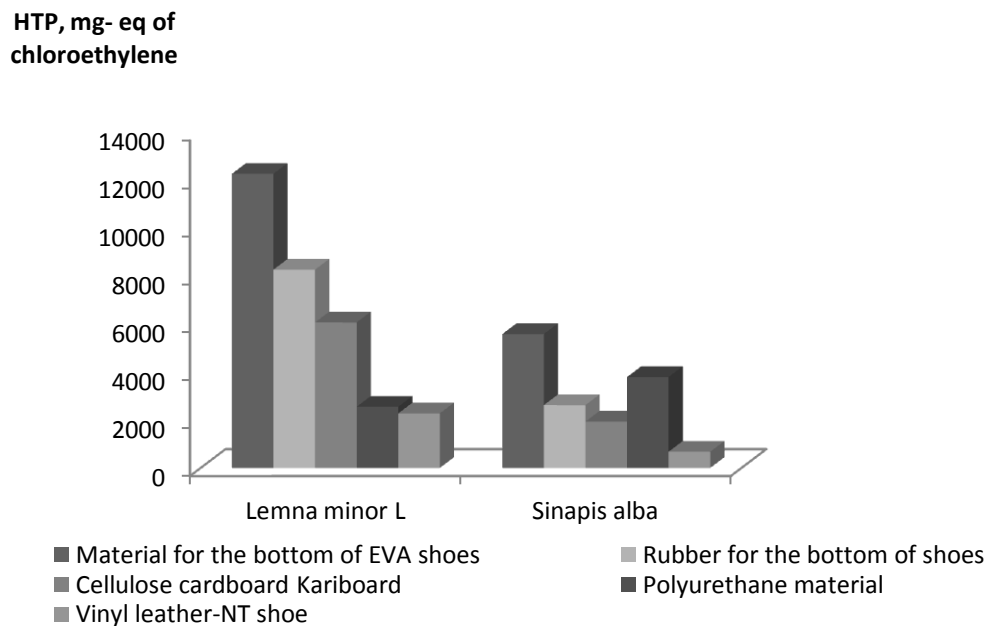


Fig. 3. Results of human toxicity potential for EVA material, porous rubber, cardboard, polyurethane material, vinyl leather

The figures show that EVA material, rubber, cardboard and leather cardboard have the highest indicators of human toxicity potential. Due to their treatment, they are toxic to the skin and have the greatest toxic effect on it. Analyzing the obtained data, the most sensitive among the test objects can be considered *D. Magna*, because it is a key species for freshwater systems and is used as a kind of indicator of the state of the environment.

Conclusions

The complex method of estimation of loadings on environment of shoe materials during their life cycle is considered. Particular attention is paid to the class of environmental impact, where the main subclass is toxicity to humans.

The main models of human toxicity assessment for different routes of exposure are analyzed. According to the key criteria, the following models were selected for further analysis: CalTOX, USES-LCA, Impact 2002 and EUSES.

The IMPACT 2002+ model takes into account multiple routes of exposure that link the concentration of a chemical in the atmosphere, soil, water, or vegetation to human absorption through inhalation or ingestion.

The CalTOX model determines the distribution of chemicals in the environment and the establishment of ways of exposure to these substances in humans, namely by inhalation of gases and particles, intake of products, fish and meat, skin contact with water and soil.

In the USEtox program, human toxicity is characterized by a characteristic factor. Two ways of getting chemicals into the human body are also taken into account: orally and by inhalation.

An algorithm has been developed extrapolation of data obtained by the method of biotesting of shoe materials on aquatic ecosystems to toxic concentrations for warm-blooded animals (rats), and then to humans when the material comes into contact with the skin. The main indicators ED_{50h} , HDF, and human toxicity potential (HTP) were calculated. Analyzing

human toxicity potential (HTP) data for different test objects, shoe materials can be ranked as follows: EVA material, rubber, cardboard and leather cardboard.

Data were analyzed HDF (DALY / kg) when taken orally and on the skin and compared with reference data obtained by ingestion of a toxic substance by inhalation.

It is established that the most dangerous way of getting a toxic substance into a person is direct contact of materials with human skin, and safe - when in contact with air, ie by inhalation.

References

1. Melnyk, L.H. & Shapochka, M.K.. (2007) Principles of Ecology. Ecological economics and nature management. Sumy: VTD «Universytetska knyha». [in Ukrainian].
2. Environmental management. Life cycle assessment. Principles and structure (2013) DSTU ISO 14040:2013 (ISO 14040:2006, IDT) from 01th July 2014. Kyiv: Derzhstandart Ukraine [in Ukrainian].
3. Ariana Arcenas, Julie Holst, Takuma Ono, Matt Valdin The Development of a Standard Tool to Predict the Environmental Impact of Footwear. Retrieved from: www.bren.ucsb.edu/research/documents/Footprint_finalreport.pdf
4. IMPACT 2002+: A New Life Cycle Impact Assessment Methodology. Retrieved from: https://www.researchgate.net/publication/226264450_IMPACT_2002_a_new_life_cycle_assessment_methodology_Int_J_Life_Cycle_Assess_8324-330
5. Edgar G. Hertwich, Sarah F. Mateles, William S. Pease, Thomas E. McKone/ An update of the Human Toxicity Potential with special consideration of conventional air pollutants. Retrieved from: <https://core.ac.uk/download/pdf/52101237.pdf>
6. Peter Fantke/ USEtox® 2.0 User Manual (Version 2) Retrieved from: https://usetox.org/sites/default/files/support-tutorials/USEtox_Manual.pdf
7. European Union System for the Evaluation of Substances 2.0 (EUSES 2.0).- Retrieved from: <https://echa.europa.eu/support/dossier-submission-tools/euses>
8. Draper, N.R., Smith, H. (1998) Applied Regression Analysis. John Wiley & Sons, Inc. Retrieved from: <https://www.twirpx.com/file/1460058/>

ACOUSTIC EMISSION DIAGNOSTICS OF COMPOSITE MATERIALS IN CAPACITOR ASSEMBLY UNDER THERMAL IMPACTS

Kovtun I., Petrashchuk S., Boiko J.

Khmelnytskyi National University, Ukraine

Introduction

The assembly of ceramic compounded capacitor, such as K 15-5, represents a ceramic disc, polymerized by compound (fig. 1). Due to difference in linear expansion coefficients between ceramics and compound when subjected to thermal impacts ceramic-compound joint undergoes a thermal stresses, which under unfavorable combination of these coefficients and mechanical characteristics of both materials may cause cracking of compound or ceramics and destruction of the joint structure.

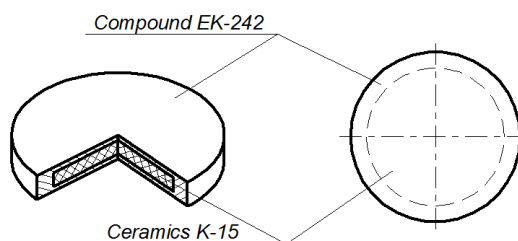


Fig. 1. Ceramic compounded capacitor assembly

The researches published in [1-3] revealed that destruction of ceramics in such structures (fig. 1) during thermal cycling is caused by the tension in direction of longitudinal axes of the disk and over the area inclined to its ends at the angle of 45° due to compression in radial directions forced by compound.

Visual inspection of capacitors destroyed by thermal impacts demonstrated that cracking of ceramics occurs in layers adjacent to compound with cracks located in planes parallel to the end planes or inclined to them at the angle of 45° . Figure 2 demonstrates cracking topography in capacitors.

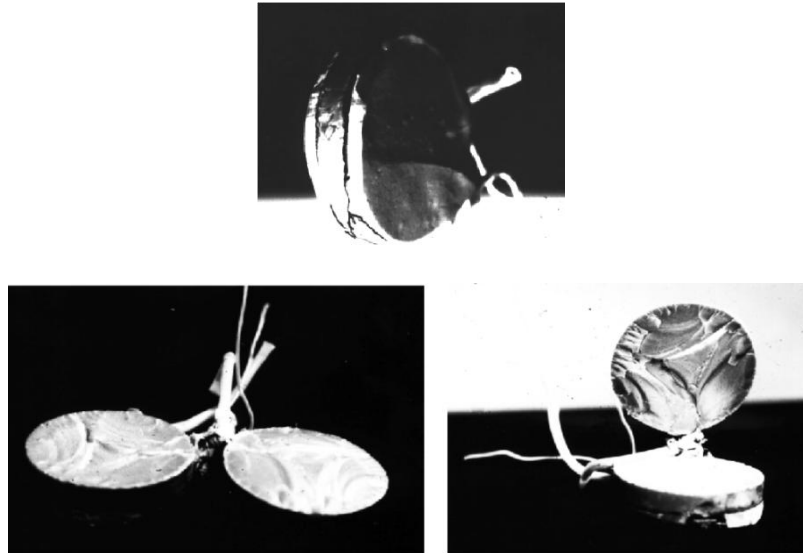


Fig. 2. The surface topography of capacitor destruction

The researches [4, 5] also revealed that stress and strain values in ceramics and compound significantly depend on the scatter of physical and mechanical characteristics α , μ , E in both ceramics and compound. For example, the possible scatter in linear expansion coefficients for ceramics and compounds may vary from -30% to $+50\%$. What brings to stress calculation errors by more than 300% . Presence of these and many other factors, which are difficult to consider, complicates strength estimation in the capacitor assembly.

Noteworthy is that stress intensity factor [6, 7] application to estimated stress field and real structure of materials may reveal growth in defects in size under $4\ \mu\text{m}$ in maximum stress spots.

In such situation providing strength of critical parts in a single or batch production relies on developing technique for non-destructive strength testing in non-detachable joints of composite materials, which are ceramics and compound. Non-destructive testing is offered to be based on method of acoustic emission, which, is sensitive to physical and mechanical properties of materials and allows monitoring microstructure condition and detecting its violation at early stages of progression.

Method

Acoustic emission researches [8-12] applied to components of ceramic capacitors were conducted for mechanical loads, such as tension and bending. As results of these researches methods were developed for non-destructive testing and diagnosing strength of components in assemblies of ceramic capacitors.

However the main causes of breakdowns, which are likely to occur in such assemblies as capacitors, are not the mechanical forces but normally the thermal impacts. Therefore this research is aimed at solving the problem of diagnosing strength of capacitors exposed to operating conditions, which are thermal cycling from +60 to –50 deg C.

The following tasks were posed for the current research:

1. finding thermal limits for operation of acoustic emission sensors made as an assembly of different materials, such as steel, ceramics, plastics, which are also capable of emitting acoustic emission signals during thermal cycling;
2. avoiding acoustic emission signals emitted by ice on the tested capacitor and the sensor during transition from positive to negative temperatures and reverse;
3. separating acoustic emission signals emitted by the ceramic base of capacitor from signals emitted by the compound shell, both at normal and negative temperatures.

Thermal tests of acoustic emission sensors were conducted in thermal chamber Faitron 3526/51. Sensors were read by acoustic emission measuring system [13]. Acoustic emission signal simulator SMA-04 generated reference signal. Tests have verified that the sensor of P113 type is capable to operate in temperature range from + 50 to –50 deg C. Figure 3 shows temperature dependence of sensor's amplitude response.

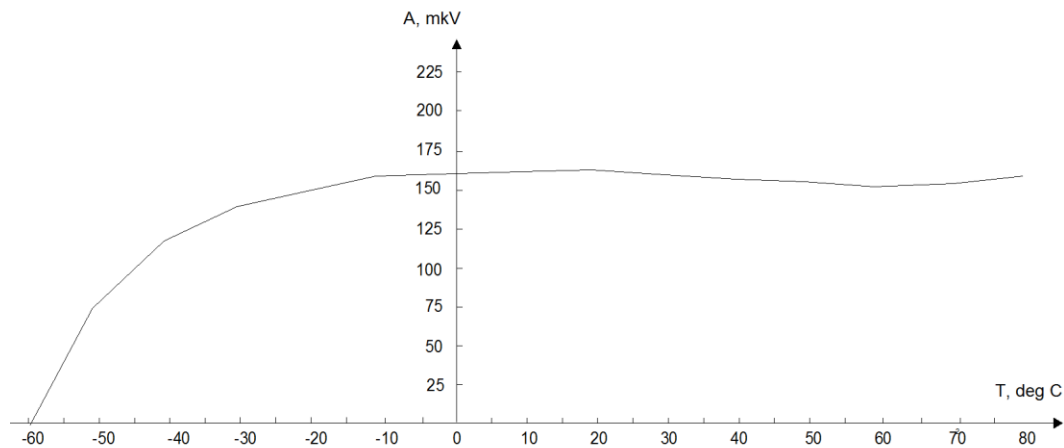


Fig. 3. Temperature dependence of sensor P113 amplitude response

However sensor readings were interfered at temperature range from +50 to +85 deg C by hindrance associated with difference in linear expansion coefficients of sensor components. False acoustic emission signals appeared while transition to negative temperatures for the same reason and also due to icing at about + 5 deg C.

To keep sensors from adverse temperatures transmission of acoustic emission was conducted through waveguides.

The following waveguides were tested: quartz, lead, titanium, bronze and steel. The most effective waveguide turned out to be the steel one with dimensions of 500x25x30 mm.

The experimental setup is represented in fig. 4. The experiment was conducted in normal conditions by using GZ-112/1 generator to generate signals through P113 (1) sensor. The second sensor P113 (2) was used as receiver of generated signals.

The sensors were attached to the ends of waveguide through the VK-1 contact adhesive layer.

Pulses supplied by generator were controlled on: voltage – by microvoltmeter (1); frequency – by frequency meter; signal shape – by oscilloscope (channel 1). The output signals were checked on: level – by microvoltmeter (2); shape – by oscilloscope (channel 2).

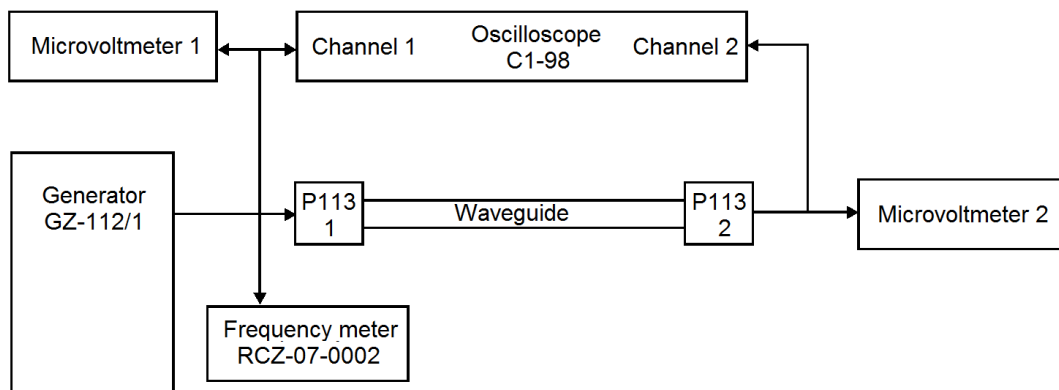


Fig. 4. The experimental setup to measure acoustic emission damping factor in the waveguide

The tests have indicated appearance of hindrances, during transitions from positive to negative temperatures and reverse, due to icing waveguide and contact layers. In order to remove icing, tests were carried out by immersing the waveguide with the sensor in the tub of alcohol. However, this method proved to be ineffective, since alcohol dissolves the contact layer and acoustic connection gets lost.

Nevertheless, use of waveguides expands the temperature range by increasing positive temperatures up to +90 deg C and negative temperatures down to -60 deg C, on condition that acoustic emission during ice formation is ignored.

To eliminate hindrance associated with formation and cracking ice during transition from positive temperatures to negative and reverse, the experiment was conducted in vacuum.

This vacuum chamber was placed inside Faitron thermal chamber. Vacuum pump provided vacuum level in the chamber (740 mm Hg), at which ice could not be formed.

Thermal cycling was carried out in temperature range from +60 to -50 deg C and reverse controlled by thermal sensor installed inside the vacuum chamber. In these conditions no icing appeared and sensor worked normally in the full temperature range [15-17].

Unfortunately, such method took extensive time for thermal cycling, for an instance transition from -50 to $+60$ deg C in the vacuum chamber took 180-190 minutes.

Finding operational frequency bands of acoustic emission signals emitted during destruction of ceramic and compound samples was accomplished by using test appliance shown in fig. 5. In this appliance samples of K-15 ceramics and EK-242 compound were installed cantilever and subjected to mechanical bending test in order to emit acoustic emission.

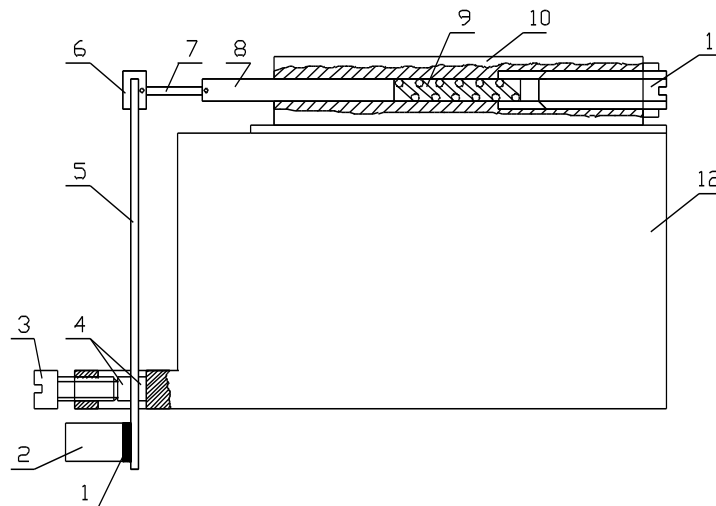


Fig. 5. Test appliance: 1 – acoustic layer; 2 – acoustic emission sensor P113; 3 – screw; 4 – fluoroplastic gasket; 5 – test sample; 6 – fluoroplastic loop; 7 – thrust; 8 – core; 9 – spring; 10 – electromagnet; 11 – adjusting screw; 12 – base

Conducted tests revealed frequency bands (table1, 2) applicable to examine both ceramic component and compound: 650-1000 kHz for ceramic component using sensor P113 (0.5-1.0 MHz); 130-300 kHz for compound component using sensor P113 (0.2-0.5 MHz).

Such destruction tests were conducted for 30 samples of ceramics and compound at negative temperatures. When temperature decreasing, starting from -35 deg C, acoustic emission appeared reaching the total count of 200 events for ceramic samples, and 120 – for compound samples. Once the temperature is stabilized these signals disappeared in 5-6 sec. Tests were conducted till the temperature reached -50 deg C. Frequency bands revealed

during negative temperature tests were identical to those obtained previously for normal conditions.

Thus, conducted tests approved that using two types of sensors P113 (0.5-1.0 MHz) and (0.2-0.5 MHz), connected via the frequency filters to separate received channels, is practicable to measure acoustic emission of ceramics and compound in their operational temperature range.

Table 1. Destruction test results of ceramics K-15 and compound EK-242

Temperature	Sensor P113 (0.5-1.0 MHz)		Sensor P113 (0.2-0.5 MHz)	
	Total count (minimal-maximal)		Total count (minimal-maximal)	
	Ceramics	Compound	Ceramics	Compound
+20 deg C	8-114	1-10	1-52	42-350
-50 deg C	1-67	1-33	2-37	1-79

Table 2. Frequency separation of acoustic emission emitted by components of capacitor K15-5

Material	Ceramics K-15	Compound EK-242
Frequency band (kHz)	650-1000	130-300

Furthermore two sensors were replaced by one wide-band sensor P113 (0.2-2.0 MHz) whose signals were transmitted to separated channels tuned on two frequency bands: 650-1000 kHz for ceramics; 150-300 kHz for compound.

Experiments

The experimental research of real capacitors K15-5 were conducted by using methods and preparations described before under thermal impacts (cycling) in the temperature range from +60 to -50 deg C. These capacitors have nominal constant voltage of 50 kV, nominal capacity of 470 pF, admissible reactive power of 10 W and mass of 80 g.

First 10 capacitors were subjected to thermal cycling in vacuum chamber, sensor P113 (0.2-2.0 MHz) was connected to measuring system of acoustic emission via the waveguide.

The experiment demonstrated that for all capacitors in range of positive temperatures acoustic emission signals are absent and appear only at temperatures of -14 deg C and below. This observation allowed further tests to be conducted in the range from normal temperatures to -50 deg C without using vacuum chamber and waveguides, but acoustic emission from icing of the sensor and capacitor at about $+5$ deg C was neglected and not recorded, what greatly simplified the experiment and reduced its duration. In the further experiments wide-band sensor was directly connected to two receiving channels tuned to ceramics and compound frequencies. Both channels were time synchronized.

Another 30 capacitors K15-5 were subjected to thermal impacts in thermal chamber. Average values of acoustic emission parameters, such as total count of oscillations, total count of events, maximum amplitudes during the first three thermal cycles are represented by graphs in fig. 6.

Data analysis revealed that acoustic emission is much more intensive in ceramic part of capacitor than in compound part, it is absent in the full range of positive temperatures and begins to appear from about $-12 \dots -15$ deg C, reaching maximum at lowest temperature of -50 deg C.

Noteworthy is that holding for 10-15 seconds at a given temperature brings to fading signals for all 30 capacitors. When temperature changed from -50 deg C to normal temperature acoustic emission signals did not appear. During the second thermal impact acoustic emission signals were not observed until about -30 deg C, and at lower temperatures their manifestation was 5-10 times lower than during the first thermal impact. This indicates the Kaiser effect [14], which testifies of sufficient strength of tested capacitors and negligible level of noise signals.

Tests of 30 ceramic compounded capacitors during thermal cycling from $+60$ to -50 deg C in 100 cycles revealed a number of facts, which were used to develop method for non-destructive strength diagnostics and control

of non-detachable ceramics and compound joints. For most of the tested capacitors, which passed the tests without destruction, acoustic emission character was identical. After a strong manifestation during the first thermal cycle and about 10 times weaker during the second one signals actually did not appear during the third and subsequent thermal cycles until the very end of the tests, which indicated the Kaiser effect and sufficient strength of the assembly, which was also confirmed by control of electrical parameters [18].

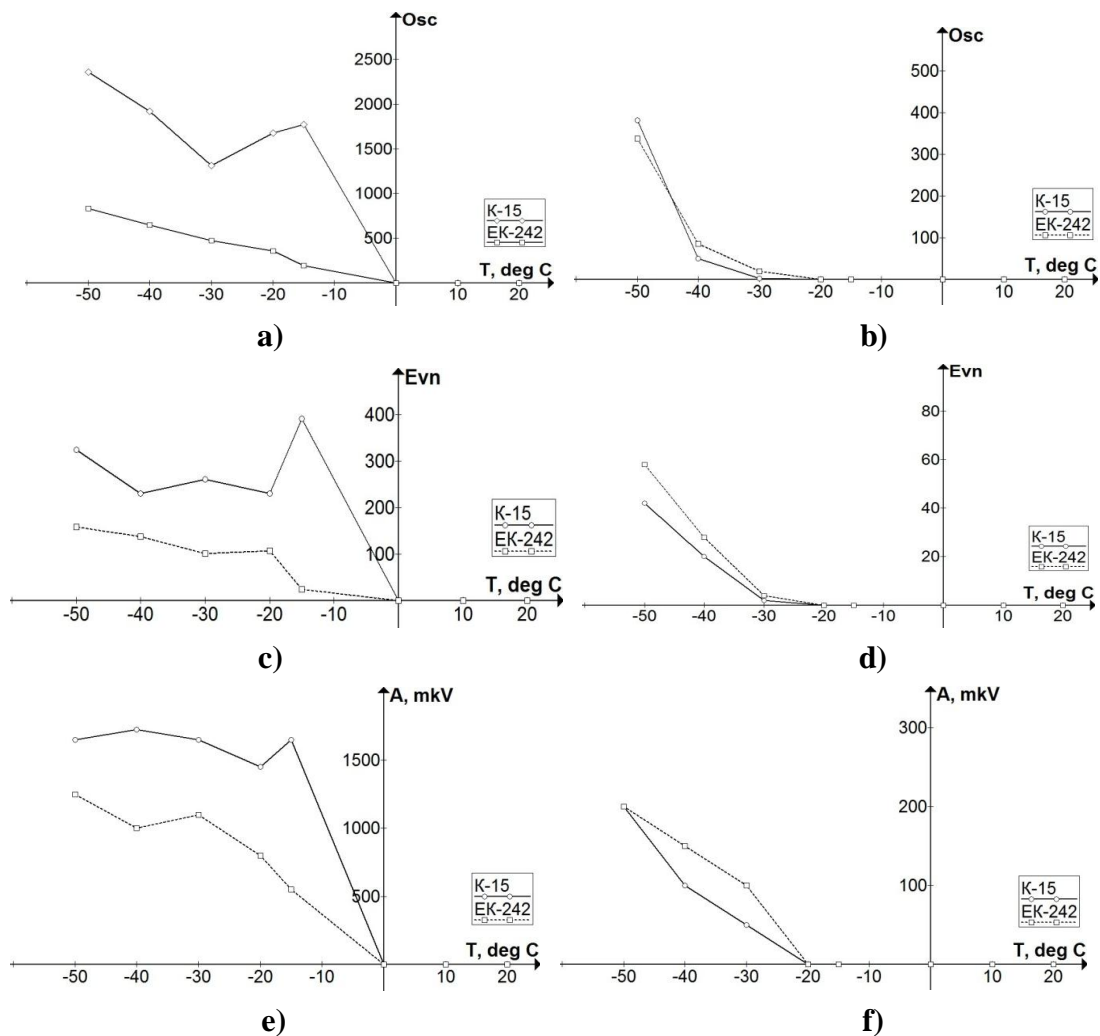


Fig. 6. Acoustic emission parameters measured during 2 thermal cycles: total count of oscillations for cycle 1 (a) and 2 (b); total count of events for cycle 1 (c) and 2 (d); maximal amplitude for cycle 1 (e) and 2 (f)

However, one of the capacitors at 69th thermal cycle emitted signals at -50 deg C, and after another 3 thermal cycles, acoustic emission bursts occurred again along with temperature raise from -40 to -15 deg C. After

another 4 thermal impacts, the electrical parameters of this capacitor deviated significantly from the specified values, so the capacitor was considered as defective, and on the 81st thermal cycle it collapsed.

Another two defective capacitors were detected by acoustic emission manifestation during the first thermal impact at temperature decrease to -50 deg C and its further progression with the temperature increase from -40 to -15 deg C in the frequency range of ceramics, which was considered as crack progression. As thermal cycles continued, one of the capacitors collapsed at the 4th thermal impact and another one at the 8th.

Conducted experiments resulted in consideration that monitoring acoustic emission is reasonable to use as non-destructive method for strength diagnostics of non-detachable ceramics and compound assemblies subjected to thermal impacts. The strength criterion in this case is the manifestation of the Kaiser effect during thermal cycling of the product.

Non-destructive strength diagnostics under thermal cycling is to be conducted by reading sensor P113 (0.2-2.0 MHz) installed on the object, in case of monitoring several objects the sensor is connected to waveguide, which provides acoustic contact with all monitored objects. Recording acoustic emission parameters is performed in the specified frequency range.

The method consists of the following steps:

1. manifestation of the Kaiser effect, i.e. the absence of acoustic emission signals after first two thermal impacts indicates of compliance with acceptable strength condition of tested assembly;

2. regaining acoustic emission signals on Nth thermal cycle, which are commensurate with signals received during the first cycle, detects beginning of destructive process and indicates that such assembly will be destroyed in 5-10 cycles;

3. observing bursts of acoustic emission signals at increasing temperature from -50 to -10 deg C indicates presence and progression of a crack in the assembly.

In last two cases the assembly is considered defective.

Conclusions

1. Thermal limits have been specified for operation of acoustic emission sensors made as an assembly of different materials, such as steel, ceramics, plastics, which are also capable of emitting acoustic emission signals during thermal cycling. Sensor P113 demonstrated reliable operation in temperature range from +50 to –50 deg C.

2. The waveguide is selected and used for transmitting acoustic emission signals from the object in the thermal chamber to the acoustic emission sensor outside the thermal chamber, what expanded the temperature range by increasing positive temperatures up to + 90 deg C and negative temperatures down to –60 deg C.

3. To eliminate hindrances associated with formation and cracking of ice during transition from positive temperatures to negative and reverse, the vacuum chamber was created. Vacuum level in the chamber equal to 740 mm Hg prevented ice formation on the samples and the waveguides.

4. The frequency separation of acoustic emission is accomplished for ceramic and compound parts of capacitor. The frequency bands are: 650-1000 kHz for ceramic component K-15; 130-300 kHz for compound component EK-242.

5. The method has been designed for non-destructive strength diagnostics of non-detachable assemblies of ceramics and compound, such as capacitors K-15-5, subjected to thermal impacts in the temperature range from +60 to –50 deg C. Manifestation of the Kaiser effect after first two thermal impacts indicates of compliance with acceptable strength condition of tested assembly, appearance of acoustic emission on Nth thermal cycle detects beginning of destructive process and indicates that such assembly will be destroyed in 5-10 cycles.

References

1. Silin R. I. (2004), Improving Reliability of Machine Units and Details by Acoustic Emission Diagnosing, Proceedings of 11th World Congress in Mechanism and Machine Science, Tianjin, China. – Tianji, pp. 2217–2221.

2. Ardebili H., Zhang J. Pecht M. G. (2019), *Encapsulation Technologies for Electronic Applications (Second Edition)*. United States, USA: William Andrew, Elsevier.
3. Phua E. J. R., Liu M., Cho B., Liu Q., Amini S., Hu X, LipGan C. (2018), Novel high temperature polymeric encapsulation material for extreme environment electronics packaging. *Materials & Design*, Vol. 141, pp.202-209.
4. Koripella C. R.. (1991), Mechanical behavior of ceramic capacitors. *IEEE Transactions on Components Hybrids and Manufacturing Technology*, 14.4, pp. 718-724.
5. Young, A. L., et al. (2007), Mechanical vs. electrical failure mechanisms in high voltage, high energy density multilayer ceramic capacitors, *Journal of materials science*, 42.14, pp. 5613-5619.
6. Kovtun I., Boiko J., Petrashchuk S., Baurienè G., Pilkauskas K. (2016), Effects of the strain transmission from the main board to the installed electronic components, *Mechanika*, Vol. 22, № 6, pp 494–489.
7. Pisarenko G. S., Kvitka O. L., Umanski E. S. (2004), *Strength of materials* 2nd edition ,Kiev.
8. Cozzolino M., Ewell G. (1980), A fracture mechanics approach to structural reliability of ceramic capacitors. *IEEE Transactions on Components, Hybrids, and Manufacturing Technology*, 3.2, pp. 250-257.
9. Kahn, S., Checkaneck, R. (1983), Acoustic emission testing of multilayer ceramic capacitors. *IEEE Transactions on Components, Hybrids, and Manufacturing Technology*, 6.4, pp. 517-526.
10. Lall P., Gupta P., Goebel K. (2011), Identification of failure modes in portable electronics subjected to mechanical-shock using supervised learning of damage progression, in 2011 Proc. IEEE 61st Electronic Components and Technology Conference (ECTC), USA, pp. 1944 - 1957.
11. Viswanadham P., Singh P. (1998), *Failure Modes and Mechanisms in Electronic Packages* in Chapman & Hall, MA, Ed. Boston : Springer.
12. Royzman V. (2002), Ways to improve strength reliability of electronics elements and systems, in Proc. IEEE Conf. Modern Problems of Radio Engineering, Telecommunications and Computer Science (IEEE Cat. No.02EX542), Lviv-Slavsko, pp.187 – 190.
13. Roizman V.P., Kovtun I.I. (1997), Software and hardware complex of acoustic emission, Measurement and computation technique in technological processes, Vol. 1, pp. 25-29.

14. Kovtun I., Royzman V.P. (2015), Development of methods for acoustic emission non-destructive strength diagnostics of components and units, Scientific collection of the National Academy of the State Border Guard Service of Ukraine. Ser.: Military and technical sciences, Vol. 3 (65). pp. 311–327.

15. Kovtun, I. I., Boiko, J. M., Petrashchuk, S. A. (2019), Reliability Improvement of Printed Circuit Boards by Designing Methods for Solder Joint Technical Diagnostics with Application of Acoustic Emission Method, Visnyk NTUU KPI Serii A - Radiotekhnika Radioaparotobuduvannia, Vol. 79, pp. 60-70.

16. Shannon R., Zucaro G., Tallent J., Collins V., Carswell J. (2019), A system for detecting failed electronics using acoustics, Instrumentation & Measurement Magazine IEEE, Vol. 22, No. 4, pp. 32-37.

17. Levikari S., Kärkkäinen T. J., Silventoinen P., Andersson C. Tamminen J. (2017), Acoustic detection of cracks and delamination in multilayer ceramic capacitors, Proc. 2017 IEEE 11 th Int. Symposium Diagnostics for Electrical Machines Power Electronics and Drives (SDEMPED), pp. 622-627.

18. Kovtun I., Boiko J., Petrashchuk S. (2018), Acoustic emission application for nondestructiv strength diagnostics of printed circuit boards, Herald of Khmelnytskyi national university, № 1. pp. 12-17.

INVESTIGATIONS ON UTILISATION CHROMIUM TANNED LEATHER RESIDUES BY CHROME RECOVERY AND BIOGAS PRODUCTION

Flisek M.¹, Wozniak B.², Schadewell Ch.³

¹Polish Chamber of Shoe and Leather Industry, Poland

²Institute for Sustainable Technologies, Poland

³Testing and Research Institute, Germany

Introduction

The production of tanned leather is very harmful for the environment. A lot of chemicals are used. The global volume of waste from the leather industry amounted to more than 800 million t per year, of which about 200 million t was generated in Europe. Approximately 210 million square meters of leather are produced per year in the European Union. About 3.5 million t of various chemical reagents and 8.4 million m³ of water are used for the production of such skins.

These figures only include waste whose chemical composition is comparable to that of finished leather. Most of these residues, as well as used leather and leather-based consumer products, are disposed of with conventional residual waste and, depending on the country, either landfilled or incinerated. The chromium and heavy metal components contained are returned to the environment either directly or via the ashes, while new chromium has to be provided for the tanning of new leathers.

For centuries leather tanning has been one of the most important industries for mankind. It is also the one producing the most polluted wastes. In general, the industry is based on the production of hides as a by-product of the meat industry. Tanneries generate plenty of wastes during all stages of their production. In the first phase, when the hide is prepared for tanning, the wastes consist mainly of untanned scraps from flashing and splitting, wastes from unhairing and pulp from degreasing. Hides are very often preserved with salts (sodium chloride). The amount of this preservative is sometimes very high - up to 300 kg per 1000 kg of hides

skins. Before the production process starts, these preserved hides skins are soaked with water, and this treatment generates large amounts of wastewater with partially extremely high salt contents. The treatment of this highly polluted waste water is very demanding and cost-intensive. The next process is tanning while the protein chains in the leather form stable complexes with chromium in case of Cr-tanning. This process is executed in water-containing chromium (III)-salts producing wastewater up to 250 kg per 1000 kg of hides. The third and last operation is finishing, which includes various process steps including glazing, polishing and coloring. It can also generate wastes containing leather dust and also chemical reagents. It can reach 100 kg per 1000 kg of hides. Generally, processing of 1000 kg of hides in tannery enables to obtain 200 kg of tanned leather, 350 kg of non-tanned solid wastes, 250 kg of tanned solid wastes and 200 kg of wastes in 45 m³ of wastewater. As chromium tanning is the most common tanning process at present, chrome is one of the chemical reagents that remains in the wastewater as well as the solid waste. Chromium is usually used and present as Cr(III), which is relatively stable, poorly soluble in water and does not generally cause health problems. But Cr(III) can be oxidized to Cr(VI) which can also occur partially through improper tanning. Cr(VI) is toxic and carcinogen, has a greater solubility compared to Cr(III) and easily penetrates biological membranes leading to a high ecological risk.

Besides high Chromium concentrations, tannery wastewaters also contain high concentrations of both organic (proteins, fats) and inorganic (salts) components. The combined wastewater usually is pretreated onsite and then transferred to local treatment plants. As chromium is a problem for sewage treatment plants, it often is precipitated previously .

Among all tanneries in Poland, 80-90% using chromium (III) as a main chemical agent. The Chromium (III) is not mentioned in 2000/60/WE Directive also after revision made in 2008/105/WE directive, but the problem is in possibility to change it in Chromium (VI) by oxidizing Most

of tannery process are made in water solution. So the wastewater are the main problem in this industry.

The method consists in adding chemical reagents such as sodium carbonate, sodium hydroxide or calcium carbonate. As a result, a precipitate of chromium (III) hydroxide is formed. The recovered chromium regenerate can be re-used in the chromium tanning process. Whereas the obtained supernatant due to the reduced chromium content can be subjected to biological treatment. The advantage of using the precipitation method is the reduction of chromium content in wastewater. On the other hand, the disadvantages are: the addition of additional chemical reagents to the wastewaters, the duration of the process depends on the alkaline agents used, the need for special filtering devices and sludge containing small amounts of chromium, as well as proteins and fats. In addition, if the chromium regenerate is not re-used, it goes to a landfill site where it is stored in a suitably protected way.

Currently, there are a lot of researches on the use of membrane techniques for the treatment of chromium tannery wastewaters. In the literature can be found information about on the use a low pressure membrane processes such as microfiltration (MF), ultrafiltration (UF) and nanofiltration (NF). However, the practical application in the separation of chromium has found the nanofiltration process (NF). By using nanofiltration processes for the treatment of chromium tannery wastewater, two streams can be obtained: permeate containing high concentration of monovalent ions salt (e.g. chlorides) and retentate containing a high concentration of chromium multivalent ions salts (e.g. sulfates). The permeate can be used as a pickling bath, whereas the retentate can be used in the tanning process. The use of pressure membrane techniques has certain advantages, including low energy demand, the possibility of enlarging the process on a larger scale (modular construction), separation processes are carried out continuously, no need for additional chemical reagents. Inconveniences appearing during the use of pressure membrane processes for wastewater treatment are: Flux decrease associated with the

occurrence of concentration polarization and fouling, as well as the resistance of the membranes used.

In recent years, a major problem is the utilization of chromium solid waste coming from the various stages of the processing of skin. These wastes are classified as particularly dangerous for the natural environment. Therefore, they cannot be stored, because after some time the chromium compounds get into the soil. Currently, technologies are being developed that allow the utilization of tannery waste by incineration while recovering chromium (III) from them. However, due to the cost of purchasing the right furnaces for this, such solutions are used to a lesser extent. During the combustion of tanning waste in conventional furnaces, chromium (III) transforms into chromium (VI), which is then released into the atmosphere. Therefore, it is necessary to search for innovative solutions enabling the recovery of chromium compounds from solid tannery wastes, which can be reused in industrial practice, among others during the processing of raw skins. Taking up such actions will contribute to the limitation of the possibility of chromium (III) compounds entering the natural environment and its transformation into carcinogenic forms of chromium (VI).

New valorization pathway for chromium tanned leather residues by a combination of protein extraction, chrome recovery and biogas production), acronym LeatherProBio.

Methods

Research will be performed by the PFI (Prüf – und Forschungsinstitut Pirmasens.V.) from Germany, and the Lukaszewicz - Institute for Sustainable Technologies (L-ITEE) and the Countrywide Polish Chamber of Leather Industry (OIBS), from Poland, both situated in Radom. The OIBS representing a large number of SME's , the PFI and Ł-ITEE have experienced research laboratories to perform the research.. OIBS will represent the leather industry and will provide extensive sample material. The SME's will be informed on a regular basis on the progress of

this precompetitive research and will have the opportunity to guide the research according to their needs.

Within the project, the goal is the development of new pathways for the recycling of chromium tanned leather residues, to re-use the contained chromium for the tanning of new leather, to minimize the release of chromium into the environment and to use the biotechnological potential of the contained biomass to save energy costs. The primary objective is the removal of chromium from tanned leather residues and subsequent combined material and energy utilization of the remaining organic content.

In order to achieve this goal, the chromium must be extracted from the leather waste and the organic material contained in the waste has to be made available to the microorganisms. This can be realized by a special physicochemical treatment process, the thermal pressure hydrolysis (TPH). After the process, the treated material can be divided into two fractions: Liquid phase and solid phase. By adapting and optimizing of the treatment conditions, the chromium content can be selectively enriched in one fraction. Chromium dissolved in the liquid phase can be made available for tanning by special processes, developed by the ITEE. The recycled chromium will be tested by the ITEE and the OIBS by performing extensive tanning tests on various leather materials to define whether the chromium can be reused. The leathers from that tanning-tests are subjected to all necessary material testing to demonstrate their recyclability and to specify the content of recycled chromium in future tanning processes. The chromium-free organic residues will be tested for their biogas potential and as additives for biotechnological applications. Based on the results from the tests energy balances for different scenarios can be established. It will be shown how much of the required energy can be recovered via biogas production from the remaining organic residues. The results are incorporated into the economic and ecological considerations.

The economic potential of the project is based on combined energy and material recovery of by-products and production waste from leather production. Currently, the solid waste is collected from the tanneries by

specialized disposal companies and usually incinerated or land filled. The costs for this disposal increase from year to year and have doubled in recent years alone to around € 150 per ton. The costs for waste water treatment are also rising continuously. The technologies developed within the framework of the project can significantly reduce the disposal costs for the tanneries. By using the solid waste for biogas production, energy costs can be significantly reduced and recovery of the chromium content from the production residues reduces the procurement costs for tanning chemicals

In the first activities in the frame of this project the actual situation with waste utilization in Polish tannery industry was investigated. The analyze was made after answers got from 53 tanneries, based in different regions in Poland.

Results

The amount of water used in this process, reported by inquired tanneries was different, and vary from 1,5 m³ up to 8 m³ per 1000 kg of hides. The average value was 2,7 m³.

So big differences are because of two reason: first - different kinds of processed leathers, so it means also different amount of salt in them and, second - the different technical condition of installations. The older, used and worm out installations are not suitable for water sawing. The actual way of waste water treatment.

Most of the examined tanneries have not their own installation for waste water treatment.

But not all tanneries gave the feedback. Only 2 tanneries reported, that they have own installation for waste water collection and clarifier at the mechanical treatment plant. All others use the other, specialized firm for waste water collection. The costs of it is also very different. The feedback information showed the value from 25 up to 80 Euro/ m³ of waste water. The differences are because of the regions in Poland have the differences in local price lists and from special conditions in agreements.

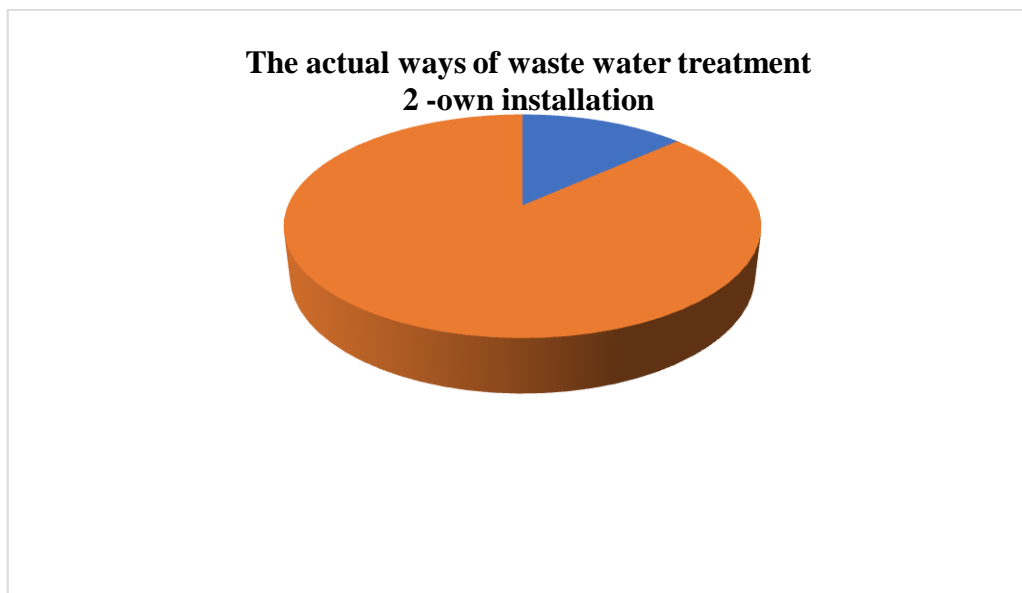


Fig 1. The actual ways of waste water treatment.

Only 6 from examined tanneries declare the water recycling. The amount of recycled water is no more than 30% of fresh water, used for operations. The main problem in increasing this amount is contaminations from salt.

The solid waste generates during tanning process.

The amounts of solid waste, reported by inquiring tanneries were different, in range 200 kg up to 600 kg of wastes for 1000 kg of hides. The average amount was 350 kg.

The amount of solid waste generated during the processing of 1 ton of hides.

The differences are because of kinds of leather and their quality are usually different in tanneries. Also technical equipment in tanneries has the influence on solid waste amount.

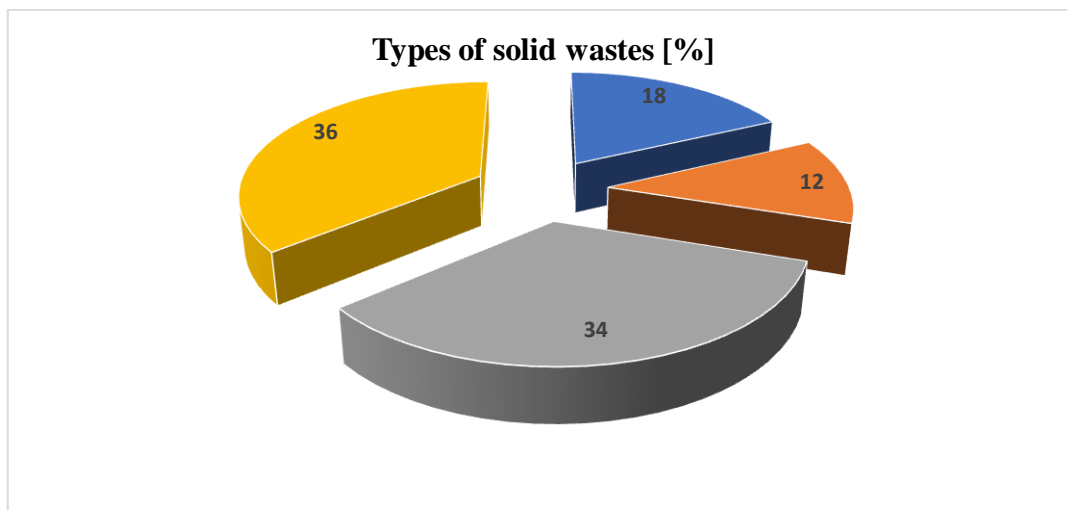


Fig 2. The percentage of solid wastes contents: Trimmings 34; Splits 36; Shaving 18; Dust 12

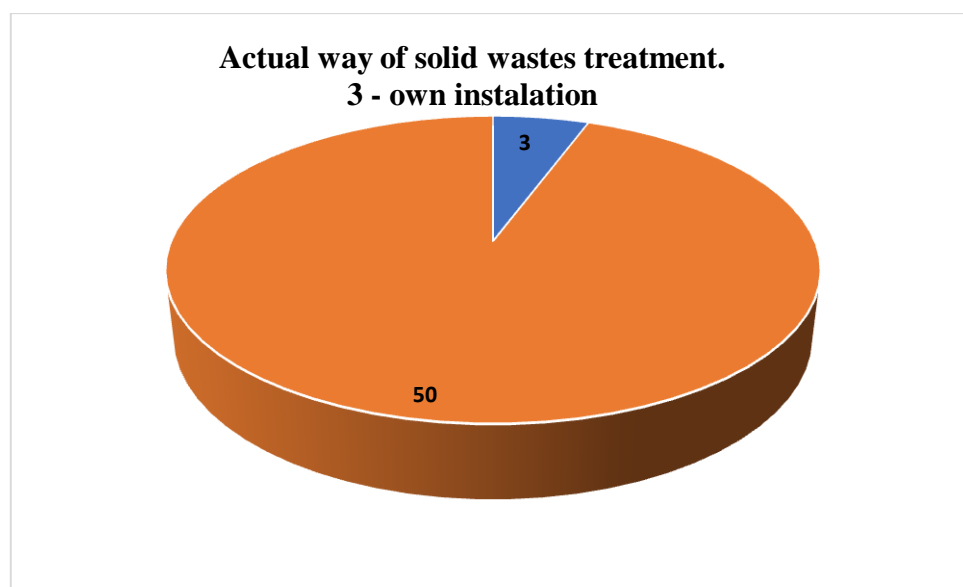


Fig 3. Actual ways of solid waste treatment

Most of the examined tanneries have not their own installation for solid waste treatment.

Conclusions

Generally, the solid wastes are collecting by outer firm, after preparing by pressing and baling for volume reducing. Only 3 middle size tanneries have their own installation for solid waste treatment.

The costs of solid waste collecting is similar in all tanneries and vary from 90 up to 120 Euro / 1000kg of waste.

CHARACTERIZATION AND PROPERTIES OF LUBRICANTS OBTAINED BY TECHNOLOGIES OF RECYCLING WASTE PRODUCTS OF THERMOPLASTICS

Prysiashna K.¹, Mandzyuk I.², Padgurskas Ju³.

^{1,2}Khmelnytskyi National University, Ukraine

³Vytautas Magnus University Agriculture Academy, Lithuania

Introduction

The term "green" means a new round of scientific thinking, which includes views on the ecological balance and principles of environmental protection. The industry of lubricants in the perspective of new thinking – "green tribology" provides among many tasks: - ecological aspects of manufacturing new lubricants with the use of renewable raw materials and their biodegradation after the end of their life cycle. Potential raw materials for the creation of environmentally friendly lubricants are vegetable oils, animal fats and synthetic alcohol esters [1, 2].

For lubricants, from the point of view of material science, it is important to solve two problems:

- to ensure the production of natural, renewable raw materials;
- to create lubricants with high tribotechnical properties and capable of independent biodegradation after the end of the cycle of operation.

In developing the technology of chemical recycling of waste polyethylene terephthalate (PET bottles) by glycerolysis, Professor Mandzyuk I.A proposed a mechanism of the process with the formation of oligomeric products - recyclables of different molecular weights [3]. The process of chemical recycling of PET, in the framework of the presented model, was considered as consisting of a sequence of reactions: the destruction of the main chain of polyethylene terephthalate under the action of degradation agent - glycerol; synthesis - polyesterification; intermolecular exchange [4, 5].

The field of technical application of natural fats continues to expand, the volume of production of products based on vegetable oils significantly

increases [6]. At the same time, attention should be focused on the fact that oil and synthetic lubricants and their components are toxic products. Some polycyclic aromatic hydrocarbons are carcinogenic. [7].

Analyzing new, modern trends in the development of tribotechnics, one should note that one of the effective directions for implementing the concept of "green tribology" is the development of new lubricant compositions based on natural ecologically safe fats capable of biodegradation. A special weightage to such scientific research is given by the use of recycling technologies of secondary raw materials [8, 9].

Methods and experimental

The aim of the work was to study the structure and tribotechnical characteristic of modified natural fats by grafting polyester oligomer (polyethylene terephthalate).

As the objects of research, the raw material: natural fats of vegetable origin – rapeseed oil and of animal origin – beef fat were considered. According to the developed technology [10], synthesized intermediate compounds of acylglycerols of natural fats [11,12], from which PET-acylglycerols of fats are synthesized. The latter were considered as the basic body of greases. To assess the structural characteristics of synthesized materials, rheometry and IR spectroscopy were used. The geometric image of the molecules and the calculation of the electrostatic potential are realized using the HyperChem programme package. The tribotechnical characteristics of the synthesized lubricants were determined on four-ball friction machine in accordance with the procedure [13].

Results and discussion

From the standpoint of the chemical structure, natural fats are compounds that are obtained as a result of the reaction between glycerol and aliphatic carboxylic acids with the formation of esters – acylglycerol (Fig. 1). By developed technologies for recycling waste PET bottles, we have obtained intermediate compounds – recyclables (PET

oligesters) the combination of which with natural fats produces PET-acylglycerols (Fig. 2).

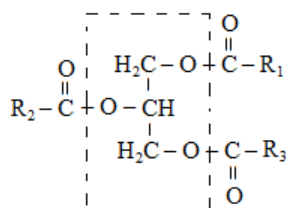


Fig. 1. Structural formula of the composition of natural fats

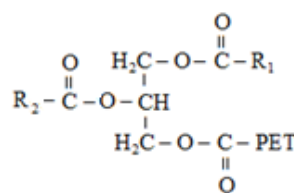


Fig. 2. Schematic form of synthesized PET-acylglycerol

On the output spectrum of rapeseed oil (Fig. 3) characteristic transmission peaks are observed, an intense band with maxima at 2966 cm^{-1} , 2887 cm^{-1} , 2843 cm^{-1} . These peaks can be attributed to stretching vibrations of $(\nu) \equiv \text{C}-\text{H}$ bond in the CH_3 groups ($2962 \pm 10\text{ cm}^{-1}$) and $=\text{CH}_2$ (2926 cm^{-1} and $2853 \pm 10\text{ cm}^{-1}$). The deformation vibrations $(\delta) = \text{CH}_2$ correspond to peaks at $(1465 \pm 10\text{ cm}^{-1})$ and 1380 cm^{-1} for $-\text{CH}_3$ and $=\text{CH}_2$. The intense band in the region of $1744 \pm 10\text{ cm}^{-1}$ is characteristic for valence vibrations of $=\text{C}=\text{O}$ bond. The stretching vibrations of the $\equiv \text{C}-\text{O}$ bond are manifested for the triacylglycerols of the three peaks of 1238 cm^{-1} , 1242 cm^{-1} , $1170 \pm 80\text{ cm}^{-1}$.

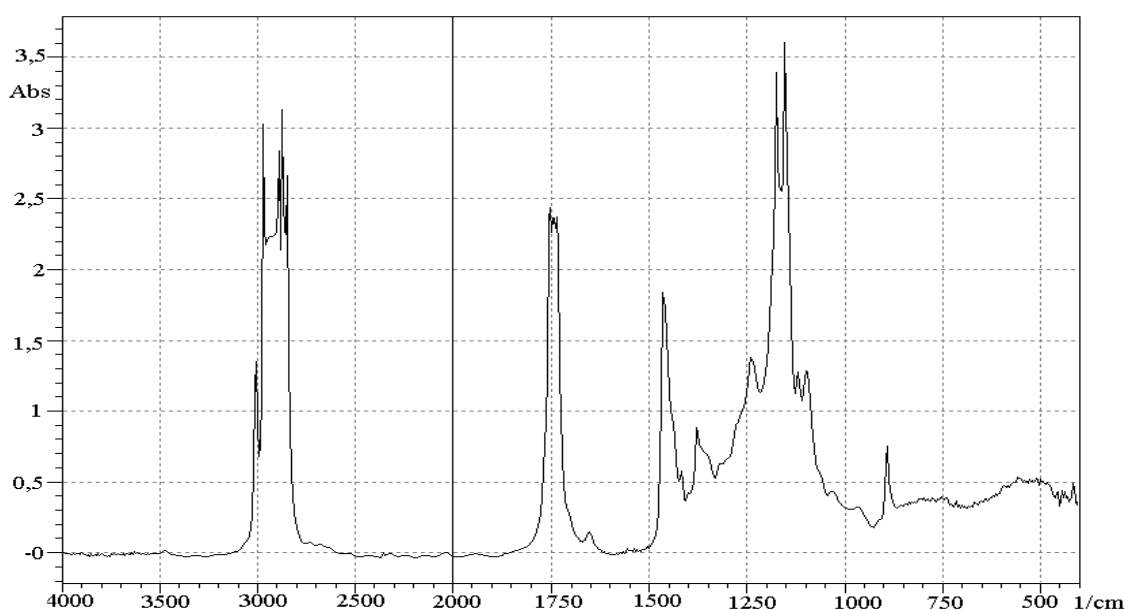


Fig. 3. IR spectrogram of rapeseed oil

On the IR spectrogram (Fig. 4) of the synthesized base bodies of lubricants base on rapeseed oil and PET waste, it should be noted the appearance of bands in the region of 1577 cm^{-1} – stretching vibrations of the C-C = benzene ring groups, deformation vibrations of the benzene ring in the plane at 1540 cm^{-1} and 1020 cm^{-1} , which indicates the presence of fragments of the PET link in the composition of acylglycerol of rapeseed oil.

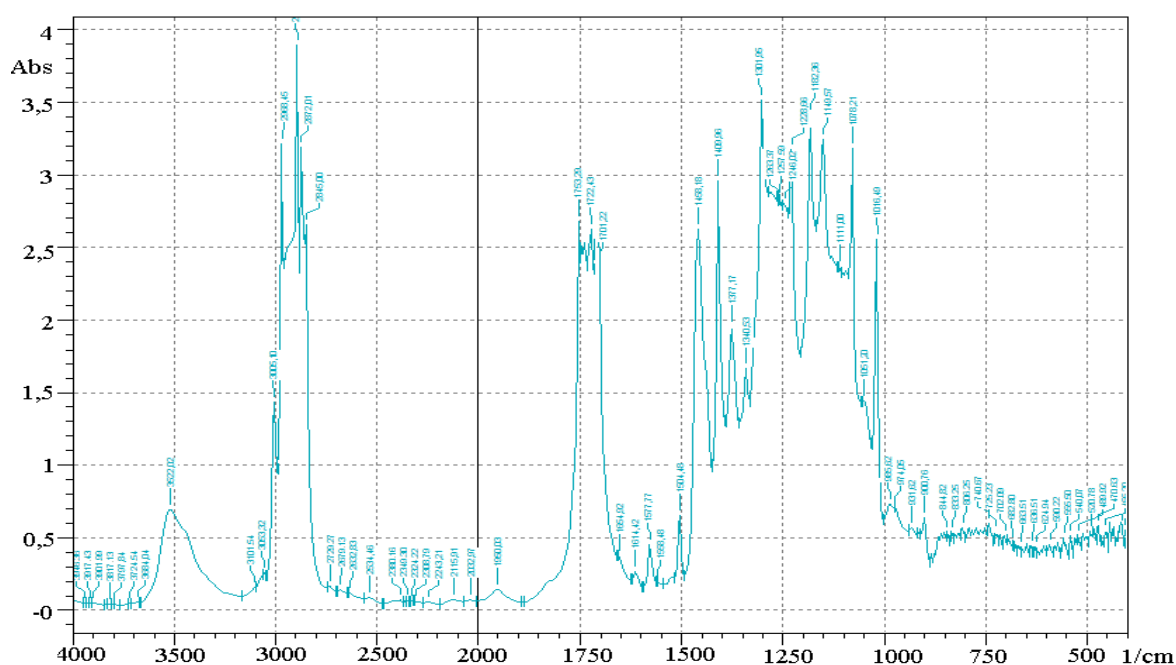


Fig. 4. IR spectrogram of PET-acylglycerol based on rapeseed oil

With the help of computer simulation using empirical calculation methods (molecular mechanics method), a geometrical image of synthesized compounds was obtained [14]. The distribution of electrostatic charge in molecules of beef fat and synthesized PET-acylglycerol is shown in Fig. 5-6.

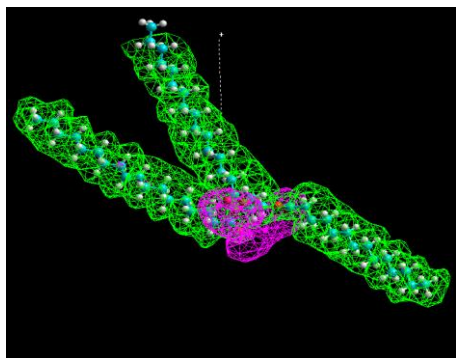


Fig. 5. The model of the beef fat molecule and the distribution of the electrostatic potential
the dashed vertical line is the direction of the vector of the dipole moment; red is negative potential, green is positive potential

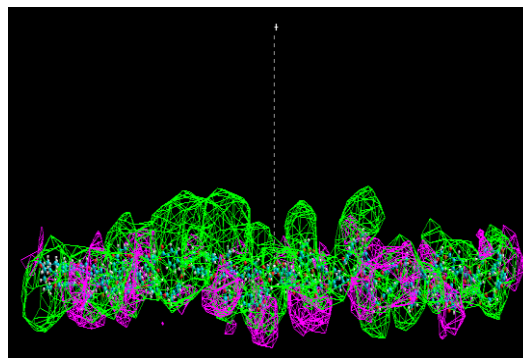


Fig. 6. The model of the beef fat molecule and the distribution of the electrostatic potential

the dashed vertical line is the direction of the vector of the dipole moment; red is negative potential, green is positive potential

The direction of the total dipole moment as regard to the horizontal plane, which can be considered a friction plane, and the distribution of the electrostatic potential clearly show the orientation of the molecules of lubricants in the adsorbed layer on the metal surface. It is the specific structure of synthesized compounds – PET-acylglycerol which allows them to be adsorbed parallel to the surface of the metal. Attention is drawn to the fact that for the PET-acylglycerol molecule, in contrast to fat, a large number of dipoles distributed along the length of the grafted oligomeric PET molecule are observed with respect to the horizontal plane.

The results of the research cycle to determine the change in tribotechnical properties, depending on the sequential complication of the system under study: natural fat – a synthesized base, with a polymer (PET-acylglycerol) – lubricating composite made from the synthesized base, containing the Irgalube (BASF) additive package are shown in Fig. 7-8.

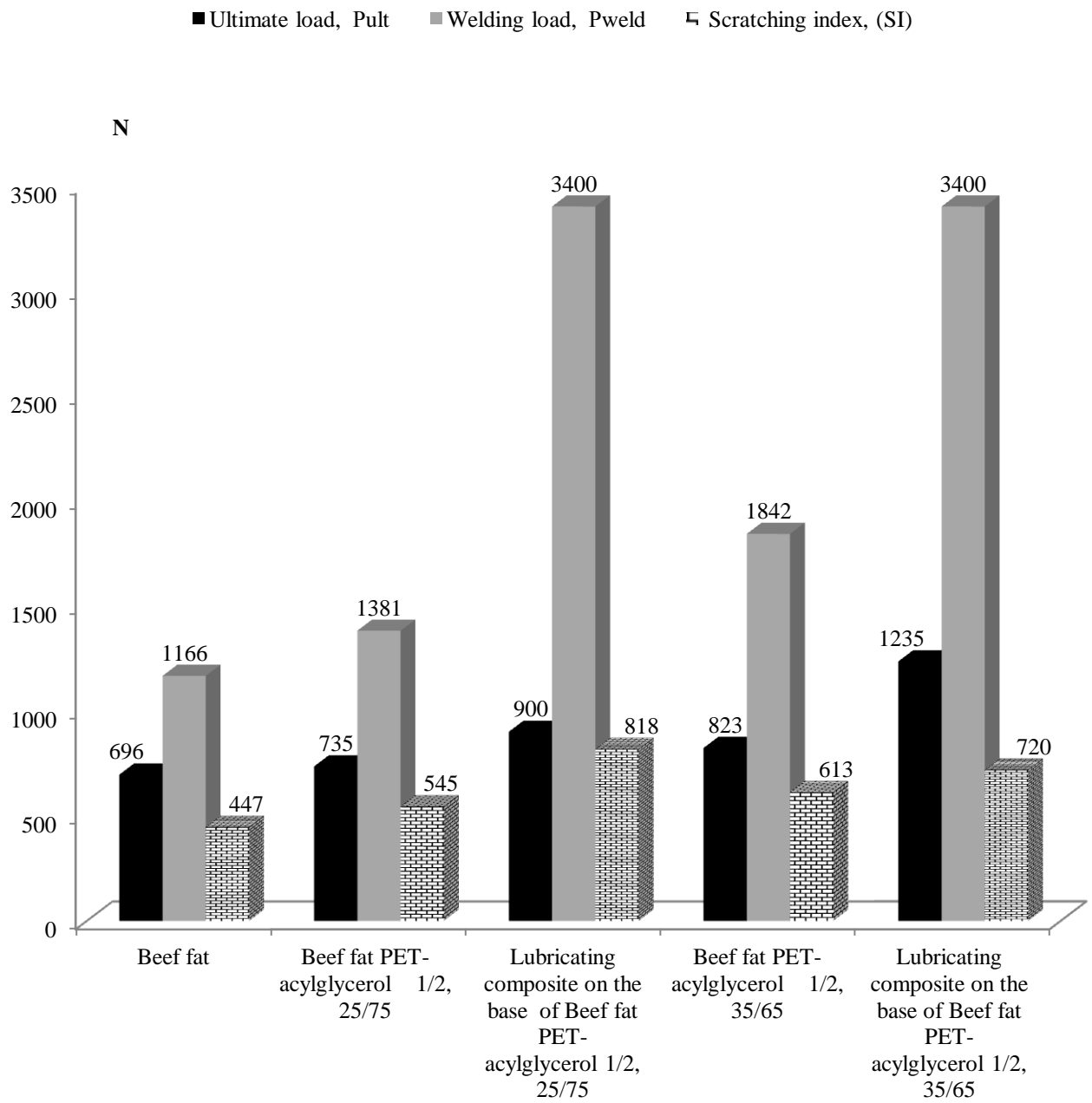


Fig. 7. Tribotechnical characteristics of the studied materials on the base of beef fat

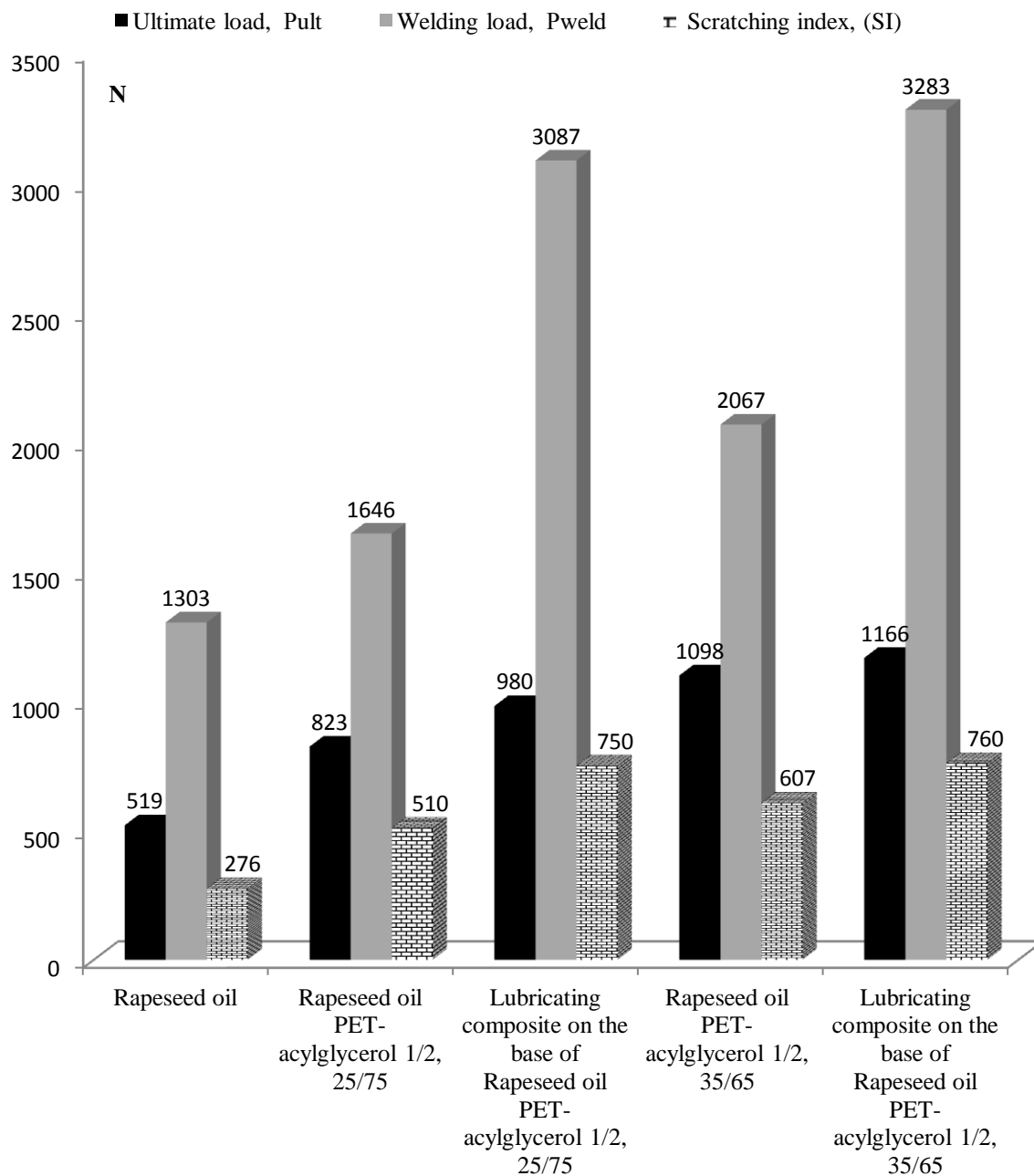


Fig.8. Tribotechnical characteristics of the studied materials on the base rapeseed oil where: 1/2 – molar ratio fat:glycerol or oil:glycerol (synthesized acylglycerol); 25/75, 35/65 – mass ratio synthesized acylglycerol:waste PET bottles

Tribotechnical characteristics of the industrial greases are shown in Fig. 9.

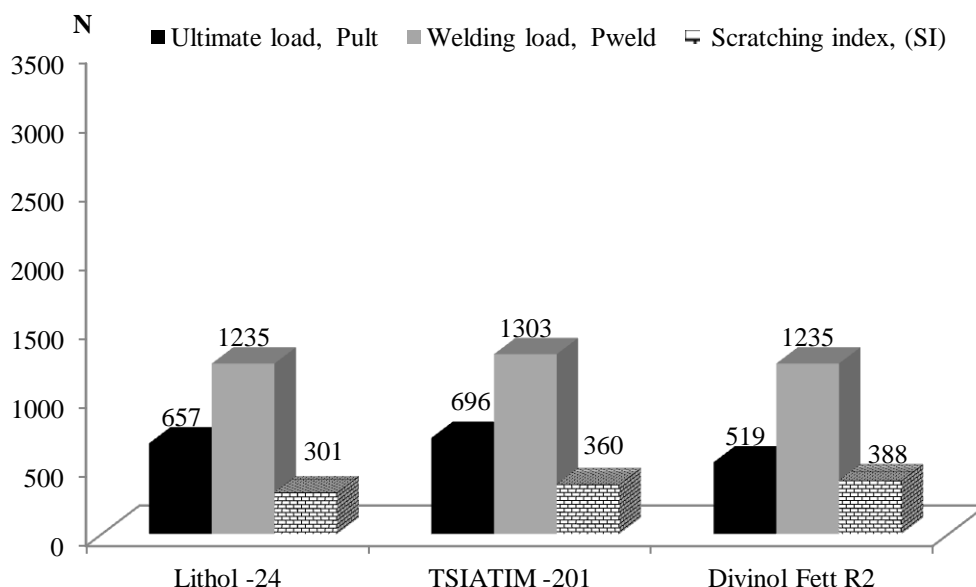
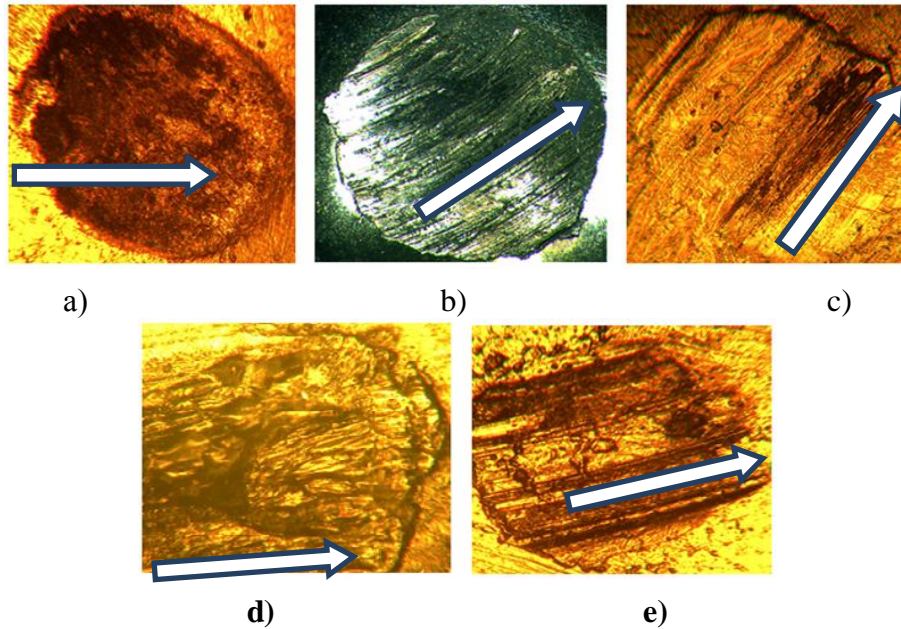


Fig. 9. Tribotechnical characteristics of the industrial greases

The results of the studies clearly demonstrate the qualitative positive change in the tribotechnical characteristics of the greases studied with the complication of their structural structure. The transition from the initial fats: beef fat and rapeseed oil to synthesized ones, on their base and PET waste, compounds (PET acylglycerol) provides an improvement in both wear indicators and a decrease in the propensity to weld.

Microphotographs of wear spots of balls investigated on the four-ball friction machine in various lubricating media are shown in Fig. 10.



a) without lubrication; b) beef fat; c) synthesized body of PET-acylglycerol 1/2, 35/65; d) lubricant based on PET-acylglycerol 1/2, 35/65; e) Lithol-24
Fig. 10. The wear spots of the balls at Pult for different lubricating oils, the arrow indicates the direction of motion. (The size of the wear spots is different, consequently the magnification range is different. It will not be correct to compare the microphotographs among themselves mechanically.)

In the picture (Fig. 10a), during friction without a lubricating oil ($P = 60\text{N}$), there are craters due to the adhesion of metal surfaces with signs of cold welding. In case of using beef fat as a lubricant, the limiting friction regime is observed with an equalization of the friction surface due to smoothing of the microroughnesses. On the surface of the spot, two paths of jamming caused by the bonding of metal surfaces can be seen, which can be explained by the failure of the film of the lubricant in the local friction zone at the indicated load value - 696N (Fig. 8). The type of wear spot when rubbing with a synthesized body (Fig. 10c) indicates the signs of plastic deformation of a thin layer of metal in the friction zone, which manifests itself in the formation of a mass of metal in front of the ball when it moves. The magnitude of plastic deformations is still insufficient to achieve setting, welding of metal surfaces. Plastic deformation of the metal is evidence of the formation of the intermediate layer in the contact zone,

due to the phenomena of adsorption of the lubricating oil on the active centers of the metal surface [14]. Specifically, a large number of dipoles, noted before, explains the extremely high degree of adhesion of PET-acylglycerol to the friction surface, which allows the lubricant film to be retained on the metal surface at high shear stresses and causes a significant improvement in tribological characteristics (Fig. 8-9).

When using a grease obtained from synthesized bodies and additives of a special purpose on the wear spot, it is clearly visible that the metal layer is inflated due to its plastic deformation. As is known [15] due to plastic deformations in the contact zone, the friction surface levels, the contact area grows, causing a decrease in wear and index of friction. In the case of tests of the industrial known lubricant of general purpose Lithol-24, on the area of the wear spot, it is possible to observe the areas of setting of metal surfaces with the formation of craters due to the extraction of the metal. This means that at a given value of the load $P_{ult} = 1235\text{N}$ and the rate, the film of the lubricant Litol-24, namely the hydrocarbon oil, ruins and it does not have time to recover and form an adsorption layer on the contact surface.

More clearly, the difference in the behavior of the lubricating oils studied and the nature of wear of the metal surface is manifested under welding load [14].

Conclusions

The conducted studies demonstrate the possibility of a new direction of development of lubricating oil bodies from natural raw materials by implantation of oligomers of different chemical nature in different amounts into fat molecule, thus regulating the rheological, adhesion, tribotechnical properties of lubricants.

References

1. Czichos Horst, Habig Karl-Heinz Tribologie Handbuch, 2010, 757 p.
2. Резников В.Д., Шестаковская Т.В., Довгопольный Е.Е. Чепурова М.Б. Зарубежные масла, смазки, присадки, технические жидкости: Международный каталог, 2005, 383 с.

3. Декл. патент 60710А Україна, МПК⁷ С 08 J11/00. Спосіб переробки відходів поліетилентерефталату / І. А. Мандзюк, В. М. Голоджко, Т. В. Іванішена (Україна) ; заявник і патентовласник Хмельницький державний університет. – № 2003021112 ; заявл. 07.02.03 ; опубл. 15.10.03, Бюл. № 10. – 3 с.
4. Mandzyuk I. A., Ivanishhena T. V. Investigation of chemical recycling - glycolysis of polyethylene terephthalate, Bulletin of Technological University of Podillya, 2002, No 5, pp 186-189.
5. Mandzyuk I. A. Questions about handling industrial and household waste, Eco-technology and resource-saving, 2003, , No 3, pp. 41-43.
6. Остриков В.В., Нагорнов С.А., Клейменов О.А., Прохоренков В.Д., Курочкин И.М., Хренников А.О., Доровских Д.В. Топливо, смазочные материалы и технические жидкости, 2008, 128 с.
7. Byrne C. J., Calder J. A. Effect of the Water-soluble Fractions of Crude, Refined and Waste Oils on the Embryonic and Larval Stages of the Quahog Clam, Marine Biology, 1977, No 40, pp. 225-231.
8. Мандзюк І. А., Присяжна Е.А. Розробка смазочних матеріалів в рамках концепції “Зеленої трибології”, Фундаментальні та прикладні дослідження у сучасній науці : зб. наук. пр. ІV наук. конференції. – Харків : Технологічний Центр, 2016. – 100 с.
9. Padgurskas J., Rukuiža R., Mandziuk I., Kupcinskas A., Prisyazhna K., Grigoriev A., Kavaliova I., Revo R. Tribological properties of beef tallow as lubricating grease, Industrial Lubrication and Tribology, 2017, Vol. 69, No 5, pp 645-654.
10. Патент на винахід 114226 С2 Україна, МПК (2017.01) С10М 177/00 С10М 105/06 (2006.01) С10М 117/00. Спосіб синтезу біодеградуючої базової основи мастильних матеріалів / І. А. Мандзюк, К. О. Присяжна (Україна) ; заявник і патентовласник Хмельницький національний університет. – № а 2015 07870 ; заявл. 07.08.2015 ; опубл. 10.05.2017, Бюл №9. – 7 с.
11. Декл. патент на корисну модель № 110856 Україна, МПК⁷ С10М 107/04, С10М 101/00, С11С 3/06, С10N 40/02. Склад консистентного мастила / І. А. Мандзюк, К. О. Присяжна ; заявник і патентовласник Хмельницький національний університет. – № u201603572 ; заявл. 04.04.2016 ; опубл. 25.10.2016, Бюл. № 20. – 3 с.
12. Декл. патент на корисну модель № 110857 Україна, МПК⁷. Консистентне мастило / І. А. Мандзюк, К. О. Присяжна ; заявник і патентовласник Хмельницький національний університет. – № u201603574 ; заявл. 04.04.2016 ; опубл. 25.10.2016, Бюл. № 20. – 3 с.
13. DIN 5135 Testing of lubricants – Testing in the four-ball tester – Parts 1-5. – Publ. 2015-03-01. – Berlin : German National Standard, 2015. – 33 p.
14. Мандзюк І. А., Присяжна К.О. Новий клас основ мастильних матеріалів за вимогами “зеленої трибології”, Проблеми трибології. – 2017. – № 1. – С. 35–40.
15. Фукс І. Г. Добавки к пластическим смазкам, М.: Химия, 1982, 248 p.

DIAGNOSING THE CONDITION OF THE TEMPOROMANDIBULAR JOINT ON THE BASIS OF MEDICAL IMAGE EXTRACTION

Glowacki M., Mazurkiewicz A., Nowicki K., Slomion M.
UTP University of Science and Technology in Bydgoszcz, Poland

Introduction

Medical imaging has become one of the most important and important aspects of preparation for treatment on many levels. Doctors are able to help with known ailments and those that they are able to see or examine, while in the case of places that show non-obvious ailments and cause considerable discomfort, they are forced to use imaging diagnostics, which deals with the creation of images of physiological and pathological changes occurring in the human body, and this is done by means of various physical interactions.

All this information, which is collected by means of imaging machines, has allowed the formation of a biomedical engineering breakthrough that uses the collected data to support doctors through printed prostheses, implants, tablets, as well as assistance in the simulation of surgical procedures and partial facial reconstructions, which is made possible by collecting the appropriate amount of data and the using additional 3D printing.

The choice of treatment that a patient should receive should not be made on the basis of a single imaging examination, so in many cases of dysfunction and injury to the head, it is important that the number of examinations carried out and the radiation strength be as low as possible, given the possible harmfulness and side effects. The extraction of medical images, and more specifically of the temporomandibular joint area due to soft tissues, has been strictly regulated by the only examination that offers the greatest diagnostic possibilities, which is magnetic resonance imaging. The pictures obtained by means of this method and their quality mainly

depend on the equipment and skills of the operator, therefore, despite the examination, it is difficult to clearly state what is wrong with the patient. To help with the diagnosis of temporomandibular joint dysfunction, the extraction of data from the magnetic resonance imaging is based on the extraction of data, which allows to obtain 3D models of the joint components, as well as to determine the correlation between themselves and any changes in structures.

Today, many imaging methods are used today to identify temporomandibular joint disorders, but to date, no gold standard has been established to identify a true clinical diagnosis. For example, arthrography has the best diagnostic results in identifying disorders within the body, but is invasive compared to magnetic resonance imaging and has poor performance among observers. Computed tomography and MRI are the gold standard in terms of joint assessment, both for the assessment of the condition of hard and soft tissues, both methods work well together,

The American Academy of Orofacial Pain (AAOP) has divided the temporomandibular joint dysfunction into two main groups: muscle and joint pain. It is estimated that this joint disorder affects approximately 30 % of the population asymptotically and is defined as internal joint damage, which includes disc displacement, structural changes associated with osteoarthritis and degenerative joint diseases. Some of the following diagnostic methods will additionally include examples presented through images obtained during these tests [1, 2].

Radiographic examination provides information about the morphological characteristics of, inter alia, bone components of the joint and certain movable links between the condyles and the joint nodules, but is not effective in assessing the soft tissues in the patient's body. There are anatomical and technical factors that can make the image unclear and distorted. Radiography is selected for the diagnosis of the temporomandibular joint, mainly when it comes to the identification of individual bone structures, a specific clinical mainly when it concerns the individual bone structures, a specifically establishes clinical disorder, or the

absence of symptomatic information on a given dysfunction that could lead to a clinical diagnosis. The type of class of radiographic techniques in which the temporomandibular joint examination is performed includes panoramic radiography, planigraphy and transcranial radiography [3, 4].

The figure below shows examples of images of individual disorders that can be seen through this diagnostic method.

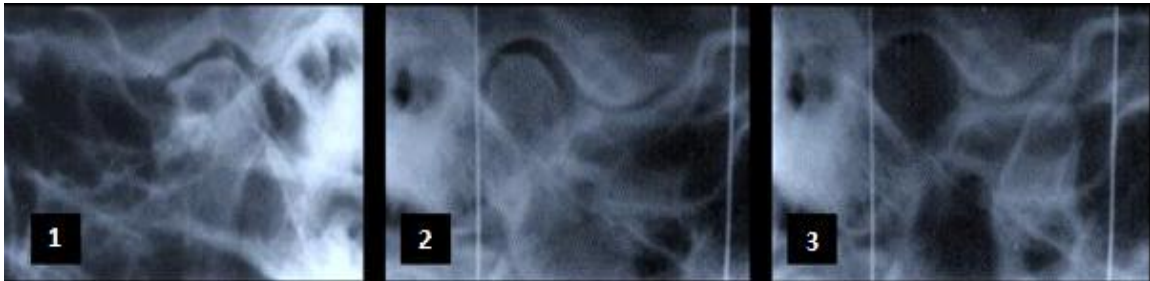


Fig. 1 Radiographic evaluation of particular disorders in the temporomandibular joint [5].

The radiological evaluation shown in Fig. 1 shows the following disorders:

1. It presents an image from a transcranial projection which states the presence of osteophytes, the so-called bone growths.
2. Allows you to determine the joint space during maximum opening.
3. It shows that the correct border of the condyle of the mandible bone has been exceeded.

Computed tomography (CT) consists of a set of images obtained using a very precise technique. For dental diagnostics, conical tomography is used, which is particularly useful in the maxillofacial region, because its main advantage is the observation of bone joint structures in three planes. Among other things, in the sagittal, coronal and axial planes, thanks to the possibility of image manipulation, it is possible to obtain a clear picture of the patient's interior at various depths. After the examination, a file in the form of a dicom is placed in the record in given diagnostic method, which enables to read three-dimensional reconstruction resulting from the examination through special software.

The main indications for CT scans of temporomandibular joint disorders include: Structural assessment of bone components of the joint, which is able to precisely determine the location and extent of bone changes, including fractures, tumours and stiffness. Erosive and degenerative changes, condylar hypertrophy, as well as intra-articular calcifications and metabolic arthritis. Indications that can be detected by this method do not include soft tissues, therefore it is not possible to assess the condition and position of the joint disc. The disadvantage, however, is exposure to significantly different levels of radiation compared to unconventional radiographic techniques and the cost of the examination itself [6, 7]. Fig. 2. present the morphological changes of bones in the temporomandibular joint made by cone-beam CT scans [5].



Fig. 2. The morphological changes of bones in the temporomandibular joint made by cone-beam CT scans

The radiological evaluation shown in Fig. 2 shows the following disorders:

1. The view from the coronal projection shows extensive erosion.
2. This example shows bone sclerosis.
3. Abnormalities in the structure of the bone bark are noticeable.

Magnetic resonance imaging (MRI) plays a major role in the study of disease processes involving soft tissues of the temporomandibular joint, such as: joint disc, ligaments, adjacent chewing muscles, smear bag contents and spinal bone components. Through this technique, we are able

to carry out analysis in the axial, coronal and sagittal plane. The gold standard for the assessment of the disc position.

Clinical conditions that indicate the need to use this diagnostic method include persistent pain in the joint or vestibular area, the presence of noises that indicate a blockage of the disc, such as a click. Quite common subluxations and dislocations, limited mouth opening motion with residual stiffness, as well as suspicions of neoplastic processes and the presence of degenerative conditions which may manifest asymptotically as the onset of osteoarthritis.

Diagnostic protocols that include registration at MHI and MMO positions with a weighted average of T1, T2 and PD proton density that quite clearly shows the anatomical details of the joint in the sagittal and coronary plane. Namely, thanks to T1 weighted images and proton density, the image is shown in a satisfactory spatial resolution, which allows you to capture possible disc movements or injuries that the disk may have suffered as a result of an impact or accident. On the other hand, T2-weighted images are used to record core bone swelling or joint exudates.

Both, as well as each method, it is the technique of diagnostic with magnetic resonance imaging that has its advantages and disadvantages. These advantages and disadvantages should be counted: Possibility of detecting changes in soft tissues, and more precisely discussing this, various types of necrosis, oedema, presence or lack of it in case of exposure to ionizing radiation. The assessment of the relationship and integrity of neuronal structures is possible by means of MRI, such as the result of neoplastic or vascular processes, which result in pain in the oral-facial region caused by strong compression of these processes. The disadvantages mainly relate to the cost of the test and the need to use high-end equipment with good resolution results [7, 8].

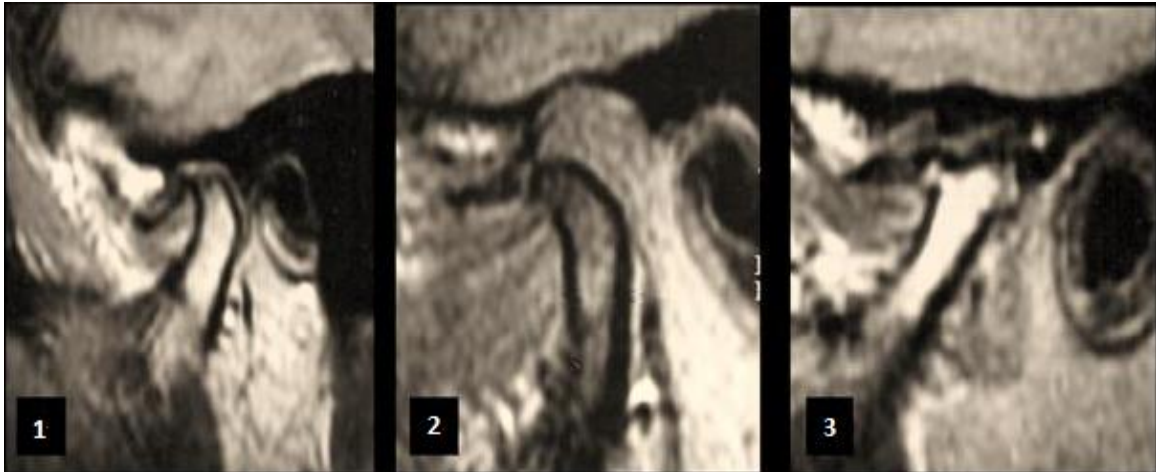


Fig. 3. Morphological changes in discs and bone structures diagnosed by MRI [5]

The assessment of changes in the temporomandibular joint is presented in Figure 3.

1. Shows a cyst for cartilage at the condyle.
2. In the figure you can see the displacement of the disc in the pond.
3. Deformations due to accident and exudate are visible.

The above mentioned methods of imaging of temporomandibular joint dysfunctions differed from each other in the degree of sensitivity, the cost of performance, the amount of ionizing radiation. Each of the methods is proven in the diagnosis of less complex symptoms in patients and the differential diagnosis of maxillo-facial inflammations.

The created method of extracting individual cases of temporomandibular joint dysfunction uses for building 3d models magnetic resonance images recorded in DICOM format. For example, two cases of joint dysfunction and one healthy joint are shown. All models were made using an open source program called Slicer, whose license allows for free and legal use. The functions include the ability to independently modify, analyze and extend existing tools necessary to properly measure and generate 3D models.

When diagnosing by means of two-dimensional images, the main focus should be on the relationship between the individual joint elements.

Sometimes it is connected with the difficulty of two-dimensionality picture and taking it in three main planes, which in turn should extend the range of possibilities for detecting dysfunction. In the case of this joint the assessment is possible only in the sagittal plane.

On the CD received from people taking radiological pictures, we usually have reference pictures, which in turn are only a preview of the best pictures selected from a set of the best ones in the smallest possible distance between them in a given projection. During the extractions, process, material in the form of a file with DICOM format was used, which thanks to its format can be used to generate 3d models.

Method of extracting of a healthy left temporomandibular joint – mandible position jaw lowered.

In the above figure, which is the first one after playing the DICOM image file, you can see the frontal plane (1), the sagittal plane (2) in which you can see the outline of the joint, the horizontal plane (3) and (4) the area where the 3d model will be displayed in the next step .

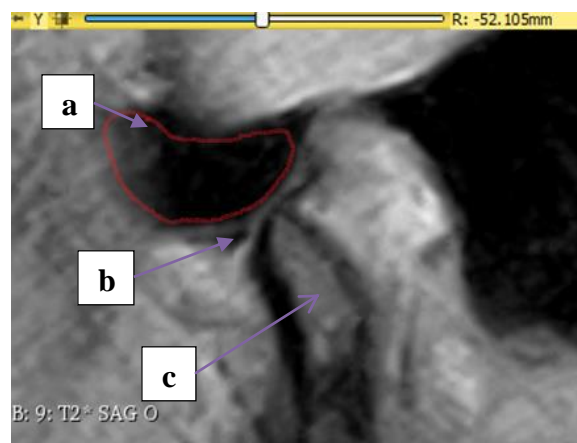


Fig. 4. Abandoned temporomandibular joint in the sagittal plane - own material

Once the area of the T1 series is been properly defined and the contrast and brightness has been adjusted to set the right visibility, the individual contours of the anatomical elements can be seen and the outlines of the joint structure can be seen. The section of the image in the dark field, which is visited by means of a red line indicates the position of the temporal bone (a), the field extending over the mandibular condyle

indicates the location of the joint disc (b), and the most visible of all the elements of the joint is the mandibular condyle (c) is the most visible of all the elements of the joint.

In order to develop a specific model of a given anatomical structure or part of the pond, it is necessary to mark by hand (on several or even several slides) a given part with a view to its displacement in relation to the photos taken at particular intervals. These distances are anatomical cuts, and the distance between them depend on the machine setting and the accuracy of the equipment. The smaller the distance, the greater the number of slides on which a given contour should be marked, but also the greater accuracy, which is characterized by a more detailed model representation.



Fig. 5. Arrow plan view and preview of a 3d model of a healthy lower joint – own material

In the above figures, we can see the marked condyle of the mandibular bones (1), the outline of which has been marked and filled with green colour, which does not have much significance that the geometric shape is the main focus here. In the figure next to (2) we have a preview of the model, which was created after putting on several slides.

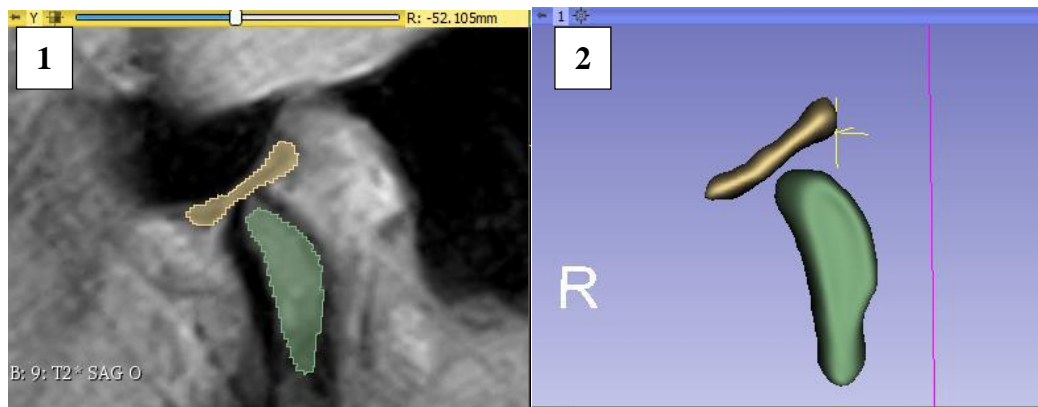


Fig. 6. Arrow plan view and preview of the 3d model of a healthy lowered joint – own material

After the condyle of the jawbone has been marked, the next step was to mark the disc on the slides in terms of their visibility (1), in the figure (2) the correct position of the disc in relation to the condyle with the mouth open.

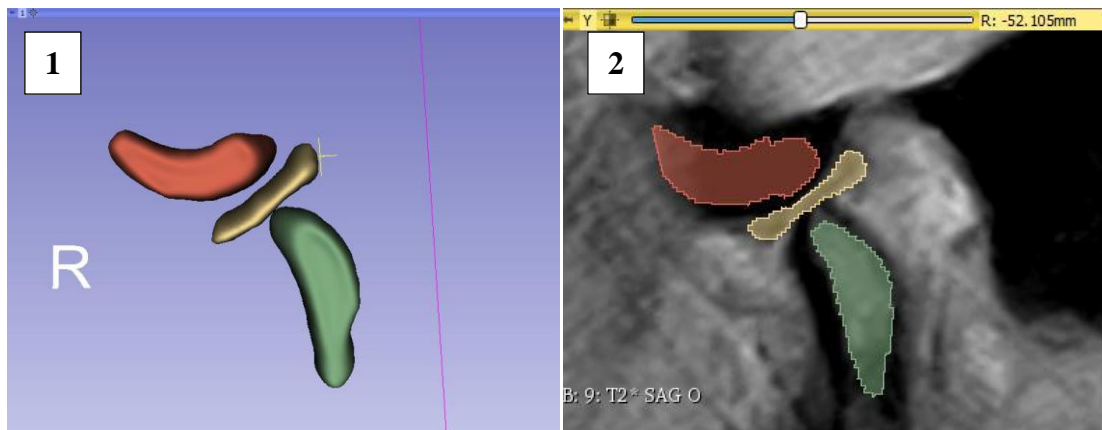


Fig. 7. Arrow plan view and preview of a 3d model of a healthy lowered pond - own material

After the above figure, an outline of the temporal bone was made, which is used only for previewing in see how closely the bone, disc and chaps' condyle correlate (2). The joint has no deviation and qualifies for as healthy one.

Method of extracting of a healthy left temporomandibular joint - raised mandible

During the reconstructing of the joint with the mandible raised and retracted, there is possibility of noting the movement of the mandible

together with the joint discs, as well as movement of the head of the mandible along the back Surface of the joint nodule from the joint hole back and upwards. This movement and the extent of the displacement can be seen when we comparing the two joints in two positions, which are visible during the lowering and raising of the mandible.



Fig. 8. The elevated temporomandibular joint in the sagittal plane - own material

When the contrast and brightness are properly set, the outlines of the joint structure can be seen, the dark box visited through a red line indicates the temporal bone position (a), extending over the condyle and on the left side of the mandibular bone, the box indicates the location of the joint disc (b), and the long oval structure marked indicates the condyle of the mandible bone (c).

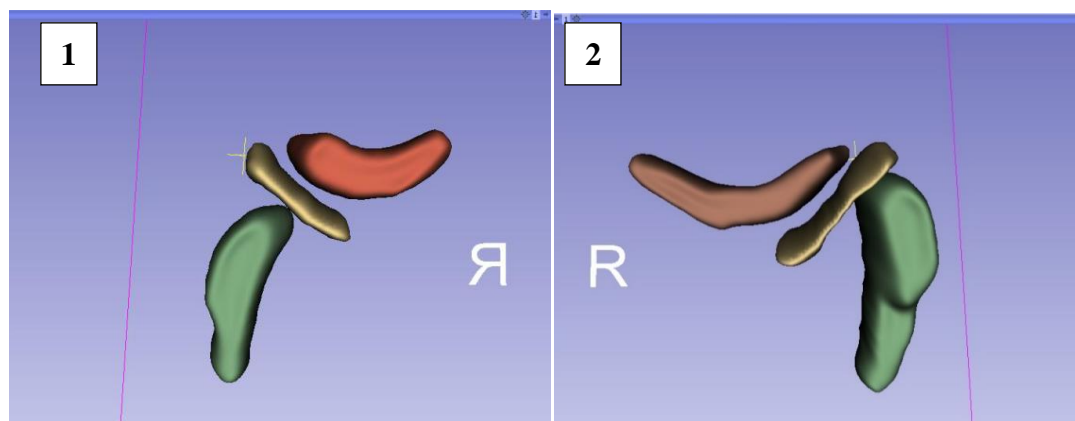


Fig. 9. The 3d model of a healthy lowered joint (1) and a raised healthy joint (2) - own material

Using the above preview, after the extraction of the patient's medical image, as well as the execution of 3d models, one can see that a given joint behaves correctly during opening and closing the mouth and the individual anatomical structures look natural to each other.

Comparison of 3d models of the temporomandibular joint in the sagittal plane during the lifting and lowering of the mandible in which the disc was moved.

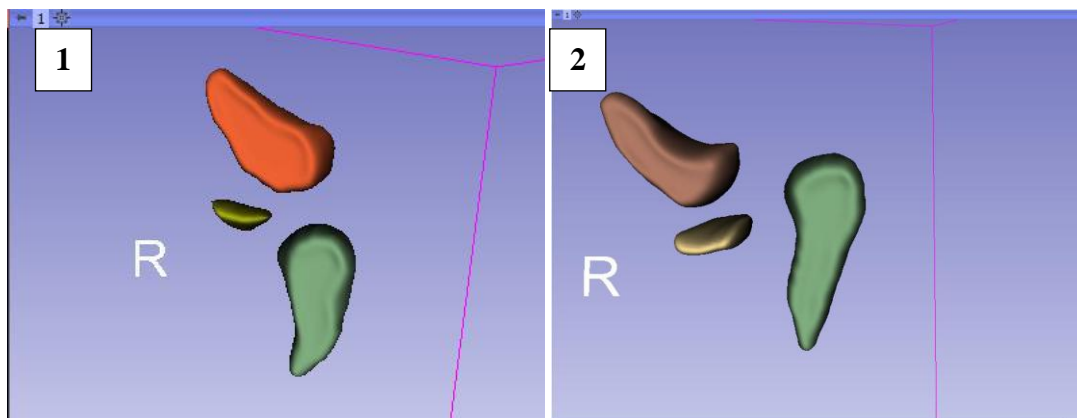


Fig. 10. The 3d model of lowered pond (1) and a raised pond (2) with a disc stirred up - own material.

The above example shows 3d models, which illustrate the joint during lifting (1) and lowering of the mandible (2), where the disc was moved. Due to the quality of the MRI image, the disc is shown in a small part, but does not change the fact that the articular disc has been blocked and is not set the correct position during the mandible lift.. This, in turn, involves quite a lot of uncomfortable and immediate need to attempt causal treatment with a temporary repositioning rail.

Research results and conclusions

The presented method of extracting medical images of the temporomandibular joint allowed, to recognize properly the components of the joint in Figures 9 and 10 with the help of the created 3d models. The problem, which concerned the determination of the position of the head of

the mandible, as well as the location and shape of the articular disc was correctly recognized. The effect was possible by means of manually adjusted contrast, sharpness and segmentation of individual parts of the joint using the presented methodology.

The presented methodology has been implemented in dentistry and effectively helps to diagnose the occlusion. Thanks to the actual scale of models developed on the basis of radiological data of patients, it is possible to design a properly fitted correction device.

By adapting the image and using the appropriate series to the correct location of the joint in the pictures that were created as a result of MRI examination, it was possible to see hard tissues that are not recognized in practice by this diagnostic method.

Thanks to the attempt to solve the problem with the diagnostics of the temporomandibular joint, the laboratories cooperating with the author, performing MRI tests implemented a new procedure. In a given procedure, only T2 series photographs are taken in all casts, bearing in mind that the most visible joint is in the coronal cast. The limitation in taking pictures of only one series of the joint in the obtuse and closed position allowed to increase the scale of accuracy of the performed examination. For example, in the past a given photo in the casts was cut with slides at a distance of 10 mm from each other and now by focusing on one cast the distance is 3 mm.

The changes in the study also included the method of taking pictures. Nowadays, they are taken separately for each joint with a specific direction, because a side effect of capturing two joints with one image was that only the joint that was closest to the calibrated direction. This resulted in the fact that the further joint was visible only in the reference pictures, so the device with which the examination was taken recorded in DICOM format only one joint.

References

1. MM Garcia, KFS Machado, MH Mascarenhas Ressonância magnética e computadorizada da articulação temporomandibular tomography: além da disfunção Radiol Bras, 41 (2008), pp. 337-342.

Advanced technologies in education, industry and the environment

2. AML Ferraz Júnior, JP Guimarães, LA Ferreira Técnicas de obtenção de imagens da articulação temporomandibular JP Guimarães, LA Ferreira (Eds.), Atlas de diagnóstico por imagiologia das desordens temporomandibulares, Editora UFJF, Juiz de Fora (2012) 28-66.
3. FA Cozzolino, A. Rapoport, SA Franzi, RP Souza, CAB Pereira, RA Dedivitis Correlação entre os achados clínicos e imaginológicos nas disfunções temporomandibulares Radiol Bras, 41 (2008), pp. 13-17.
4. SM Almeida, FN Bóscolo, TCR Pereira Estudo comparativo entre duas técnicas radiográficas transcranianas utilizando o cefalostato ACCURAD-200, nas posição de gabaritos para delimitação, 1997 51-60.
5. <https://www.sciencedirect.com/science/article/pii/S1808869415002645> access on 10/16/2020
6. SM Almeida, FN Bóscolo, TCR Pereira Estudo comparativo entre duas técnicas radiográficas transcranianas utilizando o cefalostato ACCURAD-200, nas posição de gabaritos para delimitação, 1997 51-60.
7. ACA Ramos, VA Sarmento, PSF Campos, MOD Gonzalez Articulação temporomandibular - aspectos normais e deslocamentos de disco: imagem por ressonância magnética Radiol Bras, 37 (2004), pp. 449-454.
8. EL Lewis, MF Dolwick, S. Abramowicz, SL Reeder Contemporary imaging of the temporomandibular joint Dent Clin North Am, 52 (2008), pp. 875-890.

ALPHABETICAL INDEX OF AUTHORS

- Asaulyuk T. 94
Avetisyan A.47
Boiko J. 248
Chesanovskyi I. 193
Demydchuk L. 132
Flisek M. 261
Gebrian P. 59
Glowacki M. 280
Hes L. 59
Horiashchenko K. 172
Horiashchenko S. 172
Ihnatyshyn M. 183
Ivanishena O. 235
Ivanishena T. 235
Katerynychuk I.193
Korycki R. 71, 122
Koshevko Ju.23
Kovtun I. 248
Kozar O. 33, 223
Kuleshova S. 146
Mandzyuk I. 269
Mazurkiewicz A. 280
Nowicki K. 280
Padgurskas Ju. 269
Paraska O. 59, 159
Pelekh Yu.83
Pelyk L. 83
Petrashchuk S. 248
Polishchuk O. 172
Prysiazhna K. 269
Radek N. 159
Rosul R. 183
Sapozhnyk D.132
Saribyekova Yu.94
Schadewell Ch. 261
Semeshko O. 94
Slizkov A. 47
Slomion M. 280
Synyuk O. 205
Szafranska H. 71, 122
Tkachuk H. 10
Wozniak B. 223, 261
Zakharkevich O. 23
Zasornov A. 109
Zasornova I. 109
Zhiguts Yu. 33, 223



ХМЕЛЬНИЦЬКИЙ МІСЬКИЙ ГОЛОВА

29013, Україна, м. Хмельницький, вул. Гагаріна, 3, тел. (0382) 76-50-05, 76-50-86, факс 76-43-54

Електронна пошта: rada@khn.gov.ua

Khmelnytskyi City Council recommends a monograph on "Advanced technologies in education, industry, and the environment". The monograph is a valuable source of information on the introduction of the latest technologies in production, which can be used at the enterprises of the Khmelnytskyi region by future professionals. They will use this book to deepen their knowledge while learning.

Scientists of Khmelnytskyi National University promptly respond to world trends in the need for science-intensive products, solve current scientific and industrial problems of nowadays. The activities of the university involve the active communication of scientists with representatives of the business environment. Joint scientific and practical seminars of scientists and manufacturers, international conferences, exhibitions, during which participants exchange views, ideas, discuss prospects for cooperation, and implementation of scientific developments in production have become traditional.

Oleksandr SYMCHYSHYN

Mayor

City of Khmelnytskyi

A handwritten signature in blue ink, consisting of several loops and a long horizontal stroke at the end.



УКРАЇНА

ХМЕЛЬНИЦЬКА ОБЛАСНА РАДА

Майдан Незалежності, 2, Будинок рад, м.Хмельницький, 29005

тел. 0382(2) 76-59-98, тел/факс 0382(2) 76-45-17

E-mail: oblrada@oblrada.km.ua Web: www.oblrada.km.ua Код ЄДРПОУ 00022651

2874

Manufacturing earnings and exports are stimulating economic prosperity causing nations to increase their focus on developing advanced manufacturing capabilities by investing in high-tech infrastructure and education.

Countries and companies are striving to advance to the next technology frontier and raise their economic well-being. And as the digital and physical worlds of manufacturing converge, advanced technologies have become even more essential to company- and country-level competitiveness.

In fact, technology-intensive sectors dominate the global manufacturing landscape in most advanced economies to offer a strong path to achieve or sustain manufacturing competitiveness.

The international monograph presents the results of scientific research by scientists from Ukraine, Poland, the Czech Republic and Lithuania. Research topics include innovative methods in education, physical and chemical properties of new materials, improved research methods, modeling of technological processes, resource-saving technologies, determining the impact of materials on human health.

This allows to optimize and accelerate production processes, more efficient use of funds, energy, natural resources.

Deputy Chief of
Staff of the Regional Council



Tetyana Zelenko



CENTRUM LASEROWYCH TECHNOLOGII METALI
im. Henryka Frąckiewicza
Politechniki Świętokrzyskiej i Polskiej Akademii Nauk
Dr hab. inż. Norbert Radek, prof. PŚk



Monograph nt. "ADVANCED TECHNOLOGIES IN EDUCATION, INDUSTRY AND THE ENVIRONMENT" is recommended by the Centre for Laser Technologies of Metals.

The published monograph will be a valuable source of information on innovative technologies in education, industry and the environment.

Al. Tysiąclecia Państwa Polskiego 7, PL-25-314 Kielce,
Tel. (+48-41) 34-24-504, FAX (48-41) 34-24-489.
e-mail: norrad@tu.kielce.pl



FIRMA HANDLOWA BARWA
JAROSŁAW CZAJKOWSKI



Kielce, dn. 12.10.2020 r.

F. H. Barwa Jarosław Czajkowski
Warkocz 3-5,
25-253 Kielce

F. H. Barwa rekomenduje wydanie monografii pt. **"ADVANCED TECHNOLOGIES IN EDUCATION, INDUSTRY AND THE ENVIRONMENT"**.

Wydana monografia będzie cennym źródłem informacji o zaawansowanych technologiach w edukacji, przemyśle i środowisku.


.....
Podpis



AQAP 2110:2016
PN-EN ISO 9001:2015

FIRMA HANDLOWA BARWA JAROSŁAW CZAJKOWSKI
ul. Warkocz 3-5; 25-253 KIELCE

NIP 657-023-07-86
e-mail: biuro@barwa.kielce.pl

TEL.: +48 41 302 25 70
TEL.: +48 41 302 25 72
FAX: +48 41 302 25 71

www.barwa.kielce.pl



МУКАЧІВСЬКИЙ ДЕРЖАВНИЙ УНІВЕРСИТЕТ

89600, м. Мукачево, вул. Ужгородська, 26

тел./факс +380-3131-21109

Веб-сайт університету: www.msu.edu.ua

E-mail: info@msu.edu.ua, pr@mail.msu.edu.ua

Веб-сайт Інституційного репозитарію Наукової бібліотеки МДУ: <http://dspace.msu.edu.ua:8080>

Веб-сайт Наукової бібліотеки МДУ: <http://msu.edu.ua/library/>